Establishing A High Resolution Sequence Stratigraphy & Sea-Level Curve For Tertiary Limestones, Puerto Rico

by:

DIANA LORENA ORTEGA ARIZA

Thesis submitted in partial fulfillment of the requirements for the degree of

MASTER OF SCIENCE

In

GEOLOGY

UNIVERSITY OF PUERTO RICO
MAYAGÜEZ CAMPUS
April 2009

Approved by

_____	_____
Wilson Ramírez, Ph.D. Member, Graduate Committee	Date
_____	_____
Aaron Cavosie, Ph.D. Member, Graduate Committee	Date
_____	_____
Hernán Santos, Ph.D. President, Graduate Committee	Date
_____	_____
Wilford Schmidt, Ph.D. Representative of Graduate Studies	Date
_____	_____
Aaron Cavosie, Ph.D. Department Director	Date

Abstract

A high-resolution sequence stratigraphy model for the middle Tertiary limestone formations on the north coast of Puerto Rico is presented, based on stratigraphy and recognition of exposure surfaces, using both cores and outcrops. Data obtained in this study, in addition to previous work, have been compiled to produce a more-detailed description, including microfacies analysis. Five depositional sequences and four major sequence boundaries are proposed for Oligocene to Pliocene time. These are: 1) The San Sebastian Formation-Lares Limestone; 2) The Montebello Member; 3) The Cibao Formation-Aguada (Los Puertos) Limestone; 4) The Aymamón Limestone; and 5) The Quebradillas Limestone. These are most probably related to the second-order supercycles TB1, TB2 and TB3 in terms of eustatic sea level changes (Haq et al., 1987). The cores and outcrops studied in this research show a change from well developed-complete depositional cycles to partial cycles and exposure surfaces, representing the change from green-house to ice-house systems.

Resumen

Estratigrafía secuencial es utilizada para generar un modelo de alta resolución para las formaciones calizas del Terciario medio de la costa norte de Puerto Rico. El modelo es basado en estratigrafía y superficies de exposición usando núcleos y afloramientos. Los resultados obtenidos en este estudio, además de trabajos previos fueron compilados para producir una descripción más detallada, incluyendo el análisis de micro facies. Cinco secuencias deposicionales y cuatro límites de secuencia son propuestos para las edades del Oligoceno al Plioceno. Estos son: La Formación San Sebastián-Calizas Lares; El Miembro Montebello; La Formación Cibao-Calizas Aguada (Los Puertos); La Caliza Aymamón; La Caliza Quebradillas. Probablemente estas secuencias son más relacionadas a super-ciclos de segundo orden TB1, TB2 y TB3 en términos de cambios eustáticos en nivel del mar (Haq et al., 1987). Los núcleos y afloramientos estudiados en esta investigación muestran un cambio desde ciclos deposicionales bien desarrollados y completos a ciclos deposicionales parciales y superficies de exposición, representando el cambio del sistema de "green-house" al de "ice-house".

A mis padres por ayudarme a alcanzar mis sueños… por su incondicional amor y apoyo.

Acknowledgements

I would like to gratefully acknowledge my advisor Dr. Hernán Santos for his support and guidance. I received motivation and encouragement from him during all my studies. I also want to thank the inspiration and support I received from Dr. Wilson Ramírez. Special thanks to Dr. Aaron Cavosie for his important advices, which significantly improved this research. Many thanks to the faculty, graduate, and undergraduate students from the Department of Geology; they were an important part in my development as a person and a student. They have made me feel as at home. Special thanks to Marsha Irrizarry and Wilfredo Alequin who always were willing to help me anytime. I also thank the UPRM Core Facilities at the "Finca La Montaña", located in Aguadilla, Puerto Rico.

Financial assistance (Teaching Assistant) from the Department of Geology at the University of Puerto Rico-Mayagüez as well as funds from the Exxon Mobil Geology award, used for my last semester, are also gratefully acknowledged. Financial support from the AFAMaC program is also acknowledged; special thanks to Dr. Luis Caceres chair person of this program for his support throughout these years.

Many thanks to Dr. Douglas Walker and Alvin Bonilla for the strontium isotope sample processing at the Tectonics and Geochronology Isotope Geochemistry Sample Preparation Facilities at the University of Kansas. I also extend this gratitude to Dr. Evan Franseen from the University of Kansas for collaboration in this research project.

I would like to thank my family, for their unconditional support, inspiration and love. Deeply acknowledge to Santiago Velasco who was an essential part in this Thesis achieved. Many thanks to all my friends who were with me during these years: Marggie Gonzalez, Alejo Torres and Yolanda Canabal.

Table of Contents

Abstract……...ii
Resumen……iii
Acknowledgements……v
Table of Contents……...vii
List of Figures……....ix
List of Tables……xii

Chapter 1……1
INTRODUCTION……1
1.1 Purpose……..3
1.2 Sequence Stratigraphy Model……4
1.3 Carbonate Sequence Stratigraphy……..9

Chapter 2……..12
GEOLOGICAL SETTING……12
2.1 Tectonic Setting……...12
2.2 Structure of the Tertiary rocks in Northern Puerto Rico……...16
2.3 Stratigraphy of the Tertiary rocks in Northern Puerto Rico……19
2.4 Lithologic units……24
DEPOSITIONAL SEQUENCES……30
STUDY AREA……..31

Chapter 3……..37
METHODOLOGY……..37
3.1 Synthesis of the previous work……..…….37
3.2 Test holes analysis……..……37
3.3 Field work analysis……..……38
3.4 Standard Microfacies Types (SMF) Classification……..40
3.5 Sequence Stratigraphy modeling……42
3.6 Sea level curve comparison……42
3.7 Strontium isotope stratigraphy……42
3.8 Photomosaic analysis……..……43

Chapter 4……..45
RESULTS……45
4.1 NC-5 and NC-6 Test holes……...46
4.2 PR-10 and PR-22 road outcrops……66
4.3 Photomosaic results of the PR-111 and PR-10 outcrops……77
4.4 *Kuphus incrassatus* tubes-
Strontium isotope stratigraphy (SIS) ……..82

Chapter 5……..90
INTERPRETATION……...90
5.1 Parasequences Analysis……...90
5.2 Photomosaic Analysis……..96
5.3 Correlation between cores and road outcrops……103

Chapter 6……114
DISCUSSION……114
6.1 Depositional sequences……115
6.2 Sea Level Curve…….……...120

Chapter 7……125
CONCLUSION AND FUTURE WORK...……..125
REFERENCES……..127

APPENDIX-1. NC-6 AND NC-5 STRATIGRAPHIC COLUMNS INCLUDING ROCK TEXTURE AND CONSTITUENTS

APPENDIX-2. DEPOSITIONAL ENVIRONMENTS AND PARASEQUENCES INTERPRETATIONS OF NC-6 AND NC-5 TEST HOLES, AND PR-10 AND PR-22 OUTCROPS

APPENDIX-3A. STABLE ISOTOPE ANALYSES OF *Kuphus incrassatus* TUBES AND OYSTERS FROM MARCH 10, 2009

APPENDIX-3A. STABLE ISOTOPE ANALYSES OF *Kuphus incrassatus* TUBES AND OYSTERS FROM MARCH 18, 2009

APPENDIX-4A. SUMMARY OF STRONTIUM ISOTOPE ANALYSES

APPENDIX-4B. STRONTIUM ISOTOPE ANALYSES FROM TECTONICS AND GEOCHRONOLOGY ISOTOPE GEOCHEMISTRY SAMPLE PREPARATION FACILITIES AT THE UNIVERSITY OF KANSAS

List of Figures

Figure 1.1: Location of Tertiary sedimentary basins of Puerto Rico (modified from Meyerhoff and other, 1983 *in* Renken et al., 2002)……...2

Figure 1.2: General model for a sequence-stratigraphic framework (Tucker and Wright, 1990)…6

Figure 1.3: Depositional-sequence model for an inclined carbonate platform or "ramp" located in a humid environment (Handford and Loucks, 1993 in Ward et al., 2002)……11

Figure 2.1: Location of Puerto Rico in the Caribbean region (from Renken et al., 2002)…….13

Figure 2.2: Tectonic map of the Caribbean and plate motion velocities (Modified from Mann et al., 1991)……14

Figure 2.3: Early origins of the Caribbean plate (Pindell, 2006).....…..14

Figure 2.4: Major structural elements of Puerto Rico and Mona Passage (From Meyerhoff et al., 1983)……...18

Figure 2.5: Stratigraphic nomenclature evolution and ages for Oligocene, Miocene, and Pliocene sedimentary rocks of the North Coast Tertiary Basin of Puerto Rico (modified from Ward et al., 2002)……...21

Figure 2.6: Shows the surface geology on the north coast of Puerto Rico. The map illustrates the Formation exposed in the north coast and age of its formation (modified from Rodríguez-Martínez, 1995)……..23

Figure 2.7: Sequence-stratigraphic framework of the Oligocene to middle Miocene sedimentary rocks of the North Coast Tertiary Basin, Puerto Rico (Ward et al., 2002)…….26

Figure 2.8: Aerial extent of the Northern Coast Province of Puerto Rico and the location of cities and the test holes (Rodriguez and Hartley, 1994)……...32

Figure 2.9: Location of test hole NC-5 in the Barceloneta area, Puerto Rico (Rodriguez et al., 1991)……...33

Figure 2.10: Location and surficial geology at site of test hole NC-6, Hatillo, Puerto Rico (Rodriguez and Hartley, 1994)……...34

Figure 2.11: Location of PR-22 outcrop in the Barceloneta area, Puerto Rico…….35

Figure 2.12: Location of PR-10 outcrop in the Utuado area, Puerto Rico…….36

Figure 3.1: Standard microfacies types (SMF) for homoclinal carbonate ramp settings (Flugel, 2004)……..41

Figure 4.1: Legend for both test hole and outcrop sections along the north coast of Puerto Rico…….47

Figure 4.2: Stratigraphic column equivalent to NC-6 test-hole……..48

Figure 4.3: Stratigraphic column equivalent to NC-5 test-hole……..58

Figure 4.4: Stratigraphic column equivalent to PR-10 outcrops (Modified from Ramírez, 2000).67

Figure 4.5: Lares Limestone and San Sebastian Formation contact exposed at the PR-10 and PR-6621 intersection (N18°18'52'', W66 41'05'')……..……70

Figure 4.6: Oyster layer at the base of the Montebello Member, which was defined as the Lares Limestone-Montebello Member contact (intersection of PR-10 and PR-6621)…….71

Figure 4.7: Rudstone within the Montebello Member located at the top of PR-10 outcrop……...72

Figure 4.8: *Kuphus incrassatus*-rich layer located along the PR-10 road outcrops…….....73

Figure 4.9: Erosional surface at the top of the Montebello Member (N18°23'33'', W66°41'42'', in front of the first scenic overlook from Arecibo to Utuado) (photo by W.Ramírez)……...73

Figure 4.10: Stratigraphic column equivalent to PR-22 outcrop (Modified from Matos, 2002)…76

Figure 4.11: Outcrop location on PR-111 road (Google Earth)……..77

Figure 4.12: Oyster layer at topmost of the PR-111 outcrop……..78

Figure 4.13: San Sebastian-Lares Limestone contact exposed at the base of the PR-111 outcrop……..……..79

Figure 4.14: Lares Limestone-Montebello Member contact exposed at the top of the PR-111 outcrop……80

Figure 4.15: Clinoforms dipping in a north direction at the topmost of the PR-111 outcrop…….80

Figure 4.16: Outcrop location on PR-10 road…….81

Figure 4.17: *Kuphus incrasssatus* hand samples and thin sections……84

Figure 4.18: The $\delta^{18}O$ and $\delta^{13}C$ stable isotopic analysis from the north coast *Kuphus incrassatus* tubes (Tucker and Wright V.P., 1990)……85

Figure 4.19: Absolute ages using strontium isotope stratigraphy (SIS) from the north coast *Kuphus incrassatus* tubes and oysters along the PR-111 road outcrop……..88

Figure 4.20: Absolute ages using strontium isotope stratigraphy (SIS) from the north coast *Kuphus incrassatus* tubes and oysters along the PR-10 road outcrops. All samples are from this study……88

Figure 4.21: Absolute ages using strontium isotope stratigraphy (SIS) from the north coast *Kuphus incrassatus* tubes and oysters along the NC-6, NC-11 and NC-13 test holes. All samples are from this study……..89

Figure 5.1: Photomosaic interpretation on PR-111 road outcrop……...98

Figure 5.2: Photomosaic interpretation on PR-10 road outcrop……...102

Figure 5.3: Correlation of NC-5 test hole and PR-10 outcrop along the San Sebastian Fm and Lares Limestone, using Lares-Montebello contact as datum……105

Figure 5.4: Correlation of NC-6 and NC-5 test holes along the San Sebastian Fm and Lares Limestone, using Lares-Montebello contact as datum……..106

Figure 5.5: Correlation of NC-5 test hole and PR-10 outcrop along the Montebello Member, using Lares-Montebello contact as datum……..107

Figure 5.6: Correlation of NC-6 and NC-5 test holes along the Montebello Member, using Lares-Montebello contact as datum……109

Figure 5.7: Correlation of NC-6 and NC-5 test holes along the Cibao Formation and Aguada (Los Puertos) Limestone, using Lares-Montebello contact as datum……...111

Figure 5.8: Correlation of NC-6 and NC-5 test holes, and PR-22 outcrop along Aymamón Limestone and Quebradillas Limestone, using Lares-Montebello contact as datum……...113

Figure 6.1: The San Sebastian Formation- Lares Limestone Depositional Sequence……..116

Figure 6.2: The Montebello Member Depositional Sequence……..117

Figure 6.3: The Und. Cibao Formation-Aguada (Los Puertos) Limestone Depositional Sequence……..……118

Figure 6.4: The Aymamón Limestone and the Quebradillas Limestone Depositional Sequences……120

Figure 6.5: Comparison of Tertiary eustatic sea level curves and Northwestern Puerto Rico with depositional sequences of northwestern Puerto Rico (this study)……123

List of Tables

Table 2.1: Location of NC-5 and NC-6 test-holes on the north coast of Puerto Rico……31

Table 3.1: Dunham textural classification (1962)…….....39

Table 3.2: Embry and Klovan textural classification (1971)…….....39

Table 3.3: Key textures and diagnostic constituents to identify SMF (Flugel, 2004)……40

Table 4.1: Ramp Microfacies Types (RMF) proposed to the NC-6 and NC-5 test holes based on Wilson (1975) and Flugel (2004) microfacies analysis……..56

Table 4.2: Stable isotope data from *Kuphus incrassatus* tube and oyster samples of the Tertiary limestones along the north coast of P.R……..83

Table 4.3: Age determinations from strontium isotope data of the Tertiary limestones along the north coast of Puerto Rico……..……..86

CHAPTER 1

INTRODUCTION

The middle Tertiary limestone formations of the north coast of Puerto Rico (Fig. 1.1) have been studied since the early 1900's. Most of these studies are concentrated on the lithological characteristics and economic potential of the limestones. Ward et al. (2002) worked toward the first approximation of the sequence stratigraphic framework across the limestones of north coast of Puerto Rico. They attempted to show the relationship between the carbonate units in terms of the sequence stratigraphy. They proposed five major depositional sequences occurring among these units. Ramírez (2000) studied the Tertiary rocks exposed along road PR-10 and recognized two sequence boundaries within the Montebello Member of the Cibao Formation and the Lares Limestone that correspond with those proposed by Ward et al. (2002). Matos (2000) studied the Aymamón Limestone along NC-6 and NC-5 test holes and PR-22 road, which recognized three correlated exposure surfaces.

The sequence boundaries and the time-stratigraphic boundaries proposed in previous studies are uncertain due to the poor biostratigraphic control known on the Puerto Rico North Coast Tertiary Basin. Also, the stratigraphic chronology of the formations lacks an adequate resolution due to problems with the foraminiferal assemblages used for its development, since the fossils present are mostly shallow-water forms with fairly wide stratigraphic ranges (Seiglie & Moussa, 1984).

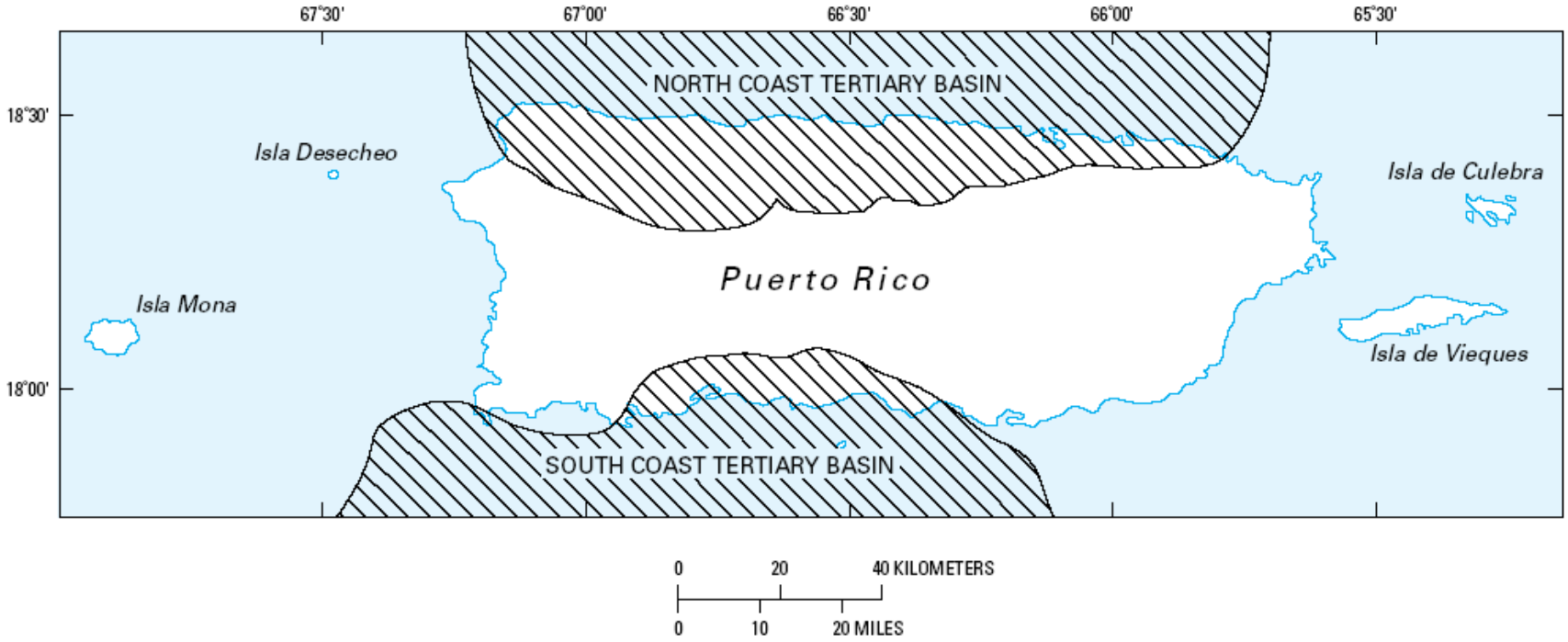

Figure 1.1: Location of Tertiary sedimentary basins of Puerto Rico (modified from Meyerhoff and others, 1983 *in* Ward et al., 2002). The northern coastal plain of Puerto Rico is underlain by as much as 2,000 m of carbonate and siliciclastic sedimentary rock, which accumulated in the North Coast Tertiary Basin during Oligocene to Pliocene time. These sedimentary rocks rest on a basement of folded and faulted Cretaceous and lower Tertiary sedimentary and igneous rocks.

In an effort to place together all the previous research, and to add resolution to the current stratigraphic knowledge the author re-examined two cores, NC-6 and NC-5, and two outcrops, PR-22 and PR-10, from Late Oligocene to Early Pliocene age in the carbonate rock section. Data obtained in this study, together with previous works, are compiled to produce more-detailed descriptions. Finally, a high-resolution sequence stratigraphy framework is produced for the Tertiary limestone formations based on surface exposures, using both outcrops and cores. This was accomplished using fundamental principles of sequence stratigraphy, characterizing the depositional environments, and describing the evolution of the paleotopography. These resulted in a model that shows and explains the development of a middle Tertiary limestone ramp of Puerto Rico over time and its relationship to global sea level.

1.1 Purpose

The concepts of sequence stratigraphy were employed to produce a detailed model for the middle Tertiary limestone formations at the north coast of Puerto Rico. This objective was achieved by using previous works to make a preliminary model based on the described methodology (Monroe, 1980; Seiggle & Moussa, 1984; Moussa et al., 1987; Hartley, 1989; Scharlach, 1990; Ramírez, 2000; Matos, 2000; Ward et al., 2002, among others). The contacts and sequence boundaries previously proposed were revised and correlated with surface exposures and cores of the corresponding formations. Relevant intervals were identified and petrographic analysis was performed where possible. Finally, a sea level curve was constructed based on the sequence stratigraphy model and compared with the global sea level curve.

1.2 Sequence Stratigraphy Model

Sequence stratigraphy is a powerful method for interpreting the stratigraphic record. Initially proposed by Vail et al. (1977) and Mitchum et al. (1977) and later refined by Posamentier et al. (1988), sequence stratigraphy "is the study of sediments and sedimentary rocks in terms of repetitively arranged facies and associated stratal geometry" (Christie-Blick and Driscoll, 1995). The definition of sequence stratigraphy establishes that shallow water sediments are deposited in distinctive packages or depositional sequences bounded by erosional unconformities or their correlative conformities. Because these major packages are separated by unconformities (sequence boundaries) and they also divide older from younger rocks, sequences have both time and genetic significance that describe periods of relative sea level changes (Mitchum et al., 1977; Van Wagoner et al., 1988; Emery and Myers, 1996; Flugel, 2004).

For the most part, the depositional architectures are products of eustatic sea level changes, regional tectonic movements, and sedimentological processes, all of which affect relative sea level. The major architectures recognized are progradational, aggradational, and retrogradational geometries (Emery and Myers, 1996). Progradational geometry occurs with high sedimentation in a static sea level scenario, and the facies belt migrates basinward. Aggradational geometry occurs when the sediment deposition and the sea level change are in balance, consequently the facies belt stack vertically. Retrogradational geometry occurs when the sediment deposition is less than the rate in which the relative sea level raises and the facies belt migrates landward (Emery and Myers, 1996).

Ideally, the sequences can be divided into “systems tracts”, units deposited during specific intervals of a third order (0.5 to 3 Million years - My) fluctuation of relative sea level (Posamentier, et al, 1988). The higher orders, first and second orders, are characterized by cycles of relative or eustatic change of sea level that have a duration in the order of 100 to 200 My and 10 to 80 My, respectively (Mitchum, 1977).

The three main systems tracts are (Fig. 1.2): Lowstand system tract (LST) at low relative sea level, Transgressive system tract (TST) as the shoreline moves landward, and Highstand system tract (HST) at high relative sea level (Van Wagoner et al., 1988). The LST can be divided into a lowstand fan (LSF), deposited during a fall in the sea level that passes the offlap break (Type sequence 1), and a lowstand wedge (LSW), deposited at the lowstand and during the early stages of a rise in the sea level. The deposits associated with this systems tract are characterized by a progradation that becomes an aggradation during the slow sea level rise (Emery and Myers, 1996; Van Wagoner et al., 1988).

The TST (middle systems tract) consist of retrogradational pattern characterized by extremely low sedimentation deposited during the subsequent rise of relative sea level. The base of this systems tract is the top of the LST in a type 1 sequence and its upper boundary is the maximum flooding surface. The upper unit (HST) is deposited during the late part of a sea-level rise and the early part of a fall resulting initially in aggradations that becomes later a progradation (Van Wagoner et al., 1988).

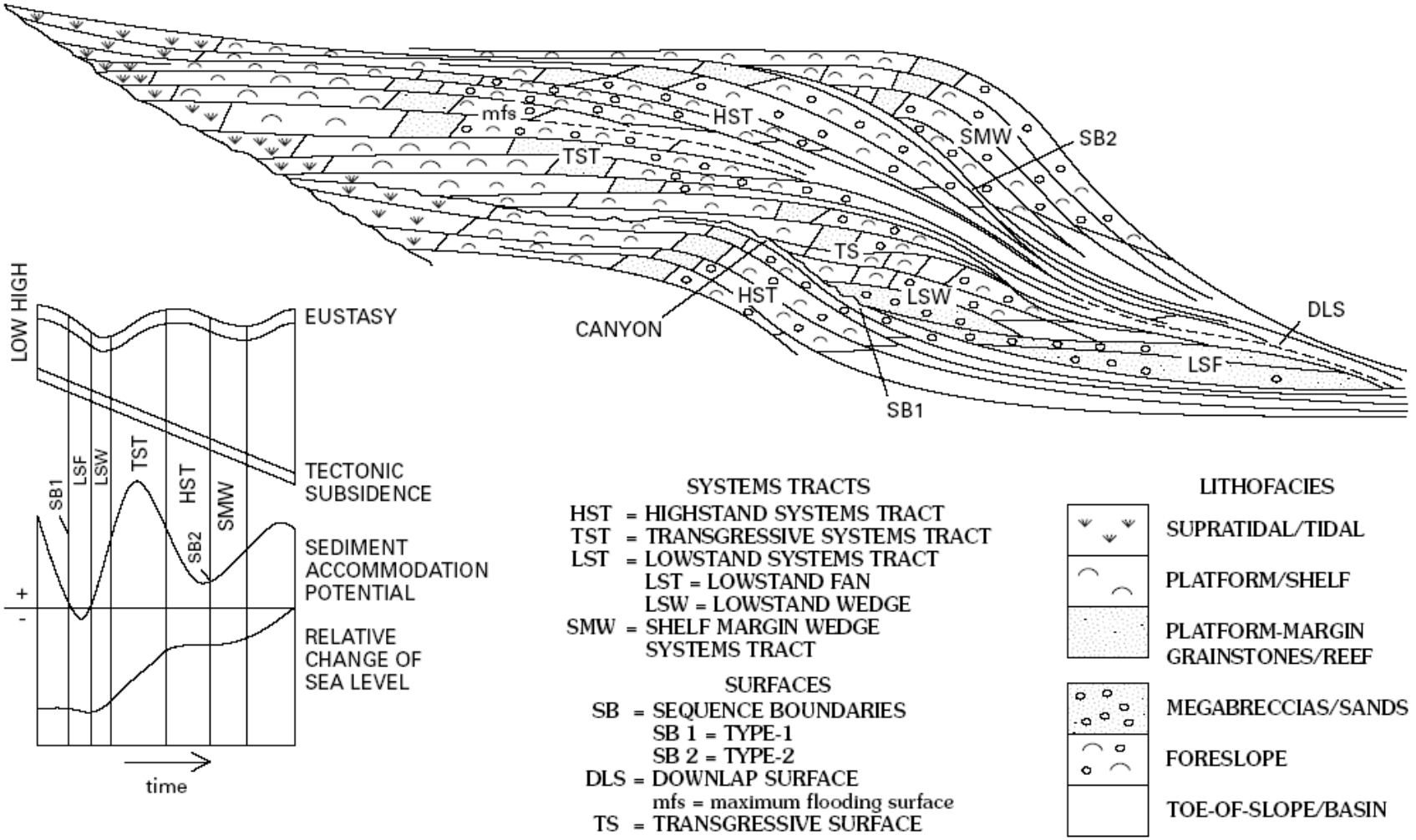

Figure 1.2: General model for a sequence-stratigraphic framework (Tucker and Wright, 1990).

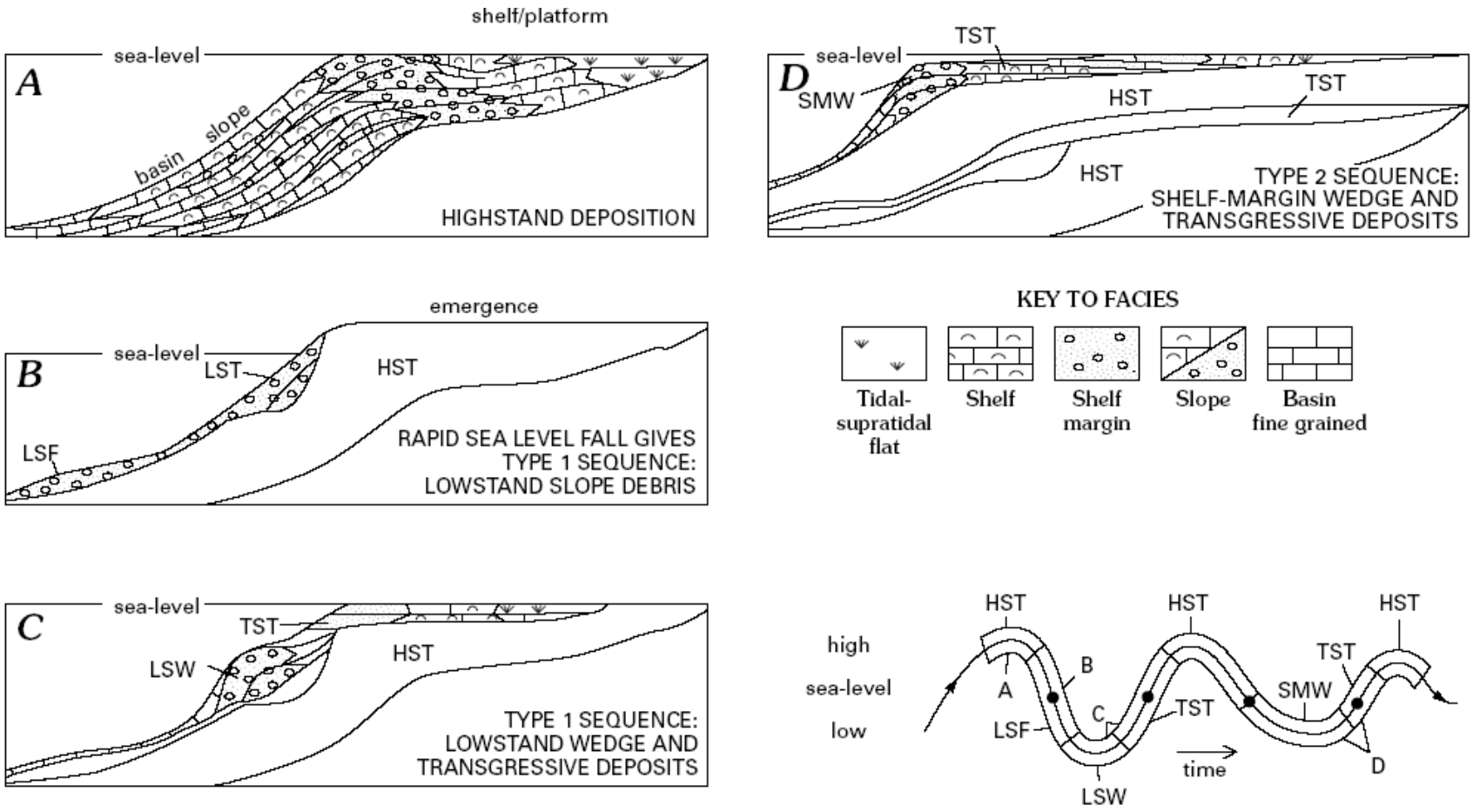

Figure 1.2 (cont.): General model for a sequence-stratigraphic framework (Tucker and Wright, 1990).

The parasequences, the smallest building block of the systems tracts, represent the sequences deposited during intervals of fourth order fluctuation of relative sea level within the LST, TST or HST. They are deposits that respond to small scale and high frequency sea level changes. These deposits are usually arranged in upward-coarsening units with shoaling-upward facies successions separated by fine sediments that represent a deeper facies succession (Emery & Myers, 1996). Furthermore, Van Wagoner (1990) described the parasequence set to each system tract as follows: the progradational parasequence set to the HST and Lowstand prograding wedge. The aggradational parasequence set to the shelf-margin system tract. Finally, the retrogradational parasequence set to the TST.

High resolution analysis provides an understanding of short periods of carbonate sedimentation (thousand to hundreds years). Deposits of higher order sea level change (fourth or higher) are expressed by minor changes in the depositional environment through the facies changes (parasequences). The parasequences in vertical progression are primarily controlled by the location of where it takes place, such as the platform, ramp or offshore settings (Flugel, 2004). In the offshore environment, parasequences are characterized by marl layers followed by thin upward shoaling units, covered by increasingly proximal tempestites. The ramp environment is characterized by oolitic and bioclastic grainstone bounded by a marine flooding surface (Flugel, 2004). While platform parasequences are characterized by flooding surfaces overlying by coral beds, oncoids beds and platform tempestites deposited under moderate energy conditions.

1.3 Carbonate Sequence Stratigraphy

Sarg (1988), and Handford and Loucks (1993) were pioneers using carbonate rocks to develop models based in sequence stratigraphy, despite the fundamental concepts of this methodology was derived from seismic stratigraphy of siliciclastic successions (Mitchum et al., 1977; Van Wagoner et al., 1988). Subsequent new carbonate models were developed by different researchers including Pomar & Ward (1991), Franseen et al. (1998), Montgomery et al. (2001), and others who recognized that these rocks are even susceptible to record with higher accuracy the relative sea-level fluctuations, changes in the carbonate sedimentation and different environmental factors, resulting in a useful technique to explain and predict the development of depositional sequences, sediment distribution and lithologic content.

Carbonate depositional systems have a different response to changes in relative sea level than siliciclastic depositional systems, especially based on the sediment supply. While siliciclastic deposits are derived from sources outside of the basin, carbonate sediments are generated in-situ.

Marine carbonate deposits are strongly influenced by environmental factors controlled by biogenic production. Therefore, they accumulate most rapidly in parts of basins where water depth, temperature, and geochemistry are optimal to this production and where the siliciclastic input is low. During times of high sea level, when large areas of continental margins are flooded with relatively shallow water and siliciclastic deposition, the rate of carbonate production is generally greatest. Falls in relative sea level may end or delay carbonate production. Even minor drops in sea level may expose

broad areas of a carbonate platform, halting carbonate sedimentation and bringing on karstification or calichification of the inner platform (Ward et al., 2002).

The model of sequence stratigraphy for carbonates is similar to that for siliciclastic rocks, where an ideal sequence is divided by system tracts: HST, TST and LST (Flugel, 2004, see Fig. 1.2). Most carbonate sedimentation has been reported in the TST and HST. The carbonate deposition in the LST is restricted to narrow areas and is recognized by abundant siliciclastic input and exposure surfaces of carbonate platforms. The TST is characterized by deepening-upward successions with progressive open marine conditions. The HST is identified by thick bedded or massive carbonate deposition, with abundant marine biota, shoaling upward successions and changes from open to restricted marine conditions (Fig. 1.3).

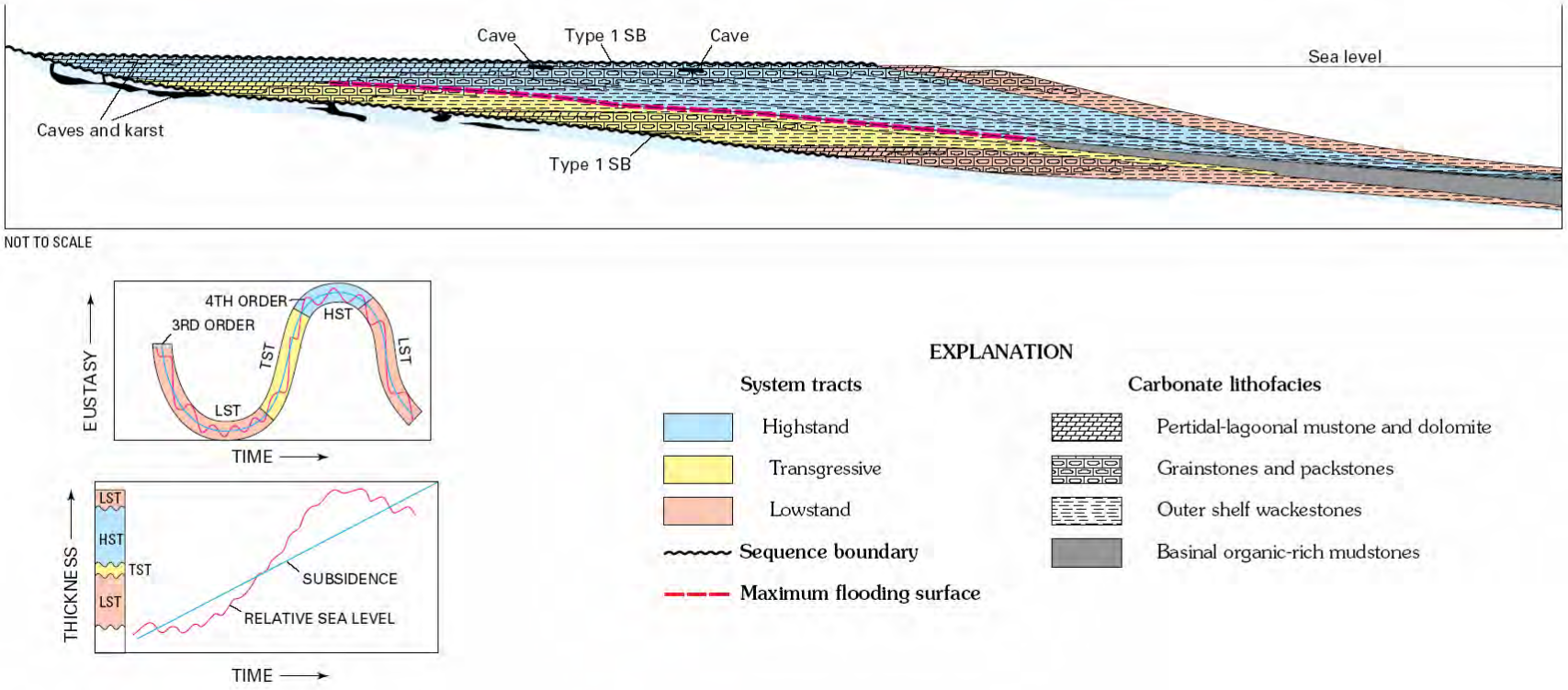

Figure 1.3: Depositional-sequence model for an inclined carbonate platform or "ramp" located in a humid environment (Handford and Loucks, 1993 in Ward et al., 2002).

CHAPTER 2

GEOLOGICAL SETTING

2.1 Tectonic Setting

Puerto Rico, the easternmost island of the Greater Antilles arc system, is located in the northeastern part of the Caribbean Sea between latitudes 17°37' and 18°31' N, and longitudes 65°14' and 67°56' W (Fig. 2.1). It is an island arc terrain with a geologic record of about 195 Ma. Together with the northern Virgin Islands it represents the subaerially exposed parts of the Puerto Rico-Virgin Islands microplate (Fig. 2.2), that lies within the seismically active Caribbean-North American Plate boundary (Byrne et al., 1985).

The most important aspects related to the tectonic development of the Caribbean, Puerto Rico and the Puerto Rico north coast Tertiary limestones are explained as follows.

About 140 Ma ago, the North America and South America plates spread apart. The Caribbean plate formed when subduction occurred beneath the Proto-Caribbean plate. Followed by the development of the Greater Antilles island arc that began during the Late Jurassic-Early Cretaceous and continued until Middle Eocene, in which time the volcanic and plutonic central part of Puerto Rico formed (Fig. 2.3, Pindell, 2006; Meyerhoff et al., 1983).

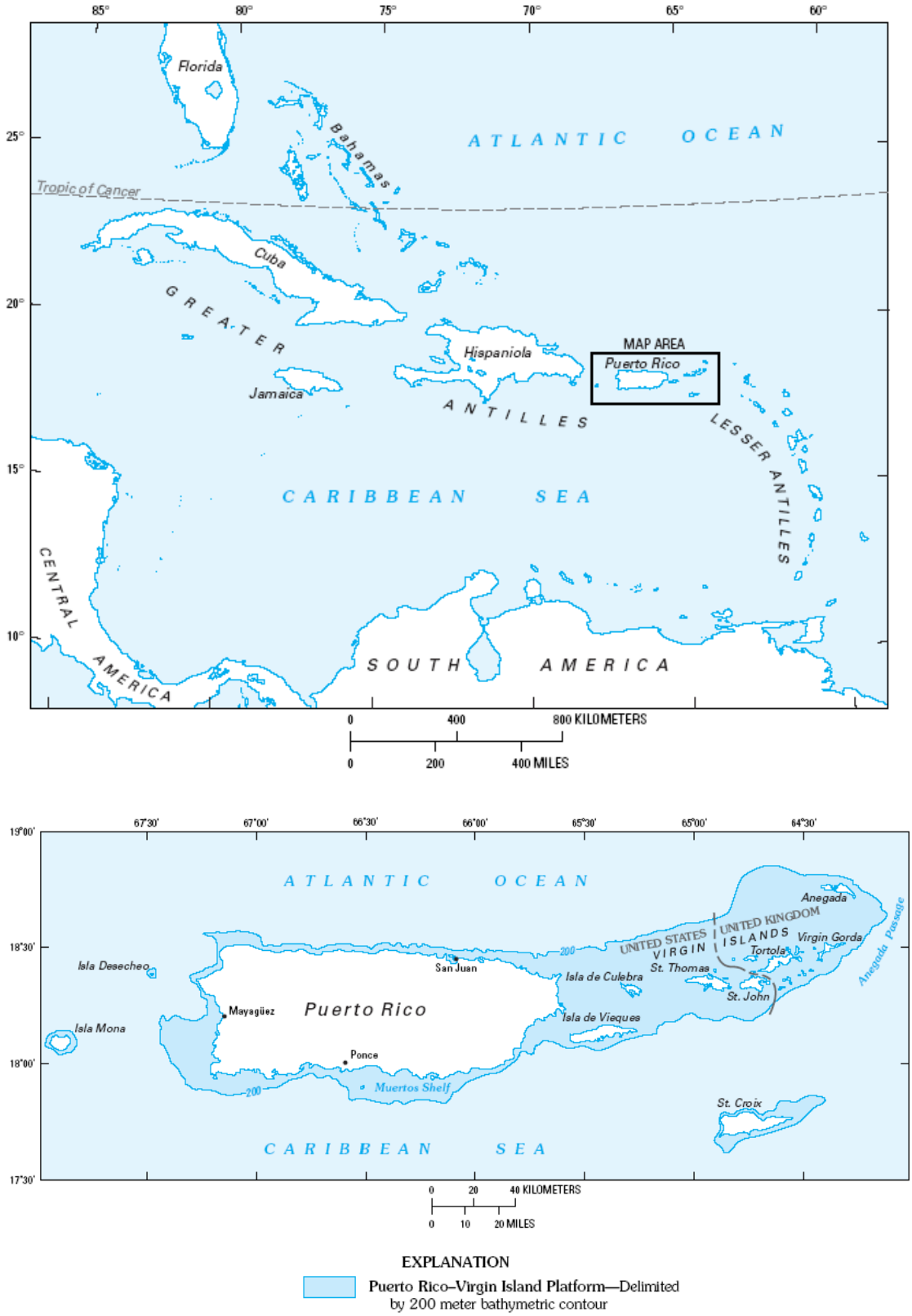

Figure 2.1: Location of Puerto Rico in the Caribbean region (from Renken et al., 2002).

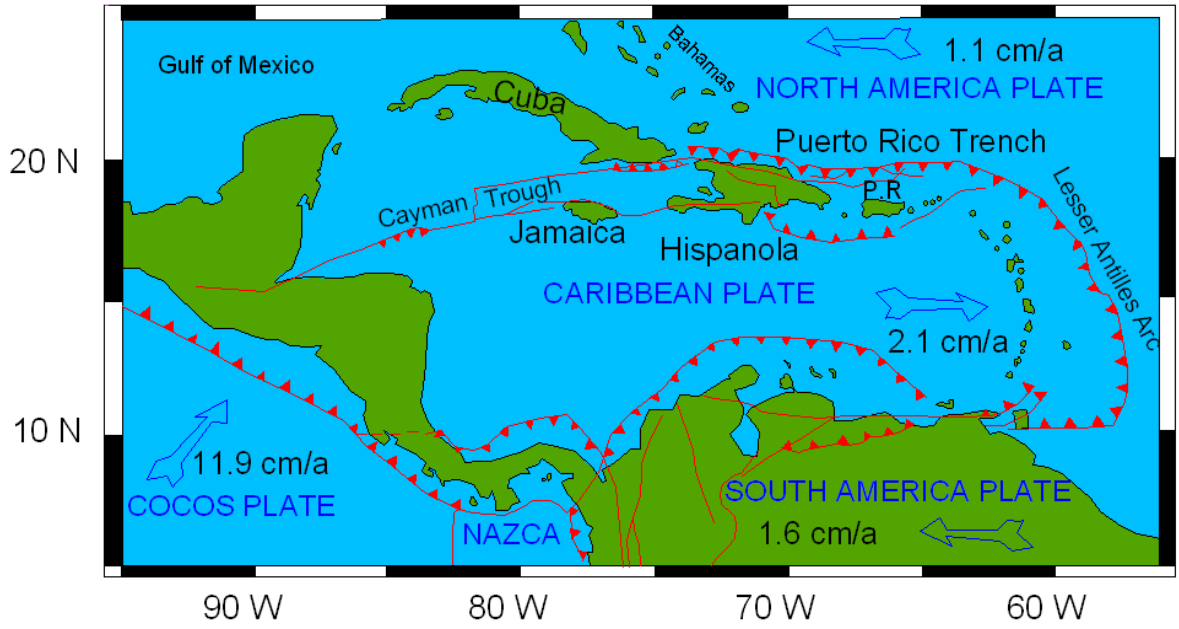

Figure 2.2: Tectonic map of the Caribbean and plate motion velocities (Modified from Mann et al., 1991)

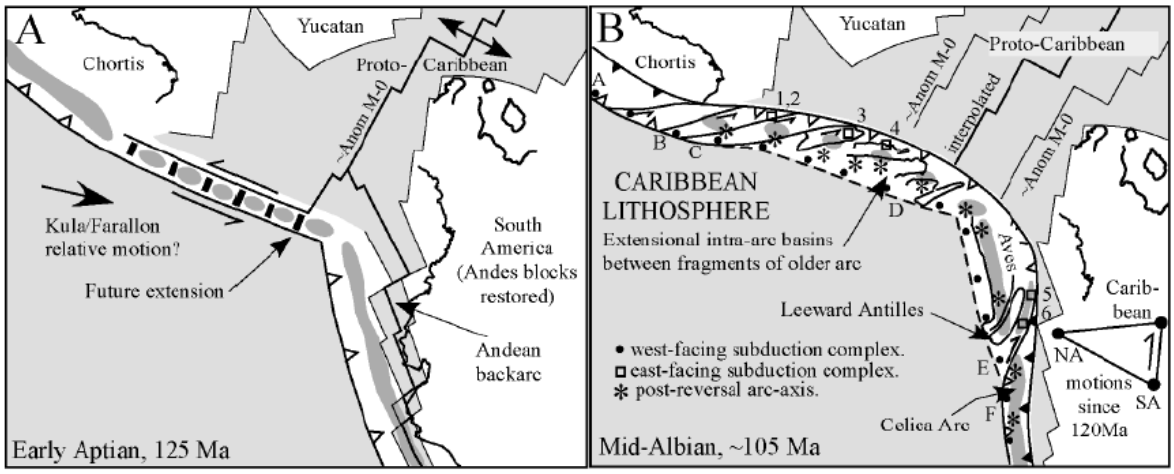

Figure 2.3: Early origins of the Caribbean plate during Cretaceous time. A) Pre-subduction-polarity-reversal time. B) Post-subduction-polarity-reversal time. Symbols: toothed lines, subduction zones; doubles lines, spreading zones; single lines or lines with arrows, transform plate boundaries (Pindell, 2006).

Sequences of deep water volcanic sediments were deposited throughout the Cretaceous, followed by a series of shallower island-arc volcanic sediments as well as carbonate and volcaniclastic deposits (Mattson, 1984). This basement of volcanic material was subjected to folding, faulting, and uplift during Late Cretaceous through Middle to Late Eocene subduction when a collision with the Bahamas platform occurred (Meyerhoff et al., 1983; Mattson, 1984).

After the collision with the Bahamas platform the volcanism in Puerto Rico stopped following the end of subduction in the Late Eocene. This event resulted in the exposure of the Puerto Rico- Virgin Islands microplate and it also changed the plate boundary between the Caribbean and the North American plates to dominantly left-lateral strike-slip (Sykes et al., 1982; Mattson, 1984). Since the Late Eocene until today, these plates show a dominance of strike-slip motion (Pindell and Barret, 1990). Eastward movement of the Caribbean plate resulted in release of stress and subsequent subsidence during the Late Oligocene to Miocene.

Both the termination of arc volcanism and the onset of orogenesis have been proposed to be related to either the collision of the western part of the Greater Antilles arc with the Bahama platform (Pindell and Barrett, 1990), subduction of the Bahama platform beneath Puerto Rico (Erikson et al., 1990), or subduction of buoyant oceanic crust (Larue, 1991).

The lack of significant deformation in the north coast Tertiary strata (Monroe, 1980) and the uniform thickness of the Tertiary sequence seen in seismic reflectors from offshore produced by Meyerhoff et al. (1983), suggest tectonic stability of the Virgin Island-Puerto Rican microplate during the Late Oligocene and Miocene. Birch (1986),

using these seismic profiles, proposed that subsidence of the northern coast of Puerto Rico occurred in three stages, each of one dominated by different physical mechanisms.

From late Middle Eocene to middle Oligocene, the first regional subsidence stage occurred. It was due to tensional crustal thinning that resulted in Puerto Rico sinking 1 to 2 km (Birch, 1986). During the second event, from the middle Oligocene to the Miocene, the region subsided almost 2 km due to sediment loading and thermal contraction from the magmatism in the previous stage. The sedimentary units considered in this study also were deposited. Finally, during the middle Pliocene the Caribbean plate subducted beneath the North American plate marking the initiation of renewed subduction again.

According to Birch (1986) these subduction episodes caused hundreds of meters of uplift in the southern portion of the North Coast Tertiary Basin (studied area), while the rest of the northern Tertiary platform (toward the trench) was tilted to the north and subsided over 4 km. Although Birch (1986) placed the uplift of the southern portion of the north Tertiary basin (studied area) during the middle Pliocene, a Late Miocene uplift is most consistent with the current stratigraphic and paleomagnetic data available (Reid et al., 1991; Renken et al., 2002).

2.2 Structure of the Tertiary rocks in Northern Puerto Rico

The island core of Puerto Rico is composed of folded and faulted Late Jurassic to Eocene metamorphic, igneous and sedimentary rocks (Mattson, 1984; Meyerhoff et al., 1983; Schellekens, 1998) intruded by multiple plutons (Smith et al., 1998).

On the north coast, these rocks are overlain by a relatively undeformed section of gently northward-dipping (homoclinal dip (1 to 8 degrees) Oligocene to Pliocene carbonate with minor terrigenous rocks deposited during shorter periods of time (Seiglie

and Moussa, 1984) (Figure 2.4), and on the south coast, by similar age but more strongly deformed rocks (Monroe, 1980). The average dip of the north coast middle Tertiary sequence is 4° to 4.5° (Briggs and Gordon, 1961).

An east-trending anticlinorium and two large left-lateral wrench faults, the Great Northern Puerto Rico fault zone, and the Great Southern Puerto Rican fault zone (Glover, 1971), are the major structural features of Puerto Rico (See Fig. 2.4). The core of the island has been subdivided into three geographic volcanic provinces using these two major fault zones (Meyerhoff et al., 1983; Larue, 1991; Schellekens, 1991; Schellekens, 1998; Jolly et al., 1998).

Structural deformation is uncommon in the Late Oligocene to Pliocene sedimentary units of the north coast basin. Faults cutting the surface are present but rare (Monroe, 1980). Some of the normal faulting within the Early Oligocene strata may be associated with the development of large structural uplifts in the basin. These are Aguadilla, Rio Grande de Arecibo, Rio Grande de Manatí (the oldest structure) and the San Juan uplifts. Monroe (1980) notes a small plunging anticline southwest of Manatí affecting the Early Miocene strata and a small domal structure near Vega Alta affecting the Miocene limestones. These two features are observed as gravity anomalies and seem to represent basement structures (Monroe, 1980).

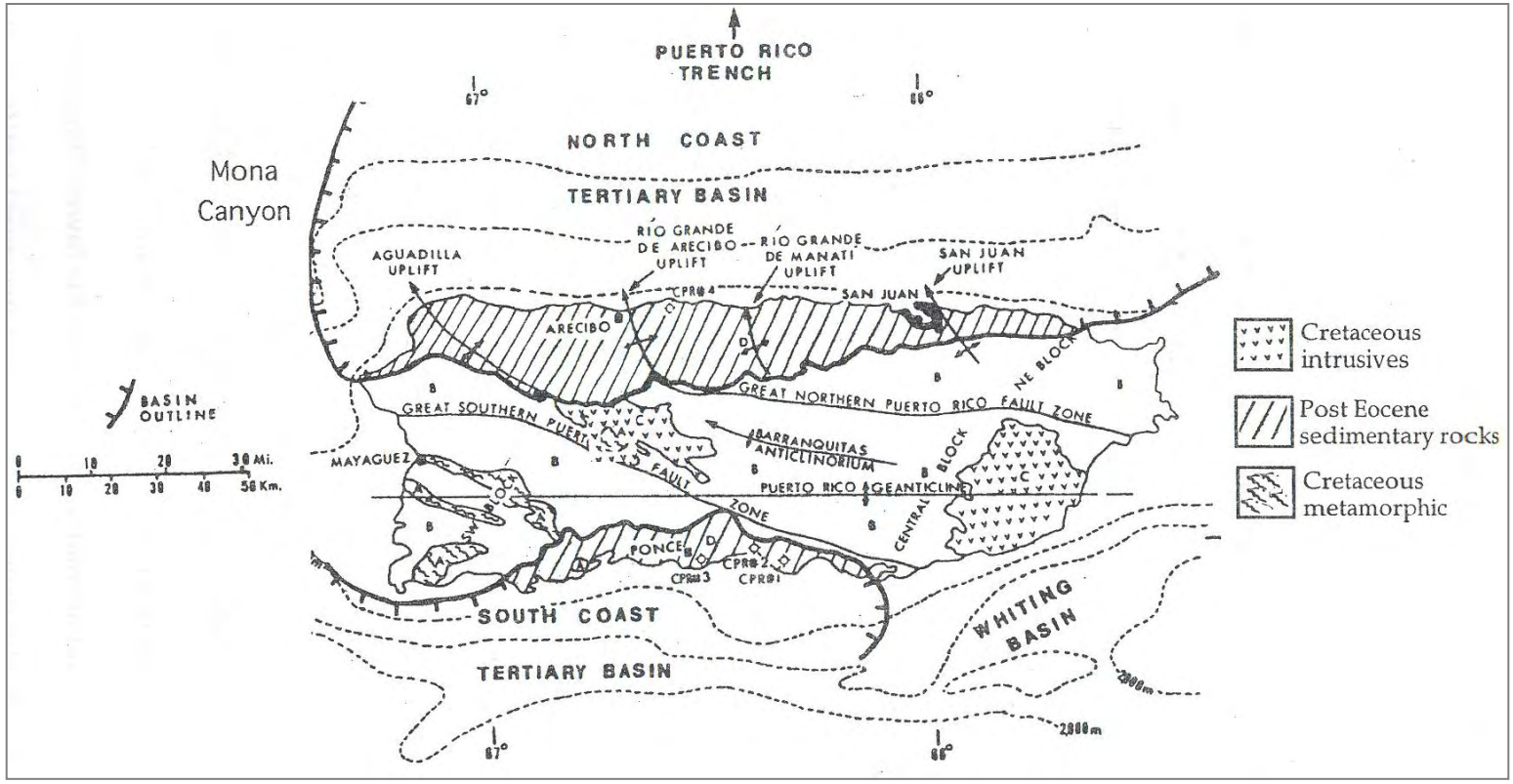

Figure 2.4: Major structural elements of Puerto Rico and Mona Passage (From Meyerhoff et al., 1983).

2.3 Stratigraphy of the Tertiary Rocks in Northern Puerto Rico

The first stratigraphic study of the Tertiary sedimentary units was published by the Council of New York Academy of Sciences (Berkey, 1915). The principal geologic features of Puerto Rico are described as "older series" of late Mesozoic rocks overlain by a "younger series" of Cenozoic rocks. The younger series was divided into the San Juan Formation and the Arecibo Formation. Later, Berkey (1919) suggested a division of the Arecibo Formation into Quebradillas (upper limestone Member) and San Sebastian (lower shale Member).

After Berkey (1919), the middle Tertiary units of northwestern Puerto Rico were divided by Hubbard (1923) into (from oldest to youngest) the San Sebastian Shale Formation, the Lares Limestone, the Cibao Formation, the Los Puertos Formation and the Quebradillas Limestone Formation (Fig. 2.5). Following Hubbard (1923), Zapp et al. (1948) divided the youngest formations deposited above the Cibao Formation into the Aguada and Aymamón Limestone formations (see Fig. 2.5).

Monroe (1969, 1980) in his stratigraphic summary of these units showed the work of Zapp et al. (1948) to be in error. The Aguada Limestone Formation type section chosen by Zapp et al. (1948) is actually the Cibao Formation proposed before by Hubbard (1923). Furthermore, Meyerhoff (1975) determined that the base of the Aguada Limestone Formation and Los Puertos Formation was at the same stratigraphic position. These observations led to the conclusion that these two formations represented the same units. Monroe (1968) tried to rectify the problem by defining a reference section for the Aguada Limestone Formation. However, Seiglie and Moussa (1975), and Meyerhoff (1975) argued that the Hubbard's (1923) name had priority, first because the type section

for the Aguada Limestone Formation was improperly defined, and second, because Hubbard (1923) proposed the name Los Puertos Formation previous to the Aguada Limestone Formation.

The former authors also argued that the Camuy Formation of Monroe (1963) is the same as the Quebradillas Limestone of Hubbard (1923) even though the Quebradillas Limestone Formation is thicker than the Camuy Formation. Seiglie and Moussa (1975) redefined the lower boundary (type section) of the Quebradillas Limestone, making it essentially equivalent to the Camuy Formation. Therefore, this invalidated the name Camuy Formation since Quebradillas Limestone name had priority (see Fig. 2.5).

Seiglie and Moussa (1984) and Meyerhoff et al. (1983) described an island-wide unconformity at the top of the Los Puertos Formation (Aguada Limestone). Meyerhoff et al. (1983) called the Moca Limestone Formation to the unit above this unconformity. This unit has not been defined formally as formation, and since the Aymamón Limestone corresponds with this stratigraphic position between Los Puertos Formation (Aguada Limestone) and the Quebradillas Limestone this name will continue to be used (see Fig 2.5).

The maximum thickness recorded in a well was 1,684 m at the test well 4-CPR, drilled between Arecibo and Barceloneta (Briggs and Gordon, 1961). Based on seismic data, the maximum onshore sedimentary rock thickness may be around 2,000 m and the maximum offshore sedimentary rock thickness may reach 2,500 m to 3,500 m (Meyerhoff et al., 1983).

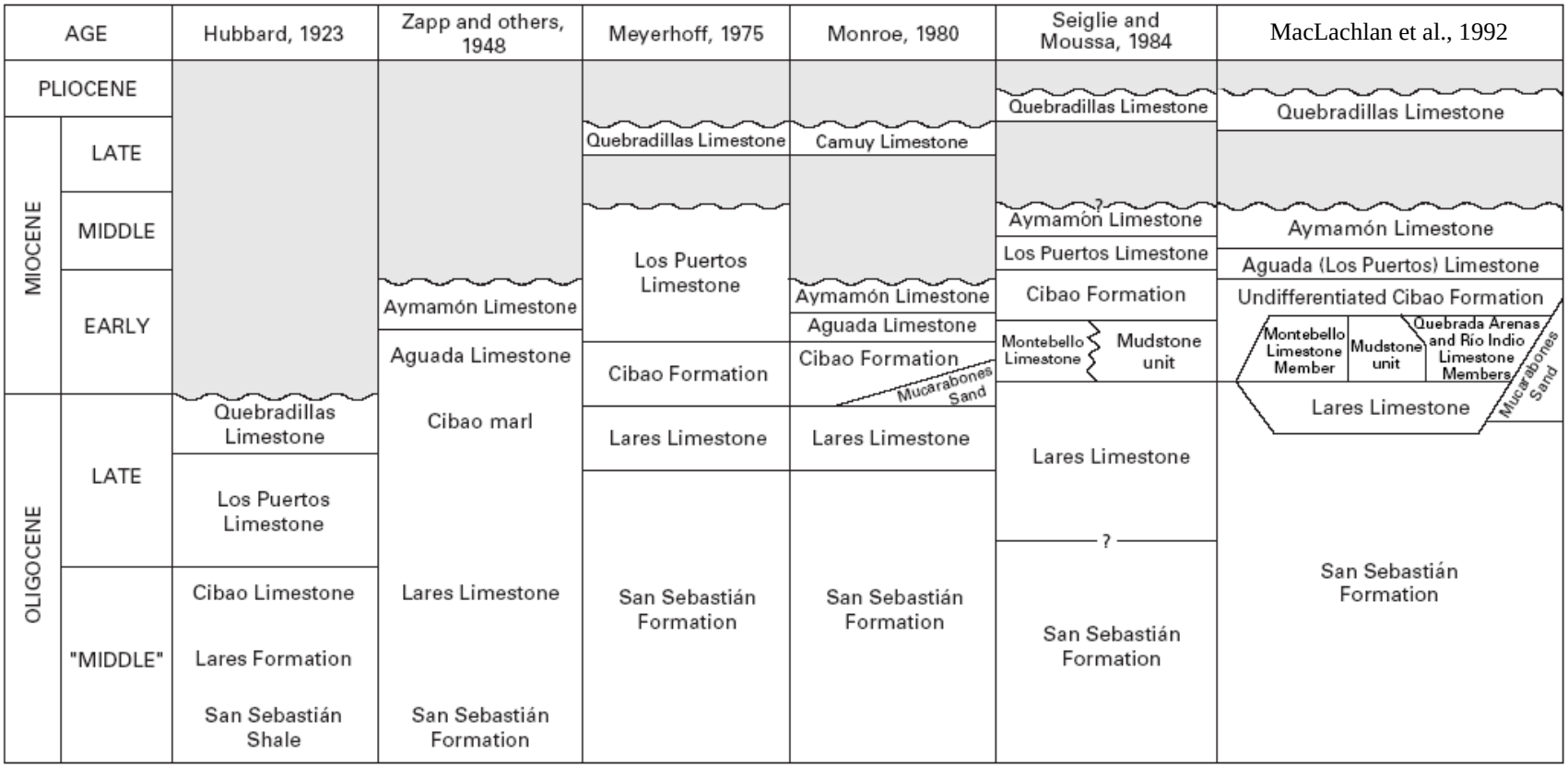

Figure 2.5: Stratigraphic nomenclature evolution and ages for Oligocene, Miocene, and Pliocene sedimentary rocks of the North Coast Tertiary Basin of Puerto Rico (modified from Ward et al., 2002).

After 1984, the U.S. Geological Survey in cooperation with various agencies of the Commonwealth of Puerto Rico carried out a series of investigations in different areas of the north coast Tertiary limestones. In these results, they describe the regional hydrogeologic units, geology and lithology of these rocks (Ward et al., 1991, Rodríguez-Martinez, 1990, Renken and Goméz-Goméz, 1994, and Torres-González et al., 1996, among others).

Until 1986, data on regional stratigraphic framework of subsurface Tertiary rocks underlying the northern coastal plain of Puerto Rico were limited to a few wells (Briggs and Gordon, 1961; Seiglie and Moussa, 1984). In 1986, an extensive core drilling program was initiated by the U.S. Geological Survey providing new data on the stratigraphy and depositional history of these units (Hartley, 1989; Scharlach, 1990; Todd, 1996; Ramírez, 2000, Renken et al., 2002; among others).

The middle Tertiary units that will be used in this study are (Fig. 2.6): from oldest (Late Oligocene) to youngest (Early Pliocene), Lares Limestone (Late Oligocene-Early Miocene age), Cibao Formation including its Montebello Limestone Member (Early Miocene age), Aguada (Los Puertos) Limestone (Early Miocene age), Aymamón Limestone (Middle Miocene age), and the Quebradillas Limestone (Late Miocene to Early Pliocene), following the nomenclature of MacLachlan et al. (1992) *in* Ward et al. (2002) (see Fig. 2.5), which follows for the most part the nomenclature used by the U.S. Geological Survey.

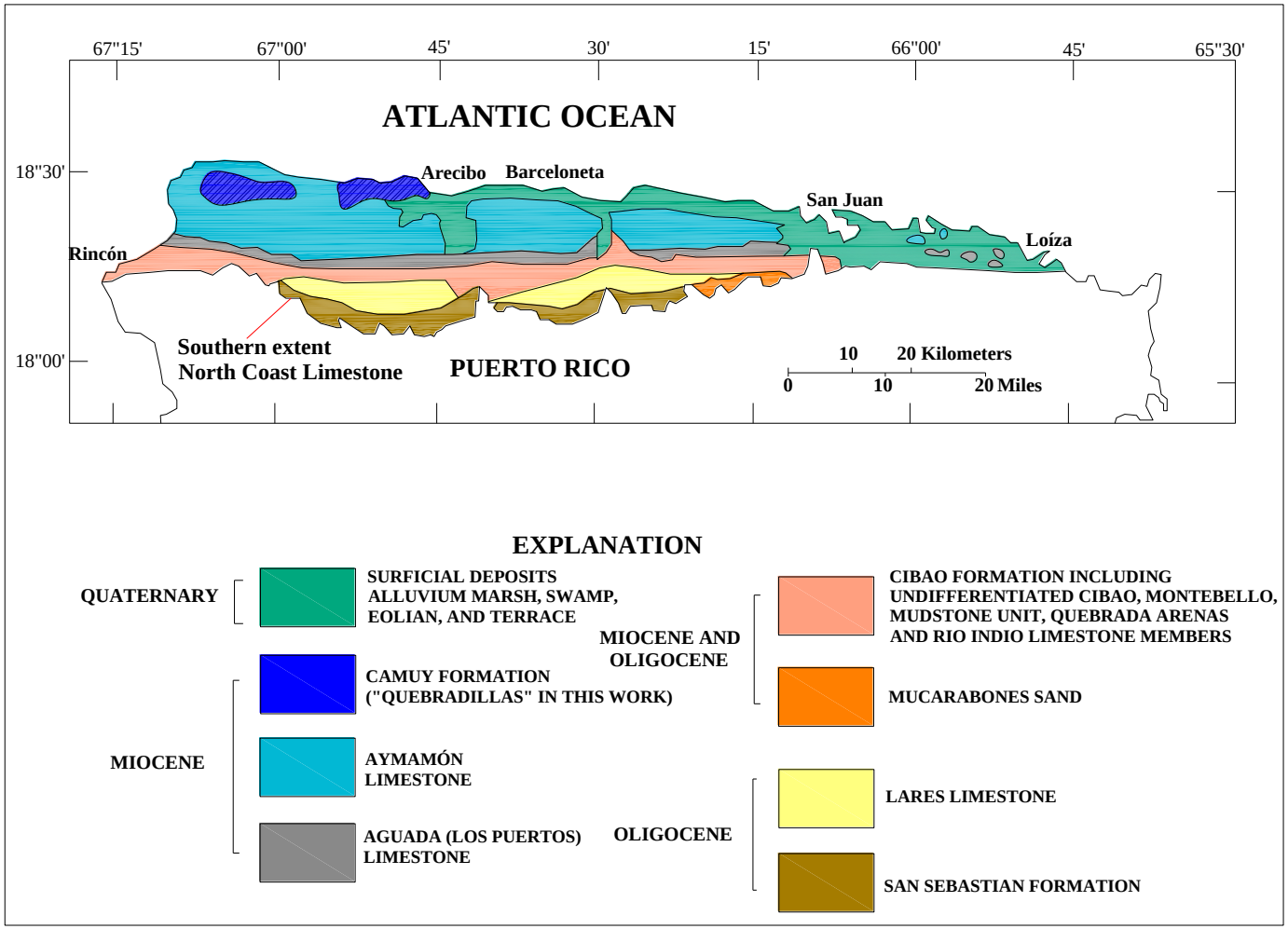

Figure 2.6: Shows the surface geology in the north coast of Puerto Rico. The map illustrates the Formation exposed in the north coast and age of its formation (modified from Rodríguez-Martínez, 1995).

2.4 Lithologic Units

The Lares Limestone

The Late Oligocene-Early Miocene (Seiglie & Moussa, 1984) Lares Limestone overlies the San Sebastian Formation or, less commonly, basement rock where larger structural uplifts occur (Monroe, 1980). The unit is composed predominantly of thickly bedded, fine to medium grained calcarenite, and in most places, is found in gradational contact with the underlying San Sebastian Formation (Hartley, 1989). This formation is mainly siliciclastic rocks while the Lares Limestone is compose mainly by carbonate rocks, so it is possible to interpret that the lower to middle Lares Limestone records a transgression that began with the upper San Sebastian Formation. This lower diachronous boundary was also interpreted by Briggs et al. (1961) and Meyerhoff et al. (1983) as deposition during a marine transgression. On the other hand, upper Lares Limestone represents a regressive stage that ended through deposition of the lower Montebello Member (Hartley, 1989). Hartley (1989) established that these transgressions and regressions represent depositional environments between lower, middle and upper Lares Limestone.

The Lares Limestone crops out in a continuous belt of limestone on the northern coast of the island. The outcrop thickness ranges from 270 m east of the Bayaney quadrangle where it has a fairly constant thickness, to a maximum thickness of 301 m in the Bayaney quadrangle (Monroe, 1980). The formation pinches out in the western and eastern edges of the outcrop belt. In the subsurface the Lares Limestone thickness ranges from 0 to 500 m (Heisel et al., 1983; Hartley, 1989; Ward et al., 2002). It is overlain by the undifferentiated Cibao Formation or by the different members of the Cibao Formation

depending on the specific location on the northern coast of the island. In the study area it is overlain by the Montebello Member.

Nelson & Monroe (1966) and Monroe (1980) in the Florida quadrangle, recognized lithologic changes between the Lares Limestone top and the contact with the Montebello Member. This contact in outcrop exposures was defined by the presence of an oyster shells bed that varies from 1 to 5 m thick. The presence of two possible sequence boundaries indicates that the Lares Limestones and the Montebello Member were exposed to weathering, erosion and meteoric water invasion twice before the undifferentiated Cibao Formation was deposited over the units (Ward et al., 2002) (Fig. 2.7).

The Lares Limestones was deposited on a broad 25 km wide shelf rich in marine organisms that were similar to those living in modern reef environments (Frost et al., 1983). The western and eastern boundaries of the basin are dominated by fluvial deposits (Monroe, 1980).

The Cibao Formation

The Cibao Formation is the most heterogeneous of the Tertiary units of northern Puerto Rico. It is a complex unit of carbonate, mixed carbonate-siliciclastic, and siliciclastic sedimentary rocks, which Monroe (1980) divided into six members on the basis of surface exposures. Typically, the formation consists of clayey skeletal wackestone and fossiliferous calcareous claystone (marl) with thin units of mudstone and sandstone. In the western-central part of the basin (the study area) the typical Cibao lithology interfingers with volcaniclastic sandstone and conglomerate and shale of the Guajataca Member.

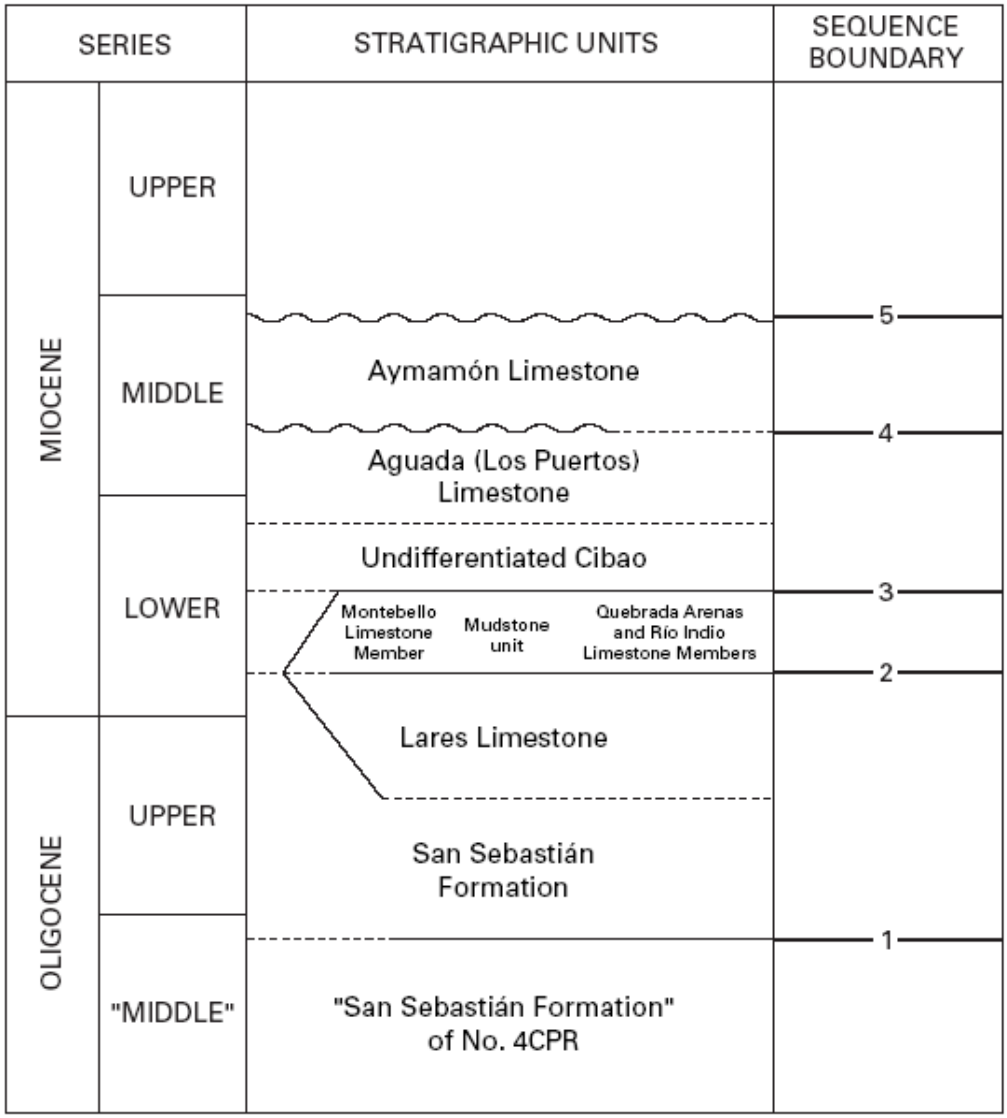

Figure 2.7: Sequence-stratigraphic framework of the Oligocene to Middle Miocene sedimentary rocks of the North Coast Tertiary Basin, Puerto Rico. The numbers (1 to 5) indicate the sequence boundaries proposed previously. The exact relation of these and the time-stratigraphic boundaries is uncertain because the lack of biostratigraphic information (Ward et al., 2002).

In the study area this formation is separated between the Montebello Limestone Member and an undifferentiated upper part. The Montebello Limestone Member is the most laterally and stratigraphically extensive member unit of the Cibao Formation and consists of mid-platform limestone. Across most of the Montebello outcrop belt, beds of large oysters mark the base of this limestone member and form the boundary with its underlying unit the Lares Limestone (Ward et al., 2002). In the subsurface, the Montebello Member is composed of shoaling upward sequences with the basal units being dominantly shallow middle-to-inner shelf deposits and the uppermost sequences composed of rocks deposited in high-energy near-shore environments (Hartley, 1989). Whereas the uppermost part of the Cibao Formation consists of claystone, marl, and limestone containing terrigenous material (Rodriguez, 1995). Seiglie and Moussa (1984) proposed an Early to Middle Miocene age to this formation while Frost et al. (1983) placed it into Early Miocene. This formation is overlain by the Aguada (Los Puertos) Limestone.

The Aguada (Los Puertos) Limestone

This Early to Middle Miocene formation crops out across the North Coast Tertiary Basin, except east of Río Bayamón where the outcrop is narrow and discontinuous (Ward et al., 2002). It consists predominantly of hard thick-bedded to massive calcarenite, alternating with beds of clayey limestone.

The Aguada (Los Puertos) Limestone is about 90 meters thick in the western part specifically on the valley of Rio Camuy and thicker farther to the east (Monroe, 1980). Thick strata of the Aguada (Los Puertos) Limestone forms a cliff-face on an escarpment above the softer Cibao Formation. It rests conformably on the Cibao Formation and in

many places “it is difficult to distinguish the two formations” (Monroe, 1980). The upper boundary is in sharp contact with the overlying Aymamón Limestone (Monroe, 1980). This contact represents an island-wide unconformity (Meyerhoff et al., 1983).

In the subsurface the Aguada (Los Puertos) Limestone typically consists of shoaling-upward cycles of grayish-orange and yellowish-gray skeletal wackestone to packstone several meters thick. Some of these depositional cycles in the lower part of this formation in the west-central area are limited by calichified zones (Ward et al., 2002).

The Aymamón Limestone

The formation consists of massive to thick bedded, fine crystalline and nearly pure limestone, which becomes dolomitic near the coast (Monroe, 1980). Most of the Aymamón Limestone is nearly white to very pale orange, but some beds are pale yellow and graynish pink. The entire thickness of the Aymamón Limestone cannot be measured directly in any single place, but estimated thickness across the outcrop belt is 190 to 200 m (Monroe, 1980; Meyerhoff et al., 1983) and the maximum subsurface thickness (incomplete section) is 218 m in the 4-CPR test well (Briggs and Gordon, 1961). Sinkholes are common in the Aymamón Limestone near the contact with the Aguada (Los Puertos) Limestone.

For the most part, the Aymamón is composed of shoaling-upward depositional cycles that range from a meter to several meters thick. Cycles commonly consist of skeletal wackestone or wackestone to packstone passing upward to packstone to grainstone. Some cycles are capped by coral rudstone or coral-red algae boundstone (Ward et al., 2002). Because of the purity of the limestone Monroe (1980) suggested that

it was deposited on a reef flat in relatively shallow water. The presence of corals, foraminifers and molds of mollusks support this conclusion.

According to Seiglie and Moussa (1975), Monroe (1980), and Meyerhoff et al. (1983), the upper boundary of the Aymamón Limestone is a paleokarst surface. In the northwestern half of the Tertiary outcrop, the Aymamón is overlain by the Pliocene Quebradillas Limestone. The boundary between these formations is an erosional unconformity.

The Quebradillas Limestone

The Quebradillas Limestone overlies paleokarst developed in the Aymamón Limestone and underlies, in some places, alluvial and coastal deposits of Quaternary age. The Quebradillas Limestone varies from calcarenite, to limestone conglomerate in a clayey matrix, to locally quartz sandstone. Monroe (1980) divided it into three parts: the lower unit is about 30 to 40 m of "chalky limestone" and calcarenite. Oyster shells and shell fragments interbedded with marl are common near the base of the formation in some localities. A middle unit consists of about 25 to 30 m of hard ferruginous calcarenite with fossiliferous beds. An upper unit is composed of more than 40 m of fossiliferous "chalk, sandy chalk, sandstone, sandy limestone, and limestone" containing abundant planktonic foraminifers (Monroe, 1980). At the subsurface the Quebradillas Limestone has been encountered only in two test wells (NC- 6 and 4-CPR) and is predominantly composed by planktonic foraminifers.

In general the Quebradillas Limestone represents a complete transgressive-regressive cycle (Seiglie & Moussa, 1984). The age of this formation is controversial.

Monroe (1980) suggests that it is Late Miocene, while Seiglie and Moussa (1984) propose that it is Pliocene.

DEPOSITIONAL SEQUENCES

Despite few published detailed descriptions of outcrop sections as well as from the cursory descriptions of cores taken during later stages of the core drilling project and lack of downdip control, the Late Oligocene through Middle Miocene sedimentary rocks (Lares Limestone throughout Aymamón Limestone) have been divided (tentatively) into four major depositional sequences by Ward et al. (2002) (see Fig. 2.7).

These sequences were proposed by identifying relative sea level changes, both in outcrop and in cores. In general terms these relative changes affect the carbonate production and siliciclastic sedimentation and they are the major characteristics useful to interpret the Tertiary limestone rocks in terms of sequence stratigraphy.

The oldest sequence comprises the upper San Sebastián Formation and the lower Lares Limestone. This interval records progressive onlap on the San Sebastian Formation during a rise in relative sea level. The top of this TST is within the middle Lares Limestone (maximum transgression). Upper parts of the Lares characterize the HST. A second depositional sequence is encountered in the Cibao Formation that represents a general transgression. The Montebello Member and the Mudstone Unit record a cycle of deposition from generally shallower to deeper and then to shallower environments which can be interpreted as a TST followed by the HST, respectively. The upper part of the Cibao Formation and the lower Aguada (Los Puertos) Limestone would represent another depositional sequence, where it is just possible to recognize the TST. Resolution of a

HST is tenuous. Finally, the Aymamón Limestone comprises the fourth depositional sequence. It is bounded both at the bottom and top by karst zones (Ward et al., 2002).

STUDY AREA

The study area is based mainly on two test holes drilled by the U.S. Geological Survey in cooperation with the Puerto Rico Department of Natural Resources as part of a comprehensive study of the north coast aquifer system of Puerto Rico. These core-holes are: NC-6, drilled to a depth of 776 m (2,574 feet) below land surface in the municipality of Hatillo; and core-hole NC-5, drilled to a depth of 772 m (2,564 feet) below land surface in the municipality of Barceloneta (Fig. 2.8 and Table 2.1). The well NC-5 is located in the north-central part of Puerto Rico, approximately 56.3 Km west of San Juan. The well is located about a half-kilometer south of highway PR-2, along highway PR-140 near Cruce Davila (Fig. 2.9). Well NC-6 was drilled in Barrio Capaez in the municipality of Hatillo, about 1.3 Km west of road 130 and 2.25 Km south of Highway PR-2 (Fig. 2.10).

Table 2.1: Location of NC-5 and NC-6 test-holes on the north coast of Puerto Rico (from Ramirez, 2000).

CORES	TOWN	Location	
		Lat N	Long W
NC-6	Hatillo	18° 27’ 57”	66° 49’ 26”
NC-5	Barceloneta	18° 25’ 43”	66° 34’ 15”

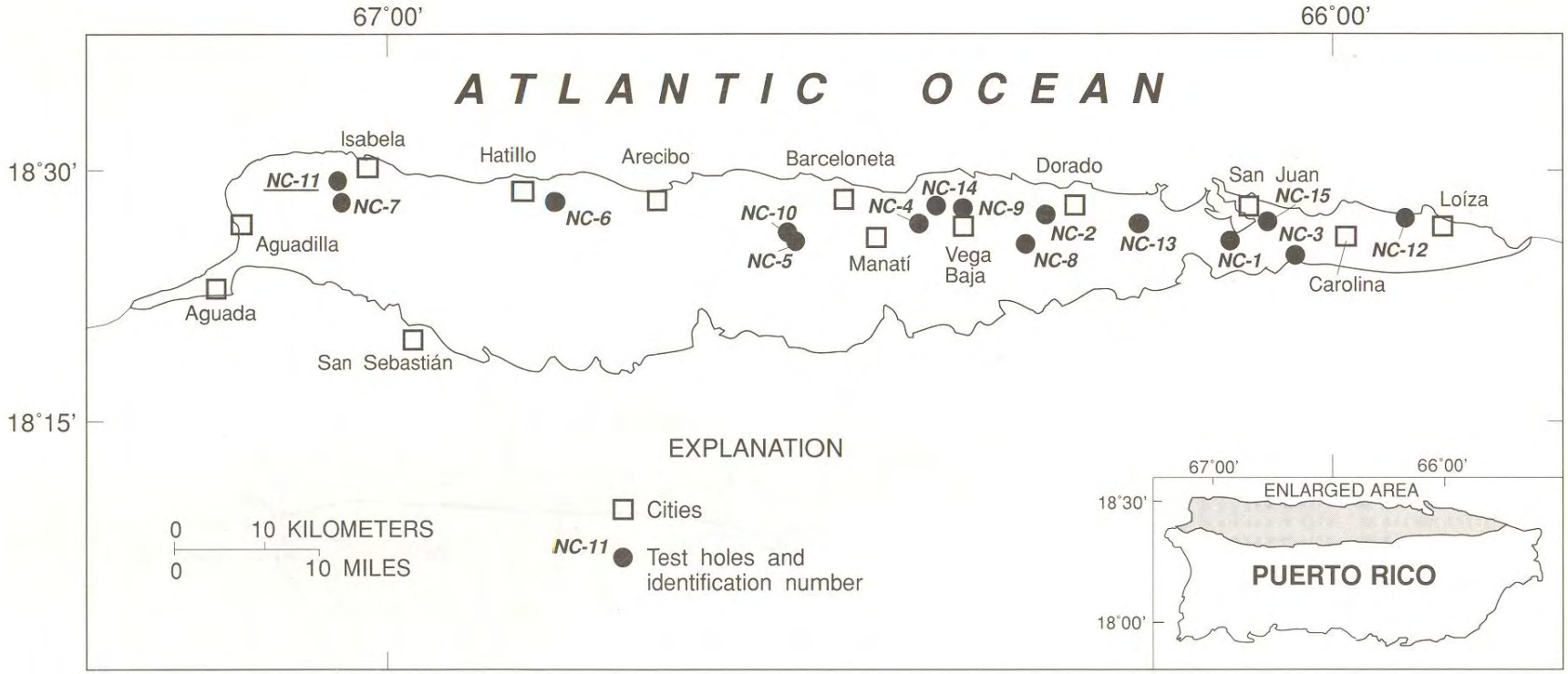

Figure 2.8: Aerial extent of the north coast province of Puerto Rico and the location of cities and the test holes (Rodriguez and Hartley, 1994).

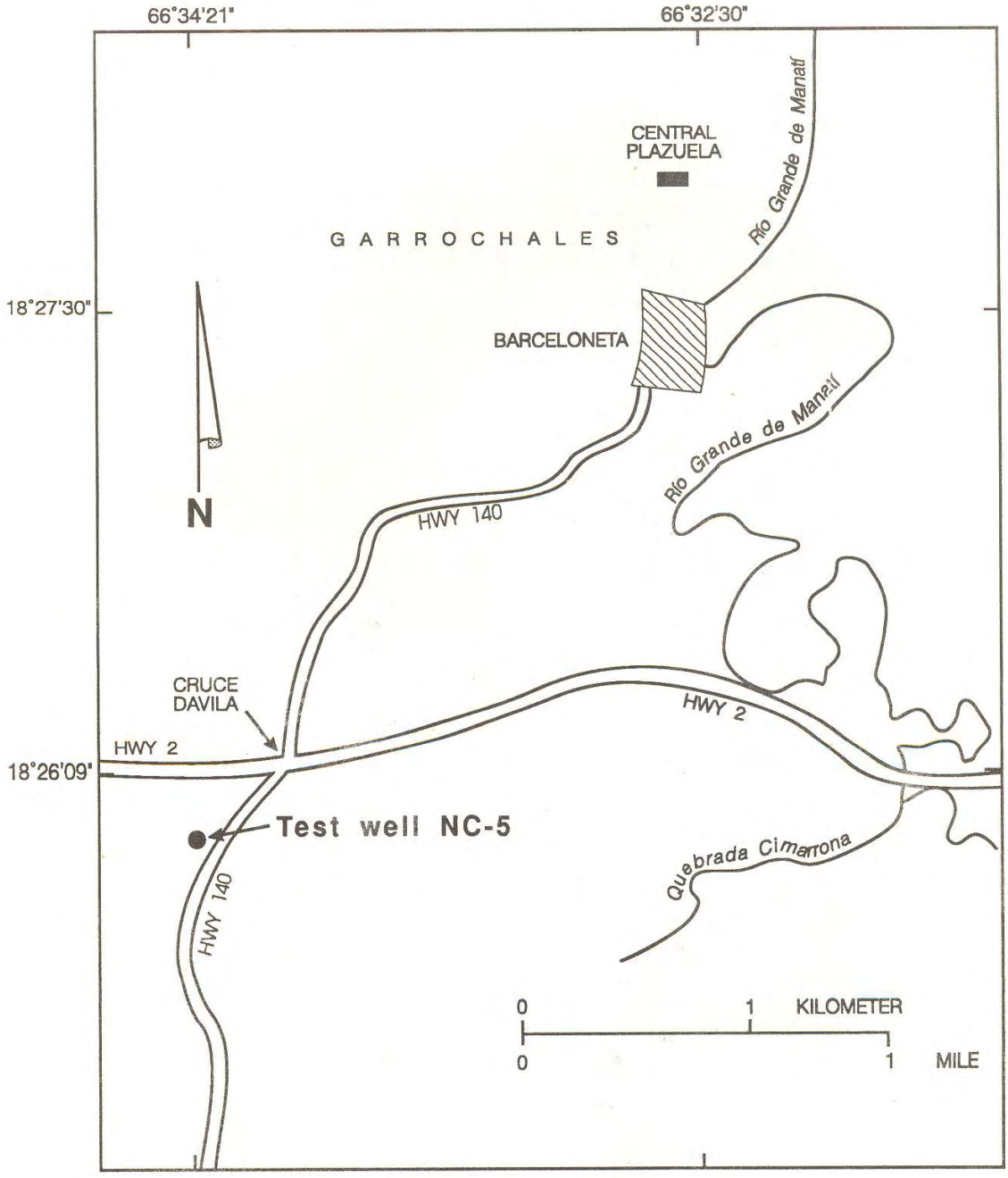

Figure 2.9: Location of test hole NC-5 in the Barceloneta area, Puerto Rico (Rodriguez et al., 1991).

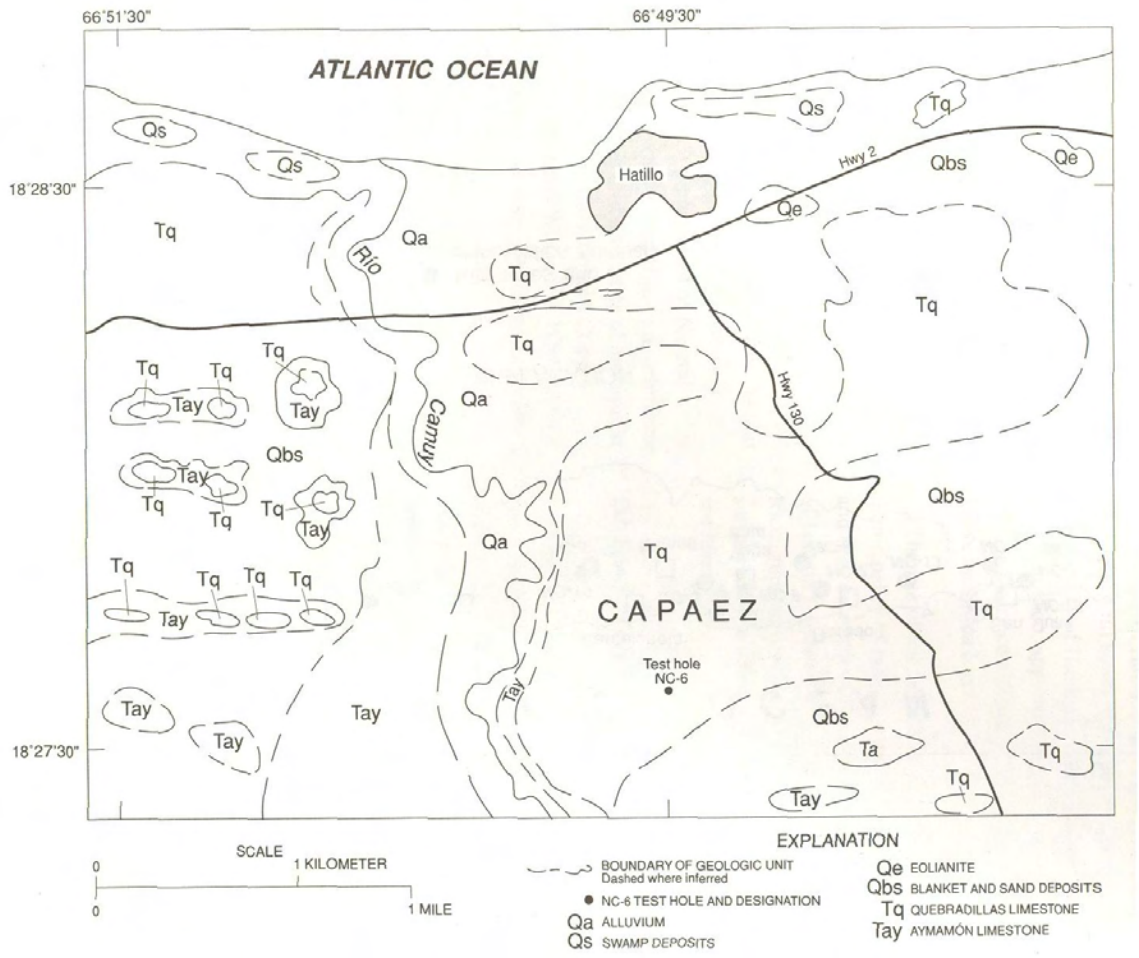

Figure 2.10: Location and surficial geology at the site of test hole NC-6, Hatillo, Puerto Rico (Rodriguez and Hartley, 1994).

Additional information was obtained from exposures along the Puerto Rico highway #22 between the municipalities of Manatí and Arecibo, and the Puerto Rico highway #10 between the municipalities of Arecibo and Utuado. The outcrop of the PR-22 is located at Km 56.6 of highway 22, San Juan to Arecibo route and it is 36.58 m in height (Figure 2.11) and it is part of a series of outcrops located along route PR-22. The PR-10 outcrops are located between the intersection of highways PR-10 and PR-6621 (N18° 18’ 52”, W66° 41’ 05”) and the first scenic overlook from Arecibo to Utuado along highway PR-10 (N18° 22’ 52”, W66° 41’ 16”) (Figure 2.12).

In order to make a complete and detail model based on the concepts of sequence stratigraphy, the areas specifically studied in outcrops and cores are locations that have been defined as contacts between formations, including the proposed sequence boundaries (See Fig. 2.7).

Figure 2.11: Location of PR-22 Outcrop in the Barceloneta area, Puerto Rico.

Figure 2.12: Location of PR-10 Outcrop in the Utuado area, Puerto Rico.

CHAPTER 3

METHODOLOGY

The main objective of this research is to construct a high-resolution sequence stratigraphy framework for the middle Tertiary limestone formations on the north coast of Puerto Rico. The sequence stratigraphy model was developed based on surface exposures and cores. Eight methodological procedures were performed to obtain these results. These methods were; 1) Synthesis of previous work; 2) Test holes analysis; 3) Field work analysis; 4) Standard microfacies types (SMF) classification; 5) Sequence stratigraphy modeling; 6) Sea level curve comparison; 7) Strontium isotope stratigraphy (SIS); and 8) Photomosaic analysis.

3.1 Synthesis of Previous Works

A review of previous work was done to make a preliminary model based on the sequence stratigraphy methodology. Several works were analyzed and described in order to develop a general model. Works that studied the NC-6 and NC-5 test holes analysis include Ward et al. (2002), Hartley (1989), Scharlach (1990), and Ramírez (2000) were used. Works that studied the PR-10 and PR-22 roads like Ramírez (2000) and Matos (2000) were also used.

The contacts and sequence boundaries previously proposed by Ward et al (2002) were revised and correlated with outcrops and test holes of the corresponding formations (See Fig. 2.7). Relevant intervals were identified and revised for each test hole and outcrop.

3.2 Test holes analysis

Two test holes, NC-6 and NC-5, drilled by the U.S. Geological Survey in cooperation with the Puerto Rico Department of Natural Resources were re-examined. The air drilling method used in these two test holes resulted in nearly continuous recovery of core. However, the recovery was fragmental in the poorly indurated and karst zones. In addition, portions of the core deteriorated during storage and have been used for research by several authors. These two test holes are stored in wooden core boxes at the Finca Montana of the UPRM in Aguadilla bunkers.

Descriptions of the cores included carbonate rock texture, amount of terrigenous material, and fossil constituents, among others, which indicated depositional environment as well as possible exposure surfaces (caliche, roots, coal layers, etc). Available thin sections (W.Ramírez, PhD collection) were also analyzed and described in terms of rock type and skeletal components. All core information was correlated with the core log records made by the U. S. Geological Survey at the time of drilling.

3.3 Field work analysis

Outcrops located along the PR-22 and PR-10 highways were used to correlate the subsurface data in order to have better control of the study area. Fieldwork was performed covering all relevant intervals recognized for development of the sequence stratigraphy model. New possible cycle boundaries, the four sequence boundaries proposed in the literature, significant surfaces and sedimentary structures, skeletal and non-skeletal components, and rock textures were studied. Rock samples were collected as part of the sedimentologic description and sequence stratigraphic analysis. Sequence

boundaries were based primarily on physical surfaces (including irregular contacts, reworking, bioturbation, and major facies changes).

The textural classification produced a general idea of the depositional environment of the limestone units. The limestone facies in rock samples were classified according to Dunham's (1962) and Embry and Klovan (1971) textural classification schemes (Tables 3.1 and 3.2). It is important to keep in mind that carbonate rocks exhibit many fabrics (micrite, wackestone, packstone and even grainstone) produced by diagenetic processes (Tucker and Wright, 1990), that can result in misinterpretations when identifying the original texture of the rocks.

Table 3.1: Dunham Textural Classification (1962).

DEPOSITIONAL TEXTURE RECOGNIZABLE					Depositional texture not recognizable
Original components not bounded together during deposition				Original components were bounded together during deposition.	
Contains mud (particles of clay and fine silt size)			Lacks mud and is grain supported		
Mud supported		Grain supported			
Less than 10% grains	More than 10% grains				
MUDSTONE	WACKESTONE	PACKSTONE	GRAINSTONE	BOUNDSTONE	CRYSTALLINE

Table 3.2: Embry and Klovan Textural Classification (1971).

ALLOCHTHONOUS LIMESTONE ORIGINAL COMPONENTS NOT ORGANICALLY ORIGINAL BOUND DURING DEPOSITION						AUTOCHTONOUS LIMESTONE COMPONENTS ORGANICALLY BOUND DURING DEPOSITION		
Less than 10% > 2 mm components contains lime mud (<0.03 mm)			No lime mud	Greater than 10% >2 mm components		by organisms which		
Mud supported		Grains-supported		Matrix-supported	> 2 mm component supported			
Less than 10% grains	Greater than 10 % grains					build a rigid framework	encrust and bind	act as baffles
Mudstone	wackestone	packstone	grainstone	floatstone	rudstone	framestone	Bindstone	bafflestone

3.4 Standard Microfacies Types (SMF) Classification

Standard microfacies types (SMF) that comprise texture, grain size, and other diagnostic constituents, for homoclinal carbonate ramp settings (Flugel, 2004; Fig. 3.1) were used. The reason to use this methodology was to do interpretations on the depositional environments present along the Tertiary limestone units on the north coast of Puerto Rico. Flugel (2004) proposed SMF Types for homoclinal ramp settings using key textures and the components in the rocks (Table 3.3).

Table 3.3: Key textures and Diagnostic constituents to identify SMF (Flugel, 2004)

Mudstone	Calcisilite	Wackestone	Floatstone	Packstone	Grainstone	Rudstone
3 Abundant planktonic microfossils	**2** Micro-bioclastic peloidal fine grained packstone/ Grainstone frabic	**1** Sponge spicules, often calcisilite matrix	**5** Densely packed whole fossils and fragments of fossils, often reef derived.	**1** Sponge spicules, often calcisilite matrix	**5** Densely packed whole fossils and fragments of fossils, often reef or platorm derived.	**4** Microbreccia, small bio- and lithoclasts.
23 Micrite or microsparite		**3** Abundant planktonic microfossils.		**4** Microbreccia, small bio- and lithoclasts.		**5** Densely packed whole fossils and fragments of fossils, often reef or platorm derived.
		8 Whole fossils, fine bioclastic micrite matrix.	**8** Whole fossils, fine bioclastic micrite matrix.	**5** Densely packed whole fossils and fragments of fossils, often reef or platorm derived.	**11** Abundant coated skeletal grains.	
		9 Abundant fragments of fossils, bioturbation.	**22** Millimeter to centimeter sized agglutinated oncoids.		**13** Millimeter to centimeter sized oncoids with tune like structutre	**6** Millimeter to centimeter sized reef derived bioclasts and fossils.
		10 Abraded and worn skeletal grains.	**24** Millimeter to centimeter sized lithoclasts.	**10** Abraded and worn skeletal grains.	**15-C** Ooids with concentric structure.	**13** Millimeter to centimeter sized oncoids with tune like structutre
		15-M Scattered micritic ooids.		**16** Non laminated very small equally sized paloids	**15-R** Ooids with radial or radial-concentric structure	**24** Millimeter to centimeter sized lithoclasts.
		22 Millimeter to centimeter sized agglutinated oncoids.			**16** Non laminated very small equally sized paloids	**26** Pisoids
				18 Abundant – rock building benthic foraminifera or calcareous algae	**17** Abundant aggregate grains	
				21 Spar filled voids within micrite or pelmicrite framework.	**18** Abundant – rock building benthic foraminifera or calcareous algae	

Carbonate Ramp

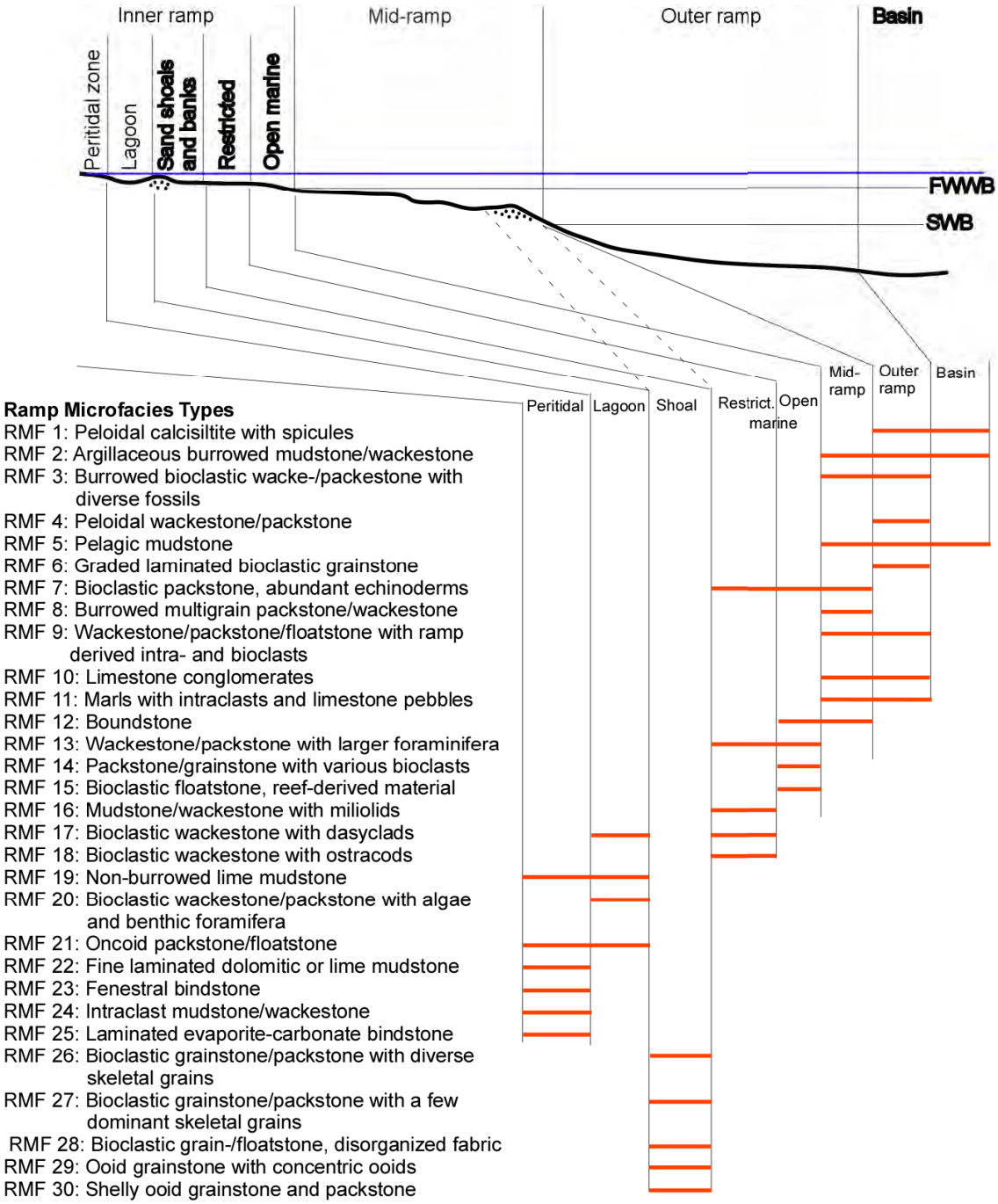

Figure 3.1: Standard microfacies types (RMF) for homoclinal carbonate ramp settings (Flugel, 2004).

3.5 Sequence Stratigraphy Modeling

A high-resolution sequence stratigraphy framework was developed using microfacies analysis, depositional environment analysis, parasequence identification, correlation of parasequences, and characterization of systems tracts.

The criteria used to define the parasequences were the texture, diagnostic constituents (skeletal and non-skeletal grains) including the presence of caliche and coal layers, standard microfacies types and tidal environments. The data is shown in stratigraphic columns in order to recognize important changes within the vertical succession.

The parasequences of PR-22 and PR-10 outcrops and the NC-6 and NC-5 test holes were then correlated, using the facies belt migration as well as the exposure surfaces identified in each one. The systems tracts (LST, TST, HST) were then correlated along the sections. The sections were placed according to location and structural dip on the north coast of Puerto Rico. The datum established to all the sections was the Montebello-Lares contact.

3.6 Sea level curve comparison

A sea level curve based on the sequence stratigraphic interpretation is included and compared with the Northwestern Puerto Rican cycles proposed by Seiglie and Moussa (1984) and the Tertiary eustatic sea-level curve (Haq et al., 1987).

3.7 Strontium Isotope Stratigraphy (SIS)

Strontium isotope stratigraphy by *Kuphus incrassatus* tubes in growth position and oysters was used to better constrain the ages of the Tertiary rocks. Stratigraphic chronology of the limestone units was poorly constrained due to problems with the

biostratigraphy based on foraminiferal assemblages (Seigle and Moussa, 1984; Ramírez, 2000). The *Kuphus incrassatus* tube and oyster samples analyzed in this study were collected on outcrops located along the PR-10 and PR-111 roads, and from the test holes NC-6, NC-5, NC-11 and NC-13.

Thin sections of the *Kuphus incrassatus* tubes were prepared and analyzed petrographycally to evaluate the extent of alteration. Altered sections of the *Kuphus incrassatus* tubes were removed. Unaltered sections were extracted and pulverized. Of these samples twenty were chosen in relevant points for oxygen and carbon isotope analysis ($\delta^{18}O$ and $\delta^{13}C$), in order to recognize if these samples have experienced diagenetic alteration that would render them unsuitable for use in strontium isotope stratigraphy.

After petrographic and isotopic analysis seventeen samples were selected for strontium isotope analysis. The samples were sent to the Tectonics and Geochronology Isotope Geochemistry Sample Preparation Facilities at the University of Kansas to acquire the $^{87}Sr/^{86}Sr$ isotopic ratios. The strontium isotopic data were compared to the database of known Sr isotopic variations in marine water (McArthur, 2001) to get an "absolute date" of the *Kuphus incrassatus* specimens. The $^{87}Sr/^{86}Sr$ age of the *Kuphus incrassatus* tubes was compared to ages of the Tertiary limestones obtained from foraminiferal assemblages in equivalent stratigraphic positions in both outcrops and test holes located on the north coast of Puerto Rico.

Stable isotope analysis description

Oxygen and carbon isotope analyses were performed in the Gas Analysis Stable Isotope Laboratory (GASI Lab) at the University of Puerto Rico-Mayaguez. Oxygen and

carbon isotope ratios were measured on a Micromass IsoPrime isotope ratio mass spectrometer operating in continuous-flow mode. For the stable isotope analyses three standard samples were used (CFN, NBS-19 and KCC). The international standard NBS-19 has a published $\delta^{13}C$ value of +1.95‰ and $\delta^{18}O$ of -2.20‰ relative to PDB. CFN and KCC are in-house standards used as monitors. The standard used to correct each analysis was NBS-19. Uncertainty of the analyses is determined by the reproducibility of NBS-19 and listed at two standard deviations (2σ). The analyses were conducted on two different dates: March 10 and March 18, 2009.

Radiogenic strontium isotope description

Strontium isotope analyses were performed in the Tectonics and Geochronology Isotope Geochemistry Sample Preparation Facilities at the University of Kansas. Strontium isotope ratios were run at a signal strength of Sr88 = 4V on a VG Sector 54 mass spectrometer operating in dynamic mode. For the strontium isotope analyses one standard sample was used (NBS-987), which has a published $^{87}Sr/^{86}Sr$ value of 0.710250. Uncertainty was assigned as the larger value between instrumental error and uncertainties associated with the Sr-seawater curve location of McArthur (2001). The Sr analyses were conducted from April 7 to April 20, 2009.

3.8 Photomosaic analysis

A Nikon D50 camera was used to take aerial photographs from a Skyhawk Cessna airplane, along the PR-111 and PR-10 highways. These photographs were used to create photo mosaics of the studied areas. This was done to identify exposure surfaces, parasequences, facies and any other important features.

CHAPTER 4

RESULTS

This chapter shows the compilation of previously published information along with the new data obtained from this study. The information in this section comes from NC-6 and NC-5 cores, and outcrops in roads PR-22 and PR-10. The results of the field and core analysis are present in Figures 4.1-4.4 and 4.10. Also included is a discussion of the different stratigraphic units found in each test well and outcrop. These results are the data base that allows the development of a sequence stratigraphic model.

The contacts between units used in this study: San Sebastian Formation, Lares Limestone, Montebello Member, Cibao Formation, Aguada (Los Puertos) Limestone, Aymamón Limestone, and Quebradillas Limestone, are included on the left side of each column. These boundaries were determined using data from Hartley (1989), Scharlach (1990), Seiglie and Moussa (1984) and Ward et al. (2002). However, new boundaries are proposed in this study, based on the sequence stratigraphy model and dates from *Kuphus incrassatus* $^{87}Sr/^{86}Sr$ isotope ratios.

The data is illustrated in stratigraphic columns in order to recognize important changes within the vertical succession. The depositional environments of the NC-6 and NC-5 test holes, and road outcrops in PR-10 and PR-22, were assigned by using the Standard Microfacies Types (RMF) proposed for the carbonate ramp environment (Flugel, 2004), and by employing the depositional lithofacies and environmental interpretations made by Ramírez (2000), Hartley (1989) and Ward et al. (2002). Rock textures and diagnostic constituents were the data base employed to define the depositional environments throughout the sections.

This chapter also includes a photomosaic analysis of the PR-111 and PR-10 outcrops, as well as the strontium isotope stratigraphy results obtained from *Kuphus incrassatus* tubes.

4.1 NC-6 AND NC-5 TEST HOLES

Hartley (1989), Ramírez (2000) and Matos (2000) described the cores NC-6 and NC-5. For this study, these cores were re-examined. The most important features relevant to this study are listed in this chapter. Stratigraphic columns with more specific details are presented in Appendix 1 and/or referenced to previous works. The inferred depositional environment and parasequence interpretations are presented in Appendix 2.

NC-6 TEST HOLE (west study area)

This core covers from the upper Lares Limestone to part of the Quebradillas Limestone. Figure 4.2 shows the units recognized in NC-6 test hole. The upper Lares Limestone is present in the first 34 meters (750-784 m) of the section. Overlaying this unit is the Cibao Formation (750-460 m), including 40 meters of the Montebello Member (680-640 m). The Aguada (Los Puertos) Limestone covers about 100 meters of the section (460-358 m). The Aymamón Limestone (358-28 m) and Quebradillas Limestone (28-0 m) are in the upper parts of the section. There are intervals within the vertical succession that are represented by empty core boxes. The cores boxes are composed of limestone fragments (625 m), breccia overlain by dark marl (408 m), dolomite and chalk (180, 190, 195 and 300 m), karst material (85, 95 m), non-data (60-73 m), and Globigerinoids chalk (28-0 m).

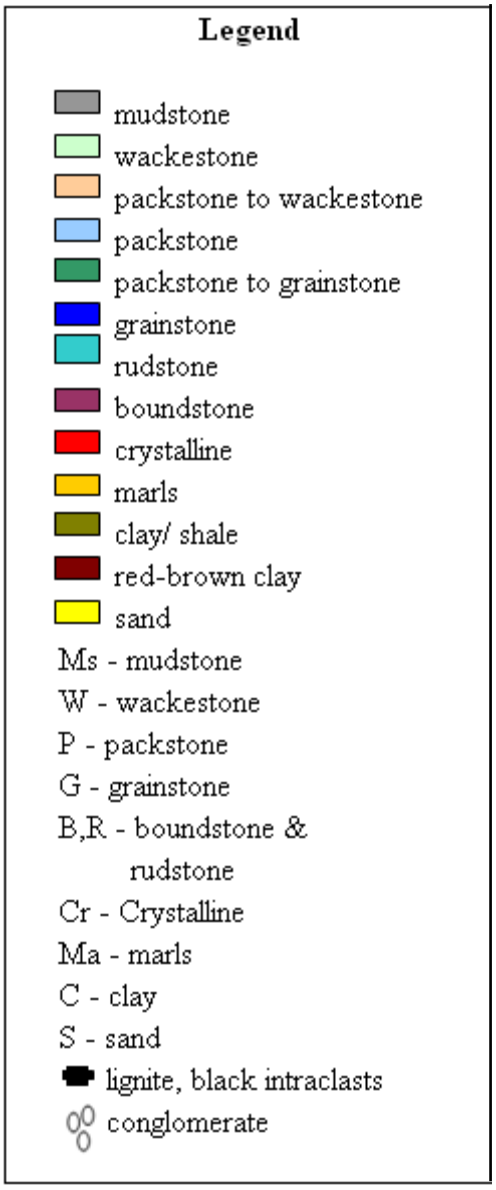

Figure 4.1: Legend for both test hole and outcrop sections along the north coast of Puerto Rico.

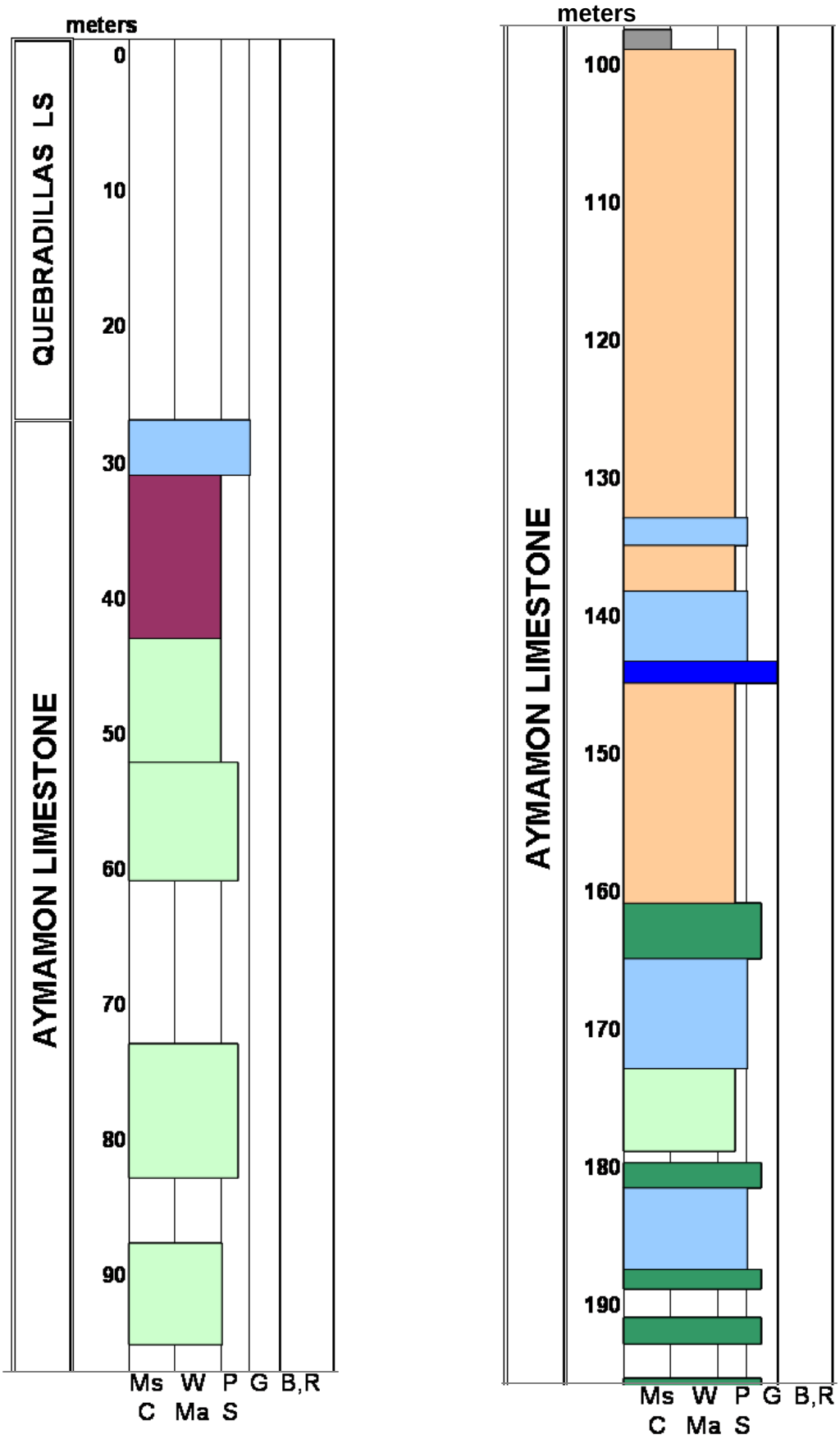

Figure 4.2: Stratigraphic column of the NC-6 test-hole.

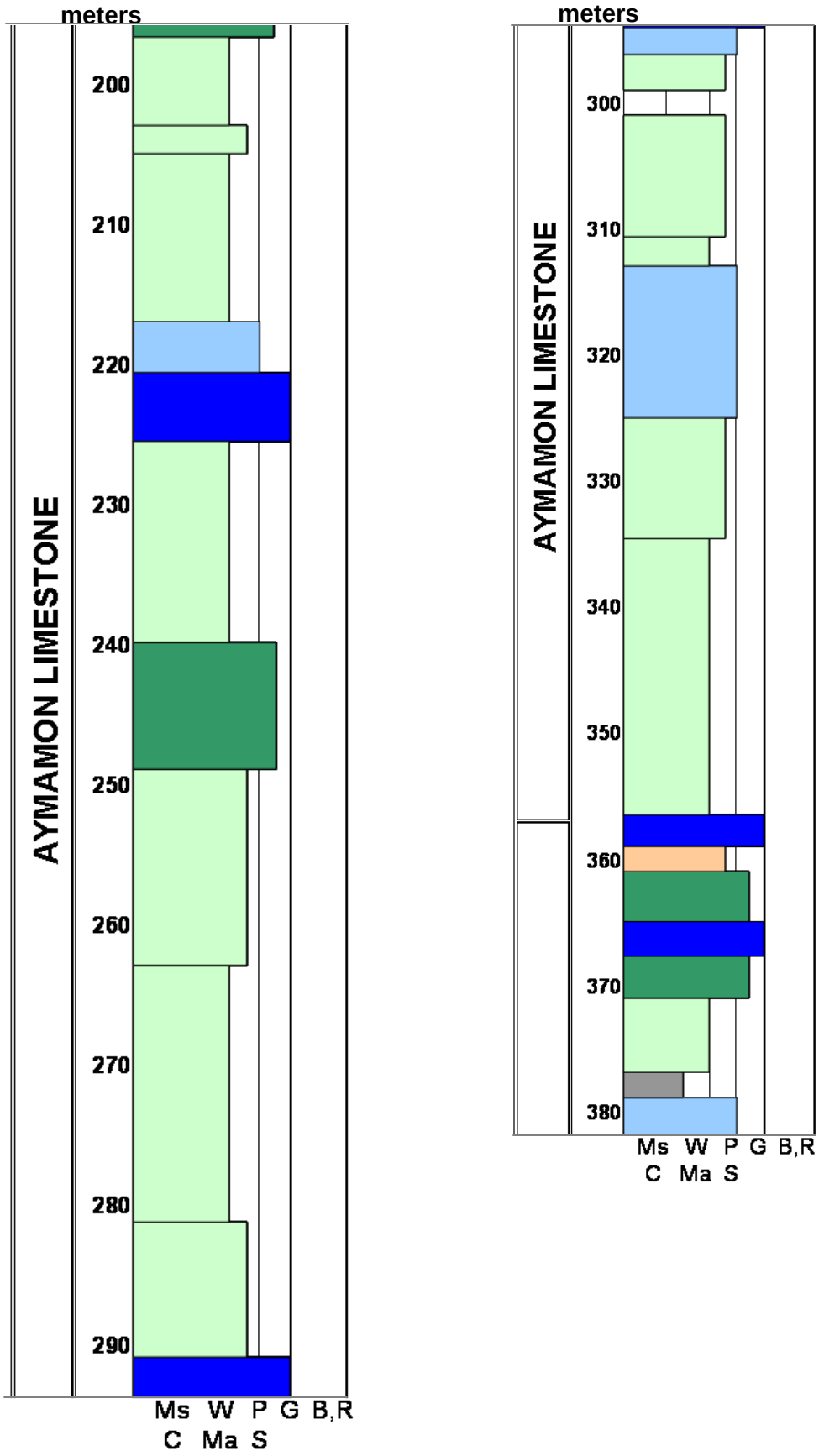

Figure 4.2: Stratigraphic column of the NC-6 test-hole (cont.).

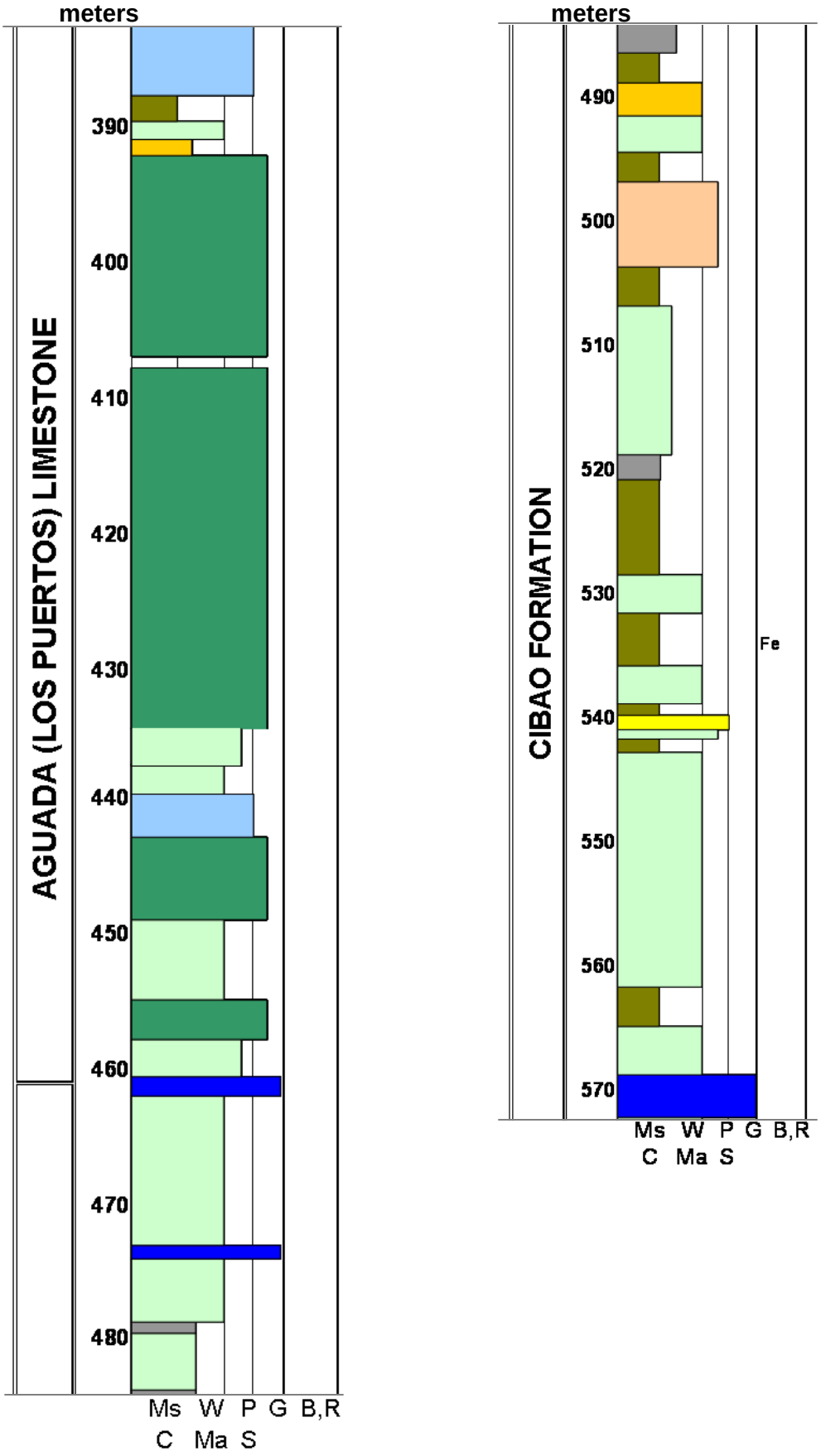

Figure 4.2: Stratigraphic column of the NC-6 test-hole (cont.).

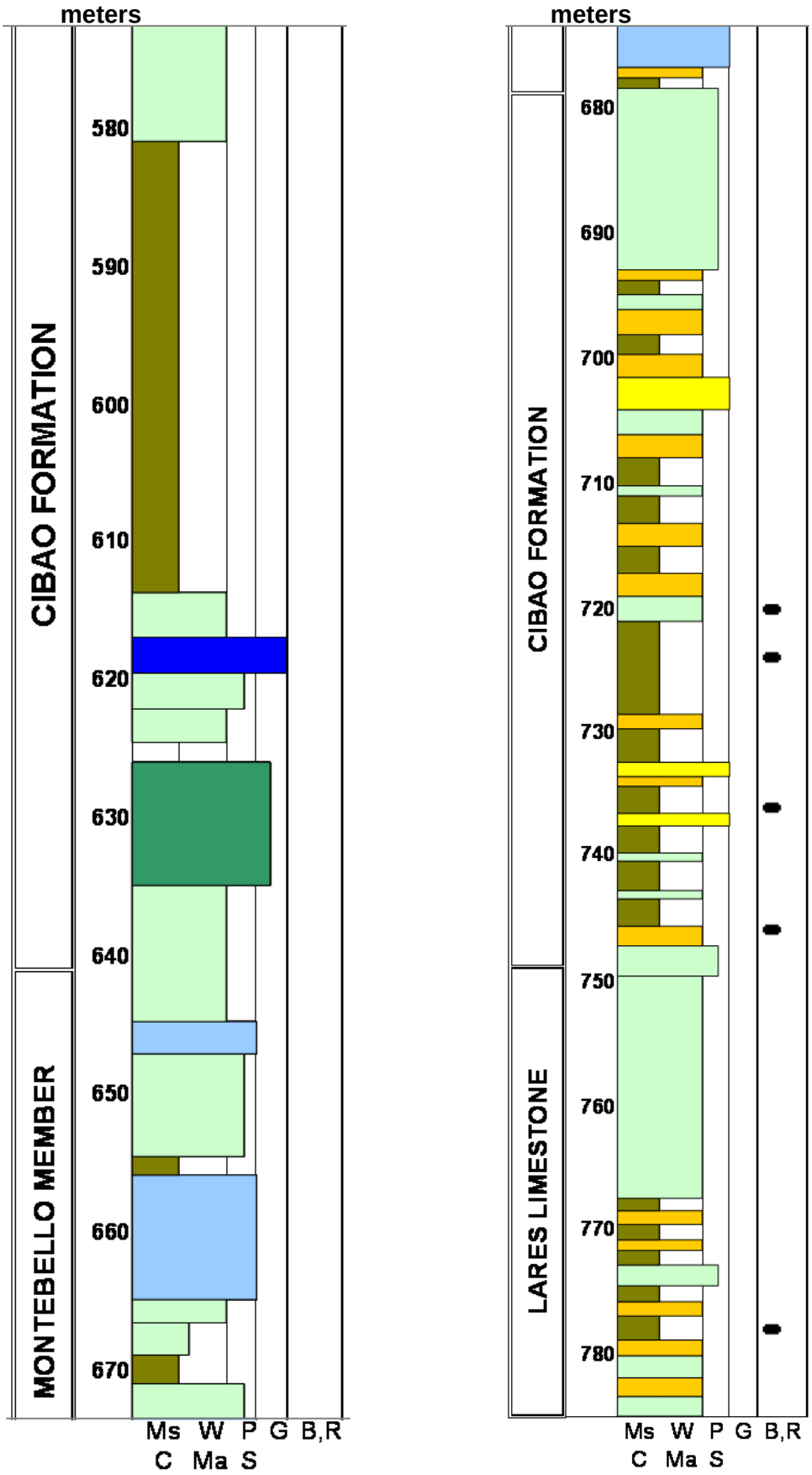

Figure 4.2: Stratigraphic column of the NC-6 test-hole (cont.).

Lithology

Wackestones and packstones are the dominant lithology throughout the section with packstone to grainstone and grainstone textures increasing upward. However, the first 300 m (480-780 m) are characterized by argillaceous composition, especially within the Cibao Formation.

We can describe this core in general terms from base to top as follows. At the base of the section (Lares Limestone and Cibao Formation) claystone layers are interbedded with marls and wackestones. Carbonaceous material occurs in the claystone and marls. The Cibao Formation which includes the Montebello Member is composed predominantly of wackestones, and wackestone to packestone textures, with some minor terrigenous sand layers, including volcanic-rock fragments, quartz and feldspar. Some of the wackestones, especially those occurring near the claystone, are slightly argillaceous and some units contain trace of organic material. The Montebello Member is composed of red-algal packstone, and packstone to grainstone. It also contains root molds in some of the packstone units toward the top.

The Aguada (Los Puertos) Limestone follows up section. It is dominantly composed by algal skeletal packstone, and packstone to grainstone. The uppermost grainstone (approximately 358 m) contains spar filled vugs. Quartz occurs in the top unit. In addition, it is important to mention that several layers of caliche breccias occur at 462, 444, 392, 388, and 362 meters of the Aguada (Los Puertos) Limestone.

Finally, a complete section of Aymamón Limestone is recognized. It is predominantly composed of limestone. In this section large intervals have been dolomitized. The dominant lithology is red-algal skeletal wackestone-packestone to

wackestone. A rhodolitic dolowackestone and, locally, boundstone containing scattered massive corals occurs between 260 and 280 m. Laminated mudstone overlain by a unit of karst material occurs between 98 and 90 m. This rock is overlain by miliolids-mollusk wackestone to packestone and grades upward to an *Amphistegina*-rich wackestone. Then red algal boundstone containing *Halimeda* and occasional massive coral and packstone forms the topmost unit of the Aymamón Limestone in this core (42-28 m). Overlying the boundstone is Globigerinid chalk of the Quebradillas Limestone which is the uppermost unit of this core.

Diagnostic Constituents

Rock texture and composition were described in order to identify the change of skeletal, non-skeletal and mineral composition from base to top throughout the section, allowing the recognition of the depositional environments and parasequence interpretation (See Appendix 1 and 2).

Skeletal

The most abundant skeletal constituents found throughout the section are benthic foraminifers, molluscs, red algae, echinoderms, and ostracodes, changing in occurrence throughout the stratigraphic column. Corals, *Halimeda*, and bryozoans, are also important, especially in the upper portion of the section. Planktonic foraminifers are only reported in the last 28 m of the section over Quebradillas Limestone.

Skeletal constituents are not abundant in the lower part of the section (Lares Limestone). Fossils include echinoderms, thin-shelled bivalves and minor amounts of *Miogypsina*, miliolid and agglutinate foraminifers, red algae and ostracodes. In the Cibao Formation the characteristic fossils include ostracodes, miliolids and soritid foraminifers,

red algae, echinoderms and diverse molluscs (mostly bivalves and gastropods with oysters and *Pecten* sp. also present). Other fossils consist of bryozoans, ostracodes, branching corals, high-spired gastropods, *Kuphus incrassatus*, encrusting foraminifers, worm tubes, and *Halimeda* (present in a few units). The Montebello Member includes *Miogypsina*, *Heterostegina*, *Amphistegina*, and *Lepidocyclina* as dominant foraminifers. Branched and massive coral are present in the packstone units as well as miliolids and soritid foraminifers and ostracodes in addition to red algae. Aguada (Los Puertos) Limestone increases in the content of red algae, *Halimeda* and bryozoans, in addition to benthic foraminifers and molluscs common along the section. The Aymamón Limestone illustrates a similar behavior of Aguada (Los Puertos) Limestone but is different in that it shows a high presence of corals fragments (especially branching type), *Amphistegina* and other large benthic foraminifers.

Non-skeletal

Non-skeletal constituents found in this core include intraclasts (NC-6: 672, 472, 380, 336, 136, and 84 m), mainly associated to packstones textures; and pelloids (NC-6: 748, 680, 646, 618, 566, 542, 480, 376, 360, 302, 226, 208, 192, 162, and 136 m), mostly related with wackestone to packstone textures.

Sedimentary Structures and Mineral Composition

Three main sedimentary structures were found along the section: bioturbation (NC-6: 748, 680, 614, 572, 544, 476, 464, 360, and 226 m), irregular lamination (NC-6: 772, 752, 614, 544, 536, and 360 m) and caliche (NC-6: 646, 624, 462, 444, 392, 388, 362, 92, and 54 m). Caliche is used to recognized possible exposure areas. In addition, a few root molds (NC-6: 560, 660, and 374 m), conchoidal fracture (600 m),

microcrystalline and fenestral voids (520, 378, 92 m), spar vugs (366 and 96 m), laminated and imbricated grainstone (462 m) were recognized and are used to find the top of the parasequences in most cases.

The mineral composition is characterized by three constituents: chalky material (term proposed in previous works), quartz contents and dolomite occurrence. In this study chalky is a term related to lithologies of finer grain size without implying any environmental interpretation. It is mainly recognized in Aguada (Los Puertos) Limestone and Aymamón Limestone. Quartz is found in minor layers within the Cibao and Aguada (Los Puertos) Limestone formations. Dolomite is limited to Aymamón Limestone, showing more abundant quantities along the section.

Depositional Environments

This core represents widespread environments that cover from the inner ramp to the outer ramp. The inner ramp environment is particularly present toward the base and middle part of the section in the Lares Limestone and the Cibao Formation. While the middle and outer ramp environments are characteristic toward the upper part in the Aguada (Los Puertos), Aymamón and Quebradillas limestones.

The Ramp Microfacies Types (RMF) found within these environments (Table 4.1) were related to Facies Zones (FZ) of a shallow inner to middle ramp settings, except for RMF 5 that represent an outer ramp environment. The RMF types present were: RMF 5, RMF 13, RMF 14, RMF 16, RMF 17, RMF 18, RMF 19, RMF 20, RMF 23, RMF 26, and RMF 27 (See Table 4.1). The environments characteristics of these RMF are: outer ramp, sand shoals and banks, open marine, restricted, lagoon, and peritidal. Two new

RMF are proposed for this test hole, RMF 32 and RMF 35. These represent marginal marine environments with terrigenous material and exposure areas.

Table 4.1: Ramp Microfacies Types (RMF) proposed to the NC-6 and NC-5 test holes based on Wilson (1975) and Flugel (2002) microfacies analysis.

RMF	Description	Environment	Key
RMF 5	Globigerinid limestone	Outer ramp	
RMF 26	Medium- and -coarse-grained bioclastic grainstone and packstone with various benthic skeletal grains.	Sand shoals and banks	
RMF 27	Bioclastic grainstone and p composed of few dominat skeletal grains (predo echino or forams)	Sand shoals and banks	
RMF 14	Packstone/grainstone with various bioclasts	Open marine	
RMF 13	Bioclastic wackestone and packestone with abundant larger foraminifera	Restricted to open marine	
RMF 16	Soritid- and -miliolid-rich wackestone	Restricted	
RMF 18	Bioclastic wackestone with ostracods	Restricted	
RMF 17	Bioclastic wackestone with dasyclad green algae	Lagoon	
RMF 20	Bioclastic wackestone and packestone with calcareous algae and benthic forams	Lagoon	
RMF 19	Non-burrowed lime mudstone	Peritidal to Lagoon	
RMF 23	Fenestral mudstone	Peritidal	
RMF 33	Argillaceous sandstone and carbonate rocks with glauconite and diverse, normal- marine fauna	Shallow open ramp	
RMF 32	Claystone olive-green, sandstone and located wackestone and marl layers, low fauna and carbonaceous material	Marginal marine/terrigenous	
RMF32B	Claystone wackestone and marl, without carbonaceous material	Marginal marine/terrigenous	
RMF 31	Claystone red-brown non-fossiliferous	Costal (Alluvial plain)	
RMF 35	Karst zones, caliche	Exposure areas	

NC-5 TEST HOLE (eastern side of study area)

This core covers from the upper San Sebastian Formation up to the Aymamón Limestone. Figure 4.3 shows the stratigraphic units recognized in NC-5 test hole. The upper San Sebastian Formation is present in the first 64 meters (780-716 m) of the section. It is overlain by the thick limestone units of the Lares Limestone (716-520 m) and the Montebello Member (520-292 m). The Cibao Formation covers approximately 90 meters of the stratigraphic section (292-205 m). The Aguada (Los Puertos) Limestone (205-118 m) and the Aymamón Limestone (118-0 m) are the stratigraphic units present in the upper parts of the section. There is an interval within the vertical section with data represented by empty core boxes.

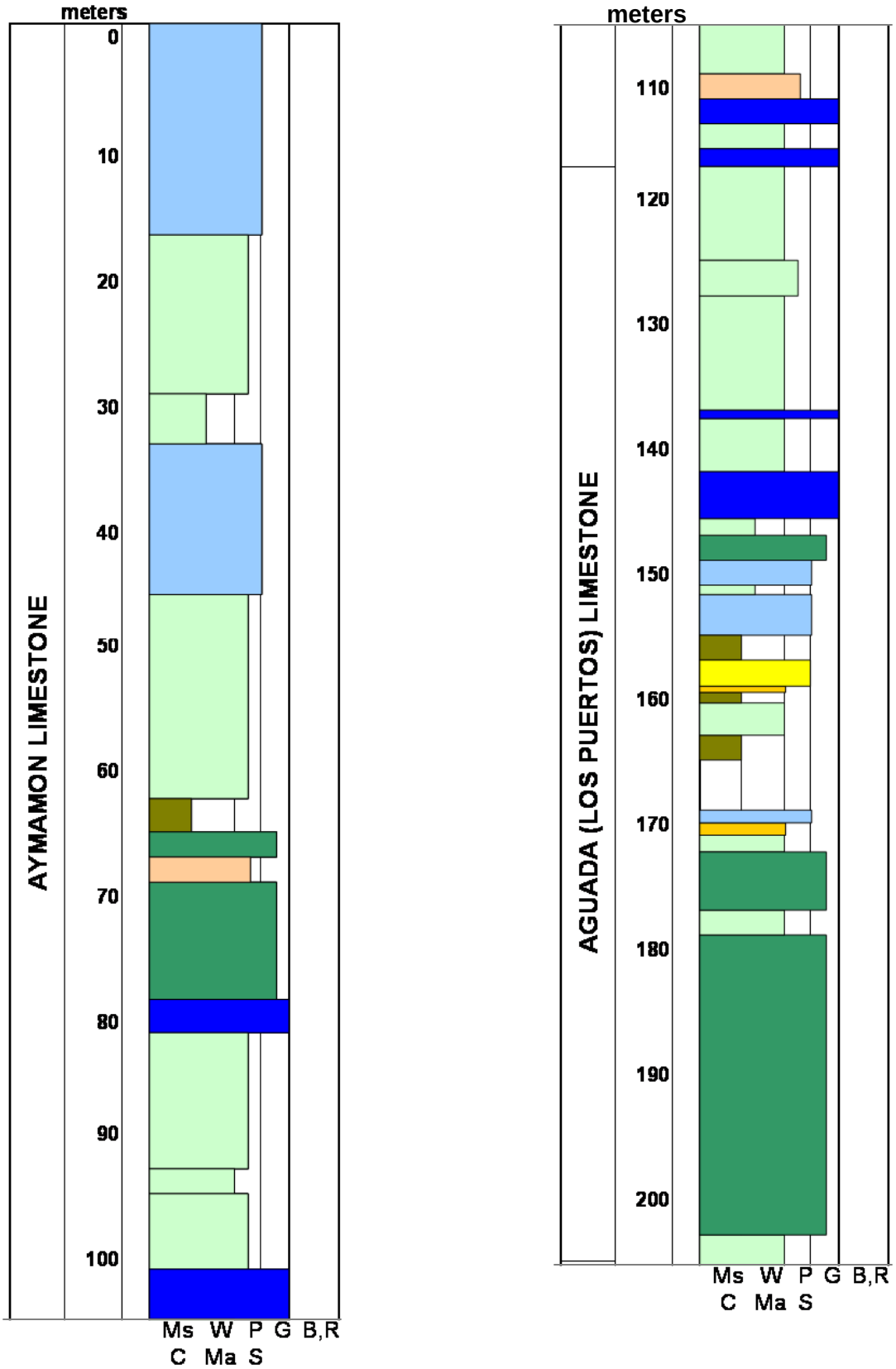

Figure 4.3: Stratigraphic column of the NC-5 test-hole.

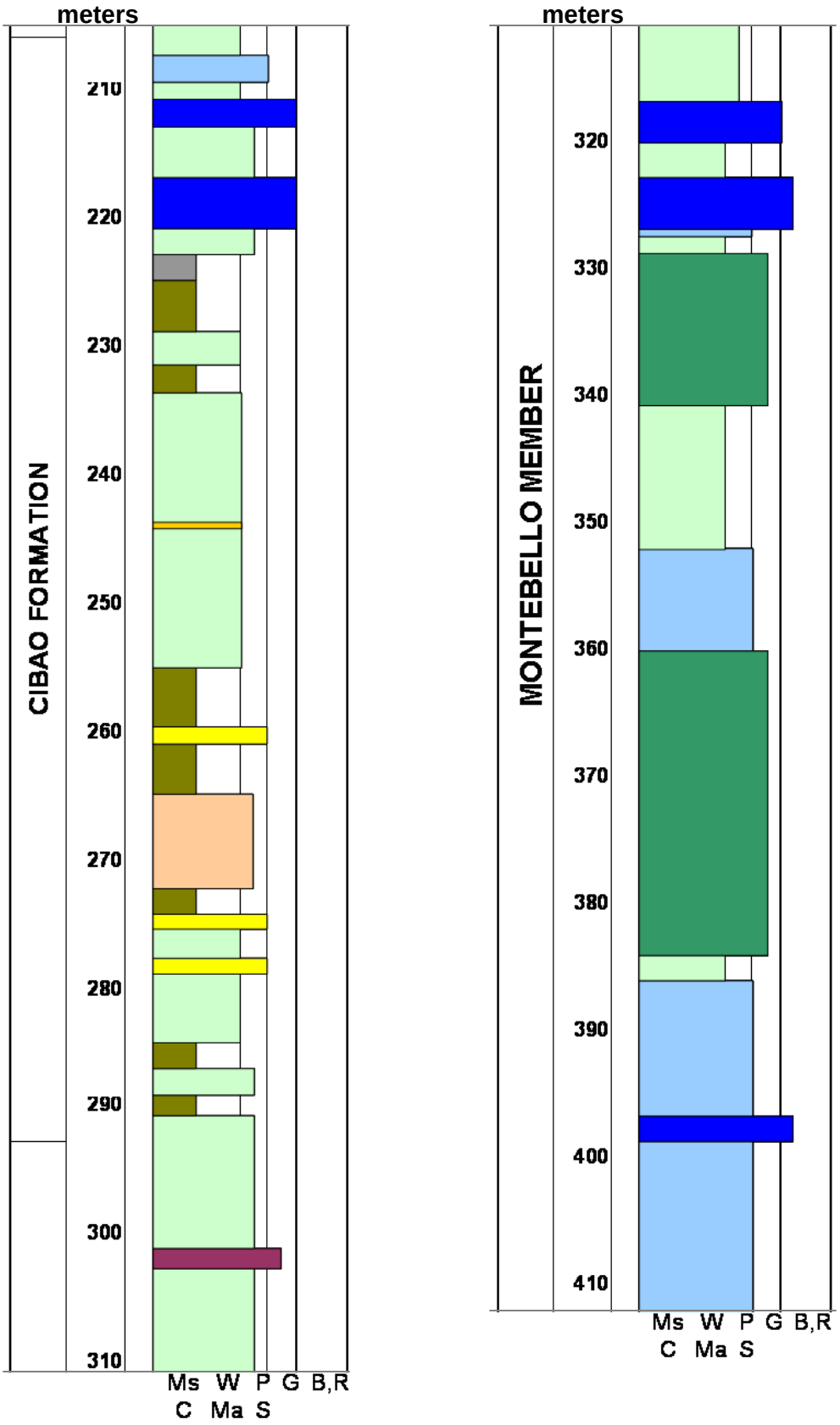

Figure 4.3: Stratigraphic column of the NC-5 test-hole (cont.).

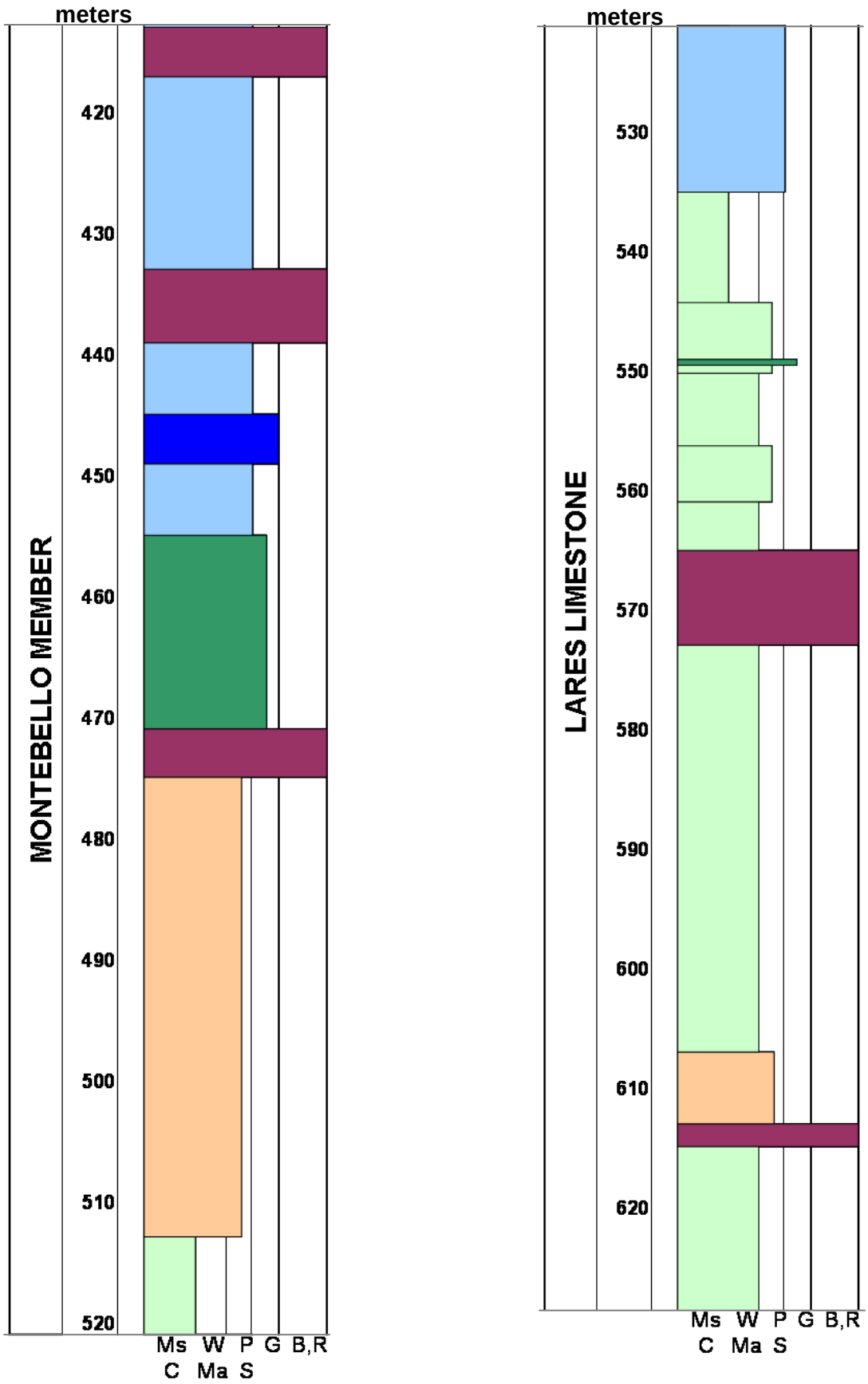

Figure 4.3: Stratigraphic column of the NC-5 test-hole (cont.).

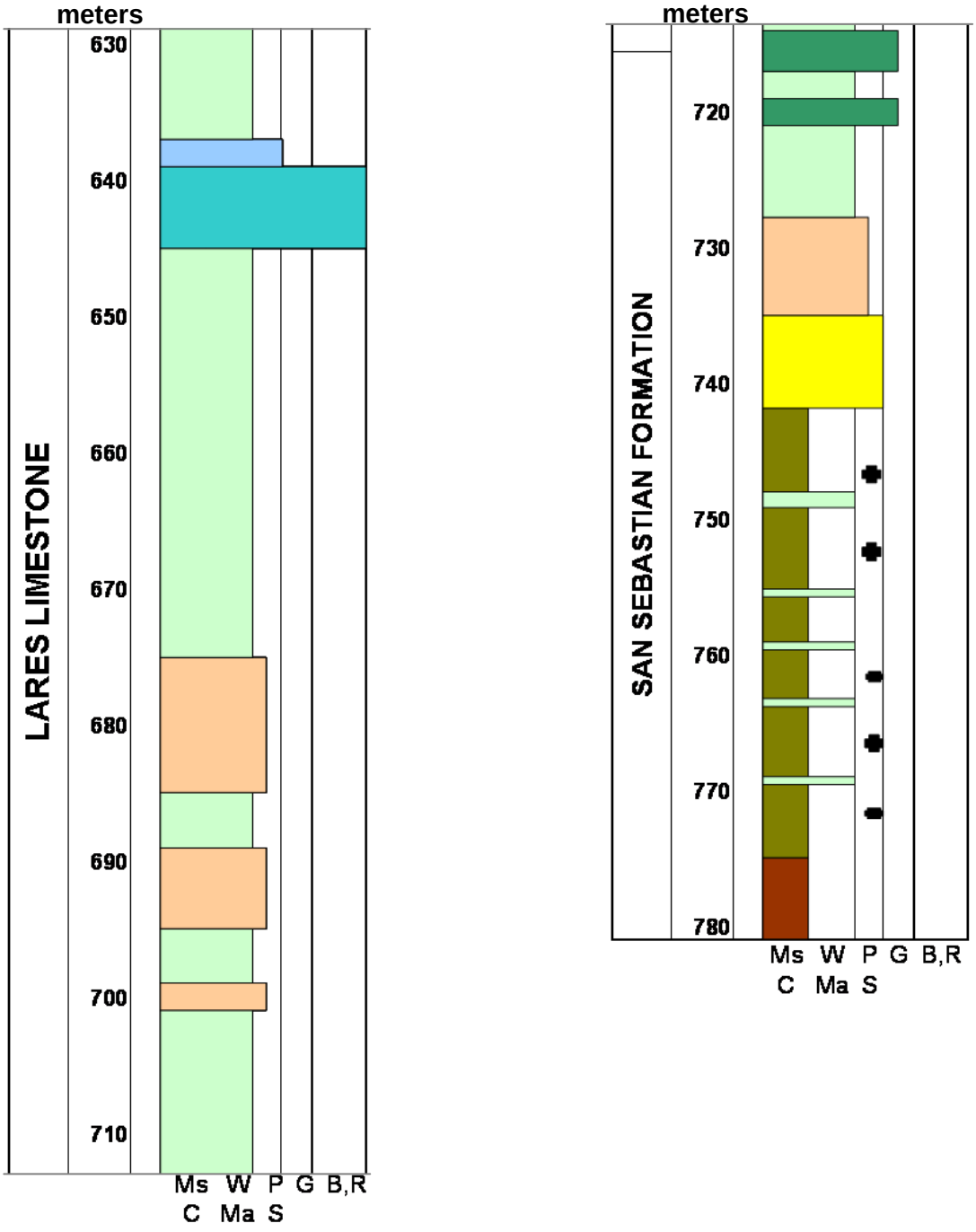

Figure 4.3: Stratigraphic column of the NC-5 test-hole (cont.).

Lithology

The NC-5 core is characterized by red-brown and olive-green claystone in the basal 742-780 m of the section, similar to NC-6 core. The claystones are interbedded with thin wackestone and carbonaceous black shale beds. The top of this sequence (San Sebastian Formation) is characterized by quartz and glauconite wackestone and grainstone. A sand layer marks the transition from dominant claystones to wackestone and packstone (Lares Limestone and Montebello Member). Branched-coral boundstone, interpreted as patch reefs are present as discreet units, from 612 to 302 m. A rudstone composed of branching coral is present at 640 m. In the Montebello Member, packstone and packstone to grainstone become the major limestone rock component. The dominant lithology of the Cibao Formation is wackestone and wackestone to packstone along with two molluscan-rich grainstone units near the top of the formation (218 and 212 m).

In the NC-5 core the limestone material increases up the section, with clay and terrigenous sand layers (including volcanic rock fragments, quartz, and feldspars) limited to the San Sebastian Formation and the Cibao Formation along with some minor beds found in the Aguada (Los Puertos) Limestone (275, 278, 260, and 158 m). The Aguada (Los Puertos) Limestone is characterized by red-algal skeletal packstones, and packstone to grainstone as well as several units of dolomite. Toward the top of the unit a karst zone and quartz grains are found. At the top of the core, the Aymamón Limestone is mainly composed of recrystallized limestone from packstone to wackestone lithologies in addition to several grainstone layers.

Diagnostic Constituents

Rock texture and composition were described in order to identify the change in skeletal vs. non-skeletal, as well as mineral composition from the base to the top the section. This allowed the recognition of the depositional environments and parasequences interpretation (See Appendix 1 and 2).

Skeletal

Benthic foraminifers and molluscs are the most common fossils found throughout the section, while ostracodes (NC-5: 728, 650, 640, 586, 566, 546, 172, 126, and 82 m), planktonic foraminifers (NC-5: 728, 650, 638, 566, 438, 96, 90, and 18 m) and bryozoans (NC-5: 742, 714, 522, and 440 m) are limited to specific intervals. Corals are present to common from the base of the core (Lares Limestone -*Porites* and massive head corals-) and also higher stratigraphically. However, they are abundant within the Montebello Member. Red algae, including rhodolites (abundant in the middle Lares Limestone) are common along the core except in the Cibao Formation and the San Sebastian Formation. Echinoderms are present to common throughout the section. *Halimeda* is found in specific intervals (NC-5: 676, 690, 640, 546, 522, 342, 330, and 264 m).

The base of the core is mostly non-fossiliferous except by thin-shelled bivalves, high-spired gastropods, miliolids and high contents of plant material (mainly inside of the San Sebastian Formation and minor quantities in the Lares Limestone). Foraminifers are the dominant fossil and include: *Heterostegina*, miliolids, and more rarely, *Lepidocyclina*. The Lares Limestone shows similar fossil assemblage with the addition of *Amphistegina*, oyster fragments, and more abundant *Lepidocyclina*. The middle part of this formation includes additional fossil diversity such as *Myogipsina*, rotalids, and

planktonic foraminifers. Ostracodes, whole thin-shelled bivalves, bryozoans, annelid tubes, rare encrusting foraminifers, *Kuphus incrassatus* and oysters also occur. Toward the Lares Limestone top is composed of thin-shelled bivalves, gastropods, branched corals, and minor amount of soritid foraminifers, among others.

The Montebello Member is characterized by branching and massive corals which form several reefal buildups. Benthic foraminifers (*Heterostegina*, *Lepidocyclina*, *Miogypsina*, and *Amphistegina* particularly along with miliolids and soritids), and molluscs (gastropods, pelecypods, and *Kuphus incrassatus*), in addition to rhodolites and ostracodes are also present.

The Cibao Formation relative abundance of each type varies, and the assemblage includes ostracodes, miliolids and soritid foraminifers, red algae and various molluscs (mostly thin-shelled bivalves and gastropods with oysters and *Pecten* sp.). The Aguada (Los Puertos) Limestone contains miliolids and soritid foraminifers as well as ostracodes along with red algae as the most common fossil. Molluscs (bivalves, gastropods and *Kuphus incrassatus*) and coral fragments are also present. The Aymamón Limestone mainly contains red algae, *Amphistegina*, miliolid and soritid foraminifers; rotalid and encrusting foraminifers, echinoderms, and molluscs are also present and change in occurrence along the section.

Non-skeletal

Non-skeletal constituents found in this core include glauconite (NC-5: 714, 700, 690, 676 and 522 m), intraclasts (NC-5: 550, 450, 250, 210 and 116 m), and pelloids (NC-5: 714, 690, 676, 576, 562, 550, 546, 522, 450, 418, 362, 342, 330, 126, 96, 90, 70 and 58 m). Glauconite is limited to the San Sebastian Formation and the Lares

Limestone, which occurs mostly in packstone to wackestone textures. Intraclasts are recognized in minor intervals within different rock textures. They are composed of mudstone and some are brecciated. Pelloids occur in packstone to grainstone textures in the San Sebastian Formation and the Montebello Member, while it occurs in wackestone to packstone textures in the Lares Limestone and middle Aymamón Limestone (714, 690, 676, 576, 562, 550, 546, 522, 450, 418, 362, 342, 330, 126, 96, 90, 70 and 58 m).

Sedimentary Structures and Mineral composition

Three main sedimentary structures were found along the section: bioturbation (722, 704, 608, 576, 558, 342, and 18 m), lamination (640, 616, 576, 558, 536, 116, and 80 m) and caliche (264, 234, 172-202, and 118 m). In the upper part of Lares Limestone scour surfaces are recognized in addition to burrow and pelletal sections. Fractures are also present below this surface (550 m) and in some intervals up the section (150, 118 and 126 m). Clay stained and filled vugs (314, 94, 90 and 82 m) also occur, particularly along the Aymamón Limestone. In addition to breccia layers (450, 248, 114 and 108 m), root molds (178, 172 and 126 m) and geopetal structures (134, 136 and 140 m) are also present.

The mineral composition is characterized by three constituents: chalky material (term proposed in previous works), quartz contents (mainly related to sand layers) and dolomite occurrence. Dolomite is found in numerous intervals along the section but it is more abundant in the Lares Limestone and the Montebello Member.

Depositional Environments

This depositional environments present in this core are alluvial plain and marginal marine to middle-outer ramp. The alluvial plain and marginal marine depositional environments are restricted to the base of the section and correspond to the San Sebastian Formation. The inner to middle ramp environments characterize most of the section.

The Ramp Microfacies Types (RMF) found within these environments (See Table 4.1) were related to Facies Zones (FZ) in a shallow inner to middle ramp settings. The RMF types were: RMF 13, RMF 16, RMF 18, RMF 19, RMF 20, RMF 26, and RMF 27. The environments characteristics of these RMF are: sand shoals and banks, restricted to open marine, restricted, lagoon, and peritidal to lagoon. Five new RMF are proposed for this test hole, RMF 31, RMF 32, RMF 32B, RMF 33, and RMF 35, which represent shallow open ramp, marginal marine with terrigenous material, alluvial plain, and exposure areas environments.

4.2 PR-10 AND PR-22 OUTCROPS

Ramírez (2000) and Matos (2000) described the outcrops located along the PR-10 and PR-22 roads, respectively. In this study, these outcrops were re-examined in order to identify parasequences in addition to those identified within the NC-6 and NC-5 test holes. The most important features relevant to this study are presented in this chapter. Additional details, including facies, depositional environments and parasequences interpretations are presented in Appendix 2.

PR-10 OUTCROPS (Arecibo and Utuado Quadrangles)

These outcrops expose the upper part of the San Sebastian Formation, the Lares Limestone, the Montebello Member and the base of the Undifferentiated Cibao

Formation. Figure 4.4 shows the units present in PR-10 outcrops. The upper San Sebastian Formation is at the base (first 2 meters of the section). It is overlain by Lares Limestone which is 18 meters thick. The Montebello Member is about 300 meters thick along the PR-10 road outcrops. There are some intervals within the entire vertical succession that are represented by empty spaces. These zones are either covered (163-170 m, 213-221 m, 235 m, 251-262, 296 m), caliche or paleosol (303-305 and 321- 325 m).

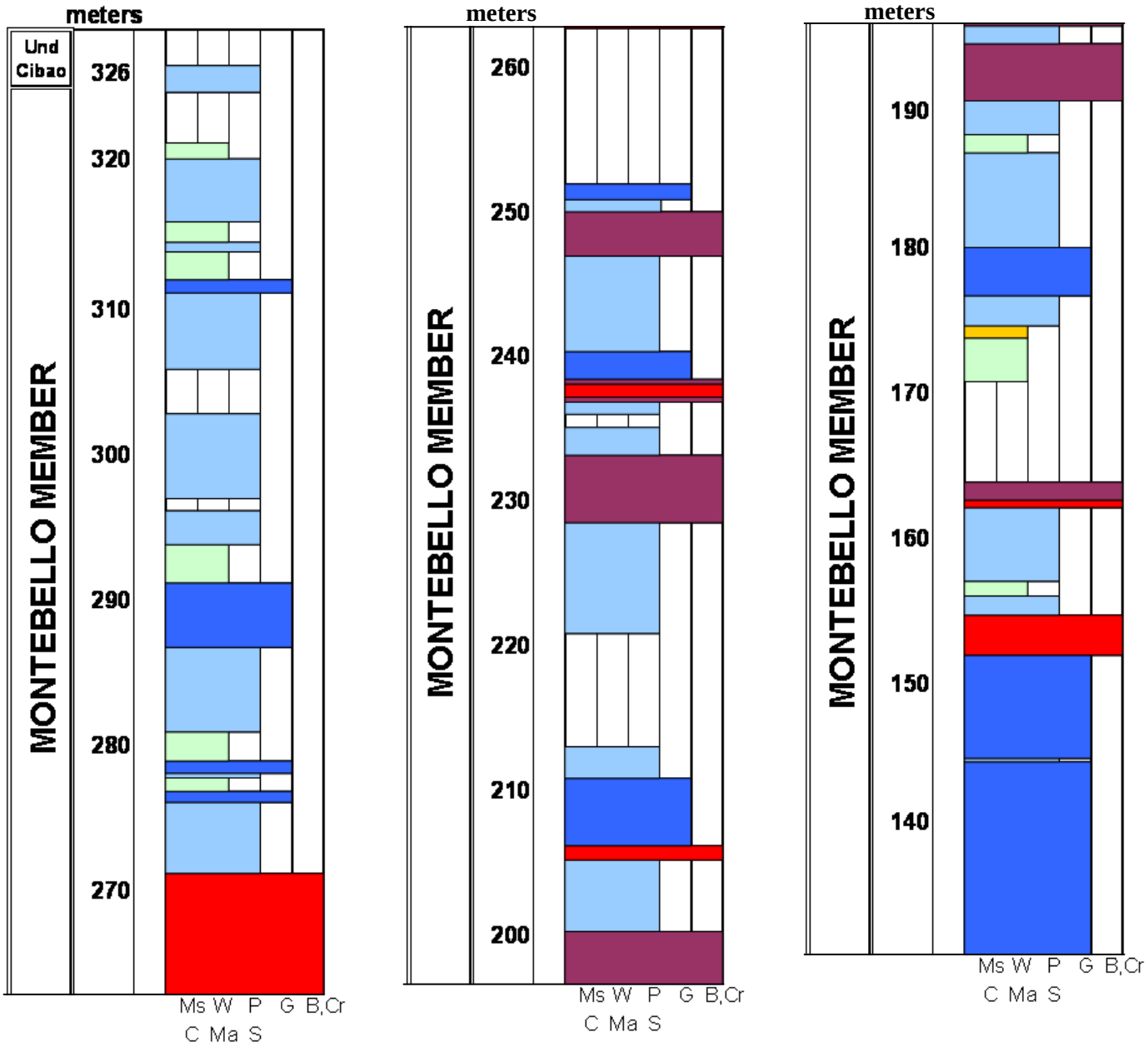

Figure 4.4: Stratigraphic column of PR-10 outcrops (Modified from Ramírez, 2000).

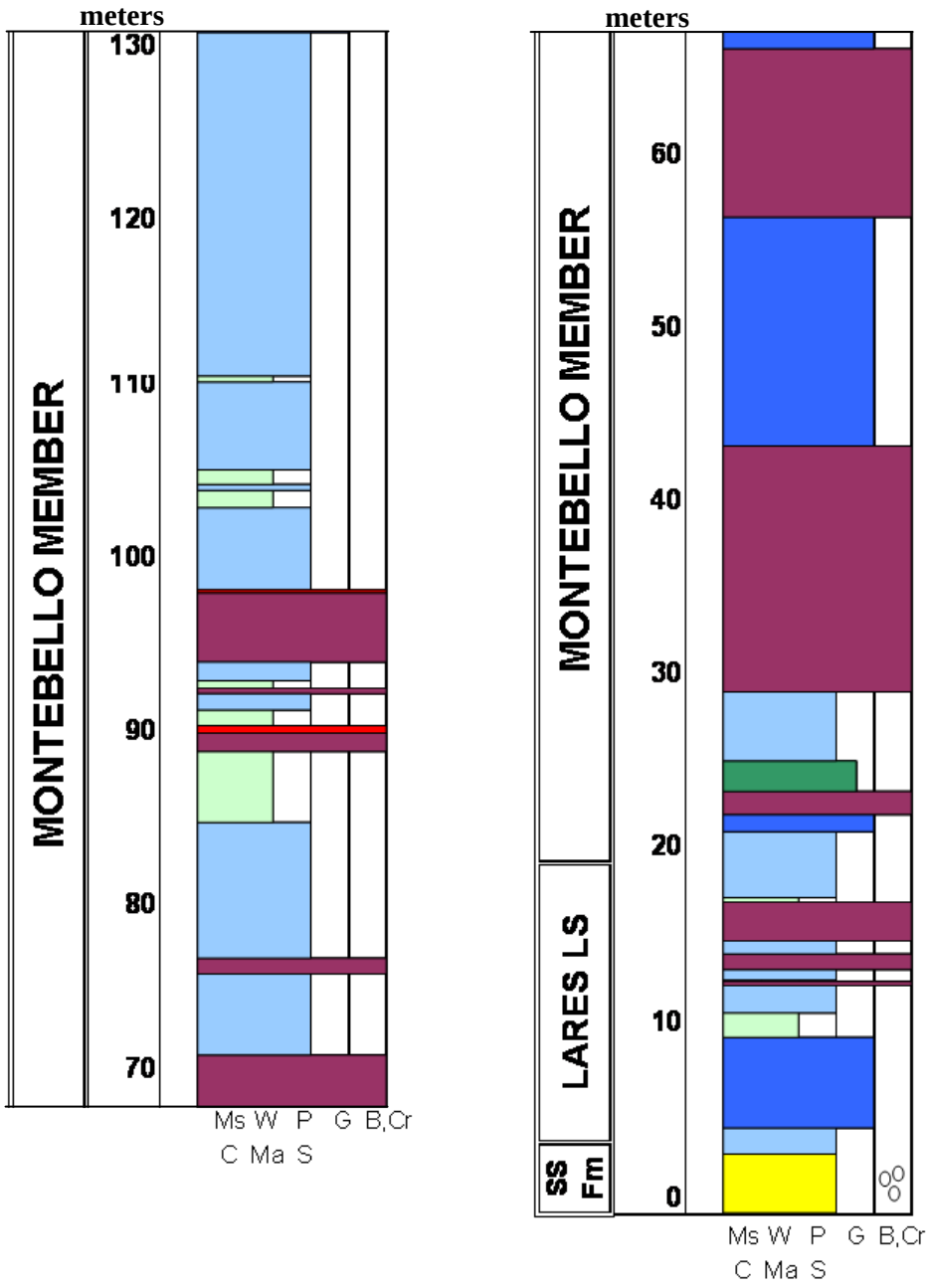

Figure 4.4: Stratigraphic column of PR-10 outcrops (Modified from Ramírez, 2000) (cont.).

Lithology and Diagnostic Constituents

The PR-10 stratigraphic section is mostly composed of pure calcium carbonate rocks (mainly packstone, grainstone and boundstone) with minor amounts of terrigenous materials (San Sebastian Formation).

The San Sebastian Formation represents the basal part of the section and is composed by sandstone, siltstone and conglomerate (from pebble to cobbles size), and some lenses of lignite. Burrows at the contact with the Lares Limestone are filled with skeletal grains from the formation above. The contact between those formations is sharp and undulatory (Fig. 4.5). The Lares Limestone consists of fossiliferous limestone, mainly grainstone with *Lepidocyclina* foraminifers (which decrease upsection), red algae, rhodolites and echinoderms (in-situ), becoming packstone and boundstone textures upsection. Cross beds and laminations are recognized within the grainstone layers.

The contact between the Lares Limestone and the overlying unit Montebello Member, is recognized by a 0.5 to 2.0 m oyster layer [proposed before by Nelson and Monroe (1966), Monroe (1980) and Ramírez (2000), and recently found at top of the PR-111 outcrop (this study)] close to the base of the Montebello Member (Fig. 4.6).

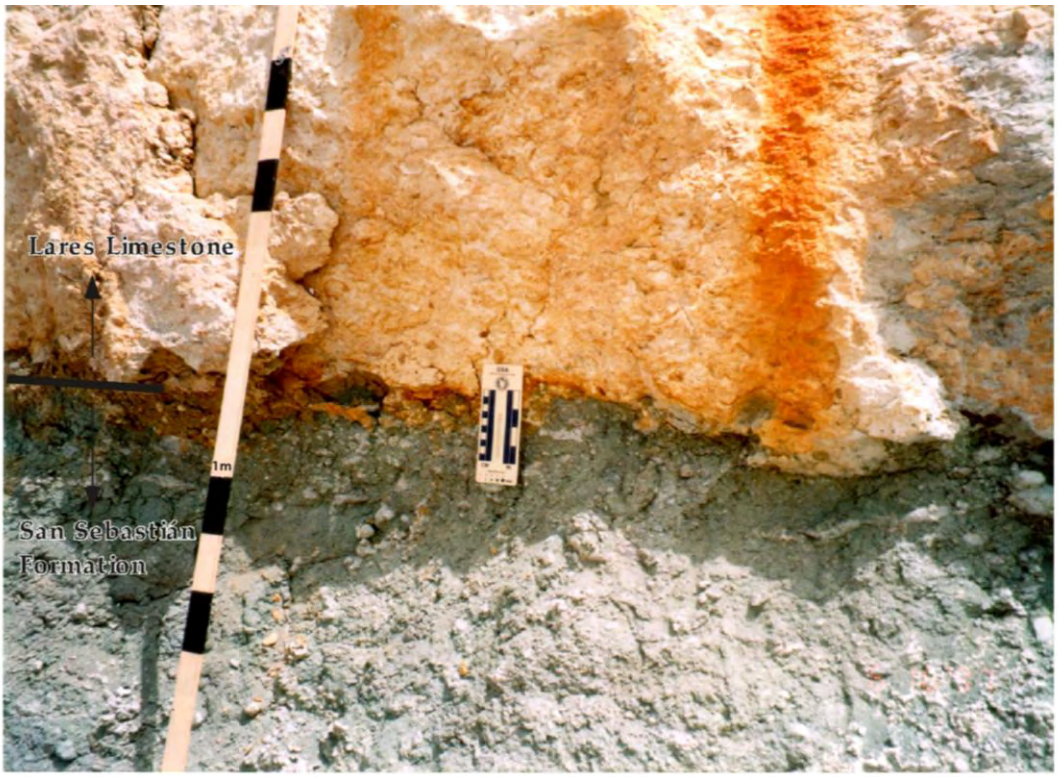

A.

B.

C.

D.

E.

Figure 4.5: A. Lares Limestone and San Sebastian Formation contact exposed at the PR-10 and PR-6621 intersection (N18°18'52'', W66 41'05'') (Photo by W.Ramírez). B. Conglomerate from the San Sebastian Formation (pebble to cobble size). C. Burrows at the contact are filled with limestone material from the Lares Limestone. D. *Lepidocyclina* foraminifers in grainstones within the Lares Limestone. E. Lignite lenses and oxidized volcanic pebbles along the contact.

A.

B.

Figure 4.6: Oyster layer at the base of the Montebello Member, which was defined as the Lares Limestone-Montebello Member contact (intersection of PR-10 and PR-6621) A. Oyster layer at the eastern side of the intersection (N18°18’58’’, W66°40’51’’). B. Oyster layer at the western side of the intersection.

The Montebello Member is mostly characterized by repetitive sequences of coral-dominated boundstone (*Porites* and head corals) and foraminifer-, red algae- and rhodolite-dominated packstones (Ramírez, 2000). Local skeletal and red algal grainstones and some wackestone layers are also present. A rudstone layer (24 m) composed of starfish fragments, corals, bivalves, rhodolites, red algae, and gastropods, among others, were also recognized (Fig. 4.7). This rudstone is the result of facies changes, laterally equivalent to packstone and grainstone composed of echinoderms, foraminifers, and red algae. *Kuphus incrassatus* layers were also identified along the Montebello Member (Fig. 4.8).

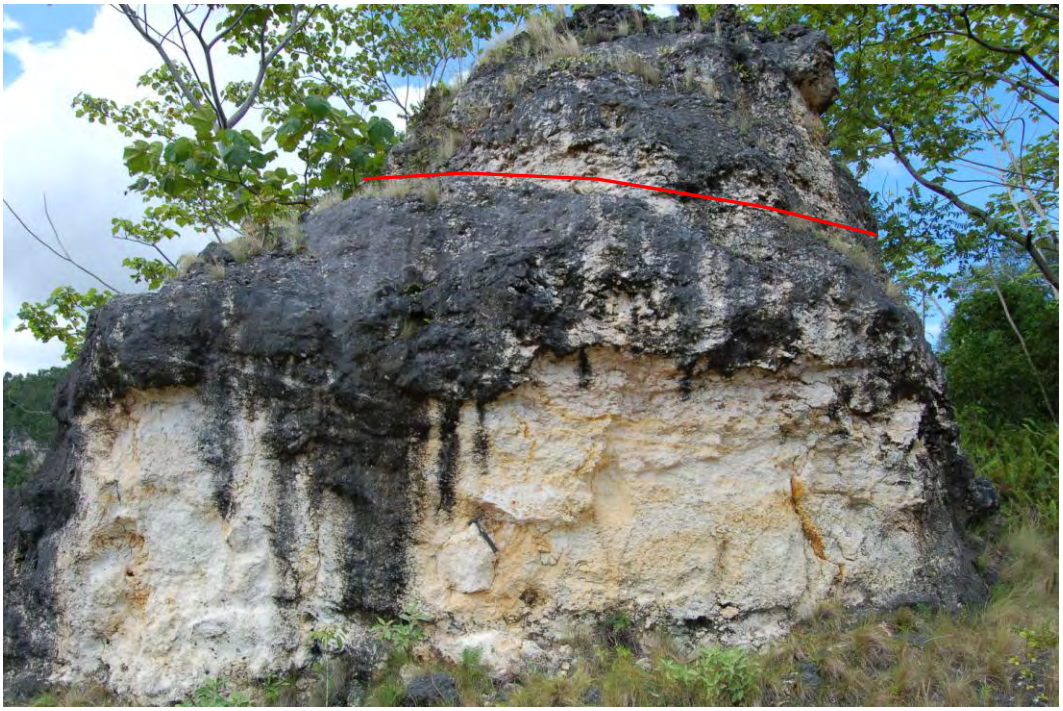

Figure 4.7: Rudstone within the Montebello Member located at the top of PR-10 outcrop (intersection of PR-10 and PR-6621), below the red line. The red line marks a *Kuphus incrassatus* layer.

Figure 4.8: *Kuphus incrassatus*-rich layer located along the PR-10 road outcrops (N18°22’35.9’’, W66°41’35.5’’).

The top of the Montebello Member is recognized by an erosional surface, represented by carbonaceous clays, conglomerates, limestone clasts, paleosol, paleosinkholes (filled with carbonaceous material and breccias), nodules, cuttons and roots casts. A thick (0.5 m) bed that contains freshwater gastropods (*Pomacea* and *Physa* genera) occurs above the contact (Fig. 4.9).

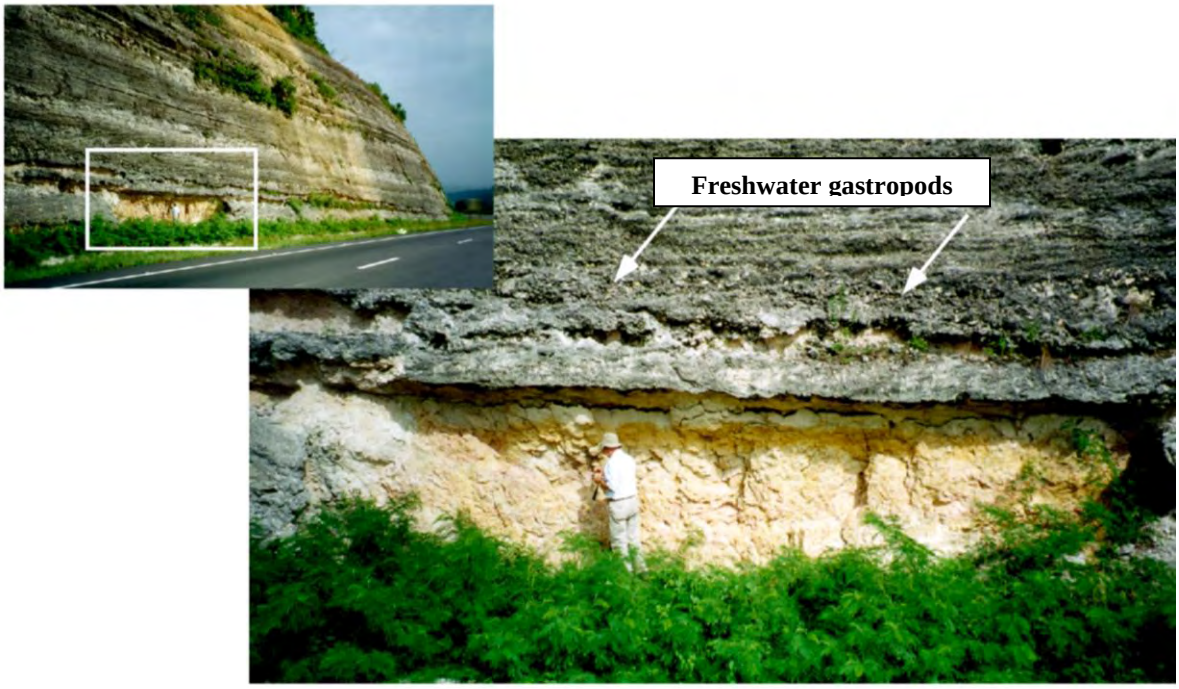

Figure 4.9: Erosional surface at the top of the Montebello Member (N18°23’33’’, W66°41’42’’, in front of the first scenic overlook from Arecibo to Utuado). The arrows are pointing the location of freshwater gastropods (photo by W.Ramírez).

A. B.

Figure 4.9 (cont.): A. Paleosinkholes filled with carbonaceous material and breccias (photo by W.Ramírez) (N18°23'33'', W66°41'42'', in front of the first scenic overlook from Arecibo to Utuado).

Depositional Environments

Four lithofacies groups were proposed based on the rock textures and the main constituents. The rock textures include wackestone, packstone, grainstone, and boundstone. The main constituents are grouped based on the abundance of foraminifers, molluscs, red algae, rhodolites, skeletal, corals, red algae-foraminifers, and skeletal-red algae (Modified from Ramírez, 2000) (See Appendix 2).

The San Sebastian Formation, at the base of the section, represents a fluvial and shallow water environment. Grainstones at the base of Lares Limestone as well as the presence of lignite beds, suggest deposition close to shore in shallow water (inner ramp). The lithofacies found in the Montebello Member suggest deposition in shallow-marine environments (middle ramp) but with higher open marine influences.

PR-22 OUTCROP

The PR-22 outcrop is located at 56.6 km of Highway 22 between Manati and Arecibo. This outcrop represents the upper part of the Aymamón Limestone and was described by Matos, 2000. Figure 4.10 shows the units recognized for PR-22 outcrop.

Lithology and Diagnostic Constituents

Matos (2000) described this outcrop as mainly composed of coral, molluscan and foraminiferal packstones and wackestones. It was divided in three sections from base to top, based on its relevant features. A *Kuphus incrassatus* layer is present at the base, followed by head corals, benthic forams and red algae toward the top form the first section. The middle part is characterized by *Amphistegina*-red algal wackestone and coral-rich packstone, in addition to molluscs, echinoderms, and ostracodes. The top of the section consists of coarse-grained packstones composed by branching and massive corals and molluscs (Matos, 2000).

Depositional Environment

The presence of corals, foraminifers and molds of molluscs suggest deposition in a middle-platform in relatively shallow water (See Appendix 2).

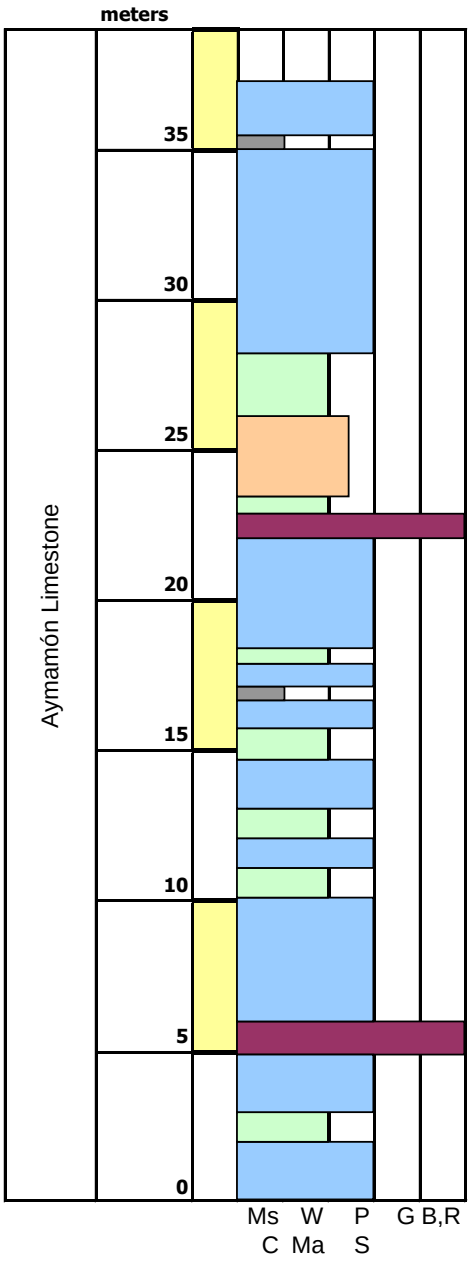

Figure 4.10: Stratigraphic column of PR-22 outcrop (Modified from Matos, 2002).

4.3 PHOTOMOSAIC RESULTS OF PR-111 (18°19’47’’N, 66°56’50’’W) AND PR-10 (N18°18’52’’, W66 41’05’’) OUTCROPS

Aerial photographs of the outcrops located on PR-111 and PR-10, together with field analysis were performed in order to get a regional view of exposure surfaces and shallowing upward sequences (cycles), in addition to the depositional environment interpretations. The cycles present in these outcrops were interpreted as parasequences.

PR-111 OUTCROP (located in the San Sebastian Quadrangle)

The PR-111 outcrop is located on road PR-111, km 27.2, between Salto Collazo and the intersection with road PR-445 (18°19’47’’N, 66°56’50’’W) (Fig. 4.11).

Figure 4.11: Location of PR-111 outcrop (18°19’47’’N, 66°56’50’’W) (Google Earth).

The units present in this outcrop are the upper part of the San Sebastian Formation, a complete section of the Lares Limestone, and the base of the Montebello Member. It is important to mention that the oyster layer, which was proposed as a regionally extensive mark at the contact between the Lares Limestone and the Montebello Member throughout the north coast of Puerto Rico (Monroe, 1980; Ramírez, 2000; among others), was also found at the top exposure at the PR-111 outcrop and can probably be correlated with the PR-10 oyster layer (Fig. 4.12).

Figure 4.12: Oyster layer at top of the PR-111 outcrop.

Lithology and Diagnostic Constituents

This outcrop, in general terms, is characterized by a sequence of carbonate rocks, including coral boundstones to mudstones, which sometimes show fissility and become shale. Grainstone and wackestone textures are also identified along the section, as well as terrigenous sediments (silt and sand).

The rock textures recognized along the section from base to top were lithic sandstones at the base (San Sebastian Formation), followed by a sequence of limestone rocks (Lares Limestone and Montebello Member), which include mudstones and wackestones with gradual development of reef environments. The contact between San Sebastian Formation and its overlaying unit, the Lares Limestone, is identified by a

grainstone mainly composed of skeletal fragments with *Kuphus incrassatus* tubes in growth position and crab crustacean fragments below the contact and *Porites* corals in a finer matrix above it (Fig. 4.13). The contact between Lares Limestone and Montebello Member, at the top of the section, is represented by a greenish paleosol, root casts, mollusk molds and dolomite (Fig. 4.14). Above this boundary, in the uppermost part of the outcrop (Montebello Member), we can observe a differentiated unit. The bedding pattern along this area show north dipped clinoforms (Fig. 4.15). The oyster layer and associated barnacle fossils were found just above the clinoforms.

The diagnostic components change their distribution both horizontally and vertically along the outcrop and include benthic foraminifers, *Kuphus incrassatus* tubes, corals (*Porites* and head corals), bivalves, gastropods, crabs, fish scales, red algae, rhodolites, bryozoans, vertebrate bones, and fossil teeth, among others, in addition to coal and Fe-oxide layers.

Figure 4.13: San Sebastian-Lares Limestone contact exposed at the base of the PR-111 outcrop (18°19’47’’N, 66°56’50’’W).

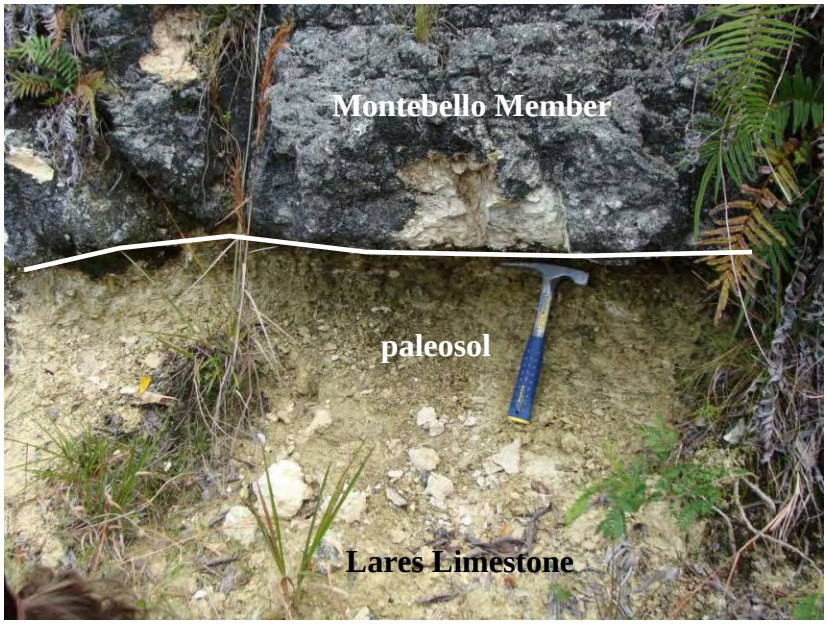

A.

B.

Figure 4.14: A. Lares Limestone-Montebello Member contact exposed at the top of the PR-111 outcrop. B. Oxidized root cast present within the paleosol.

Figure 4.15: Clinoforms dipping in a north direction at the top of the PR-111 outcrop.

PR-10 OUTCROP (Utuado and Arecibo Quadrangles)

The PR-10 outcrop studied by the photomosaic analysis is located between the intersection of the highways PR-10 and PR-6621 (N18°18’52’’, W66° 41’05’’) (Fig. 4.16).

Figure 4.16: Outcrop location on PR-10 road (N18°18’52’’, W66° 41’05’’).

The units present in this outcrop are the upper most section of the San Sebastian Formation, the Lares Limestone, and the Montebello Member.

Lithology and Diagnostic Constituents

The lithology and diagnostic constituents found in this outcrop are described in more detail in the section corresponding to PR-10 outcrops. Above the contact of the San Sebastian Formation and the Lares Limestone, which demark the change of terrigenous material (conglomerates) to carbonate rocks (*Lepidocyclina* grainstones), small units characterized by mudstones and wackestones are exposed. These units at the base of the Lares Limestone are mainly composed of corals and red algae changing upward into

grainstones units. *Porites* increase upward becoming coral boundstone to the point where 0.5-2.0 m oyster layer occurs (marker between the Lares Limestone and the Montebello Member previously mentioned). From this point to up-section repetitive sequences of massive and finger coral boundstones are present at the base of thick units, capped at the top by grainstones and packstones. At the top of the section these units are capped also by *Kuphus incrassatus* tubes.

4.4 STRONTIUM ISOTOPE STRATIGRAPHY (SIS) USING *Kuphus incrassatus* TUBES

Approximately 100 samples of *Kuphus incrassatus* tubes were collected in the north coast of Puerto Rico from both cores and outcrops. Of these, twenty were chosen for carbon and oxygen stable isotopic analysis ($\delta^{18}O$ and $\delta^{13}C$), in order to recognize if these samples have experienced diagenetic alteration (Table 4.2). However, the potential alteration in the *Kuphus incrassatus* tubes is low since they are composed of Low-Magnesium Calcite, which represent a stable mineralogy. Four of the samples are analyzed from oysters collected at the base of the Montebello Member.

The samples were selected based on their stratigraphic location within the Tertiary basin, close to the formational contacts and close to the depositional boundaries between sequences in terms of sequence stratigraphy. The first method to identify zones of diagenetic alteration was performed by doing a petrographic analysis of the tube (Fig. 4.17). In most cases examination of the *Kuphus incrassatus* tubes in thin sections showed that their inner linings were less altered than the outer linings which commonly were recrystallizated.

Table 4.2: Stable isotope data from *Kuphus incrassatus* tube and oyster samples of the Tertiary limestones along the north coast of P.R.

Sample ID	Lithologic unit	*Kuphus* / Oyster	$\delta^{13}C$ Corr. Run 1	$\delta^{13}C$ Corr. Run 2	$\delta^{13}C$ Avg Run 1-2	$\delta^{18}O$ Corr. Run 1	$\delta^{18}O$ Corr. Run 2	$\delta^{18}O$ Avg Run 1-2
NC-13-526	Aymamón Ls	K	2.39	2.40	**2.40**	-0.66	-0.15	**-0.41**
NC-11-1145-1	Aguada (Los Puertos) Ls	K	1.17	1.21	**1.19**	-0.68	-0.52	**-0.60**
NC-11-1145-2	Aguada (Los Puertos) Ls	K	2.39	2.40	**2.40**	-1.29	-1.04	**-1.17**
NC-11-1149-46	Aguada (Los Puertos) Ls	K	1.08	1.05	**1.07**	0.02	-0.06	**-0.02**
NC-11-1165-4	Aguada (Los Puertos) Ls	K	1.42	1.43	**1.43**	-0.79	-0.67	**-0.73**
NC-6 LP 1380-77-1	Aguada (Los Puertos) Ls	K	0.30	0.34	**0.32**	-2.34	-2.49	**-2.42**
NC-11-1181-2	Cibao Formation	K	2.06	2.22	**2.14**	-0.80	-0.25	**-0.53**
C1-CIBAO	Cibao Formation	K	-7.84	-7.88	**-7.86**	-4.19	-4.14	**-4.17**
C2-CIBAO	Cibao Formation	K	-7.04	-7.22	**-7.13**	-4.22	-4.38	**-4.30**
PR-10 GAS3	Montebello Mbr	K	-7.10	-7.14	**-7.12**	-4.46	-4.34	**-4.40**
PR-10 2 K1-4	Montebello Mbr	K	-4.06	-3.95	**-4.01**	-1.62	-1.33	**-1.48**
PR-10 3 M2	Montebello Mbr	K	-3.57	-3.47	**-3.52**	-1.73	-1.64	**-1.69**
PR-10 Km 67.6-2	Lares Ls-Montebello Mbr	O	-0.17	-0.53	**-0.35**	-1.02	-1.65	**-1.34**
PR-10 Km 67.6-3	Lares Ls-Montebello Mbr	O	-1.40	-1.43	**-1.42**	-1.69	-1.66	**-1.68**
PR-111 OL-2	Lares Ls	O	0.75	0.76	**0.76**	-1.97	-1.84	**-1.91**
PR-111 OL-3	Lares Ls	O	-0.96	-1.03	**-1.00**	-1.64	-1.67	**-1.66**
PR-111 GPS	Lares Ls	K	1.57	1.83	**1.70**	-1.76	-1.43	**-1.60**
PR-111 T1	Lares Ls	K	1.92	1.97	**1.95**	-0.88	-0.53	**-0.71**
PR-111 M2	Lares Ls	K	-1.14	-1.08	**-1.11**	-2.29	-2.01	**-2.15**
PR-111 M8	Lares Ls	K	-0.92	-1.19	**-1.06**	-1.85	-2.25	**-2.05**

Measured isotope ratios and standard results are listed in Appendix 3A and 3B.
All samples corrected to published value of NBS-19.
All δ values are in ‰ on the PDB scale.
Ls = Limestone; Mbr = Member; Corr. = Corrected; Avg = Average

Figure 4.17: *Kuphus incrasssatus* hand samples and thin sections.

Stable isotopic analysis produced $\delta^{18}O$ values ranging from –2.97 to –1.56 ‰ (PDB) for the *Kuphus incrassatus* tube and oysters samples in the Lares Limestone at the PR-111 outcrop. The $\delta^{13}C$ values ranged from -1.25 to 1.81 ‰ (PDB). The *Kuphus incrassatus* tubes and oysters from the Lares Limestone and the Montebello Member at the PR-10 outcrops have $\delta^{18}O$ and $\delta^{13}C$ values that range from -2.37 to –1.70 ‰ (PDB), and from –1.51 to –0.28 ‰ (PDB), respectively (see Table 4.2).

In contrast, the NC-6 core *Kuphus incrassatus* tube sample in the Aguada (Los Puertos) Limestone shows $\delta^{18}O$ values of -3.02 ‰ (PDB) and $\delta^{13}C$ values of 0.19 ‰ (PDB). The NC-11 test hole *Kuphus incrassatus* samples from the Cibao Formation and Aguada (Los Puertos) Limestone show $\delta^{18}O$ and $\delta^{13}C$ ranging from -1.97 to -0.66 ‰ (PDB), and from 2.28 to 0.97 ‰ (PDB), respectively. In the NC-13 well *Kuphus incrassatus* tubes from the Aymamón Limestone showed $\delta^{18}O$ values of -1.34 ‰ (PDB) and $\delta^{13}C$ values of 2.28 ‰ (PDB) (see Table 4.2).

The carbon and oxygen isotopic *Kuphus incrassatus* and oyster data results are plotted and compared to modern isotopic signatures of molluscs by Tucker & Wright (1990). Fifteen of the twenty samples fell within the field of shallow water molluscs and

foraminifera, indicating minimum alteration if any (Fig. 4.18). Petrographic and isotopic analyses suggested that these fifteen samples have not been significantly altered. In addition to samples number 10 and 11, which fell close to the field that indicates minimum recrystallization and have similar oxygen isotopic signature of those fifteen samples. The seventeen samples were analyzed for the strontium isotope stratigraphy (SIS) (Table 4.3).

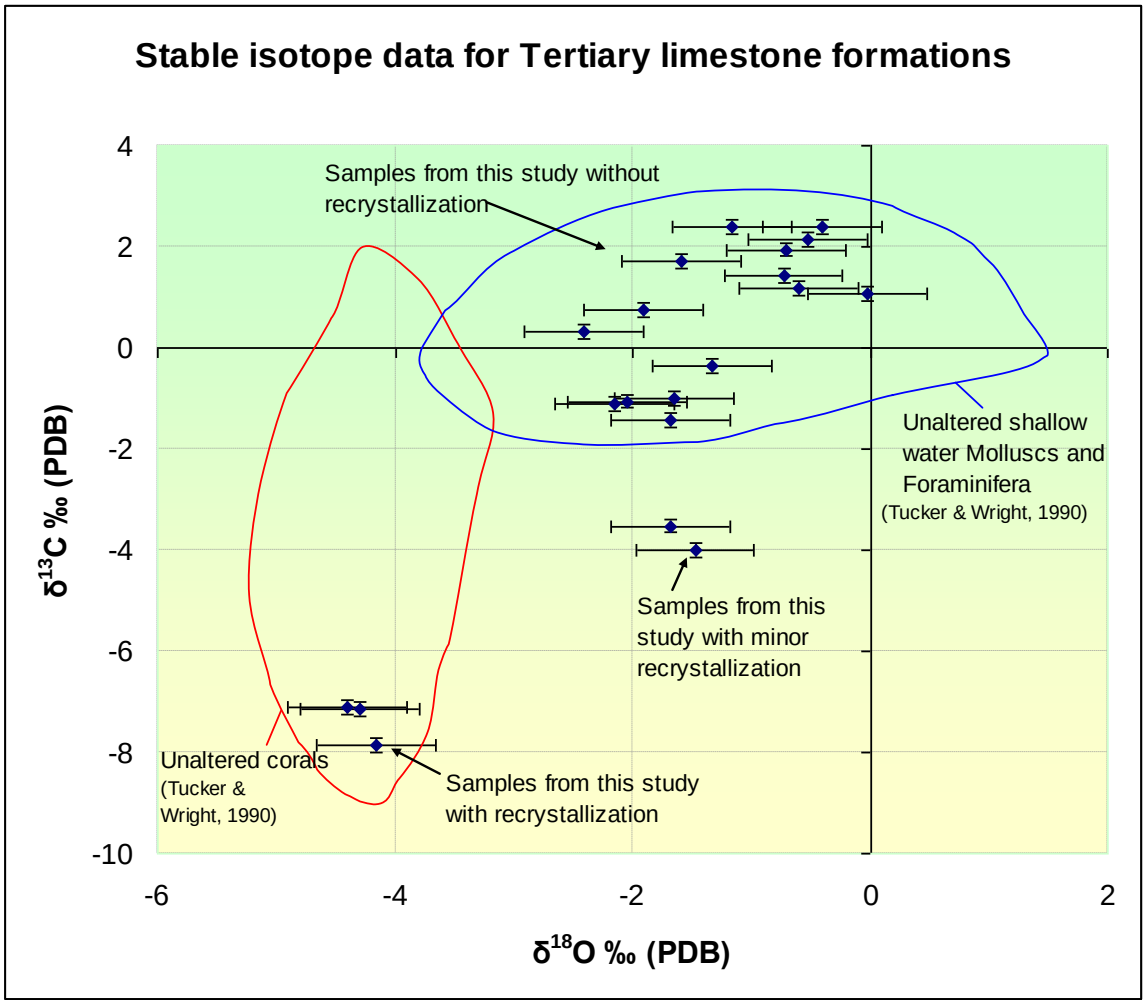

Figure 4.18: Stable isotope results from the north coast *Kuphus incrassatus* tubes and oysters. The blue field shows the values expected in skeletons of unaltered shallow water molluscs and foraminifera. Samples within the red field are recrystallized (Tucker and Wright, 1990). Samples within the red field were not analyzed for Sr isotopes.

Table 4.3: Age determinations from strontium isotope data of the Tertiary limestones along the north coast of Puerto Rico.

Sample ID	Lithologic unit	$^{87}Sr/^{86}Sr$	Absolute Age (Ma)	Instr. error (Ma)	Curve error (Ma)	Best age* (Ma)
NC 13-526	Aymamón Ls	0.708858	10.91	0.34	0.26	**10.91+/-0.34**
NC-11 1145-2	Aguada (LP) Ls	0.708854	11.06	0.37	0.26	**11.06+/-0.37**
NC 11-1145-1	Aguada (LP) Ls	0.708851	11.18	0.46	0.29	**11.18+/-0.46**
NC 11-1149-46	Aguada (LP) Ls	0.708845	11.45	0.54	0.45	**11.45+/-0.54**
NC 11-1165-4	Aguada (LP) Ls	0.708843	11.59	0.51	0.41	**11.59+/-0.51**
NC-6 LP 1380-77 -1	Aguada (LP) Ls	0.708795	14.60	0.89	0.37	**14.60+/-0.89**
NC-11 1181-2	Cibao Formation	0.708835	12.07	0.53	0.37	**12.07+/-0.53**
PR-10 10 3M2	Montebello Mbr	0.708198	24.07	0.12	0.16	**24.07+/-0.16**
PR-10 2K1-4	Montebello Mbr	0.708128	25.76	0.18	0.28	**25.76+/-0.28**
PR-10KM67.6 #3	Lares Ls-Montebello Mbr	0.708109	26.43	0.25	0.34	**26.43+/-0.34**
PR-10KM67.6 #2	Lares Ls-Montebello Mbr	0.708085	27.24	0.24	0.29	**27.24+/-0.29**
PR111OL-3	Lares Ls	0.708146	25.23	0.19	0.26	**25.23+/-0.26**
PR 111-OL-2	Lares Ls	0.708171	24.60	0.13	0.21	**24.60+/-0.21**
PR111-GPS	Lares Ls	0.708167	24.69	0.14	0.22	**24.69+/-0.22**
PR-111 T1	Lares Ls	0.708162	24.81	0.15	0.22	**24.81+/-0.22**
PR-111 M2	Lares Ls	0.708130	25.70	0.18	0.27	**25.70+/-0.27**
PR-111 M8	Lares Ls	0.708121	25.97	0.24	0.32	**25.97+/-0.32**

Measured isotope ratio results are listed in Appendix 4.

All samples corrected to published value of NBS-987 ($^{87}Sr/^{86}Sr$ = 0.710250).

Ls = Limestone; Mbr = Member; LP = Los Puertos; Ma = Millions years;

Instr. = Instrumental; Curve error based on McArthur (2001)

* Uncertainty assigned as the larger error between instrumental and curve location.

The strontium isotope analysis results indicate that the *Kuphus incrassatus* tubes analyzed from the PR-111 outcrop collected at the base of the Lares Limestone (Ramírez et al., 2006), show $^{87}Sr/^{86}Sr$ isotopic values that range from 0.7080 to 0.7081. These values suggest ages of *Kuphus incrassatus* tube formation of 26 to 27 million years (27.17 +/- 0.73 Ma, 27.10 +/- 0.74 Ma) (see Table 4.3 and Fig. 4.19). The Lares Limestone unit was previously assigned a Late Oligocene (30 to 23.7 Ma) age based on foraminiferal assemblages (Seiglie and Moussa, 1984). The *Kuphus incrassatus* tube age provides a better constraint age for the base of this formation that is also consistent with the ages of previous work.

The *Kuphus incrassatus* tubes from the middle part of PR-111 outcrop (Lares Limestone) resulted in $^{87}Sr/^{86}Sr$ isotopic values that range from 0.708130 to 0.708121. These values suggest ages of *Kuphus incrassatus* tube formation of 25.70 +/- 0.27 Ma to 25.97 +/- 0.32 Ma. The *Kuphus incrassatus* tubes from the top of PR-111 outcrop (Lares Limestone) resulted in $^{87}Sr/^{86}Sr$ isotopic values that range from 0.708167 to 0.708162. These values suggest ages of *Kuphus incrassatus* tube formation of 24.69 +/- 0.22 Ma to 24.81 +/- 0.22 Ma. The oysters at top of PR-111 outcrop (Lares Limestone) resulted in $^{87}Sr/^{86}Sr$ isotopic values that range from 0.708146 to 0.708171. These values suggest ages of *Kuphus incrassatus* tube formation of 25.23 +/- 0.26 Ma to 24.60 +/- 0.21 Ma (see Table 4.3 and Fig. 4.19).

The *Kuphus incrassatus* tubes from the Lares Limestone-Montebello contact (Km 67.6) in PR-10 outcrop resulted in $^{87}Sr/^{86}Sr$ isotopic values that range from 0.708109 to 0.708085. These values suggest ages of *Kuphus incrassatus* tube formation of 26.43 +/- 0.34 Ma to 27.24 +/- 0.29 Ma (see Table 4.3 and Fig. 4.20).

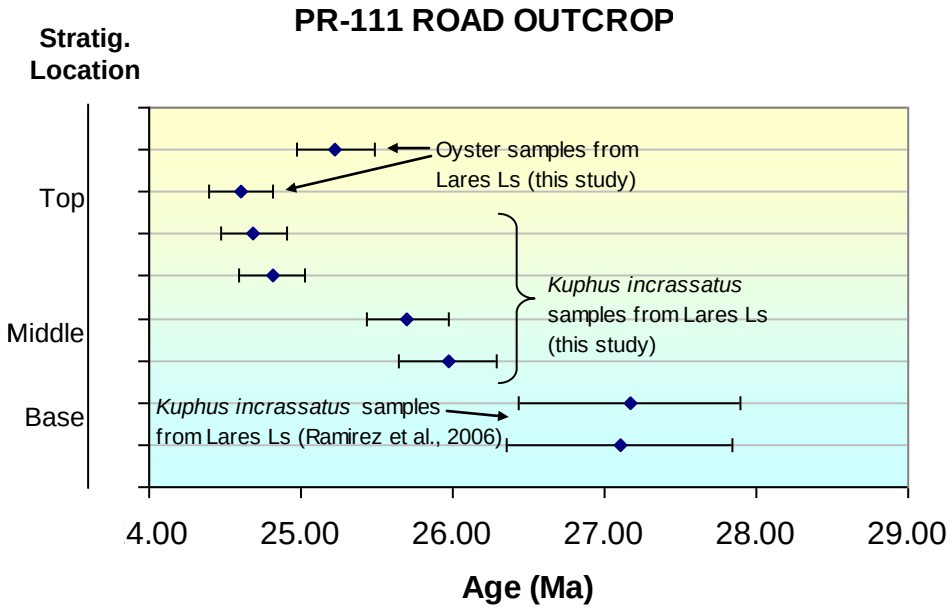

Figure 4.19: Absolute ages using strontium isotope stratigraphy (SIS) from the north coast *Kuphus incrassatus* tubes and oysters along the PR-111 road outcrop.

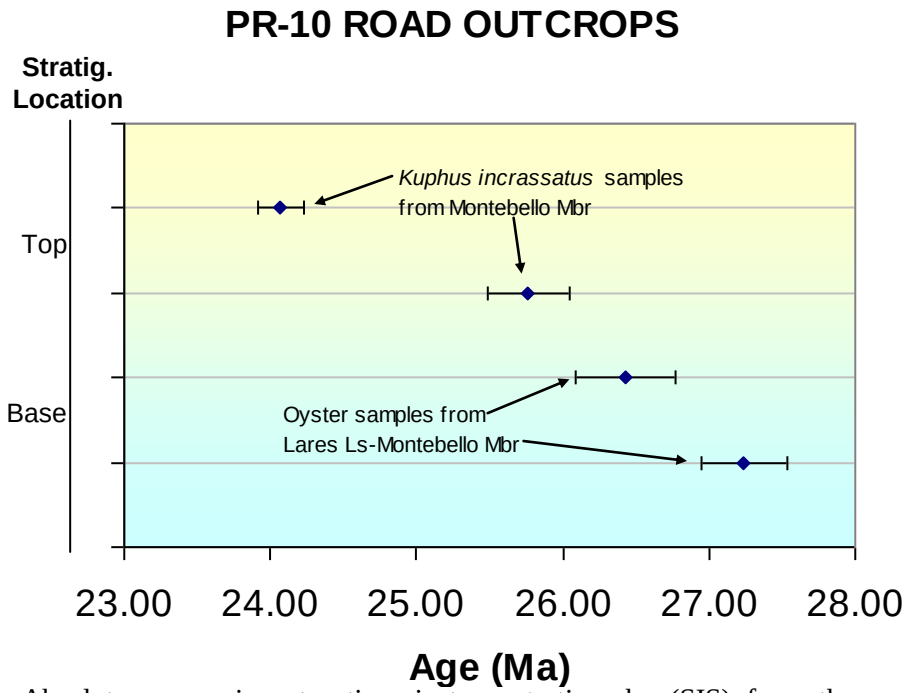

Figure 4.20: Absolute ages using strontium isotope stratigraphy (SIS) from the north coast *Kuphus incrassatus* tubes and oysters along the PR-10 road outcrops. All samples are from this study.

The *Kuphus incrassatus* tubes at top of PR-10 outcrop (intersection of PR-10 and PR-6621) resulted in $^{87}Sr/^{86}Sr$ isotopic values that range from 0.708198 to 0.708128.

These values suggest ages of *Kuphus incrassatus* tube formation of 24.07 +/- 0.16 Ma to 25.76 +/- 0.28 Ma (see Table 4.3 and Fig. 4.20).

In contrast, the *Kuphus incrassatus* tubes from the Cibao Formation and Aguada (Los Puertos) Limestone in NC-11 core resulted in $^{87}Sr/^{86}Sr$ isotopic values that range from 0.708835 to 0.708854. These values suggest ages of *Kuphus incrassatus* tube formation of 12.07 +/- 0.53 Ma to 11.06 +/- 0.37 Ma. The *Kuphus incrassatus* tubes from the Aguada (Los Puertos) Limestone in NC-6 core resulted in $^{87}Sr/^{86}Sr$ isotopic value of 0.708795. This value suggests an age of *Kuphus incrassatus* tube formation of 14.60 +/- 0.89 Ma. The *Kuphus incrassatus* tubes from the base of Aymamón Limestone in NC-13 core resulted in $^{87}Sr/^{86}Sr$ isotopic value of 0.708858. This value suggests an age of *Kuphus incrassatus* tube formation of 10.91 +/- 0.34 Ma (see Table 4.3 and Fig. 4.21).

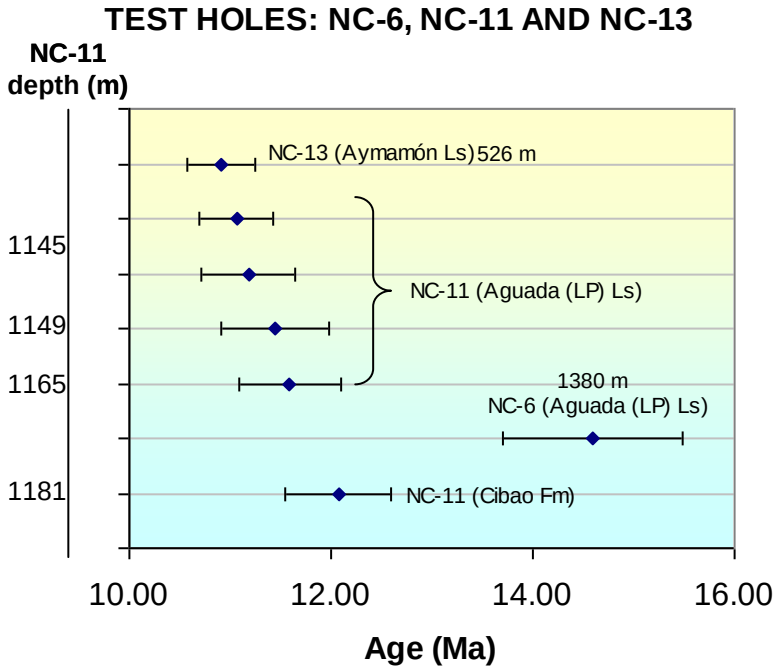

Figure 4.21: Absolute ages using strontium isotope stratigraphy (SIS) from the north coast *Kuphus incrassatus* tubes and oysters along the NC-6, NC-11 and NC-13 test holes. All samples are from this study.

CHAPTER 5

INTERPRETATION

The NC-6 (2572 ft- 785 m) and NC-5 (2560 ft- 780 m) cores, as well as the PR-10 (326 m) and PR-22 (36 m) outcrops, in addition to aerial photographs taken along PR-10 and PR-111 highways, were used to interpret the Tertiary limestone units along the north coast of Puerto Rico, based on the concepts of sequence stratigraphy.

5.1 PARASEQUENCES ANALYSIS

The parasequences analysis was carried out after depositional environments were documented on both test holes and outcrops (see Appendix 2). The criteria to determine parasequences (shallowing upward sequences) was the presence of diagnostic constituents and lithologic composition, which define the different depositional environments.

NC-6 TEST HOLE

The NC-6 test hole contains 69 parasequences which are distributed as follow; seven in the upper Lares Limestone, twelve in the lower Cibao Member, four in the Montebello Member, fifteen in the Undifferentiated Cibao Formation, ten in the Aguada (Los Puertos) Limestone, twenty in the Aymamón Limestone and one in the Quebradillas Limestone.

The parasequences toward the base in the NC-6 test hole generally are thinner (2 to 5 m) representing lesser accommodation space (upper Lares Limestone and lower Cibao Formation). These are characterized in most cases by wackestone at the base, with claystone and marls lithologies at the top. Carbonaceous material and sand layers are also present toward the top of individual parasequences especially within the lower Cibao

Formation. The thinner tendency of these parasequences change toward the top of the lower Cibao Formation, where they become thicker (5 to 15 m), and the carbonate component (packstone and wackestone) become abundant with lesser to absent claystone (Montebello Member). The top of some parasequences are characterized by exposure surfaces evidenced by caliche. Within the overlying unit (upper Cibao Formation) the parasequences continue to be thick (12 to 14 m), with an extensive layer of claystone material (approx. 30 m), which may represent a paleosol. The top of most parasequences within this formation return to be claystone in most cases, except by a parasequence at the base of the formation that ends up in grainstone and a parasequence at the top of the formation that ends up in caliche. Despite the presence of claystone at the top of the parasequences, limestone (especially wackestone) units are thicker (approximately 120 m), being the parasequences thicker as well. The top of some parasequences toward the top of this formation are also characterized by microcrystalline and fenestral mudstone.

The Aguada (Los Puertos) Limestone parasequences are characterized by limestone, with wackestone at the base and packstone to grainstone at the top. The parasequences are thinner (approx. 6m) at the base and thicker (approx. 12 m) toward the middle and upper parts, where they are capped by caliche (exposure surface). At the upper part of the formation a thin (4 m) parasequence of claystone and marl layer is present, bounded by an exposure surface above, as well as another one formed by packstone at the base and mudstone at the top. The top of the Aguada (Los Puertos) Limestone is characterized by texture recognized as karst.

The Aymamón Limestone is characterized by thicker parasequences (approx. 18 m, some reach over 40 m). These shallowing upward sequences show wackestone at the

base changing upward to packstone, grainstone or packstone to grainstone at the top. Some parasequences are thinner (1 to 4 m) in the middle part of the formation and are composed of packstone to grainstone at the base and limestone fragments at the top. Toward the top of the formation parasequences are usually capped by mudstone lithologies and exposure surfaces. The top of the Aymamón Limestone is characterized by textures associated to an extensive karst that can be traced across the entire north coast basin.

The Quebradillas Limestone has only one parasequence (28 m) in the NC-6 core that is the last parasequence at the top of the NC-6 core. It is composed of planktonic foraminifers in a chalk matrix at the base, followed by benthonic foraminifers toward the top (See Appendix 2).

Matos (2000) recognized six exposure surfaces within the Aymamón Limestone in the NC-6 core. The upper one, located at 85 m, is composed of laminated crust and microcrystalline calcite. Coral mollusk wackestone to packstone with occasional iron oxides is present above the exposure surface, while highly fractured foraminiferal wackestone is below it. The second exposure surface, located at 131 m, is characterized by caliche crust, fractures, rhyzomorphs and iron oxides. The third exposure surface, located at 171 m, is composed of 45 cm of thick caliche layer. The fourth exposure surface, located at 183 to 184 m, is characterized by a brecciated horizon and micritic laminations. Mudstone was identified above the exposure surface, while wackestone below it. The fifth exposure surface, located at 216 m, is composed of molluskan packstone above the exposure to a patchy dolomitic wackestone. The sixth exposure

surface located at 268 m is characterized by laminations, iron oxide and fractures. Red algae packstone is present above it, while dolomitic packstone is below it (Matos, 2000).

NC-5 TEST HOLE

The NC-5 test hole contains 68 parasequences distributed as follow. Ten in the San Sebastian Formation, twelve in the upper Lares Limestone, fifteen in the Montebello Member, twelve in the Undifferentiated Cibao Formation, twelve in the Aguada (Los Puertos) Limestone, and seven in the Aymamón Limestone.

The parasequences toward the base are thinner (approx. 6 m). They are characterized by layers of wackestone at the base, changing to claystone and carbonaceous layers at the top. Towards the top of the San Sebastian Formation the limestone content increases, with parasequences composed of wackestone at the base and packstone to grainstone at the top. Claystone is absent from this interval to the Undifferentiated Cibao Formation. The parasequences along the basal Lares Limestone are thinner (approx. 13) and composed of wackestone at the base and wackestone to packstone at the top. Parasequences become thicker (approx. 25 m) toward the middle part of the formation, and are characterized by thick wackestone layers at the base changing upward to coral boundstones at the top. The upper part of the Lares Limestone shows thinner (approx. 15 m) parasequences composed of wackestone to packstone textures.

The parasequences in the Montebello Member are mainly characterized by wackestone (sometimes packstone) at the base, changing to boundstone and grainstone at the top. The presence of boundstones at the top of parasequences is more common in the middle part of the formation, while grainstones occur toward the top. Parasequences are

thicker (18 m, with some reaching up to 24 m) in the lower part of the formation, while thinner ones (approx. 10 m) occur at the top, particularly the last one which is capped by claystone.

The Undifferentiated Cibao Formation parasequences are thinner (4 to 7 m) and are characterized by wackestone at the base and claystone at the top (sometimes sand in the basal part of the formation). Caliche and mudstone cap some parasequences, while grainstone caps parasequences toward the top. The basal Aguada (Los Puertos) Limestone presents parasequences compose of wackestone at the base coarsening upward to packstone to grainstone at the top, with exposure surfaces (caliche) associated. Toward the middle part of the formation thinner (approx. 3 m) parasequences are interpreted as successions that change from wackestone at the base to clay and sand material at the top. This may represent a pulse of local terrigenous input within the limestone sections. Parasequences at the upper part of the formation are composed of wackestone that change upward into grainstone. The uppermost of the formation shows characteristics associated with karst. The Aymamón Limestone parasequences are thinner (approx. 6 m) in the lower part of the formation, becoming thicker (approx. 24 m) toward the middle and upper sections. They are composed of wackestone to grainstone in the lower Aymamón Limestone changing into wackestone to packstone toward the top. Some parasequences are capped by claystone and mudstone at the top (See Appendix 2).

Matos (2000) recognized three exposure surfaces within the Aymamón Limestone in the NC-5 core. In general terms, the first one located at 29 m is recognized by caliche crust with laminations and iron oxides. Coral packstone is present above the exposure surface, while unknown skeletal fragment-mollusk wackestone unit is below it. The

second exposure surface located at 30.5 m is characterized by caliche crust with some laminations, iron oxides and fractures. The third exposure surface located at 72 m is represented by fractures, rhizomorphs, and iron oxides. Rich fossiliferous packstone is present above the exposure surface, while red-algae packstone occurs below (Matos, 2000).

PR-10 ROAD OUTCROPS

The PR-10 outcrops expose the San Sebastian Formation, Lares Limestone and Montebello Member. These contain 43 parasequences distributed as follow: five in the Lares Limestone and thirty eight in the Montebello Member.

Parasequences in the Lares Limestone are thinner (approx. 3 m) with respect to those along the Montebello Member. They are composed of packstone and wackestone at the base, changing to grainstone and packstone at the top. Boundstones are present at the base of parasequences toward the top of the Lares Limestone. The parasequences in the basal Montebello Member are mainly characterized by coral boundstones ranging in thickness from 3 to 14 m at the base, changing upward to grainstone and packstone lithologies. Toward the middle section of the Montebello Member exposure the parasequences are made of packstone (sometimes wackestone) at the base to thick grainstone layers (ranging in thickness from 4 to 14 m) at the top. Stratigraphically upward the parasequences are composed of boundstone at the base, changing to packstone and grainstone at the top. Finally, the upper part of this member is represented by wackestone at the base, changing upward to grainstone at the top. The last parasequence shows evidence of an exposure associated with a relative fall in sea level. This is based on the presence of a paleosol, freshwater gastropods, breccias, root traces

and paleosinkholes. This boundary also serves as the lithologic contact between the Montebello Member below and the Undifferentiated Cibao Formation above (See Appendix 2).

PR-22 ROAD OUTCROP

Matos (2000) recognized four exposure surfaces along the PR-22 road outcrop. The first exposure surface is characterized by a microcrystalline matrix, crust, iron oxide minerals and rhizoliths. Red algae-foraminiferal packstone with ocassional *Halimeda* and skeletal fragments is present below the exposure, while mollusk wackestone above it. The second one is composed of microcrystalline calcite matrix, iron oxides, and fractures. Coral mollusk packstone is present below the exposure, and foraminiferal mollusk packstone above it. The third one is characterized by caliche, iron oxides, and glaebules. Foraminiferal packstone is present below the exposure, while mollusk packstone with occasional *Amphistegina* and miliolids above it. The fourth one is characterized by microcalcite, matrix hardpan and iron oxides. Foraminiferal packstone with common mollusk and coral fragments is present above it, while coral mollusk packstone is below it (See Appendix 2).

5.2 PHOTOMOSAIC ANALYSIS

PR-111 ROAD OUTCROP

At least nine parasequences were identified along this outcrop. These are organized from base to top along the outcrop (Fig. 5.1). The fossils present like benthic foraminifers, *Kuphus incrassatus*, corals, bivalves and gastropods, among others, change in distribution, both vertically and horizontally, along the outcrop, helping to further interpret the parasequences. The first parasequence is identified within the San Sebastian

Formation. It is characterized by massive and branching corals in a finer matrix at the base, changing upward to grainstone with *Kuphus incrassatus*-rich and crab fragments at the top. This parasequence is interpreted to represent the San Sebastian Formation-Lares Limestone contact (Late Oligocene), based on the change from mainly terrigenous to mostly carbonate rocks. The second parasequence is represented by *Porites* coral boundstone at the base, to coal layers and organic rich sediments (fine grain). The third one is composed of mudstone to wackestone at the base, to coal fragments and *Kuphus incrassatus*, skeletal grains, and oxidized fractures at the top, with lateral facies changes represented by corals boundstone.

The fourth parasequence is composed of sparse massive corals in growth position, red algae and bivalves in a finer matrix (carbonate shales), changing upward to abundant branching and massive corals, mostly in growth position (North side). This parasequence change laterally and is correlated with bryozoans at the base and corals at the top in the south side. The fifth parasequence is characterized by wackestone mainly composed of foraminifers and bivalves, changing upward to massive corals, most of them in growth position. The sixth parasequence is composed of mudstone to wackestone with terrigenous influence (silt-showing fissility), changing to grainstone with *Kuphus incrassatus*-rich layers at the top. The seventh and eighth parasequences, just visible at the top of the north side of the outcrop, are characterized by *Porites* and massive corals (most are not in growth position). At the top of the seventh parasequence, in the northern section, flat (platy) corals are distinguished locally. The eight parasequence is capped by a *Kuphus incrassatus*-rich layer.

A.

B.

Figure 5.1: Photomosaic interpretation of PR-111 road outcrop. A. Complete PR-111 outcrop section and B. West-side PR-111 outcrop. The red lines mark the lithologic contact between units.

Figure 5.1 (cont.): Photomosaic interpretation of PR-111 road outcrop. C. Central-side PR-111 outcrop and D. East-side PR-111 outcrop (below). The red lines mark the lithologic contact between units.

Finally, the ninth parasequence is composed of finer matrix (mudstone to wackestone) at the base, changing to pelletal grainstone at the top. Dolomite is present at the top of the parasequences.

The burrowed olive green claystone, with organic material, root casts and scarce fossils above the dolomite, which is interpreted as a paleosol, is proposed as the new Lares Limestone-Montebello Member contact (Early Miocene), rather than the oyster layer used by previous authors. At this exposure, the oyster layer mentioned is found at the topmost part of the section, several meters above the paleosol and on top of the clinoforms. The clinoforms dipping towards the north, and above the paleosol, are interpreted as result of new and rapid relative rise in sea level.

In general terms, the parasequences along the PR-111 outcrop are represented by mudstones and wackestones at the base, with gradual development of coral boundstones. In some parasequences the boundstones occur at the top but in others a wackestone and/or grainstone, interpreted as lagoonal and beach environments, are present.

PR-10 ROAD OUTCROP

The outcrop comprises at least thirteen parasequences. These are organized from base to top along the outcrop (Fig. 5.2). The first parasequence is identified within the Lares Limestone with a packstone to grainstone texture at the base, changing to grainstone with echinoderms, benthic foraminifers and cross beds at the top. *Lepidocyclina undosa* is abundant at the base of this parasequence and decreases upward. The second shallowing upward sequence is composed of wackestone at the base changing upward to foraminiferal grainstone. The third one is characterized of mudstone to wackestone, changing to boundstone with delicate and flat corals. The fourth, fifth and

six parasequences are represented by mudstone to wackestone at the base, to mainly *Porites* corals in a fine grain matrix at the top.

The sixth one is capped at the top by grainstone, in addition to a laterally continues oyster layer. It also represents the lithologic contact between the Lares Limestone and the Montebello Member.

The next parasequences show similar arrangement, being thicker than those below the oyster layer. They are composed of repetitions of massive corals boundstone at the base, changing upward to foraminiferal grainstones. *Kuphus incrassatus* layers occur at the top of some parasequences in the upper section of the outcrop.

In general terms, from the San Sebastian Formation-Lares Limestone contact thirteen parasequences are recognized, regardless of the fact that the Lares Limestone is thinner in this area. The parasequences change in thickness from thicker (higher accommodation space) to thinner ones (lesser accommodation space). Thicker foraminiferal grainstones parasequences (numbers 1 and 2) gradually change to thinner parasequences (numbers 3, 4 and 5). The sixth parasequence below the oyster layer is thick again. This tendency continues above the oyster layer where thicker coral boundstone parasequences (numbers 7 to 13) are clearly identified. Furthermore, the oyster layer is inside the first thick parasequence.

Figure 5.2: Photomosaic interpretation on PR-10 road outcrop. The red lines mark the lithologic contacts between units.

5.3 CORRELATION BETWEEN CORES AND OUTCROPS

The correlation between NC-6 and NC-5 cores, and PR-10, PR-111 and PR-22 outcrops is shown in Figures 5.3 to 5.8. The Lares Limestone-Montebello Member contact is used as datum.

The oldest unit recognized in this study is the upper part of the San Sebastian Formation, which together with the Lares Limestone represent a transgression event over the Cretaceous to early Tertiary basement (Figs. 5.3 and 5.4). This is evidenced by the siliclastic material gradually changing to carbonate rocks (transition from fluvial to marine environments).

The NC-5 core, PR-10 and PR-111 outcrops record this transgression of the San Sebastian Formation and the lower half of the Lares Limestone. Both represented by thick parasequences. The change into thinner parasequences in the PR-10 and PR-111 outcrops toward the contact with the Montebello Member, represent a decrease of accommodation space, as the sea level record a maximum flooding. These thinner parasequences of the Lares Limestone are interpreted as a Highstand System Tract (HST) and can be correlated in the distal (NC-5 core) with thick parasequences (higher accommodation space) of the prograding package. In the PR-111 the Lares Limestone-Montebello Member contact is represented by an exposure surface and in the PR-10 by influx of siliciclastics within grainstones, reflecting a relative drop of sea level (sequence boundary).

The NC-6 core only contains the upper part of the Lares Limestone (See Fig. 5.4). This is because the San Sebastian Formation and the Lares Limestone units are deeper at the NC-6 site. The paleotopography also plays an important role controlling the

deposition toward the western regions. These units pinch out to the west. The lower Cibao Formation in NC-6 core represents a facies change of the Montebello Member. The lower Cibao is a clay rich limestone due to terrigenous influx. The parasequences of terrigenous sediments in the west suggest a fluvial input during the Oligocene (San Sebastian Formation) and Miocene (Cibao Formation) time.

The NC-6 core at its base also record the change from retrogradational (TST) to progradational pattern (HST), allowing the deposition of more terrigenous overlying units (the lower Cibao Formation). Furthermore, the lower Cibao Formation was deposited due to a relative fall in sea level after final deposition of the Lares Limestone.

A relative rise in sea level is represented by the Montebello Member in the central part of the basin. The thickening of the parasequences (higher accommodation space) within this member suggests another transgression (TST). In the NC-5 core (distal area) the transgression is represented by abundance of branched and massive corals boundstones and rhodolites, while purer limestones with thick units of coral boundstone are present within the PR-10 outcrops (Fig. 5.5). The PR-111 outcrop includes part of the Montebello Member deposited over the exposure surface (sequence boundary 1), showing a progradational pattern (clinoforms dipping in a north direction), which are produced after a rapid relative rise in sea level (HST).

The maximum relative rise in sea level (maximum flooding surface-MFS) within the Montebello Member is located where coral boundstones are abundant, which is toward the middle part of this unit (NC-5 core and PR-10 outcrop) (See Fig. 5.5).

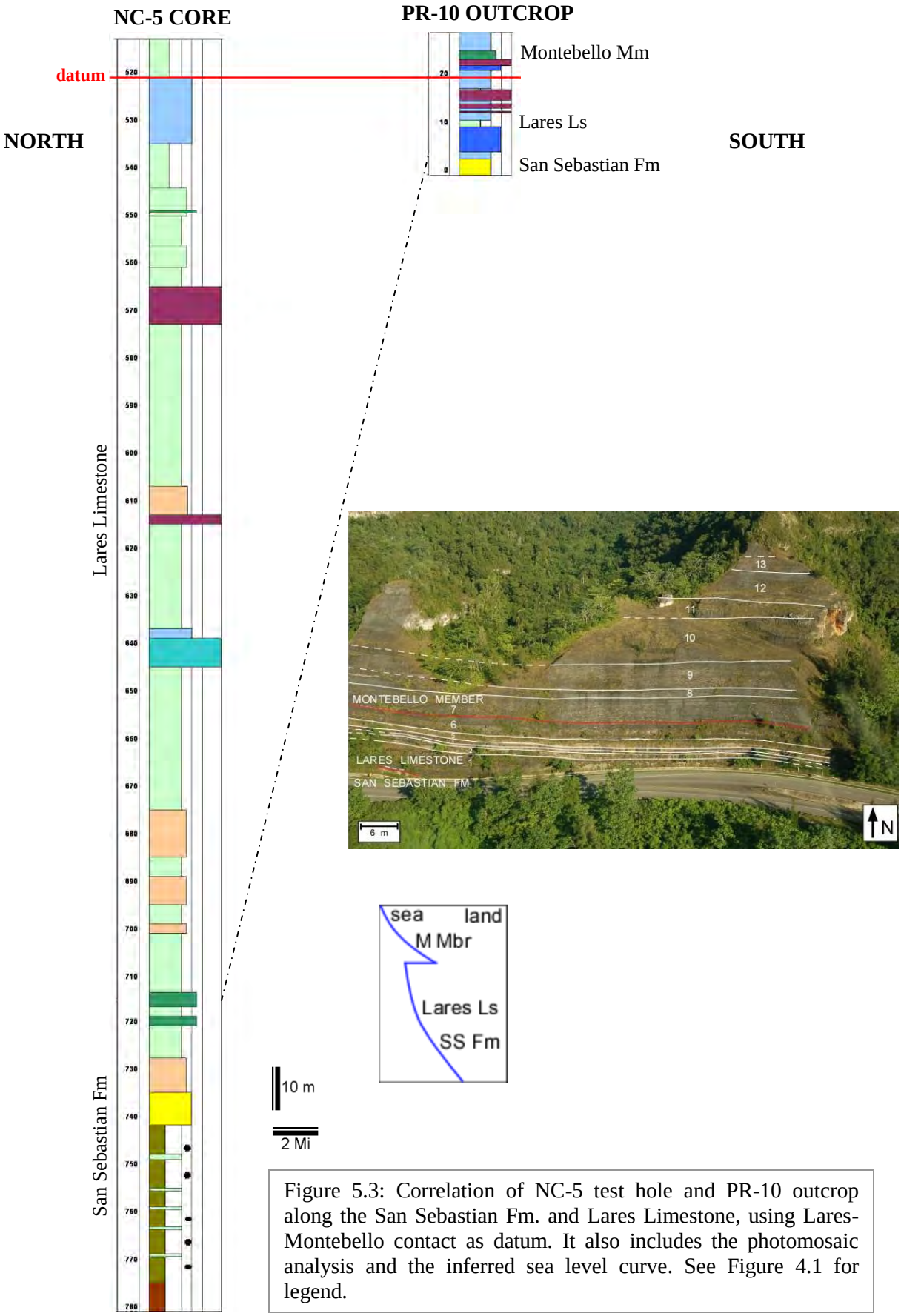

Figure 5.3: Correlation of NC-5 test hole and PR-10 outcrop along the San Sebastian Fm. and Lares Limestone, using Lares-Montebello contact as datum. It also includes the photomosaic analysis and the inferred sea level curve. See Figure 4.1 for legend.

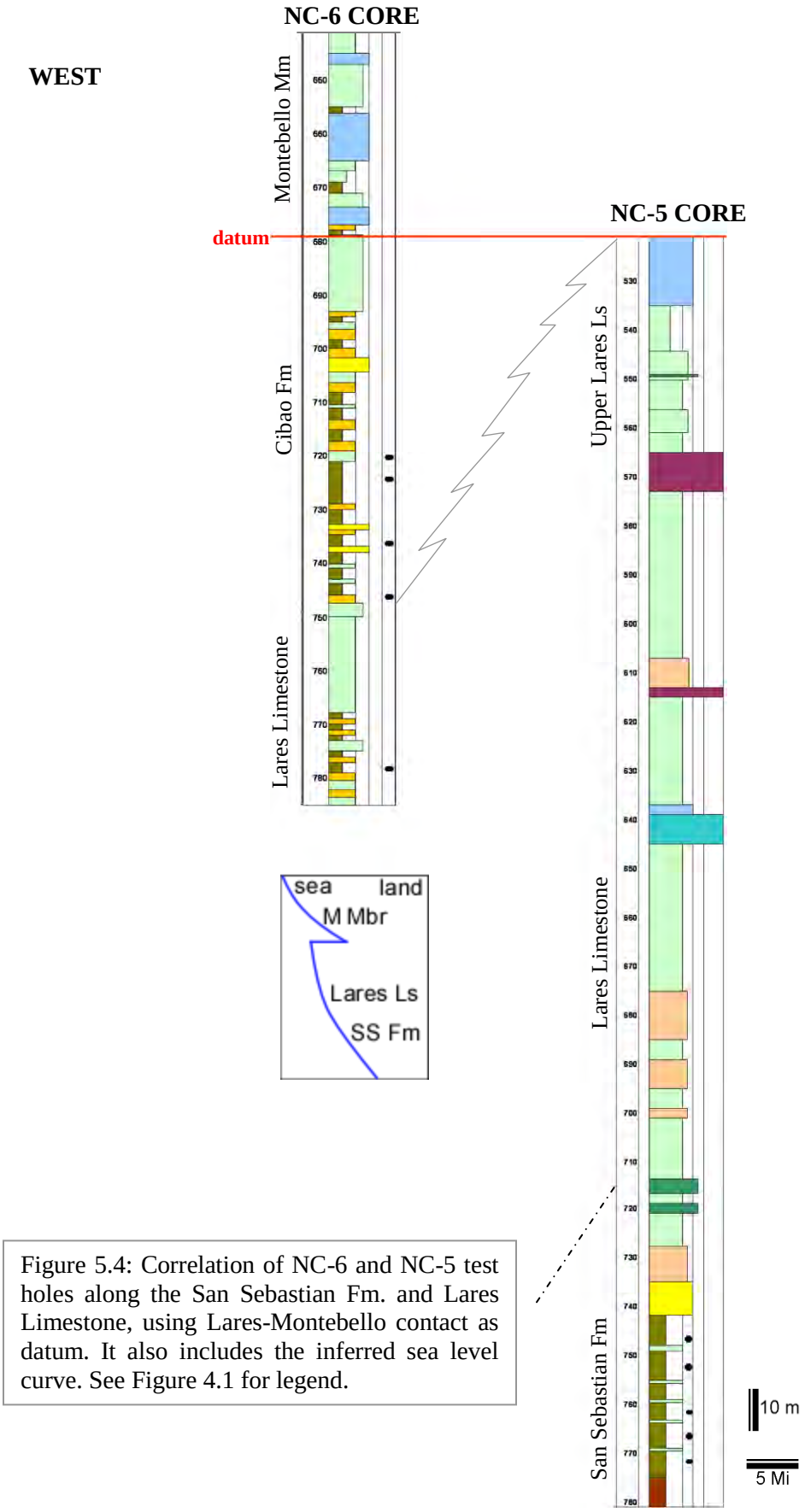

Figure 5.4: Correlation of NC-6 and NC-5 test holes along the San Sebastian Fm. and Lares Limestone, using Lares-Montebello contact as datum. It also includes the inferred sea level curve. See Figure 4.1 for legend.

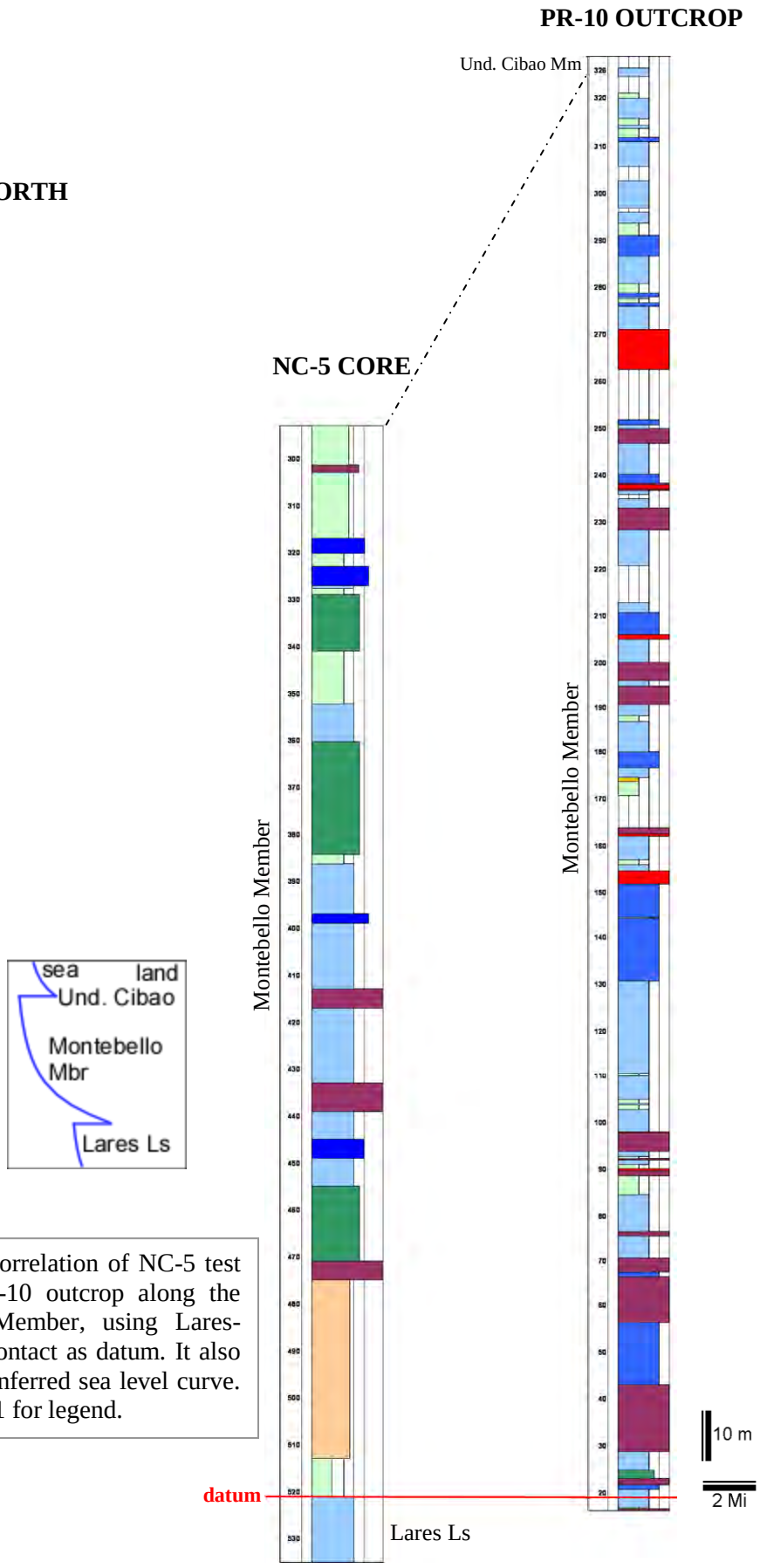

Figure 5.5: Correlation of NC-5 test hole and PR-10 outcrop along the Montebello Member, using Lares-Montebello contact as datum. It also includes the inferred sea level curve. See Figure 4.1 for legend.

After that point, parasequences become thinner, characterized by packstone and grainstone rather than thicker coral levels. This is interpreted as a decrease in accommodation space characteristic of Highstand System Tract (NC-5 core and PR-10 outcrop). Both NC-5 and NC-6 cores (Fig. 5.6) record a shallower environment to exposure at the top of the Montebello Member as evidenced by caliche in NC-6 core, and a change to thicker organic rich claystone deposits (Undifferentiated Cibao Formation). In the PR-10 outcrop (proximal area) the sea level drop is represented by an exposure surface (sequence boundary) at the top of the Montebello Member containing paleosol and paleosinkholes, together with freshwater gastropods and rhizoliths.

In the NC-6 core deposition of the more terrigenous lower Cibao is followed by deposits of the Montebello Member as the transgression continued (TST). Deposits of the Montebello Member in the NC-6 core ended as the sea level drop resulting in deposition of the thick marginal marine Undifferentiated Cibao Formation (upper Cibao unit, NC-6 and NC-5 cores). Laterally this correlates with the exposure surface (sequence boundary 2) in the top of the Montebello Member in the PR-10 outcrop.

The Undifferentiated Cibao Formation is thicker toward the west in response to more terrigenous influx due to the paleotopography in the area during the Early Miocene (NC-6 core) (Fig. 5.7). The parasequences (NC-6 core), in general, are thinner, but they show a particular pattern. They are thicker at the base and thinner toward the top, because claystone material gradually decreases and carbonate rocks become abundant, reflecting a new relative rise in sea level.

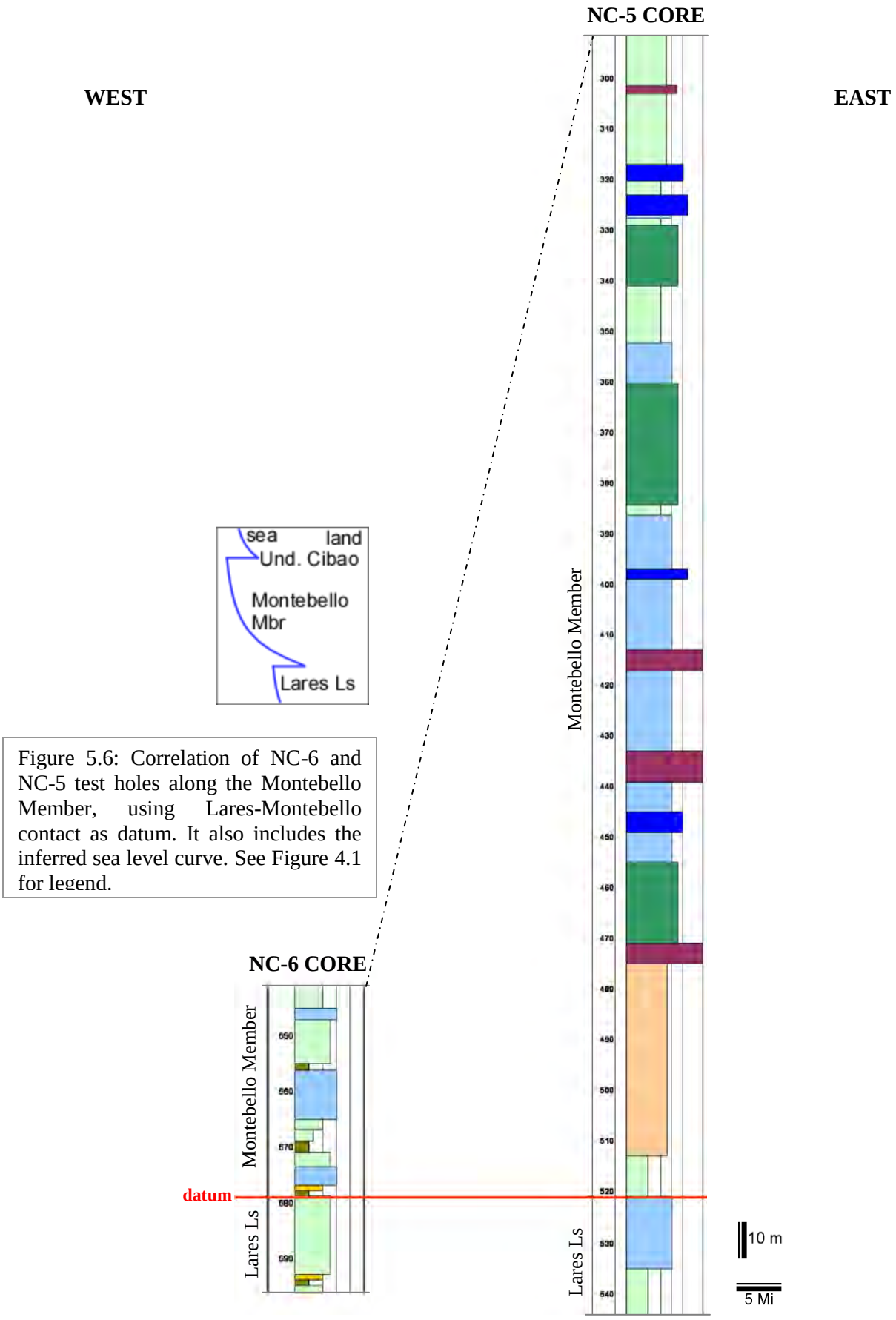

Figure 5.6: Correlation of NC-6 and NC-5 test holes along the Montebello Member, using Lares-Montebello contact as datum. It also includes the inferred sea level curve. See Figure 4.1 for legend.

The NC-5 core also shows the same tendency of NC-6 core toward the top. Microcrystalline and fenestral mudstones at the top of the formation (NC-6 and NC-5 cores), which are deposited in tidal flat setting, provide evidence of a shallower environments and the beginning of a high amplitude sea level fluctuations within the basin. These are also supported in both NC-6 and NC-5 cores with caliche (partial and pisolites) layers and volcanic rock fragments associated to an exposure surfaces.

The NC-6 and NC-5 cores show approximately the same succession along the Aguada (Los Puertos) Limestone (See Fig. 5.7). The shallowing upward sequences are composed of limestone rocks, in most cases, passing from wackestone, packstone to grainstone. The NC-5 core differs from NC-6 core in that it presents more clay, sand and marl layers, which form thinner parasequences. The karst zone identified at the top of the Aguada (Los Puertos) Limestone within the NC-5 test hole, which is correlated with the grainstone containing spar filled vugs in NC-6 test hole, is interpreted as result of a relative drop in sea level. In both NC-6 and NC-5 cores various caliche (breccia and pisolite) layers, root molds and fenestral mudstones (NC-6 core) are interpreted as exposure surfaces.

A relative rise in sea level (TST) that started with the Undifferentiated Cibao Formation and continued with the Aguada (Los Puertos) Limestone shows repeated episodes of subaerial exposure within these units. Together with those occurring within the overlying Aymamón Limestone, reflect the high amplitude sea-level fluctuations during Miocene time.

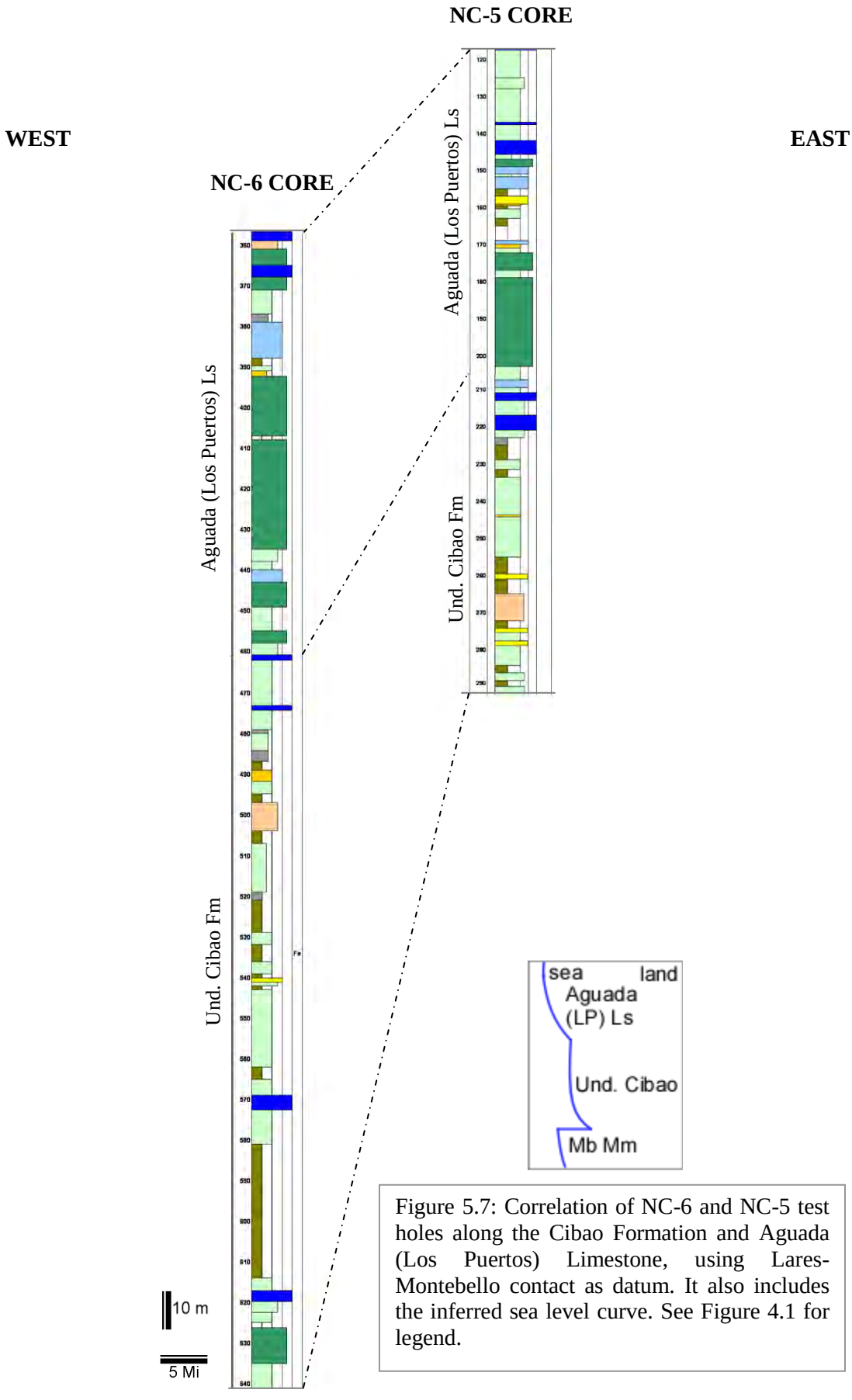

Figure 5.7: Correlation of NC-6 and NC-5 test holes along the Cibao Formation and Aguada (Los Puertos) Limestone, using Lares-Montebello contact as datum. It also includes the inferred sea level curve. See Figure 4.1 for legend.

The Aymamón Limestone shoaling upward sequences in both NC-6 and NC-5 cores are characterized by complete limestone successions from wackestone to grainstone (Fig. 5.8). Branched corals, red algae, planktonic foraminifers (especially within the NC-6 core) and *Amphistegina* foraminifers are also important along this formation. These parasequence patterns represent a new transgression (TST) after the exposure and karstification occur in the top of Aguada (Los Puertos) Limestone and before deposition of the Aymamón Limestone. The top of the Aymamón Limestone is also characterized by a widespread karst surface that represents another relative drop in sea level, which produces a regional unconformity along the whole North Coast Tertiary Basin. The high amplitude of sea level fluctuation results in deposition of limestone followed by exposure surface represented by caliche. Following this idea each limestone deposition represents a transgressive to highstand system tract.

The Quebradillas Limestone is only found in the NC-6 core (western area) and is Pliocene in age based on its foraminiferal association (See Fig. 5.8). Therefore, the unconformity between the Aymamón Limestone and this unit would correspond to the Late Miocene, where a period of a higher fall in sea level is interpreted. The Quebradillas Limestone represents the last relative rise in sea level within the Oligocene-Pliocene time. The relative sea level rise was the highest and extended further south into the island resulting in open marine deposition at NC-6 core as evidenced by deposition of planktonic foraminifer chalks.

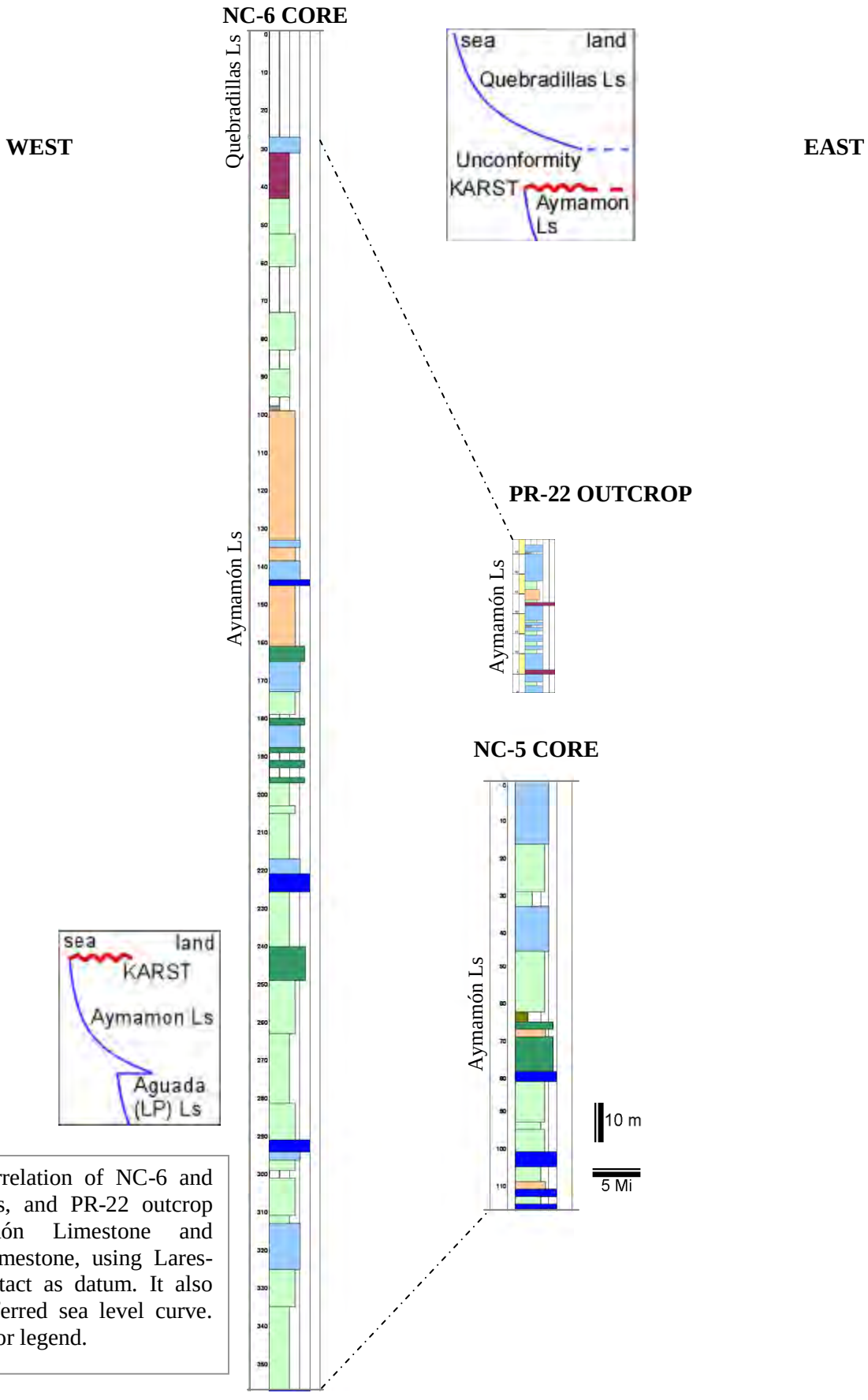

Figure 5.8: Correlation of NC-6 and NC-5 test holes, and PR-22 outcrop along Aymamón Limestone and Quebradillas Limestone, using Lares-Montebello contact as datum. It also includes the inferred sea level curve. See Figure 4.1 for legend.

CHAPTER 6

DISCUSSION

Parasequences interpretations using NC-6 and NC-5 cores, together with the PR-10, PR-22 and PR-111 outcrops (Chapter 5) are discussed in this chapter. A sequence stratigraphic model is proposed for the Tertiary limestone formations along the north coast of Puerto Rico (Figs. 6.1, 6.2, 6.3 and 6.4). In addition, a sea level curve based on the sequence stratigraphic interpretation is included and compared with the Puerto Rican cycles proposed by Seiglie and Moussa (1984) and the eustatic sea-level curve (Haq et al., 1987) (Fig. 6.5).

Cross sections were constructed to visualize the changes along the North Coast Tertiary Basin of Puerto Rico, in both sequence stratigraphic and paleotopographic aspects. Consequently, cross sections were generated to tie NC-5 test hole to the outcrops exposed in PR-10 and PR-111 roads in an approximately North-South direction. The PR-10 and PR-111 outcrops are located landward (toward the south), while NC-5 test hole (and NC-6 test hole), and PR-22 outcrop are located seaward (toward the north). The advantage to have control in both surface and subsurface regions, helps to better understand the changes that occurred in the basin from Late Oligocene to Early Pliocene time.

Five depositional sequences and four major sequence boundaries are proposed. These are: 1) The San Sebastian Formation-Lares Limestone; 2) The Montebello Member; 3) The Cibao Formation-Aguada (Los Puertos) Limestone; 4) The Aymamón Limestone; and 5) The Quebradillas Limestone. These depositional sequences are similar to those proposed by Ward et al. (2002).

6.1 DEPOSITIONAL SEQUENCES

After the collision with the Bahamas Platform (Eocene time), cessation of volcanism, subsidence, cooling and tilting (3 to 6 degrees) of the north coast Tertiary platform, conditions for the deposition of thick limestone sequences developed. The limestone units were deposited over the existing paleotopography during Oligocene to Pliocene time.

1. THE SAN SEBASTIAN FORMATION-LARES LIMESTONE DEPOSITIONAL SEQUENCE

The upper San Sebastian Formation represents fluvial to marginal marine environment. The Lares Limestone corresponds to inner to middle ramp carbonates. Together, they characterize a complete depositional sequence (See Figure 6.1). The San Sebastian Formation and the lower half Lares Limestone represent a Transgressive System Tract (TST), with the maximum flooding surface (MFS) and the Highstand System Tract HST being represented by the upper half of the Lares Limestone. Parasequences present in the San Sebastian Formation and the lower half of Lares Limestone show thickness associated with the creation of accommodation space during the transgression. Repetition of coral boundstone units represent reef parasequences where probable the MFS occur. Parasequences in the upper part of the Lares Limestone, above the MFS, are thinning as the accommodation space decrease due to progradation during the HST. The upper boundary of this depositional sequence at the top of the Lares Limestone characterizes the first Sequence Boundary (SB-1) of this study. The SB-1 is present in the PR-111 outcrop as an exposure surface (paleosol and dolomite), and in the PR-10 outcrop by a grainstone with siliciclastic grains.

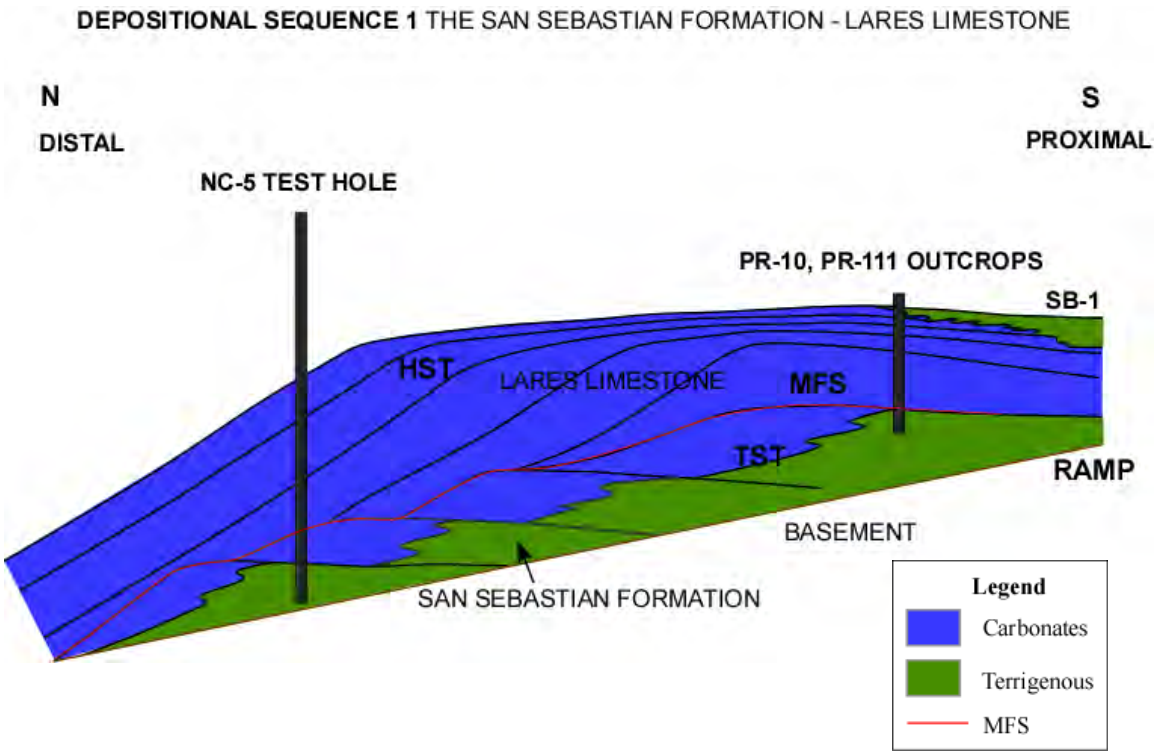

Figure 6.1: The San Sebastian Formation- Lares Limestone Depositional Sequence.

2. THE MONTEBELLO MEMBER DEPOSITIONAL SEQUENCE

Deposition of the Montebello Member represents a complete depositional sequence by itself (See Fig. 6.2). The depositional sequence records a cycle of deposition from inner to middle ramp as a transgression (TST) occur and returns to inner ramp during the HST. Repetition of coral boundstone parasequences exposed in PR-10 outcrop and present in NC-5 core represent the MFS. The exposure surface at the top of the Montebello Member proposed by Ramírez (2000) in PR-10 outcrop represents the upper boundary (Sequence Boundary-2) of this depositional sequence. Paleosinkholes, freshwater gastropods (*Physa* and *Pomacea*), a paleosol, and nodules, among others, are associated with this exposure.

Previous authors recognized separate transgressive-regressive cycles within the Lares Limestone and the Montebello Member based on subsurface studies (Seiglie and Moussa (1984); and Hartley (1989). In the surface the contact between those is proposed to occur several meters below a continuous oyster layer exposed in an East-West trend along the Lares-Utuado area (Monroe, 1980). In this study an exposure surface mainly represented by paleosol, rhizoliths, and dolomite was found several meters below to an oyster layer in the San Sebastian-Lares area (PR-111outcrop). Siliciclastic-rich grainstones various meters below of the oyster layer in the PR-10 outcrop are correlated with this surface. This study suggests the Sequence Boundary-1 as the new lithologic contact between the Lares Limestone and the Montebello Member.

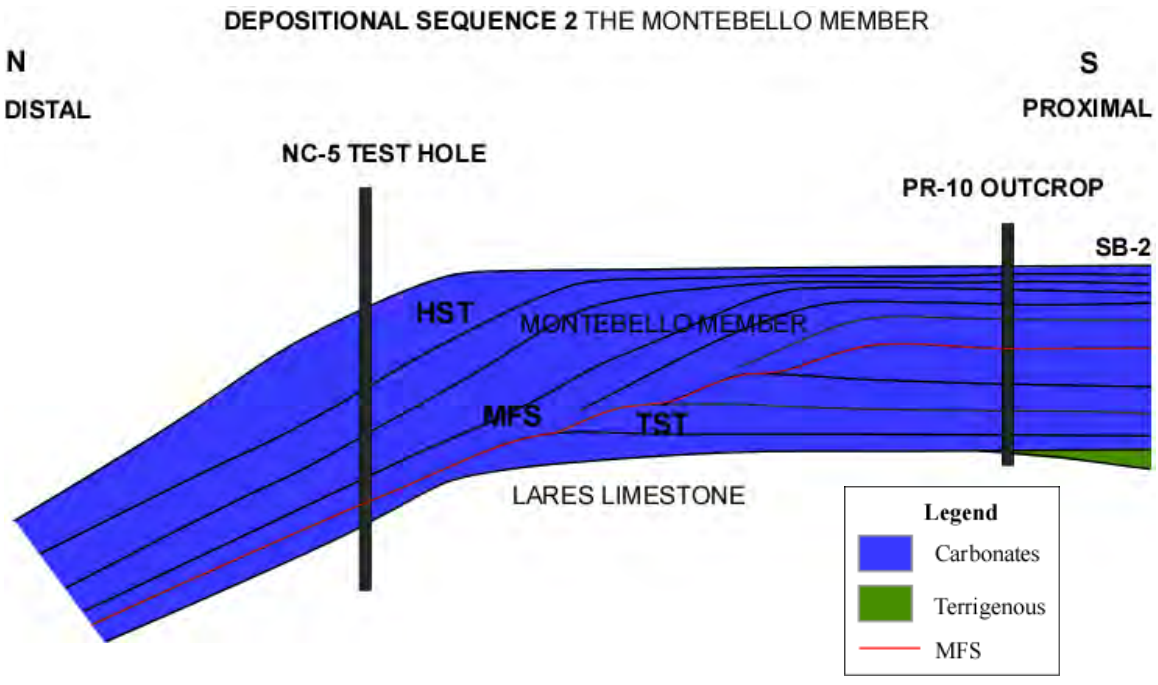

Figure 6.2: The Montebello Member Depositional Sequence.

3. THE UNDIFFERENTIATED CIBAO FORMATION- AGUADA (LOS PUERTOS) LIMESTONE DEPOSITIONAL SEQUENCE

The Undifferentiated Cibao Formation- Aguada (Los Puertos) Limestone interval records a new rise in relative sea level (TST). The Undifferentiated Cibao Formation with high percent of terrestrial input represents a gradual rise in sea level with parasequences representing a retrogradational pattern (TST). This TST extend into cleaner carbonates lower Aguada (Los Puertos) Limestone where thick parasequences composed of packstone to grainstone probably represent the MFS. Thinner parasequences with terrigenous influx toward the top of the Aguada (Los Puertos) Limestone represents a transition into the HST. The Sequence Boundary-3 (SB-3) in this study occurs at the top of the Undifferentiated Cibao Formation-Aguada (Los Puertos) Limestone depositional sequence and is represented by an exposure surface with caliche breccias, associated with karst. Repeated episodes of subaerial exposure inside this depositional sequence reflect the high amplitude sea-level fluctuations within an ice-house system during Miocene time (See Figure 6.3).

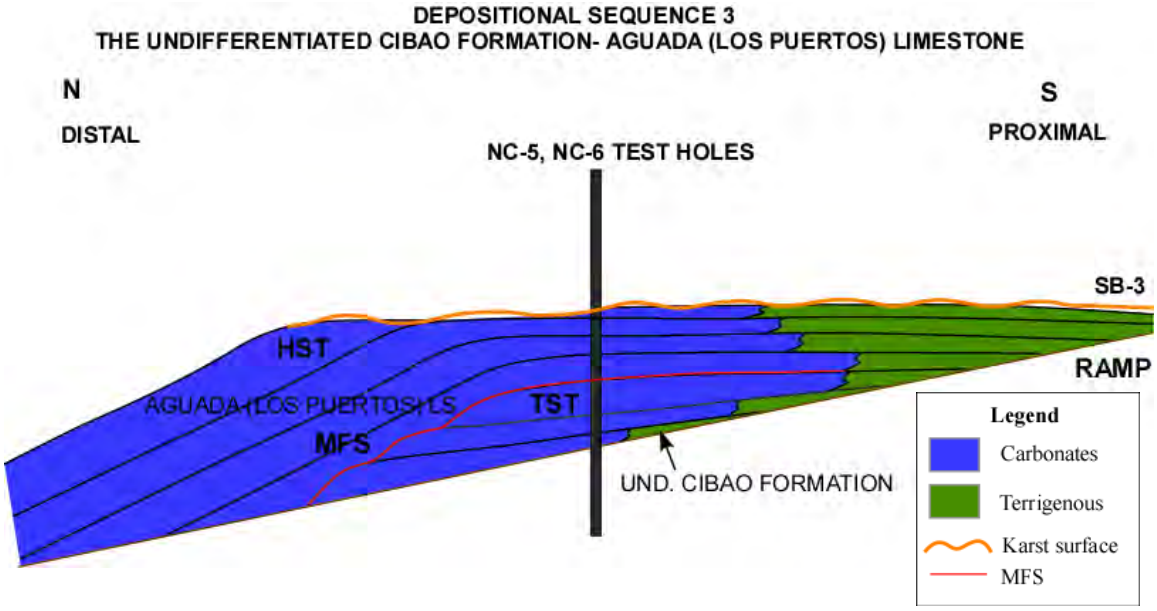

Figure 6.3: The Und. Cibao Formation-Aguada (Los Puertos) Limestone Depositional Sequence.

4. THE AYMAMON LIMESTONE DEPOSITIONAL SEQUENCE

The Aymamón Limestone bounded both at the base and top by exposure and karstification represents the four depositional sequence recognized in this study (See Figure 6.4). Much frequent episodes of subaerial exposure inside this depositional sequence further support the high amplitude sea-level fluctuations within more ice-house conditions during Middle Miocene time. These fluctuations result in deposition of limestone followed by exposure surface represented by caliche. Following this idea each limestone deposition represents a transgressive (TST) to highstand system tract (HST). The TST and HST correspond with the remnant of Aymamón Limestone after erosion and karst occurred due to exposition. The exposure surface (extensive karst zones) at the top of Aymamón Limestone is the upper boundary of this depositional sequence (Sequence Boundary-4).

5. THE QUEBRADILLAS LIMESTONE DEPOSITIONAL SEQUENCE

The Quebradillas Limestone represents the last relative rise in sea level (TST) within the Oligocene-Pliocene time after the exposure (SB-4) at the top of Aymamón Limestone occurred. This relative sea level rise during Pliocene was the highest and extended further south into the island resulting in open marine deposition (See Figure 6.4).

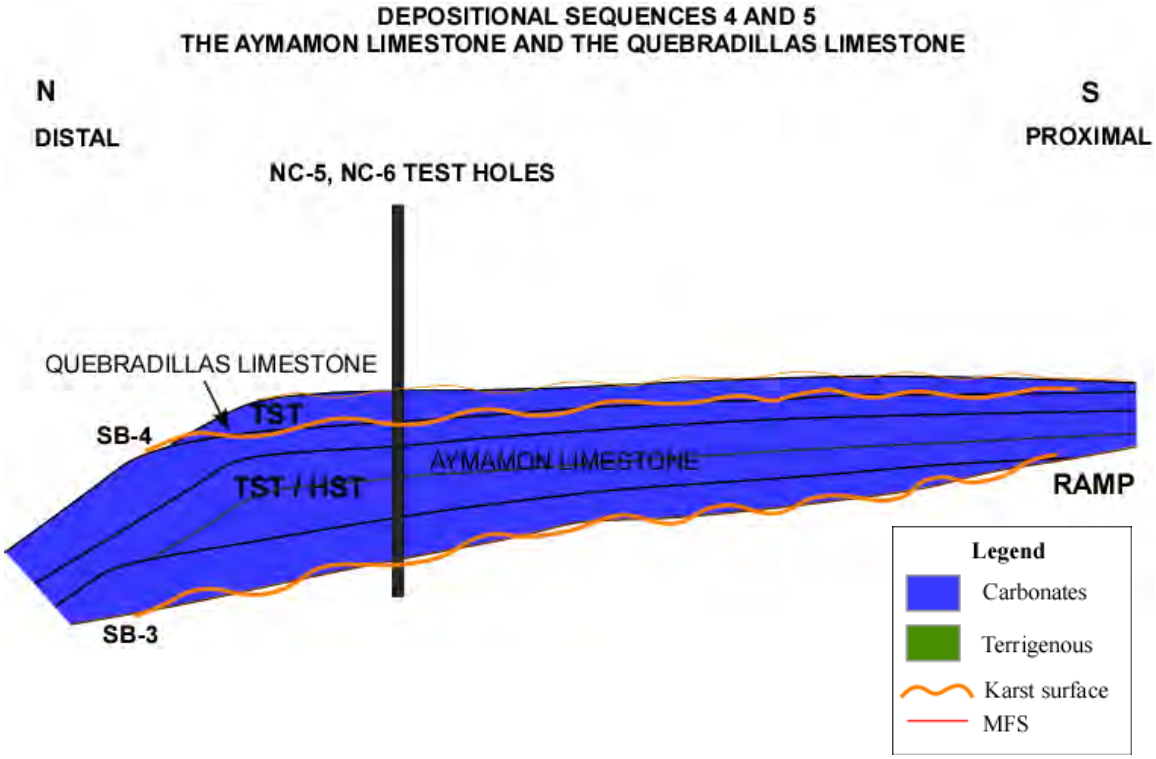

Figure 6.4: The Aymamón Limestone and the Quebradillas Limestone Depositional Sequences.

6.2 SEA LEVEL CURVE

The north coast platform has been tectonically stable since Oligocene (Meyerhoff et al., 1983; Monroe, 1980). Following this idea is plausible to compare the five depositional cycles proposed in this study, with the Puerto Rican cycles (Seiglie and Moussa, 1984) and with the eustatic sea-level curve (Haq et al., 1987) (See Fig. 6.5). Furthermore, despite ages of the Tertiary limestone units, which were established on benthic foraminifers (Seiglie and Moussa, 1984), are still approximated, the inferred sea level curve from these depositional sequences can be correlated. However, this comparison is estimated since the ages are not well constrained. However, a *Kuphus*

incrassatus strontium isotope age of 27.17+/-0.73 Ma at base of the Lares Limestone (PR-111 outcrop) is used as reference.

The five depositional sequences are most probably related to the second-order supercycles TB1 (depositional sequences 1 and 2), TB2 (depositional sequences 3 and 4), and TB3 (depositional sequence 5) (Haq et al., 1987) (See Fig. 6.5). The general eustatic-sea level rise during the Late Oligocene-Early Miocene is represented by the first depositional sequence between the San Sebastian Formation and the Lares Limestone. The second depositional sequence represented by the Montebello Member is visible after the eustatic-sea level fall recognized at the PR-111 outcrop (SB-1) and is followed by an eustatic-sea level rise. The third depositional sequence (Undifferentiated Cibao Formation-Aguada (Los Puertos) Limestone) started after the eustatic-sea level fall, which is evidenced at the top of the Montebello Member in the PR-10 outcrop (SB-2), and eustatic-sea level rise. The karst surface at the top of this depositional sequence (SB-3) can be correlated with one noticeable eustatic-sea level fall during Early to Middle Miocene. The forth depositional sequence represented by the Aymamón Limestone is correlated with an eustatic-sea level high. At its top (SB-4) an extensive karst surface is correlated with the major sea-level fall along the eustatic-sea level curve. The exposure surfaces along second and third depositional sequences which probably were developed during fourth or higher-order fluctuation in sea level may also be correlated with those along eustatic-sea level curve.

Finally, the Quebradillas depositional sequence corresponds with the first and major eustatic-sea level rise during Pliocene time, following the regional unconformity resulting from eustatic-sea level fall.

ICE HOUSE AND GREEN HOUSE SYSTEMS

Many factors determine whether complete systems tracts develop or not. One of the important considerations is that the systems tract models were developed for 3rd order scale. The north coast of Puerto Rico includes the Oligocene-Miocene boundary where a change from green house to ice house world occurred (See Fig. 6.5). During ice house high frequency and high magnitude fluctuations in sea level were associated. Especially under those conditions, complete systems tracts may not develop.

The limestones at the north coast of Puerto Rico represent depositional cycles of Oligocene to Pliocene age. Therefore, a change in sequence character is observed, reflecting the transition into more icehouse conditions, within higher order sea level fluctuations. The cores and outcrops studied in this research show a change from well develop-complete depositional cycles to partial cycles and exposure surfaces, representing a change to high amplitude fluctuations. Based on data presented in this study the change occurs from the Undifferentiated Cibao Formation to Aguada (Los Puertos) Limestone until the Aymamón Limestone where an increase in exposure surfaces is noted.

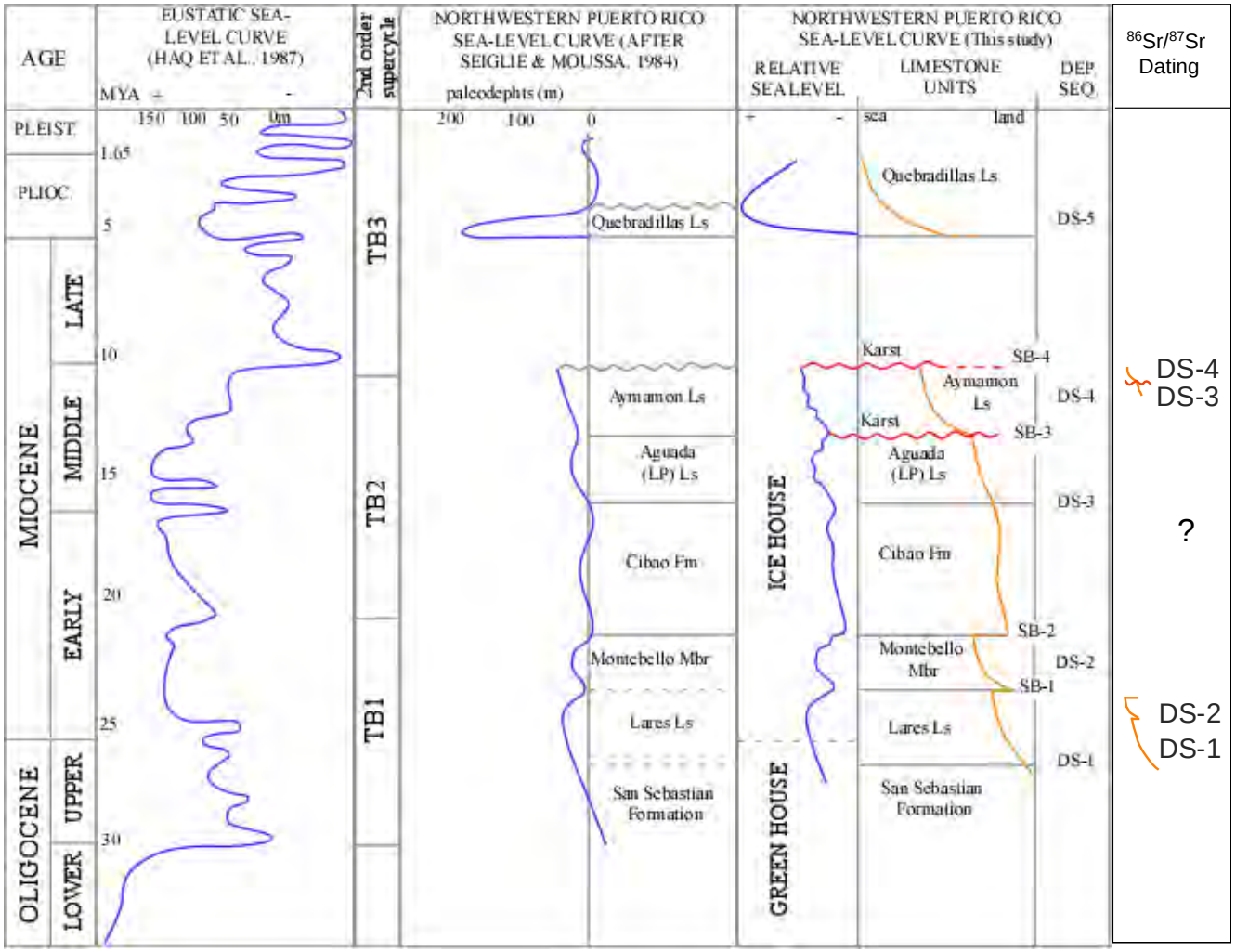

Figure 6.5: Comparison of Tertiary eustatic sea level curves (Haq et al., 1987) and Northwestern Puerto Rico (Seiglie and Moussa, 1984) with depositional sequences of northwestern Puerto Rico (this study). Age determinations from strontium isotope data are also included.

STRONTIUM ISOTOPE STRATIGRAPHY

Age determinations by strontium isotope stratigraphy (SIS) were used in attempt to better constrain the previous relative ages proposed to the north coast Tertiary limestones. The ages are mostly Oligocene and Miocene (see Table 4.3 and Figs. 4.19, 4.20 and 4.21). Based on these new dates, the results of the sequence stratigraphy for the north coast Tertiary limestones change significantly. Two tight groups can be observed: 1) a Late Oligocene to Early Miocene (25.97+/-0.32 to 24.07+/-0.16 Ma) that represents the San Sebastian Formation, Lares Limestone and Montebello Member; and 2) late Middle Miocene (12.07+/-0.53 to 10.91+/-0.34 Ma) that represents the Cibao Formation, Aguada (Los Puertos) Limestone and Aymamón Limestone.

Figure 6.5 shows the stratigraphy using the absolute ages obtained from $^{87}Sr/^{86}Sr$ ratios with depositional sequences 1 and 2 in Late Oligocene to Early Miocene, and a stratigraphic gap until late Middle Miocene and depositional sequences 3 and 4 in the late Middle Miocene. When comparing the new stratigraphy with the eustatic sea level curve, the local curve proposed in this study differs. The eustatic curve shows a high sea level during a time when the North Coast Tertiary Basin was exposed producing a sequence boundary between the Montebello Member and the Cibao Formation. This suggests a local relative sea level curve to the Tertiary limestone formations along the north coast of Puerto Rico probably due to tectonics.

CHAPTER 7

CONCLUSION AND FUTURE WORK

The main purpose of this Thesis is to construct a high-resolution sequence stratigraphy model for the middle Tertiary limestone formations on the north coast of Puerto Rico. Parasequences interpretations based on both outcrops and cores were used to accomplish this objective.

Five depositional sequences and four major sequence boundaries during Oligocene-Pliocene time are proposed. These are: The San Sebastian Formation-Lares Limestone; The Montebello Member; The Cibao Formation-Aguada (Los Puertos) Limestone; The Aymamón Limestone; and The Quebradillas Limestone. These are most probably related to the second-order supercycles TB1 (depositional sequences 1 and 2), TB2 (depositional sequences 3 and 4), and TB3 (depositional sequence 5) in terms of eustatic sea level changes (Haq et al., 1987).

The cores and outcrops studied in this research show a change from well develop-complete depositional cycles to partial cycles and exposure surfaces, representing the change from green-house to ice-house systems, i.e. to high amplitude sea level fluctuations.

This study proposes the Sequence Boundary-1 represented by an exposure surface (paleosol and dolomite) in the PR-111 outcrop and by siliciclastic-rich grainstones in the PR-10 outcrop, as the new lithologic contact between the Lares Limestone and the Montebello Member.

As a suggestion for future work the author emphasize the importance of constraining the Tertiary limestone formations ages by using recently developed methods for absolute dating like strontium isotope stratigraphy (SIS), in order to establish more precise sea level changes.

REFERENCES

Berkey, C.P., 1915, Geological reconnaissance of Porto Rico: New York Acad. Sci. Annals, v.26, p.1-70.

Berkey, C.P., 1919, Introduction to the geology of Porto Rico: New York Acad. Sci., Sci. Survey of Porto Rico and the Virgin Islands, v.1, pt.1, p.1-10.

Birch, F.S., 1986, Isostatic, thermal and flexural models of subsurface of the north coast of Puerto Rico: Geology, v. 14, p. 427-429.

Briggs, J.C. and Gordon, 1961, Geology of Kewanee Interamerican Oil Company test number 4CPR, *in* Oil and gas possibilities of Northern Puerto Rico; San Juan, Puerto Rico Mining Comm. p.1-23.

Dunham, R. J., 1962, Classification of carbonate rocks according to depositional texture. In: Flugel, E. 2004, Microfacies of Carbonate Rocks: Analysis, Interpretation and Application. Springer, Germany, p. 348-355.

Embry, AF, and Klovan, JE, 1971, The expanded and revised classification from Dunham, 1962. In: Flugel, E. 2004, Microfacies of Carbonate Rocks: Analysis, Interpretation and Application. Springer, Germany, p. 348-356.

Emery, D. & Myers, K. J., 1996, Sequence Stratigraphy, Blackwell Science Ltd, UK, 290p.

Erikson, J.P., Pindell, J.L., & Larue, D.K., 1990, Mid-Eocene-Early Oligocene Sinistral Transcurrent Faulting in Puerto Rico Associated with formation of the Northern Caribbean Plate Boundary Zone: Journal of Geology, 98, p.365-384.

Franseen, E., Goldstein, R., Farr, M., 1998, Quantitative controls on location and architecture of carbonate depositional sequences: Upper Miocene, Cabo de Gata Region, SE Spain. Journal of Sedimentary Research, v.68, No. 2, p.283-298.

Fluguel, E., 2004, Microfacies of Carbonate Rocks: Analysis, Interpretation and Application. Springer, Germany, 976p.

Frost, S.H., Harbour, J.L., Beach, D.K. Realini, M.J., and P.N. Harris, 1983, Oligocene reef track development, southwestern Puerto Rico: The Comparative Sedimentology Laboratory, Division of Marine Geology and Geophysics, Rosenstiel School of Marine & Atmospheric Science, University of Miami, 144p.

Glover, L., 1971, Geology of the Coamo area, Puerto Rico, and its relation to the volcanic arc-trench association: U.S.G.S. Professional Paper, 636, 102p.

Handford, C.R., and R.G. Loucks, 1993, Carbonate depositional sequences and systems tracts - responses of carbonate platforms to relative sea-level changes, *in* R.G. Loucks and J.F. Sarg, eds., Carbonate Sequence Stratigraphy: Recent Developments and Applications: AAPG Memoir 57, p. 3-41.

Haq, B.U., Hardenball, J., Vail, P., 1987, Mesozoic and Cenozoic chronostratigraphy and cycles of the sea level change, *in* Wilgus *et al.*, 1988, Sea-level changes: An integrated approach, SEPM Special Publication #42, p. 71-108.

Heisel, J.E., Gonzalez, J.R., and Cruz, C., 1983, Analog model analysis of the north coast limestone aquifers, Puerto Rico: U.S.G.S. Open File Report, 82-52, 49p.

Hartley, J.R., 1989, Subsurface Geology of the Tertiary carbonate rocks, Northwestern Puerto Rico: [unplub. M.S. thesis]: University of New Orleans, 213p.

Hubbard (1923), The Geology of Lares District, Puerto Rico: New York Academy of Science, Scientific Survey Puerto Rico and Virgin Islands, v. 3, p. 1-115.

Jolly, W.T., Lidiak, E.G., Dickin, A.P., and Tsai-way, W., 1998, Geochemical diversity of Mesozoic island arc tectonic blocks in eastern Puerto Rico: *in* Lidiak, E.G. and Larue, D.K. editors, Tectonics and Geochemistry of the Northeastern Caribbean, G.S.A. Special Paper 322, p. 67-99.

Larue, D.K., 1991, The Toa Baja drilling project, Puerto Rico: scientific drilling into a non-volcanic island arc massif: Geophysical Research Letters, v.18, p.489-492.

Matos, R., 2000, Controls on porosity in the North Coast Aymamón limestone: [unplub. M.S. thesis]: University of Puerto Rico at Mayaguez, 85p.

Mattson, P.H., 1984, Caribbean structural breaks and plate movements: G.S.A. Memoir 162, p. 131-153.

McArthur, J.M., 2001, Strontium Isotope Stratigraphy: LOWESS Version 3: Best Fit to the Marine Sr-Isotope Curve for 0-509 Ma and Accompanying Look-up Table for Deriving Numerical Age: The Journal of Geology, volume 109, p.155-170.

Meyerhoff, H.A., 1975, Stratigraphy and petroleum possibilities of middle Tertiary rocks in Puerto Rico (discussion): AAPG Bulletin, v.59, n.1, p. 169-172.

Meyerhoff, H.A., Krieg, E.A., Cloos, J.D. and Taner, I., 1983, Petroleum potential of Puerto Rico, Oil and Gas Journal, v.81, p.113-120.

Mitchum, R.M., Vail, P.R. & Thompson, S., 1977, Seismic Stratigraphy and Global Changes of Sea Level, Part 2: The Depositional Sequence as a Basic Unit for Stratigraphic Analysis, in Payton C. E. (ed): AAPG Memoir 26 Seismic Stratigraphy- Applications to Hydrocarbon Exploration, p. 53-62.

Mitchum, R.M., 1977, Seismic Stratigraphy and Global Changes of Sea Level, Part 11: Glossary of Terms used in Seismic Stratigraphy, in Payton C. E. (ed): AAPG Memoir 26 Seismic Stratigraphy- Applications to Hydrocarbon Exploration, p. 205-212.

Monroe, W.H., 1968, The Aguada Limestone of northwest Puerto Rico: U.S.G.S. Bull 1274-G, p. G1-G12.

Monroe, W.H., 1969, Geological Map of Moca and Isabella quadrangles, Puerto Rico: U.S.G.S. Miscellaneous Geological Investigation Map I-565, scale 1:20,000.

Monroe, W. H, 1975, Stratigraphy and petroleum possibilities of middle Tertiary rocks in Puerto Rico (reply): AAPG Bulletin, v. 59, n. 1, p. 172-173.

Monroe, W. H., 1980, Geology of the middle Tertiary formations of Puerto Rico: U.S. Geological Survey Professional Paper 953, 93p.

Monroe, W. H., 1963, Geology of the Camuy Quadrangle, Puerto Rico, U.S. Geological Survey, MAP GQ-197, scale 1: 20,000.

Montgomery, P., Farr, M., Franseen, E. & Goldstein, R (2001): Constraining controls on carbonate sequences with high-resolution chronostratigraphy: Upper Miocene, Cabo de Gata region, SE Spain. Journal of Palaeogeography, Palaeoclimatology, Palaeoecology # 176, p. 11-45.

Moussa, M., Seiglie, G., Meyerhoff, A. & Taner, I., 1987, The Quebradillas Limestone (Miocene-Pliocene), northern Puerto Rico, and tectonics of the northeastern Caribbean margin. Geological Society of America Bulletin, v. 99, p. 427-439.

Nelson, A. E., 1967, Geologic Map of the Utuado Quadrangle, Puerto Rico, U.S. Geological Survey, Miscellaneous Geologic Investigations, MAP I-480, scale 1:20,000.

Nelson, A. E., Tobisch O.T., 1968, Geologic Map of the Bayaney Quadrangle, Puerto Rico, U.S. Geological Survey, Miscellaneous Geologic Investigations, MAP I-525, scale 1:20,000.

Nelson, A.E., and Monroe, W.H., 1966, Geology of the Florida Quadrangle, Puerto Rico: U.S.G.S. Bull, 1221-C, 22p.

Pindell, J.L., and Barret, S.F., 1990, Geological Evolution of the Caribbean region: a plate tectonic perspective: *in* Dengo, G., and Case, J.E., eds., The Caribbean Region: Boulder Colorado, G.S.A., The Geology of North America, v. H, p. 405-432.

Pindell, J., Kennan, L., Stanek, K., Maresch, W. and Draper, G., 2006, Foundations of Gulf of Mexico and Caribbean evolution: eight controversies resolved: Geologica Acta, Vol.4, Nº1-2, 2006, p. 303-341.

Pomar, L. & Ward, W., 1991, Características de las secuencias deposionales de alta frecuencia en el sistema arrecifal del Mioceno superior de Mallorca. Acta Geológica Hispánica, V. 26, N 3-4, p. 181-194.

Posamentier, H.W., Jervey, M.T., Vail, P.R., 1988, Eustatic controls on clastic deposition. I. Conceptual framework: *in* Wilgus, C.K., Hastings, B.S., Kendall, C.G.St.C., Posamentier, H.W., Ross, C.A., Van Wagoner, J.C. (Eds.), Sea Level Changes—An Integrated Approach, vol. 42. SEPM Special Publication, p. 110–124.

Posamentier, H.W., Vail, P.R., 1988, Eustatic controls on clastic deposition. II. Sequence and systems tract models: *in* Wilgus, C.K., Hastings, B.S., Kendall, C.G.St.C., Posamentier, H.W., Ross, C.A., Van Wagoner, J.C. (Eds.), Sea Level Changes—An Integrated Approach, vol. 42. SEPM Special Publication, p. 125– 154.

Ramírez, W., 2000, Dolomitization and evolution of the Puerto Rico North Coast confined aquifer system, Ph.D Thesis, Tulane University. 337p.

Ramírez, W.R., Johnson, C., Martinez, M., Torres, M., Ortiz, V., and Velez, J., 2006, Strontium Isotope Stratigraphy from *Kuphus incrassatus*, Cenozoic Limestones, Puerto Rico, Abstract in GSA Annual Meeting, Abstracts with Program, Vol. 39, No. 7, p. 90.

Reid, J.A., Plumley, P.W., and Schellekens, J.H., 1991, Paleomagnetic evidence for Late Miocene counter-clockwise rotation of north coast carbonate sequence, Puerto Rico: Geophysical Research Letters, v.18, No.3, p. 565-568.

Renken, R., Ward, W.C., Gill I.P., Gómez-Gómez, F., Rodríguez-Martínez, J. and others, 2002, Geology and Hydrogeology of the Caribbean Islands Aquifer System of the Commonwealth of Puerto Rico and the U.S. Virgin Islands Regional Aquifer-System Analysis. U.S. Geological Survey, Professional Paper 1419, 148p.

Renken, R.A., and Gómez-Gómez, F., 1994, Potentiometric surfaces of the upper and lower aquifers, North Coast limestone aquifer system, northern Puerto Rico: U.S. Geological Survey Open-File Report 93-499, 16p.

Rodriguez-Martinez, J., 1995, Hydrogeology of the North Coast Limestone Aquifer System of Puerto Rico: U.S.G.S. Water Resources Investigations, Report 94-4249, 22p.

Rodriguez-Martinez, J. and Hartley, J.L., 1994a, Geologic and hydrologic data collected at test holes NC-6 and NC-11, Hatillo and Isabela, Northwestern Puerto Rico: U.S.G.S. Open File Report, 93-465, 39p.

Rodriguez-Martinez, J., Hartley, J.L., and Torres-Gonzalez, A., 1991a, Geologic and hydrologic data collected at test well NC-5, Barceloneta, Puerto Rico: U.S. Geological Survey Open File Report, 90-390, 30 p.

Rodríguez-Martínez, J., 1990, The hydrogeologic framework of the northern coastal province aquifer system of Puerto Rico, in Gómez-Gómez, Fernando, Quiñones-Aponte, Vicente, and Johnson, A.I., eds., Regional aquifer systems of the United States--Aquifers of the Caribbean Islands: American Water-Resources Association Monograph Series No. 15, p. 5-16.

Sarg, J.F., 1988, Carbonate Sequence Stratigraphy: *in*: C.K. Wilgus, B.S. Hastings, C.A. Ross, H.W. Posamentier, J. C. Van Wagoner and C. G. S. C. Kendall, eds., Sea-level Changes, an Integrated Approach: SEPM Special Publication 42, p. 155-181.

Schellekens, J.H., 1998, Geochemical evolution and tectonic history of Puerto Rico: Geological Society of America Special Paper 322: Tectonics and Geochemistry of the Northeastern Caribbean, p. 35-66.

Schellekens, J.H., 1991, Late Jurassic to Eocene geochemical evolution of volcanic rocks of Puerto Rico: Geophysical Research Letters, v.18, p.533-556.

Seiglie, G. & Moussa, M., 1975, Paleoenvironments of Quebradillas Limestone (Tertiary), northern Puerto Rico, and their geologic significance: AAPG Bulletin, v. 59, p. 2314-2321.

Seiglie, G. & Moussa, M., 1984, Late Oligocene-Pliocene Transgressive-Regressive Cycles of Sedimentation in Northwestern Puerto Rico: AAPG Memoir 36, p. 89-95.

Scharlach, R. A, 1990, Depositional History of Oligocene-Miocene carbonate rocks, subsurface of Northeastern Rico: [unplub. M.S. thesis]: University of New Orleans. 242p.

Smith, A., Schellekens, J.H. & Muriel-Díaz, A., 1998, Batholiths as markers of tectonic change in the northeastern Caribbean: Geological Society of America Special Paper 322: Tectonics and Geochemistry of the Northeastern Caribbean, p. 99-122.

Sykes, L.R., Mccann, W.R., and Kafka, A.L., 1982, Motions of the Caribbean Plate during the last seven million years and implications for earlier Cenozoic movements: Journal of Geophysical Research, v.87, p.1065-1076.

Todd, P.C., 1996, Lithology and depositional history of the Oligocene-Miocene section in two wells in northern Puerto Rico: [unpb. M.S. Thesis]: University of New Orleans, 74p plus appendixes.

Torres-González, S., Planert, M., and Rodríguez, J.M., 1996, Hydrogeology and simulation of ground-water flow in the upper aquifer of the Río Camuy to Río Grande de Manatí area, Puerto Rico: U.S. Geological Survey Water Resources Investigations Report 95-4286, 102p.

Tucker, M. & Wright, V. P., 1990, Carbonate Sedimentology Chapter 2, Blackwell Science Ltd, UK, p. 28-67.

Vail, P.R., Mitchum, R.M., and Thompson, S., 1977, Global cycles of relative changes in sea level : *in* C.E. Payton, ed. Seismic Stratigraphy-applications to hydrocarbon exploration, A.A.P.G. Memoir, v26, p. 83-89.

Van Wagoner, J.C., Posamentier, H.W., Mitchum, R.M., Vail, P.R., Sarg, J.F., Loutit, T.S., Hardenbol, J., 1988, An overview of sequence stratigraphy and key definitions: *in* Wilgus, C.K., Hastings, B.S., Kendall, C.G.St.C., Posamentier, H.W., Ross, C.A., Van Wagoner, J.C. (Eds.), Sea Level Changes—An Integrated Approach, vol. 42. SEPM Special Publication, p. 39–45.

Van Wagoner, J.C., Mitchum Jr., R.M., Campion, K.M., Rahmanian, V.D., 1990, Siliciclastic sequence stratigraphy in well logs, core, and outcrops: concepts for high-resolution correlation of time and facies. American Association of Petroleum Geologists Methods in Exploration Series 7, 55p.

Ward, W.C., Scharlach, R.A., and Hartley, J.R., 2002, Geology of the North Coast ground-water province of Puerto Rico: *in* Renken R.A., and others, Geology and Hydrogeology of the Caribbean-Islands Aquifer System of the Commonwealth of Puerto Rico and the U.S. Virgin Islands: U.S. Geological Survey Professional Paper 1419, p. 45-76.

Ward, W.C., Scharlach, R.A., and Hartley, J.R., 1991, Controls on porosity and permeability in subsurface Tertiary carbonate rocks of northern Puerto Rico in Gómez-Gómez, Fernando, Quiñones-Aponte, Vicente, and Johnson, A.I. eds., Regional aquifer systems of the United States--Aquifers of the Caribbean Islands, American Water-Resources Association Monograph Series No. 15, p. 17-23.

Wilson, J.L., 1975, Carbonate facies belt in geologic history: Springer-Verlag, New York, Heidelberg, Berlin, p. 471.

Zapp, A.D., Berquist, H.R., and Thomas, C.R., 1948, Tertiary geology of the coastal plains of Puerto Rico: U.S.G.S. Oil and Gas Investigation Preliminary Map 85.

APPENDIX 1
NC-6 AND NC-5 STRATIGRAPHIC COLUMNS INCLUDING ROCK TEXTURE AND CONSTITUENTS

NC-6 AND NC-5 ROCK TEXTURE AND COMPOSITION

LEGEND

Foraminifers		**NON-SK**	Non-skeletal
B	Benthics	**Intra**	Intraclasts
P	Planktonics	**Pello**	pelloids
COR	Corals	**SED. STR.**	Sedimentary structures
ALG	Algae	**BIOT**	bioturbation
RA	Red algae	**LAM**	lamination
HAL	Halimeda	**CALI**	caliche
MOL	Mollusks	**MIN. COMP.**	Mineral composition
ECH	Echinoderms	**CHAL**	chalky
BRY	Bryozoans	**QZ**	quartz
OST	Ostracodes	**DOL**	dolomite

NC-6 TEST HOLE

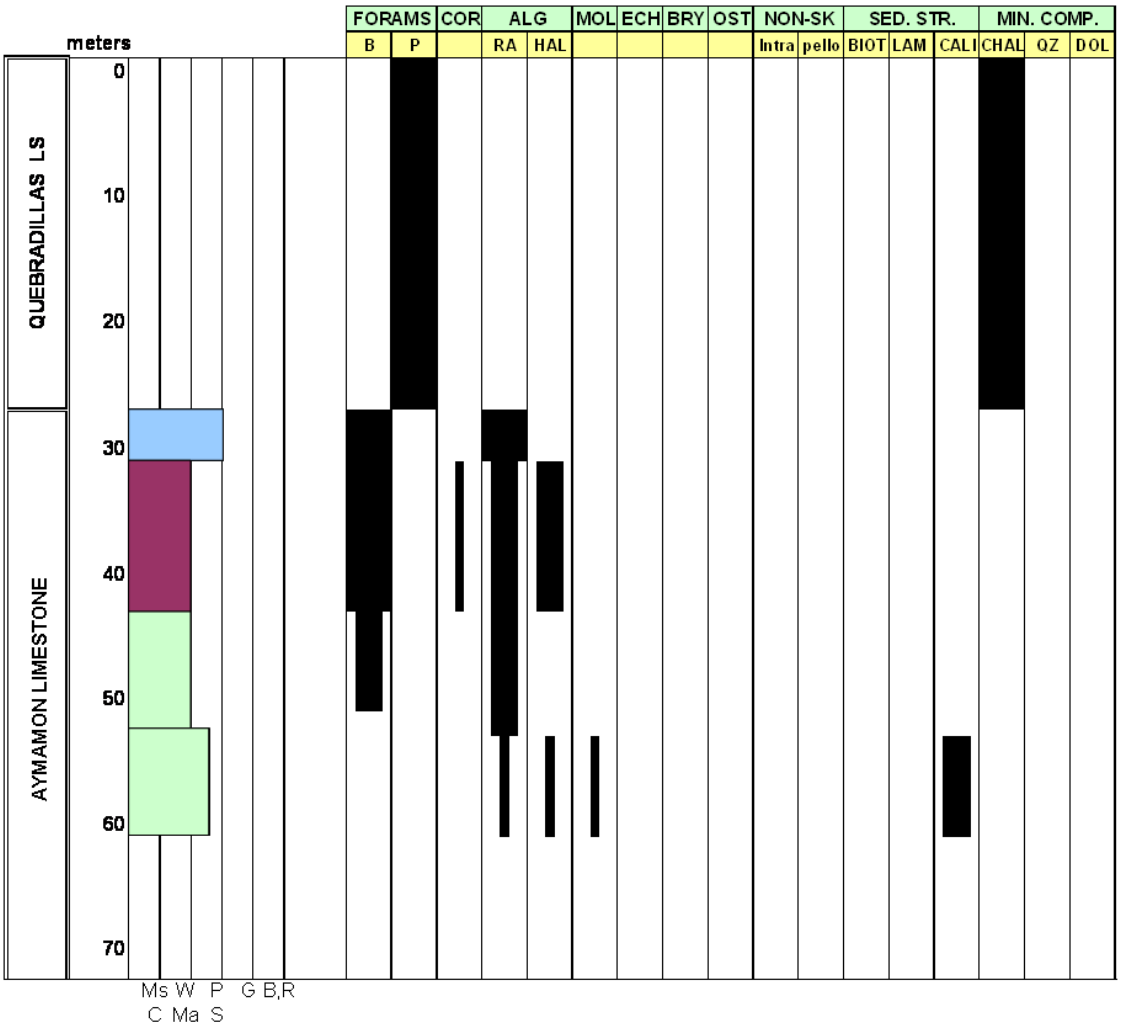

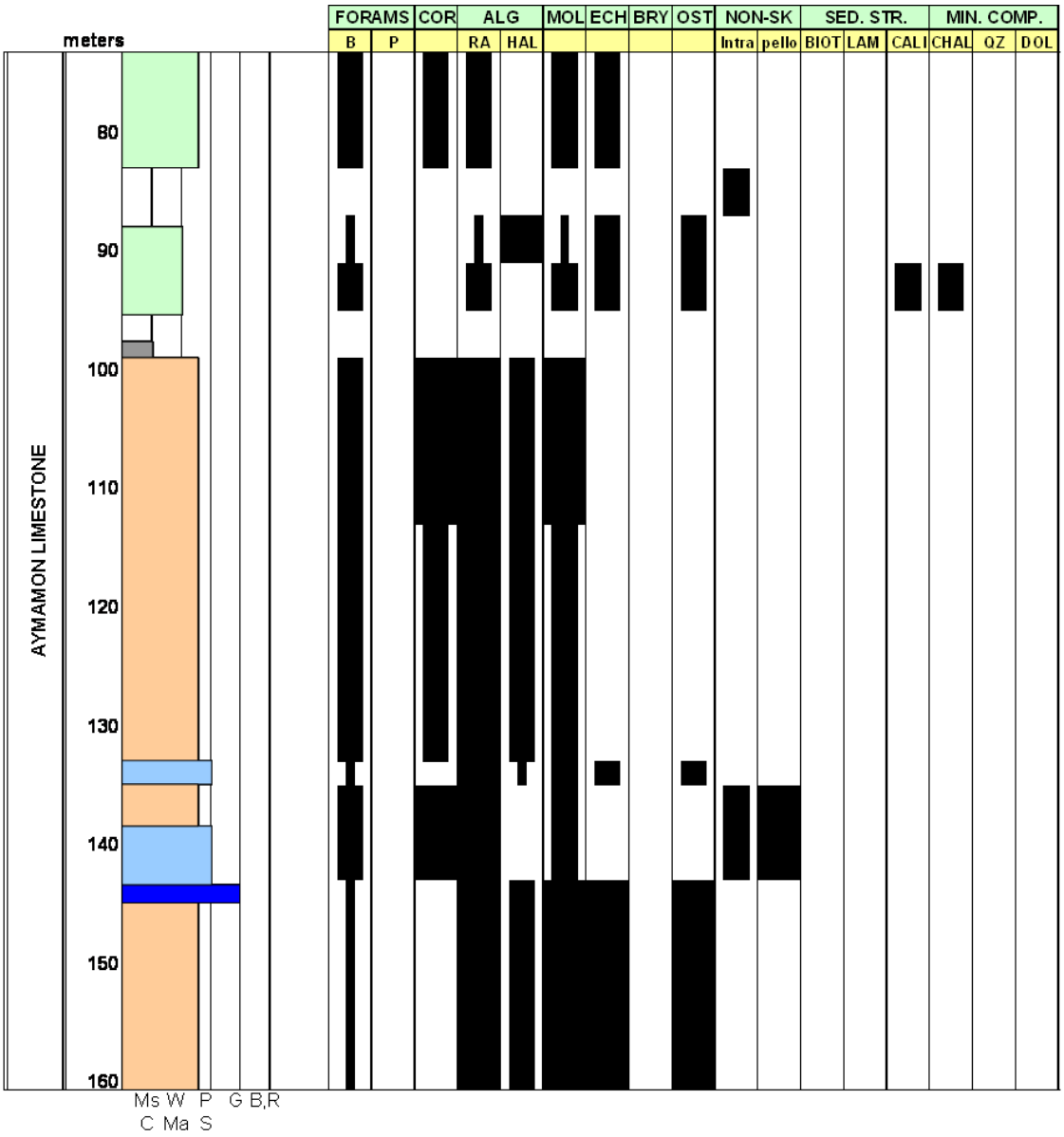
FORAMS
COR
ALG
MOL
ECH
BRY
OST
NON-SK
SED. STR.
MIN. COMP.
B
P
RA
HAL
Intra
pello
BIOT
LAM
CALI
CHAL
QZ
DOL
meters
80
90
100
110
120
130
140
150
160
AYMAMON LIMESTONE
Ms W P G B,R
C Ma S

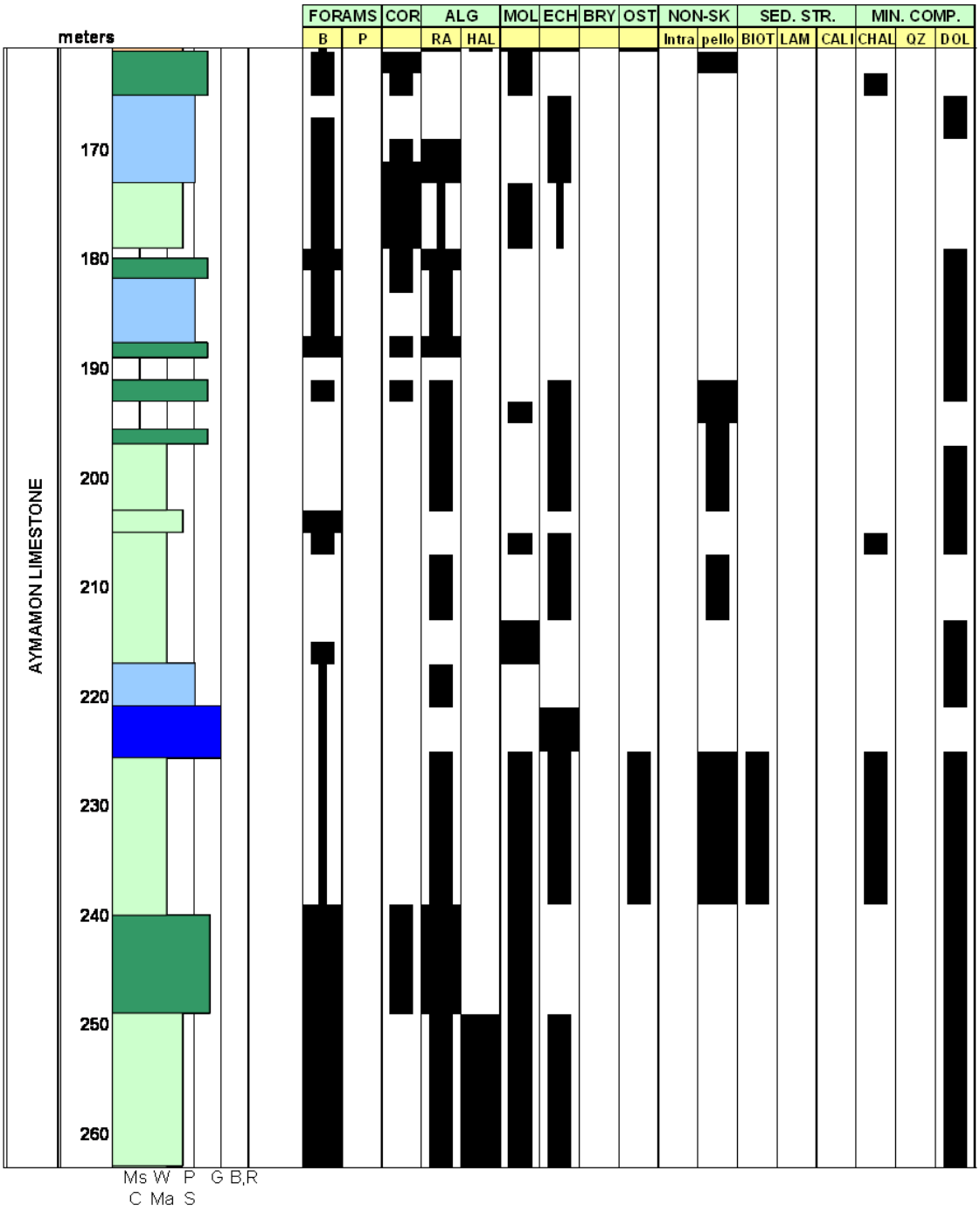
meters
AYMAMON LIMESTONE
170
180
190
200
210
220
230
240
250
260
Ms W P G B,R
C Ma S
FORAMS
B
P
COR
ALG
RA
HAL
MOL
ECH
BRY
OST
NON-SK
Intra
pello
SED. STR.
BIOT
LAM
CALI
MIN. COMP.
CHAL
QZ
DOL

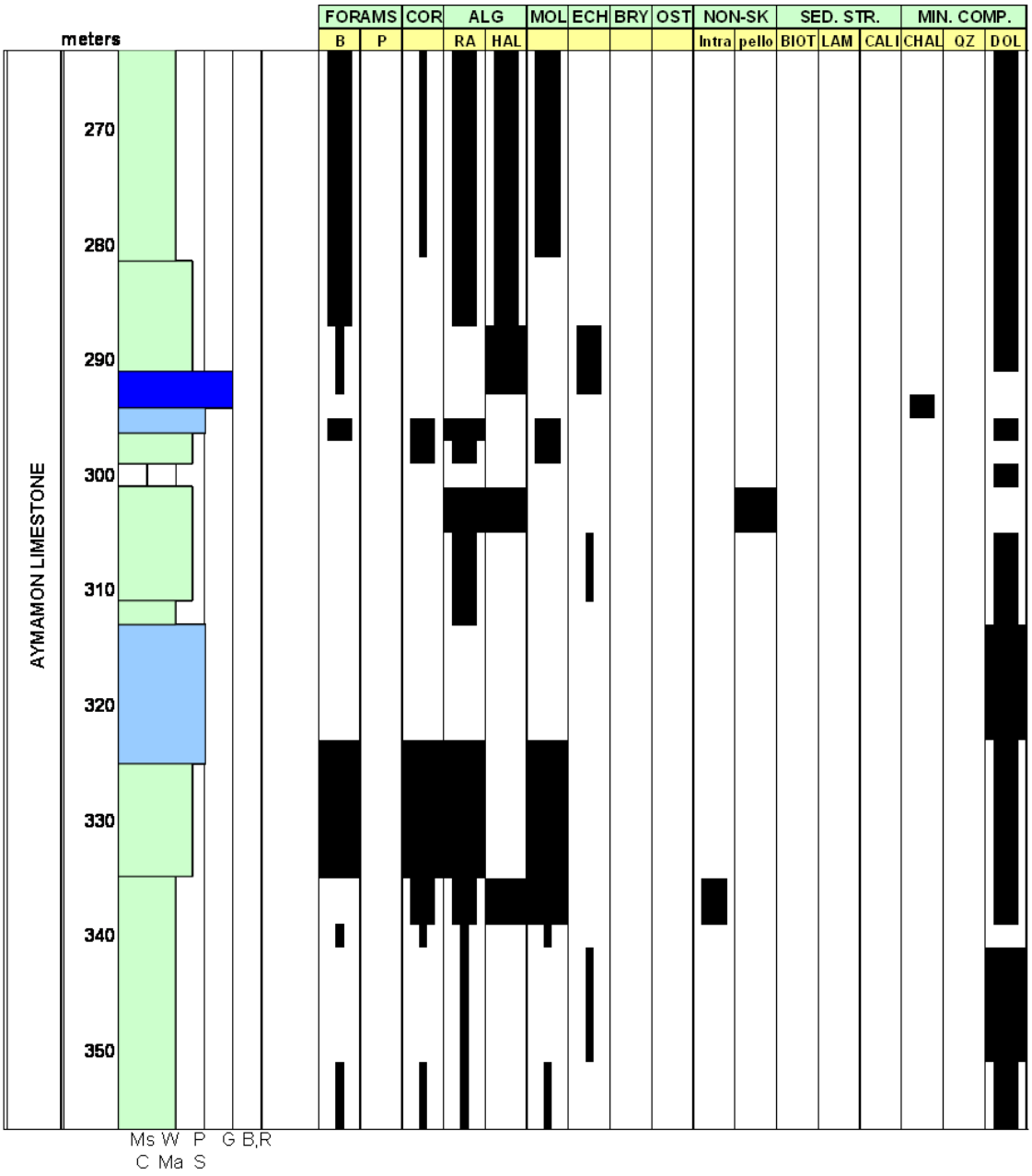
meters
FORAMS
COR
ALG
MOL
ECH
BRY
OST
NON-SK
SED. STR.
MIN. COMP.
B
P
RA
HAL
Intra
pello
BIOT
LAM
CALI
CHAL
QZ
DOL
AYMAMON LIMESTONE
270
280
290
300
310
320
330
340
350
Ms W P G B,R
C Ma S

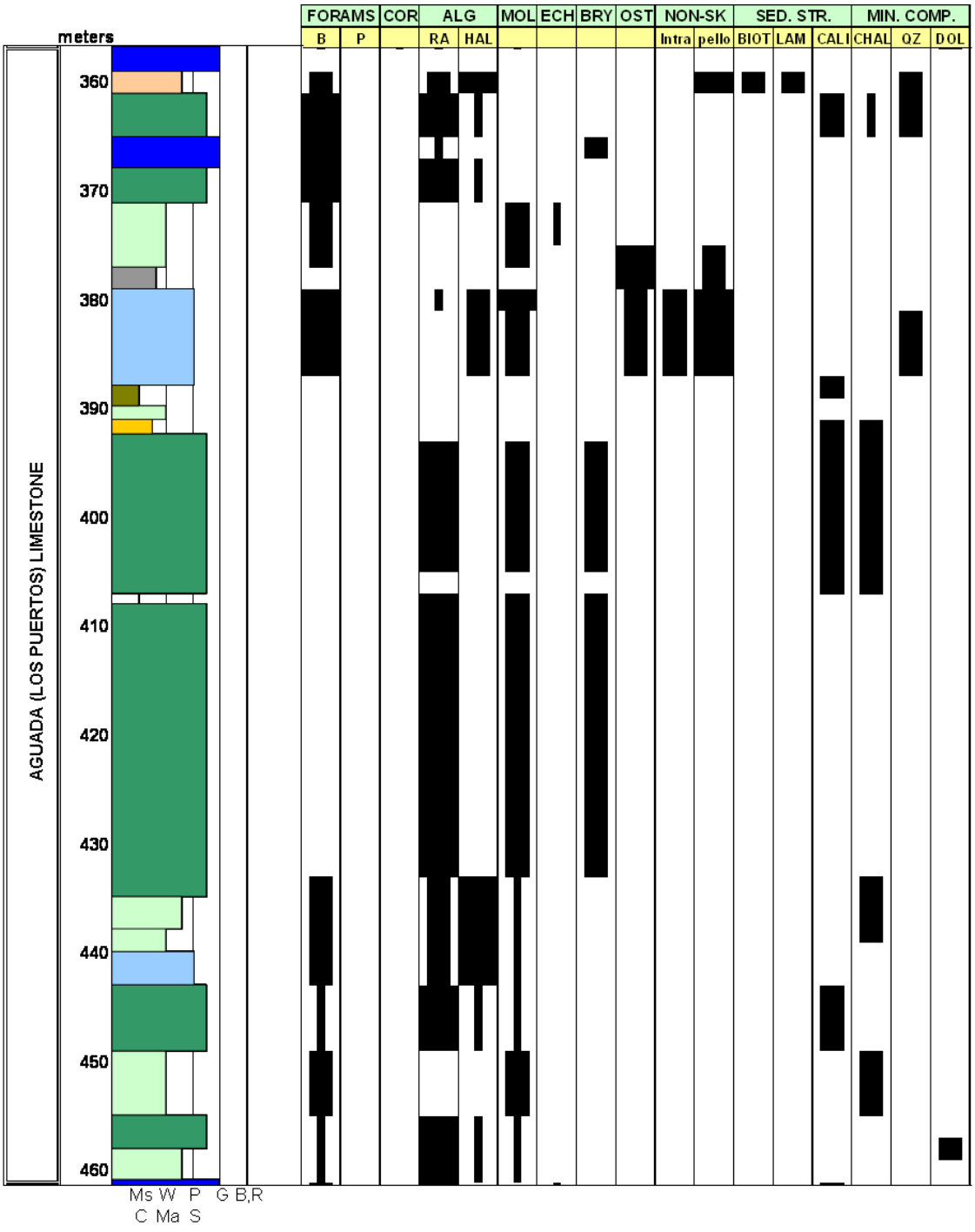
AGUADA (LOS PUERTOS) LIMESTONE
meters
360
370
380
390
400
410
420
430
440
450
460
FORAMS
B
P
COR
ALG
RA
HAL
MOL
ECH
BRY
OST
NON-SK
Intra
pello
SED. STR.
BIOT
LAM
MIN. COMP.
CALI
CHAL
QZ
DOL
Ms W P G B,R
C Ma S

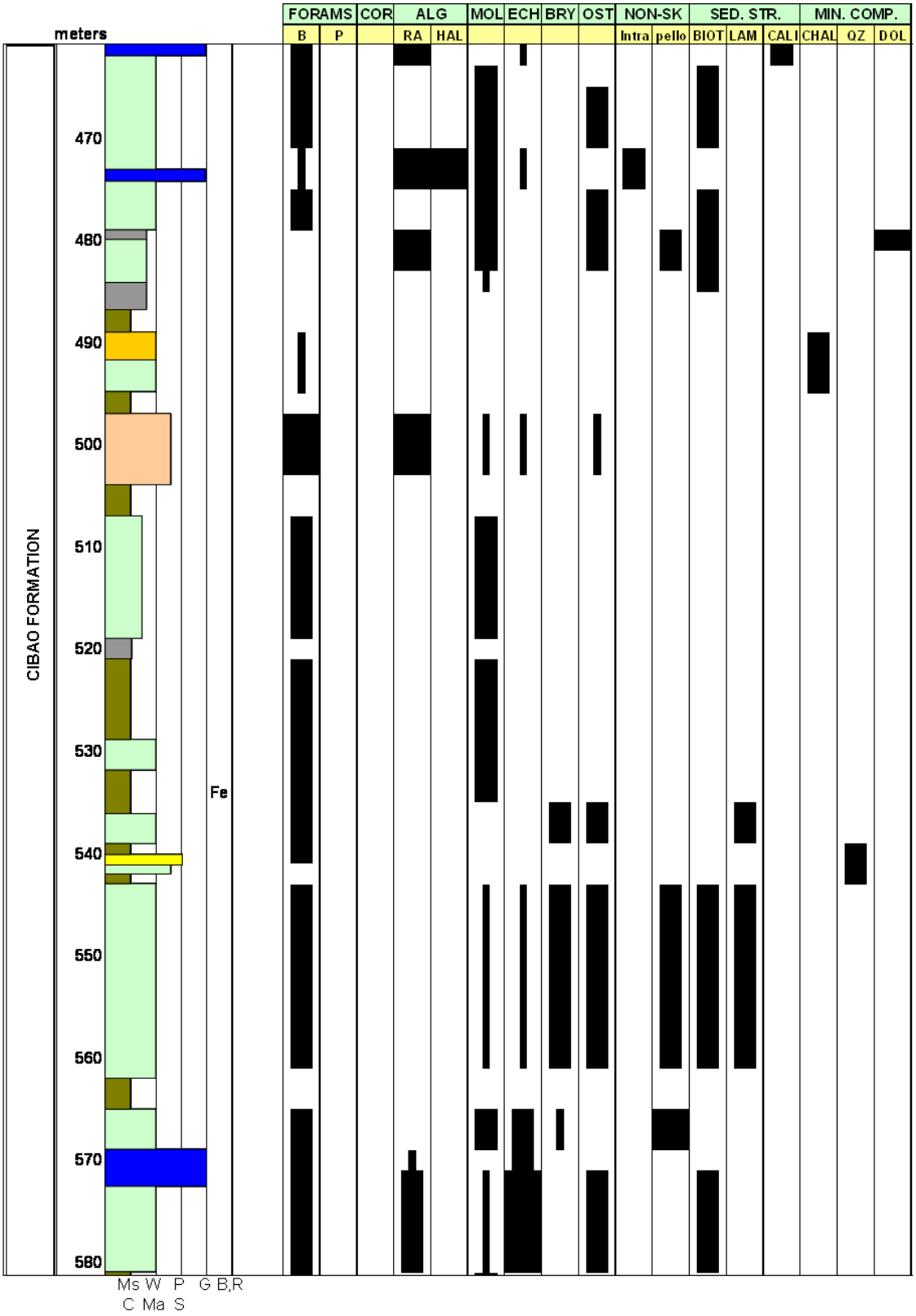
meters
FORAMS
COR
ALG
MOL
ECH
BRY
OST
NON-SK
SED. STR.
MIN. COMP.
B
P
RA
HAL
Intra
pello
BIOT
LAM
CALI
CHAL
QZ
DOL
CIBAO FORMATION
470
480
490
500
510
520
530
540
550
560
570
580
Fe
Ms W P G B,R
C Ma S

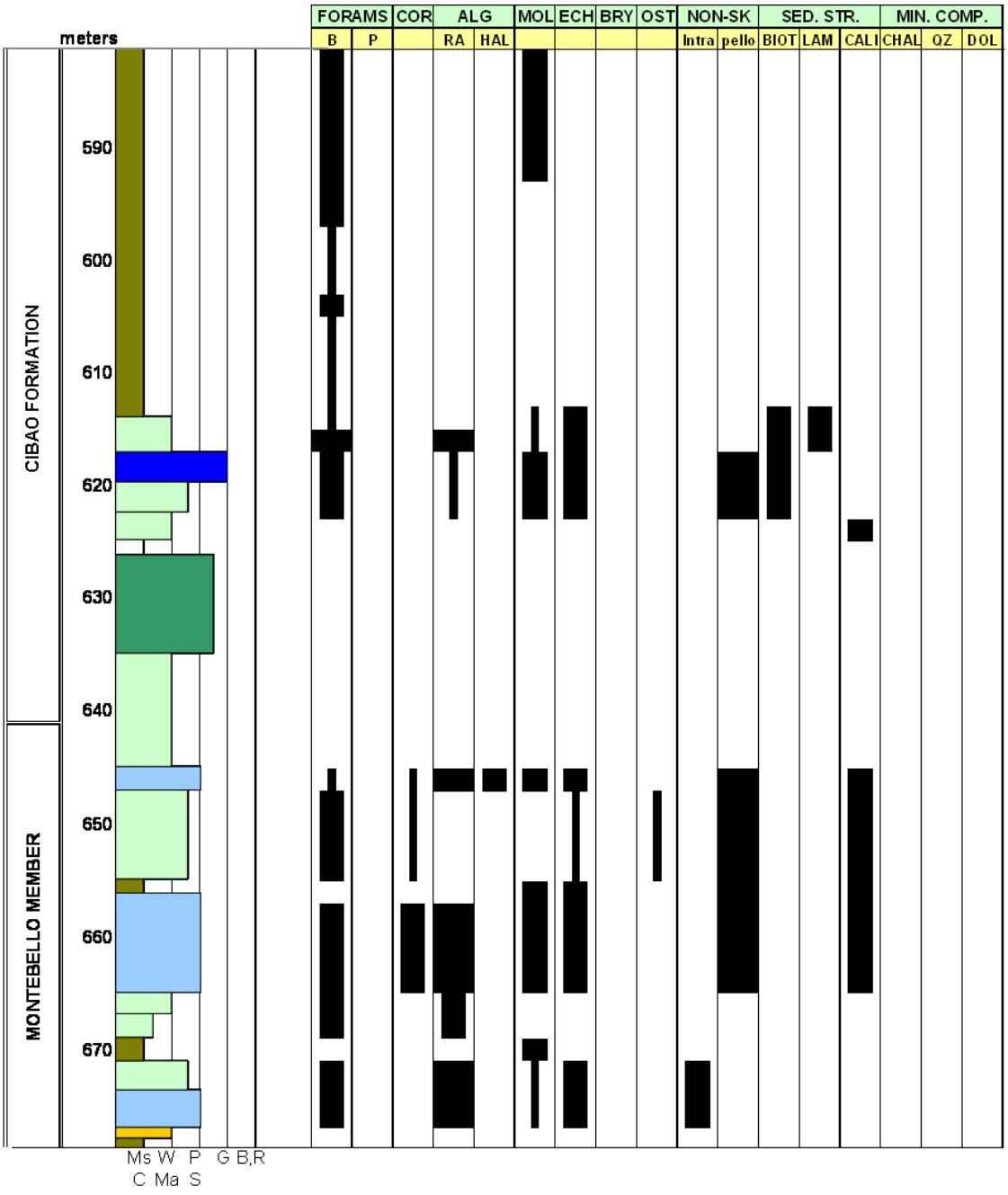
meters
FORAMS
COR
ALG
MOL
ECH
BRY
OST
NON-SK
SED. STR.
MIN. COMP.
B
P
RA
HAL
Intra
pello
BIOT
LAM
CALI
CHAL
QZ
DOL
CIBAO FORMATION
MONTEBELLO MEMBER
590
600
610
620
630
640
650
660
670
Ms W P G B,R
C Ma S

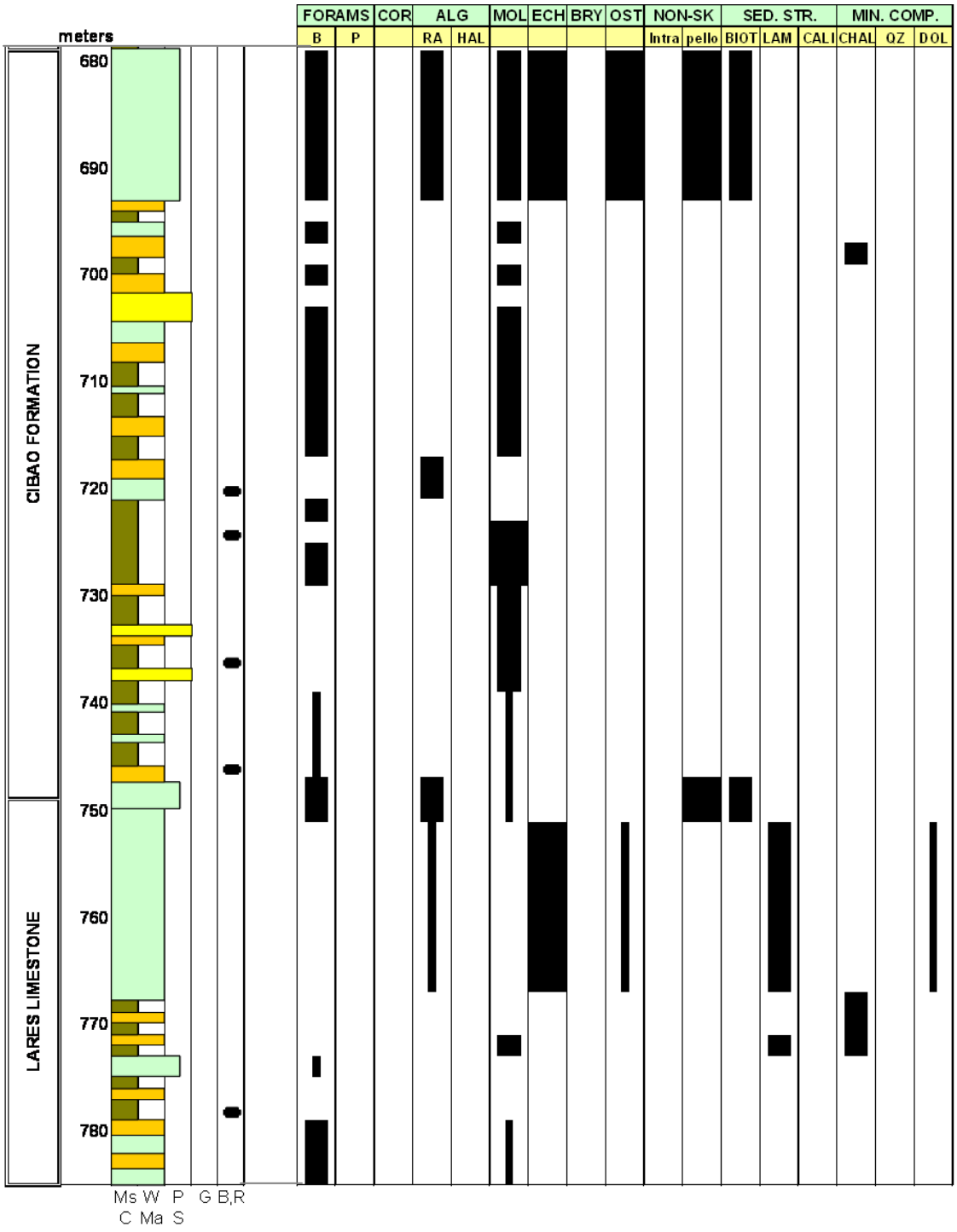
meters
680
690
700
710
720
730
740
750
760
770
780
CIBAO FORMATION
LARES LIMESTONE
FORAMS
B
P
COR
ALG
RA
HAL
MOL
ECH
BRY
OST
NON-SK
Intra
pello
SED. STR.
BIOT
LAM
CALI
MIN. COMP.
CHAL
QZ
DOL
Ms W P G B,R
C Ma S

NC-5 TEST HOLE

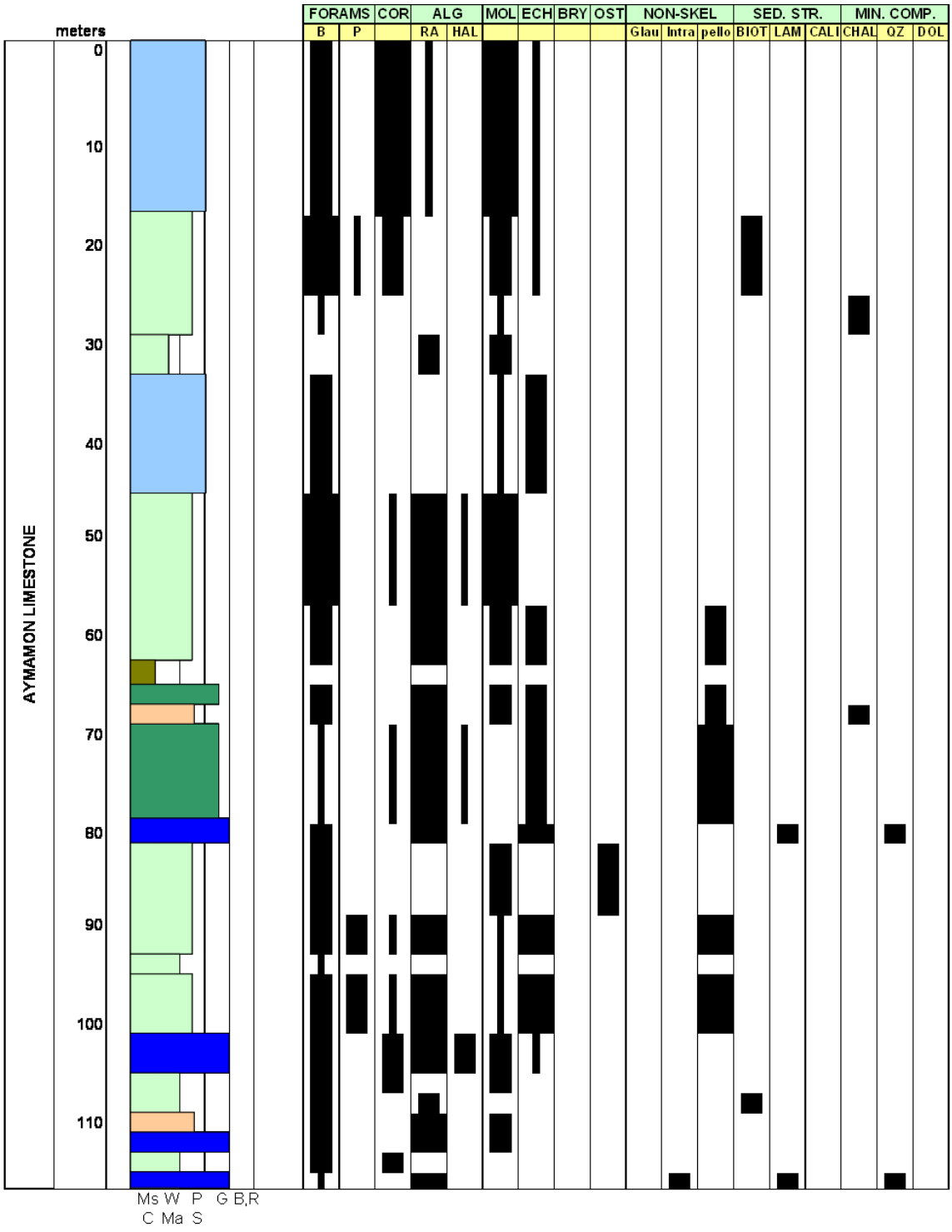

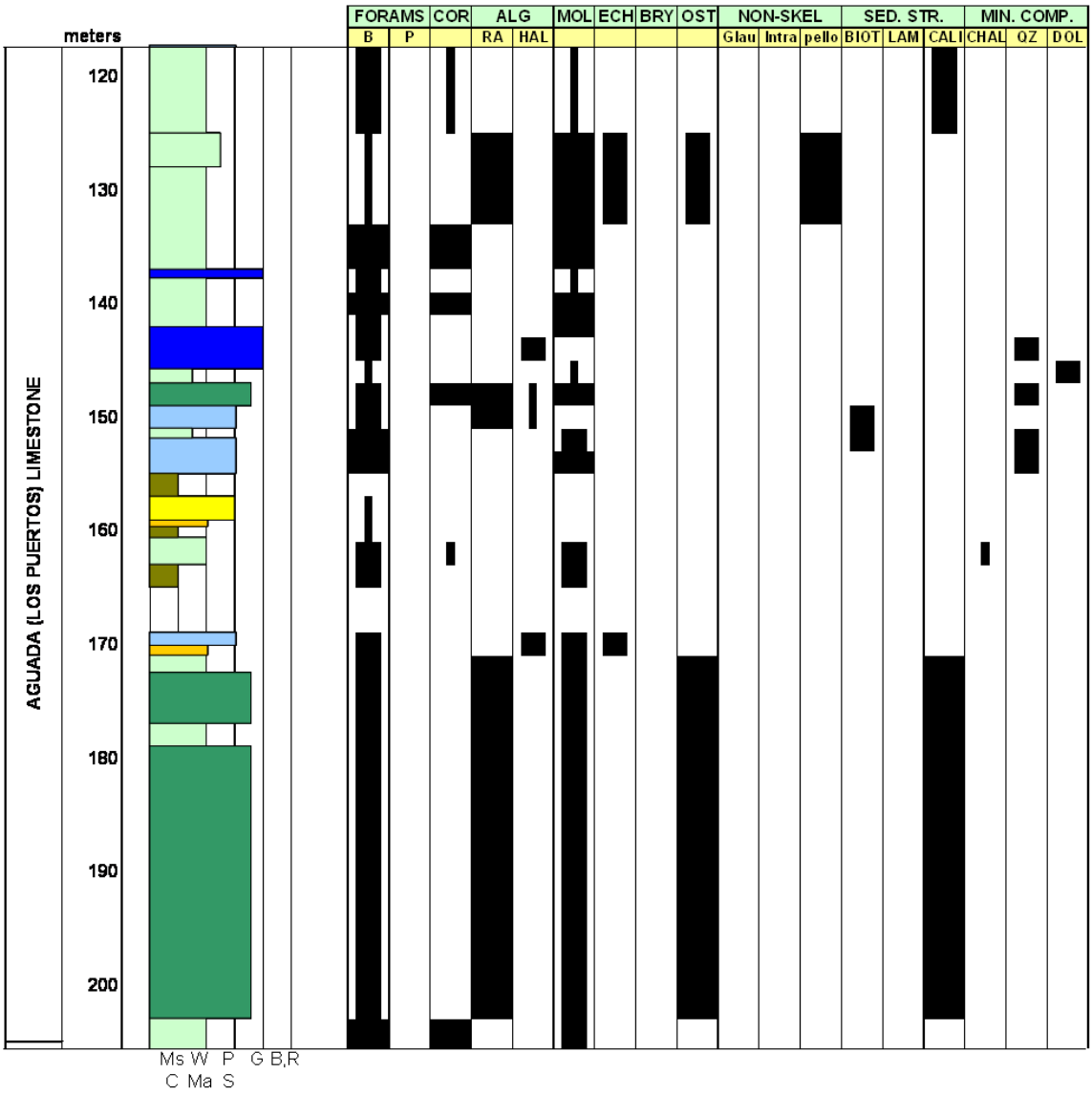
FORAMS
COR
ALG
MOL
ECH
BRY
OST
NON-SKEL
SED. STR.
MIN. COMP.
B
P
RA
HAL
Glau
Intra
pello
BIOT
LAM
CALI
CHAL
QZ
DOL
meters
120
130
140
150
160
170
180
190
200
AGUADA (LOS PUERTOS) LIMESTONE
Ms W P G B,R
C Ma S

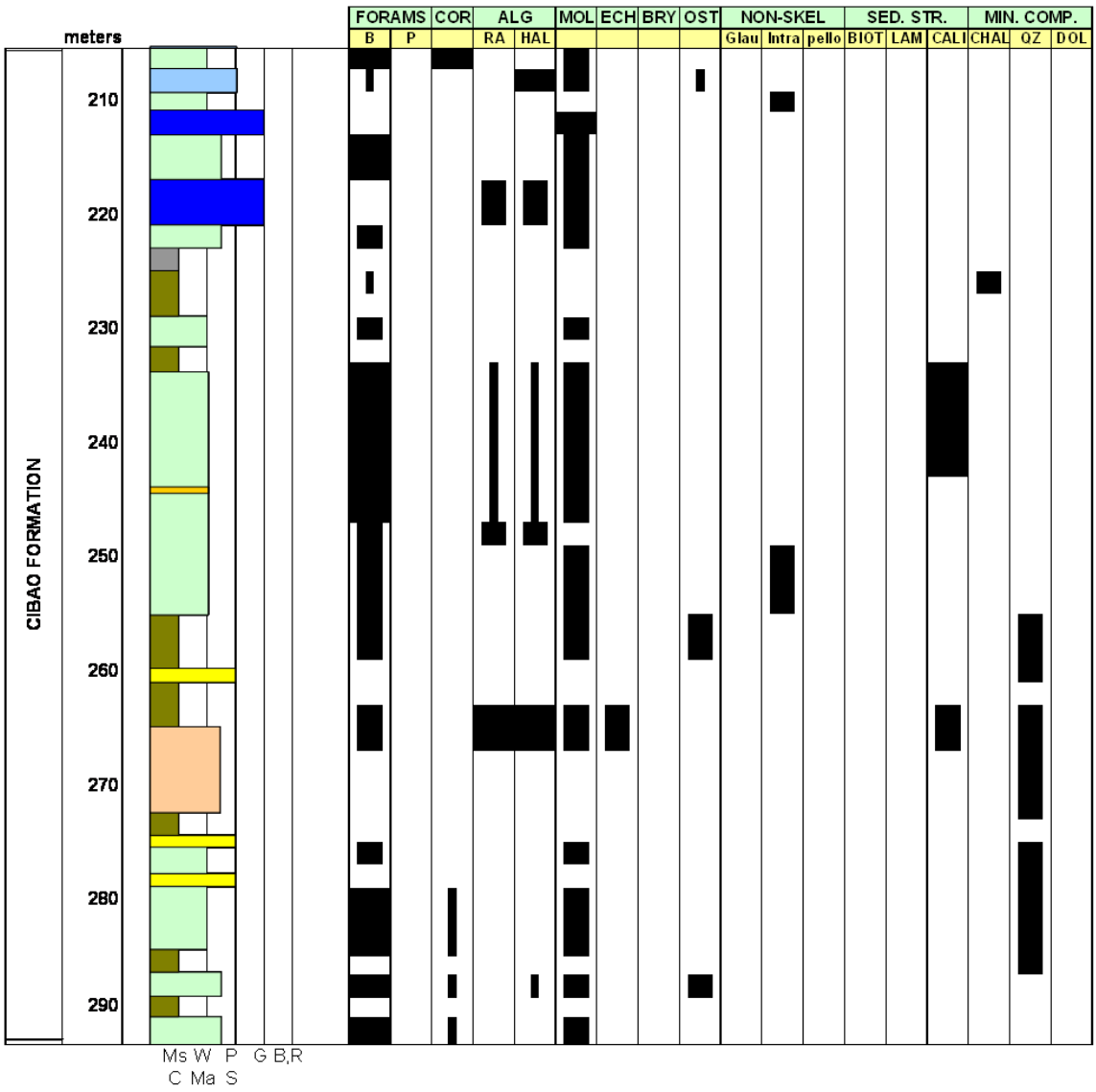
meters
CIBAO FORMATION
210
220
230
240
250
260
270
280
290
FORAMS
B
P
COR
ALG
RA
HAL
MOL
ECH
BRY
OST
NON-SKEL
Glau
Intra
pello
SED. STR.
BIOT
LAM
CALI
MIN. COMP.
CHAL
QZ
DOL
Ms W P G B,R
C Ma S

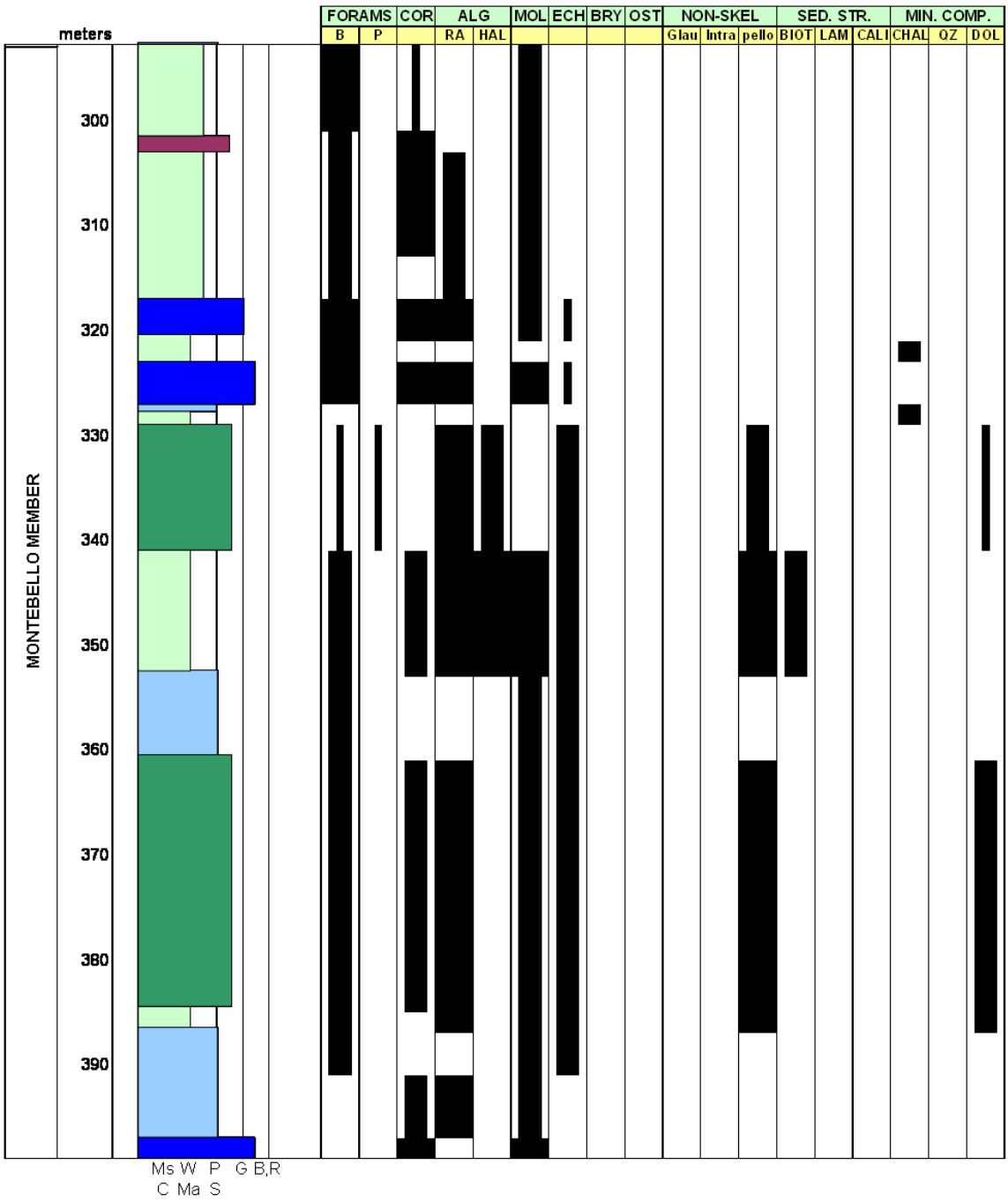
meters
FORAMS
COR
ALG
MOL
ECH
BRY
OST
NON-SKEL
SED. STR.
MIN. COMP.
B
P
RA
HAL
Glau
Intra
pello
BIOT
LAM
CALI
CHAL
QZ
DOL
MONTEBELLO MEMBER
300
310
320
330
340
350
360
370
380
390
Ms W P G B,R
C Ma S

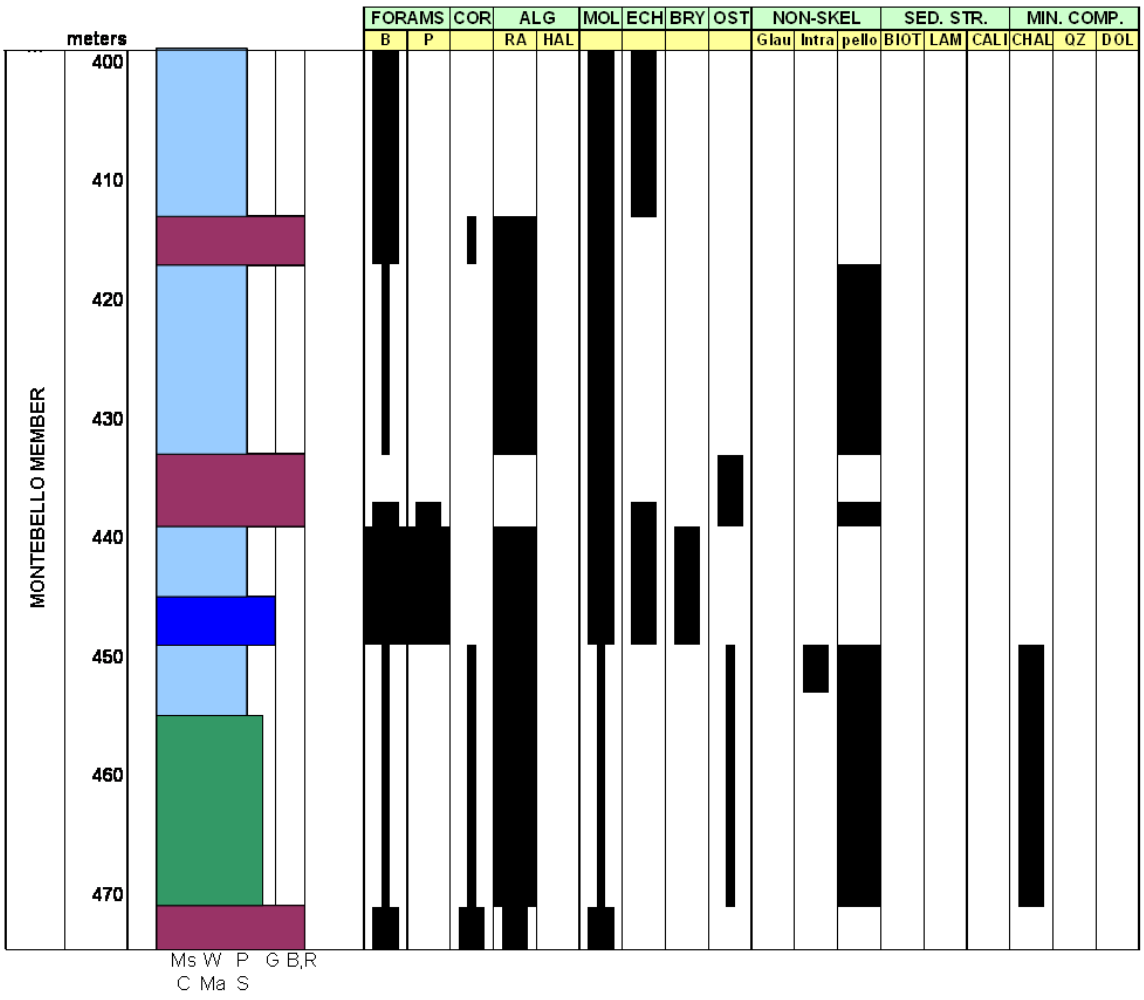
meters
FORAMS
COR
ALG
MOL
ECH
BRY
OST
NON-SKEL
SED. STR.
MIN. COMP.
B
P
RA
HAL
Glau
Intra
pello
BIOT
LAM
CALI
CHAL
QZ
DOL
400
410
420
430
440
450
460
470
MONTEBELLO MEMBER
Ms W P G B,R
C Ma S

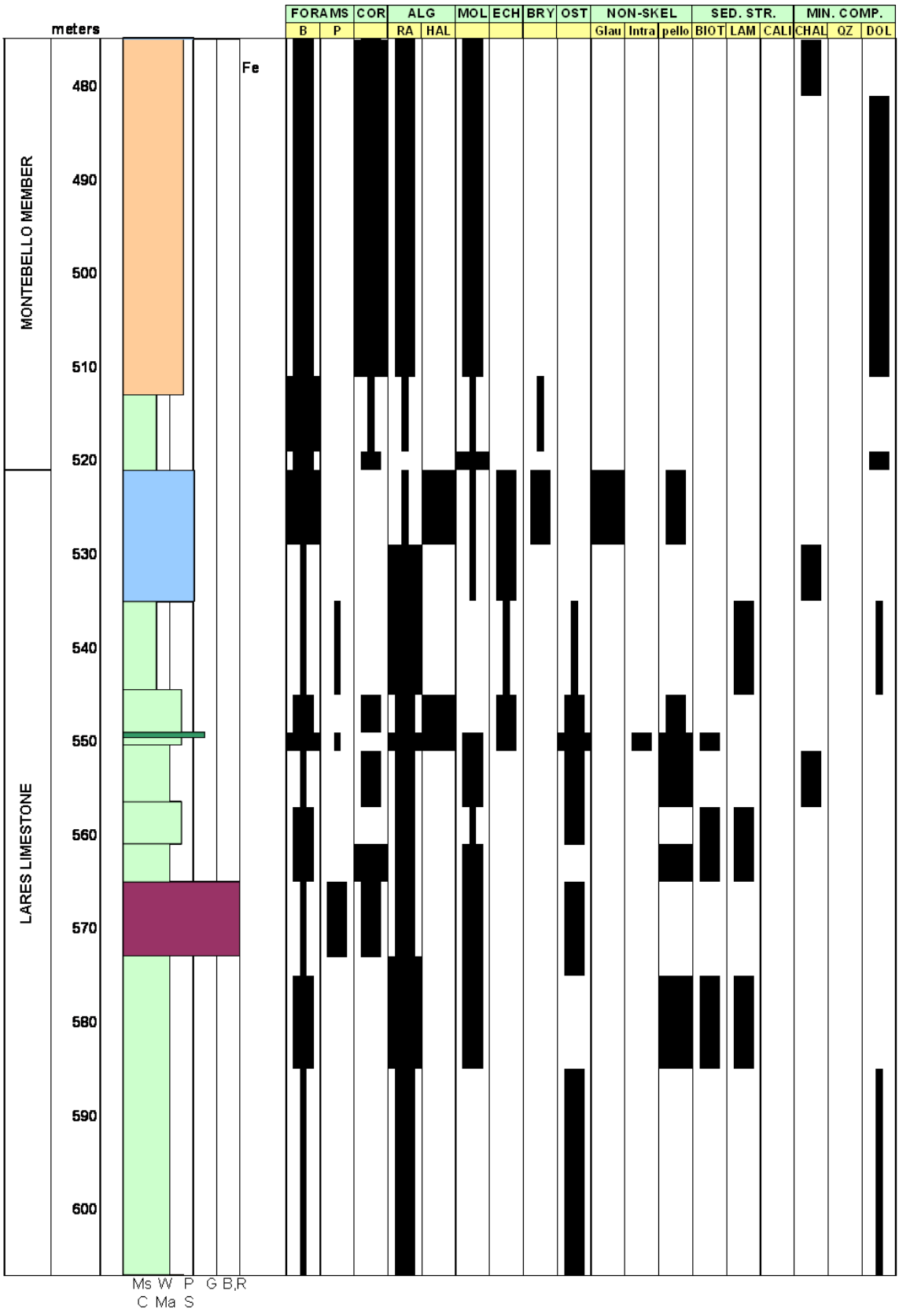
meters
FORAMS
B
P
COR
ALG
RA
HAL
MOL
ECH
BRY
OST
NON-SKEL
Glau
Intra
pello
SED. STR.
BIOT
LAM
CALI
MIN. COMP.
CHAL
OZ
DOL
Fe
MONTEBELLO MEMBER
LARES LIMESTONE
480
490
500
510
520
530
540
550
560
570
580
590
600
Ms W P G B,R
C Ma S

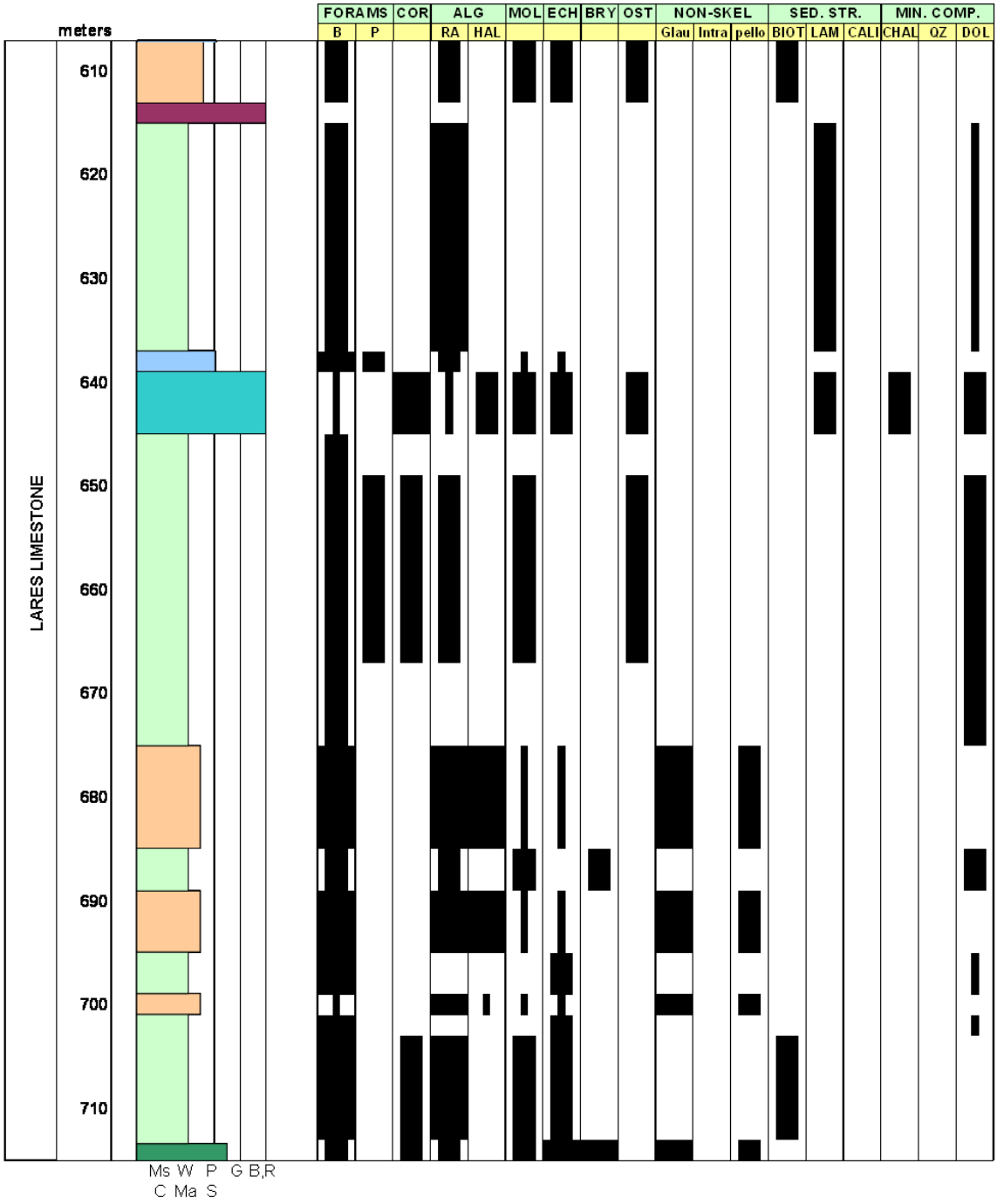
meters
FORAMS
COR
ALG
MOL
ECH
BRY
OST
NON-SKEL
SED. STR.
MIN. COMP.
B
P
RA
HAL
Glau
Intra
pello
BIOT
LAM
CALI
CHAL
OZ
DOL
610
620
630
640
650
660
670
680
690
700
710
LARES LIMESTONE
Ms W P G B,R
C Ma S

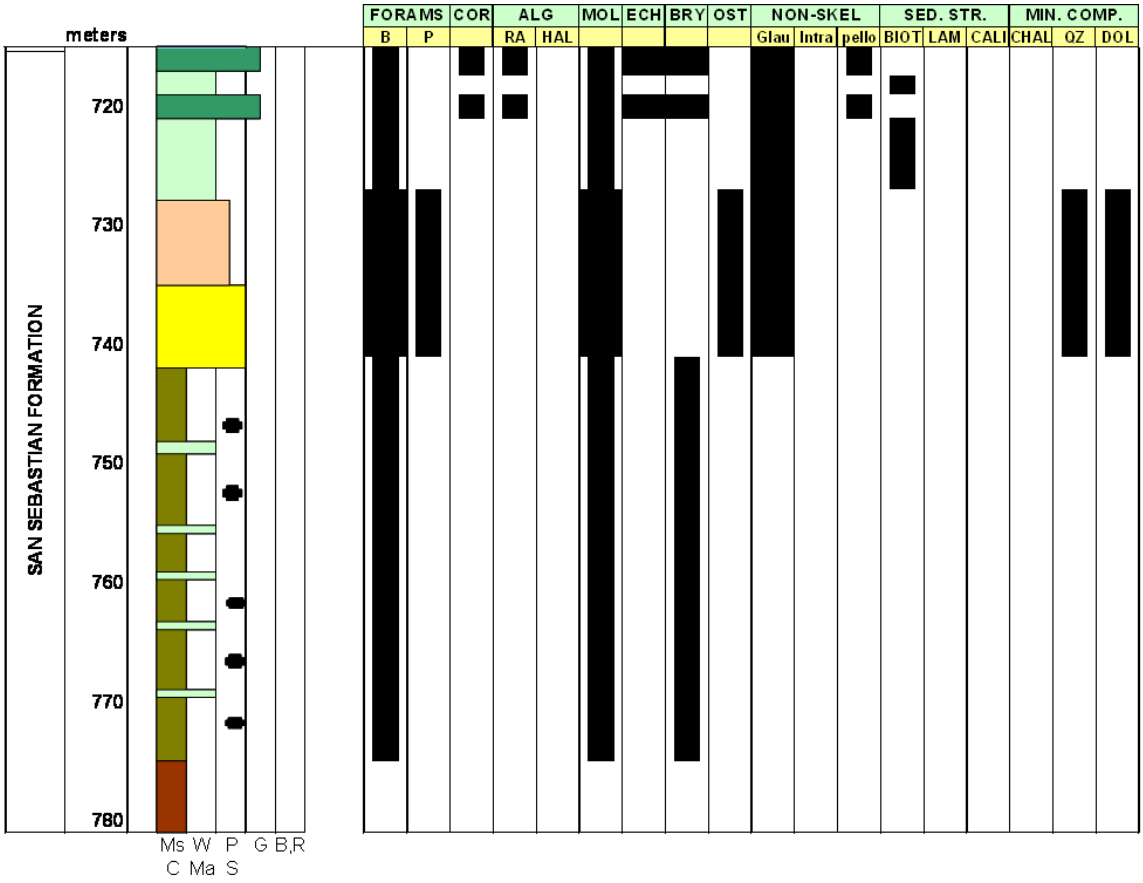
meters
SAN SEBASTIAN FORMATION
720
730
740
750
760
770
780
Ms W P G B,R
C Ma S
FORAMS
B
P
COR
ALG
RA
HAL
MOL
ECH
BRY
OST
NON-SKEL
Glau
Intra
pello
SED. STR.
BIOT
LAM
CALI
MIN. COMP.
CHAL
OZ
DOL

APPENDIX 2
DEPOSITIONAL ENVIRONMENTS AND PARASEQUENCE INTERPRETATIONS OF NC-6 AND NC-5 TEST HOLES, AND PR-10 AND PR-22 OUTCROPS

NC-6 AND NC-5 TEST HOLES: STANDARD MICROFACIES TYPES (RMF), DEPOSITIONAL ENVIROMENTS AND PARASEQUENCES INTERPRETATIONS

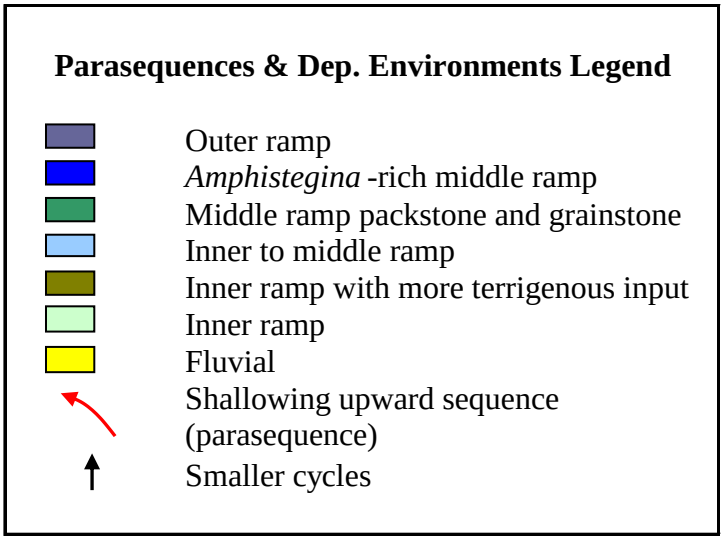

Legend also applies to PR-10 and PR-22 outcrops.

Ramp Microfacies Types (RMF) proposed to the NC-6 and NC-5 test holes based on Wilson (1975) and Flugel (2002) microfacies analysis.

RMF	Description	Environment	Key
RMF 5	Globigerinid limestone	Outer ramp	
RMF 26	Medium- and -coarse-grained bioclastic grainstone and packstone with various benthic skeletal grains.	Sand shoals and banks	
RMF 27	Bioclastic grainstone and p composed of few dominat skeletal grains (predo echino or forams)	Sand shoals and banks	
RMF 14	Packstone/grainstone with various bioclasts	Open marine	
RMF 13	Bioclastic wackestone and packestone with abundant larger foraminifera	Restricted to open marine	
RMF 16	Soritid- and -miliolid-rich wackestone	Restricted	
RMF 18	Bioclastic wackestone with ostracods	Restricted	
RMF 17	Bioclastic wackestone with dasyclad green algae	Lagoon	
RMF 20	Bioclastic wackestone and packestone with calcareous algae and benthic forams	Lagoon	
RMF 19	Non-burrowed lime mudstone	Peritidal to Lagoon	
RMF 23	Fenestral mudstone	Peritidal	
RMF 33	Argillaceous sandstone and carbonate rocks with glauconite and diverse, normal- marine fauna	Shallow open ramp	
RMF 32	Claystone olive-green, sandstone and located wackestone and marl layers, low fauna and carbonaceous material	Marginal marine/terrigenous	
RMF32B	Claystone wackestone and marl, without carbonaceous material	Marginal marine/terrigenous	
RMF 31	Claystone red-brown non-fossiliferous	Costal (Alluvial plain)	
RMF 35	Karst zones, caliche	Exposure areas	

NC-6 TEST HOLE

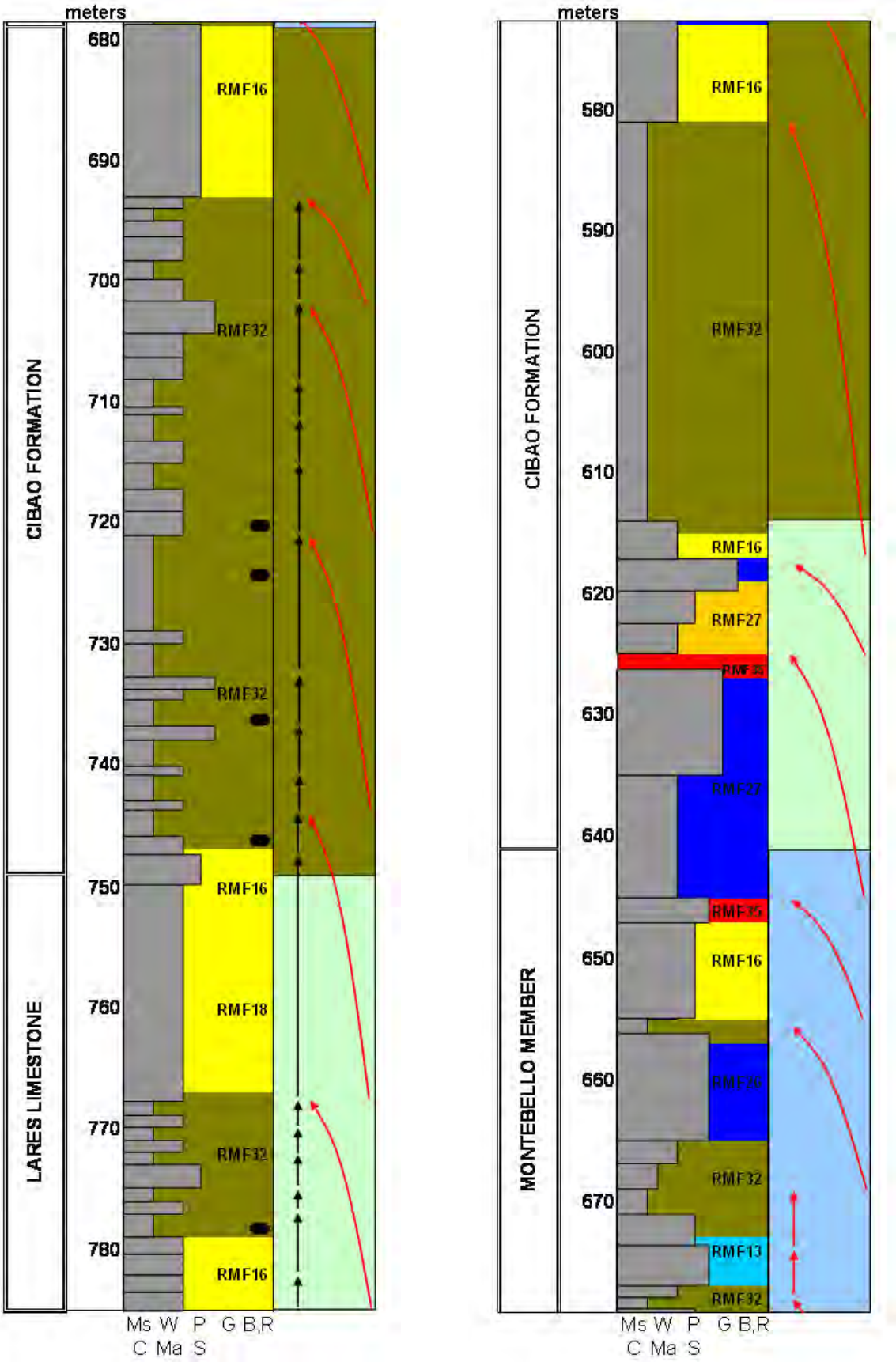

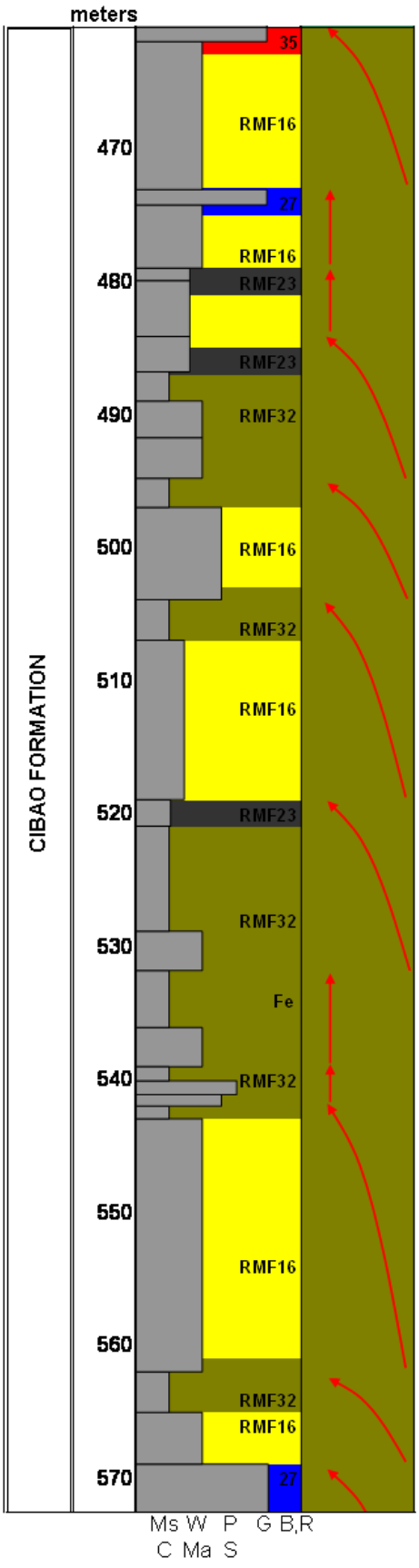
meters
CIBAO FORMATION
470
480
490
500
510
520
530
540
550
560
570
35
RMF16
27
RMF16
RMF23
RMF23
RMF32
RMF16
RMF32
RMF16
RMF23
RMF32
Fe
RMF32
RMF16
RMF32
RMF16
27
Ms W P G B,R
C Ma S

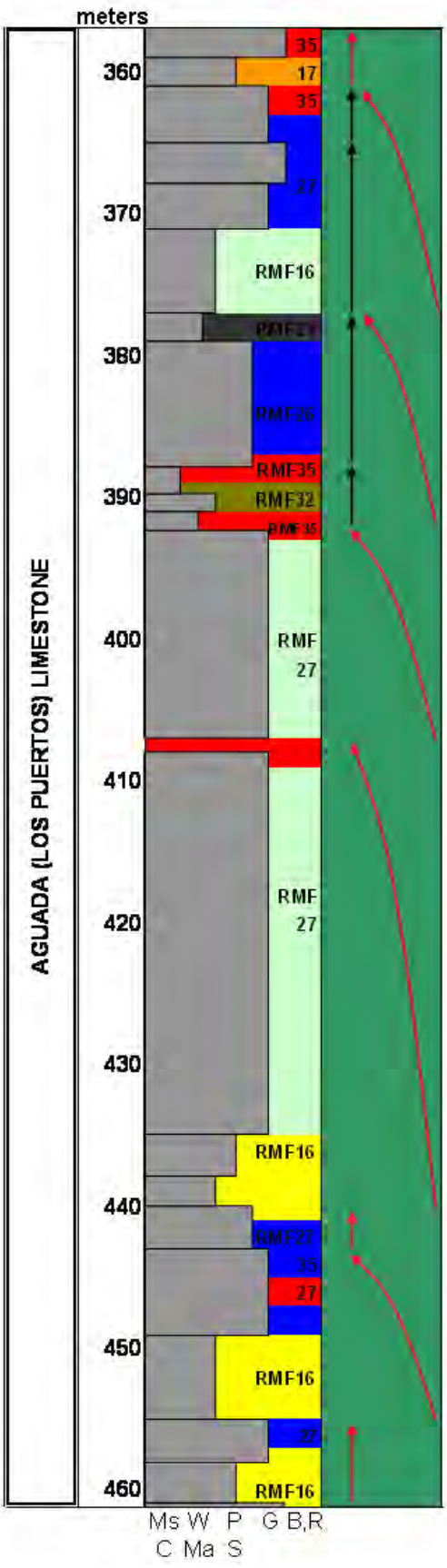
meters
AGUADA (LOS PUERTOS) LIMESTONE
360
370
380
390
400
410
420
430
440
450
460
35
17
35
27
RMF16
RMF26
RMF35
RMF32
RMF
27
RMF
27
RMF16
RMF27
35
27
RMF16
27
RMF16
Ms W P G B,R
C Ma S

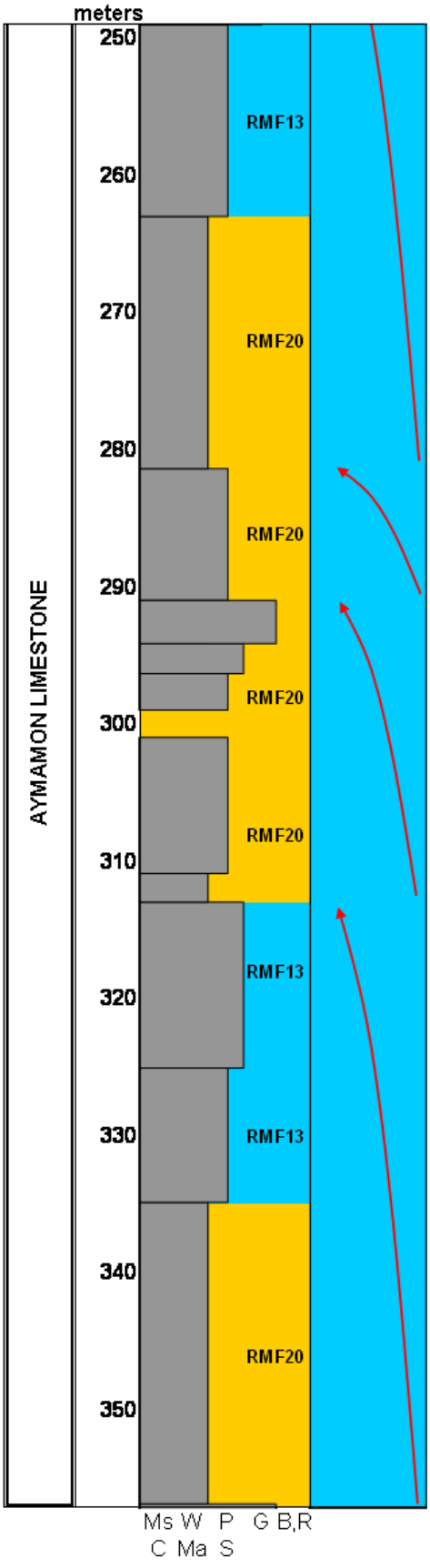
meters
AYMAMON LIMESTONE
250
260
270
280
290
300
310
320
330
340
350
RMF13
RMF20
RMF20
RMF20
RMF20
RMF13
RMF13
RMF20
Ms W P G B,R
C Ma S

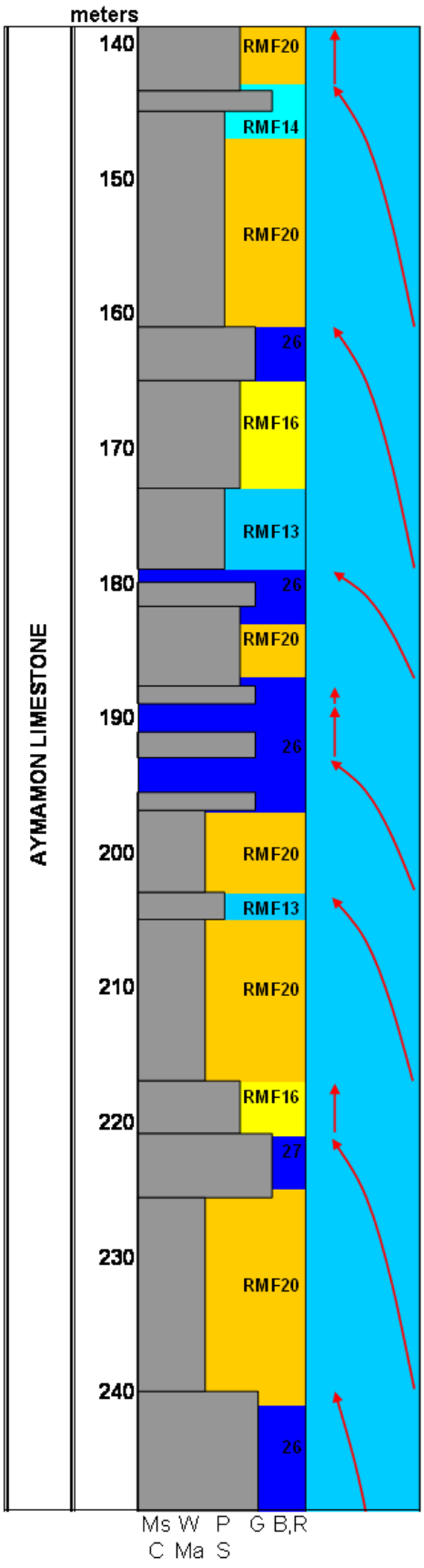
meters
AYMAMON LIMESTONE
140
150
160
170
180
190
200
210
220
230
240
RMF20
RMF14
RMF20
26
RMF16
RMF13
26
RMF20
26
RMF20
RMF13
RMF20
RMF16
27
RMF20
26
Ms W P G B,R
C Ma S

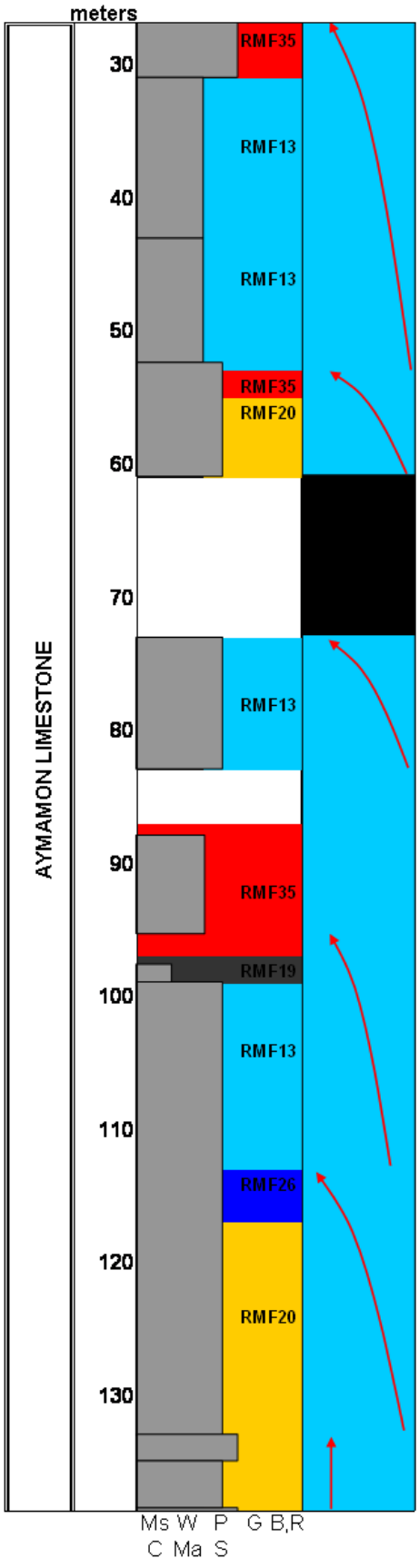
meters
AYMAMON LIMESTONE
30
40
50
60
70
80
90
100
110
120
130
RMF35
RMF13
RMF13
RMF35
RMF20
RMF13
RMF35
RMF19
RMF13
RMF26
RMF20
Ms W P G B,R
C Ma S

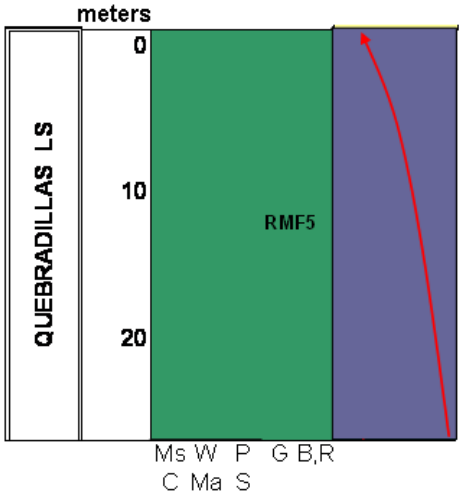
meters
QUEBRADILLAS LS
0
10
20
RMF5
Ms W P G B,R
C Ma S

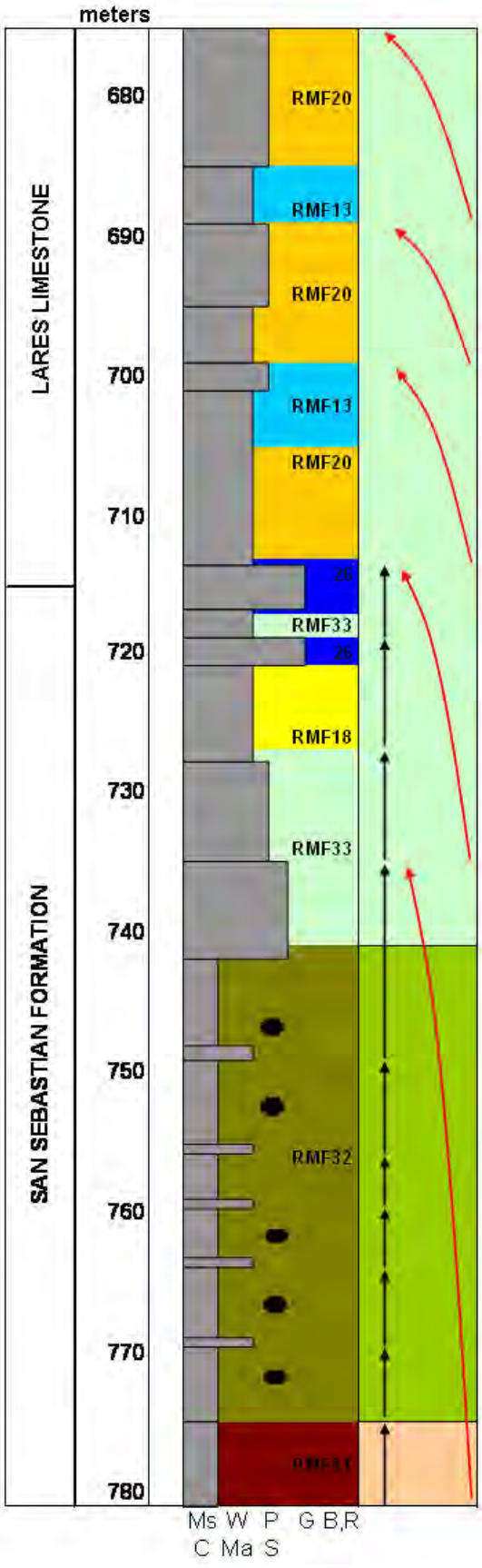
meters
LARES LIMESTONE
SAN SEBASTIAN FORMATION
680
690
700
710
720
730
740
750
760
770
780
RMF20
RMF13
RMF20
RMF13
RMF20
26
RMF33
26
RMF18
RMF33
RMF32
Ms W P G B,R
C Ma S

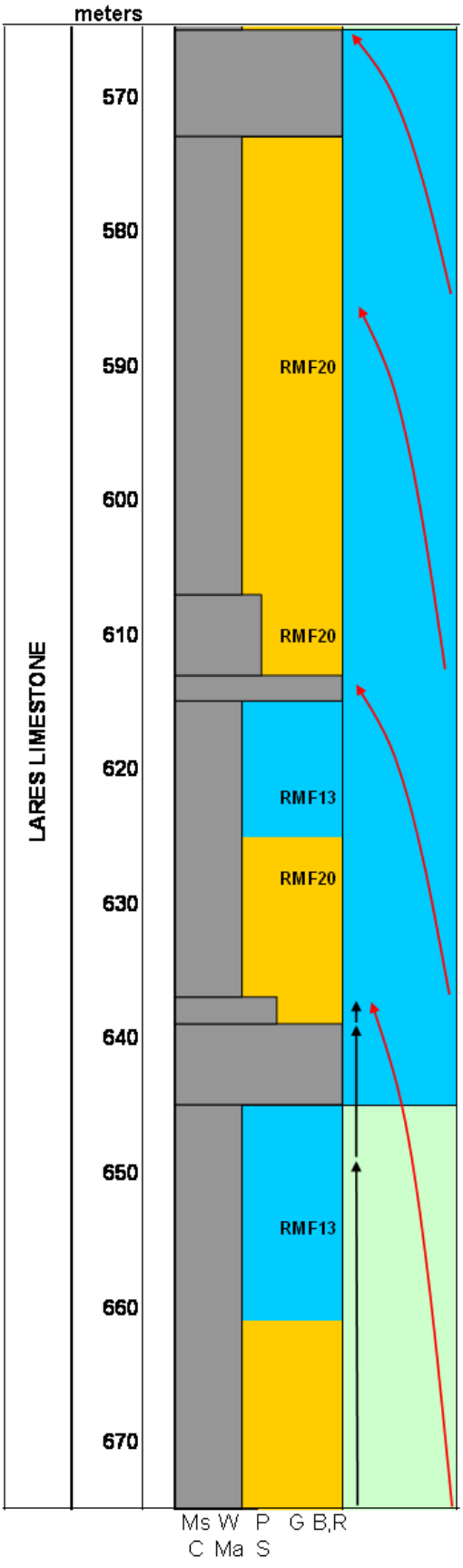
meters
LARES LIMESTONE
570
580
590
600
610
620
630
640
650
660
670
RMF20
RMF20
RMF13
RMF20
RMF13
Ms W P G B,R
C Ma S

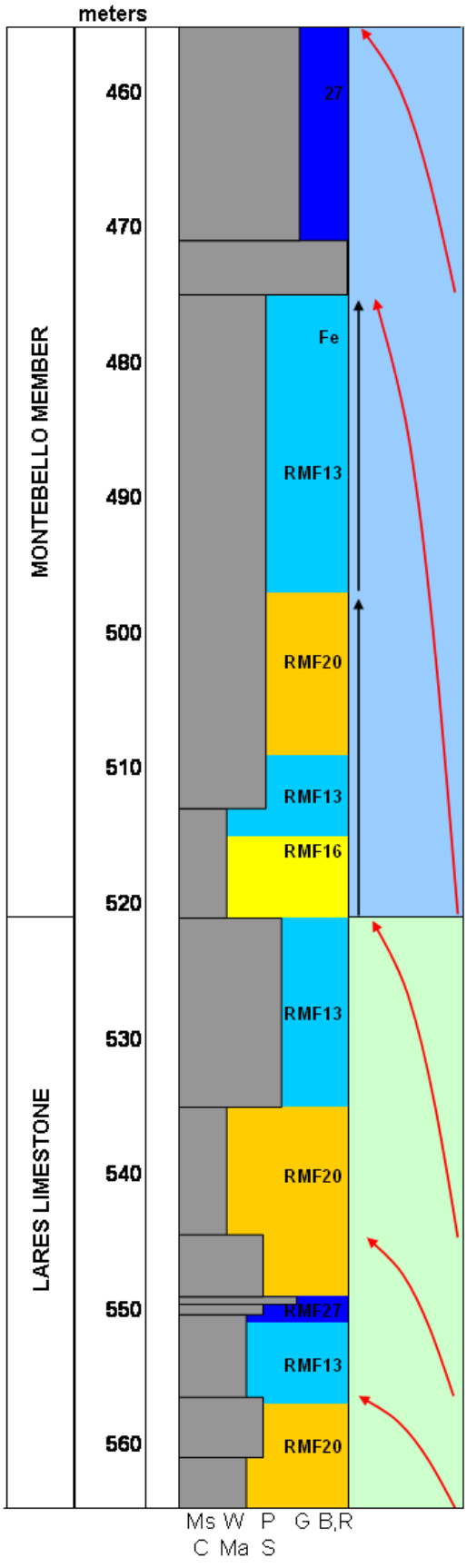
meters
MONTEBELLO MEMBER
LARES LIMESTONE
460
470
480
490
500
510
520
530
540
550
560
27
Fe
RMF13
RMF20
RMF13
RMF16
RMF13
RMF20
RMF27
RMF13
RMF20
Ms W P G B,R
C Ma S

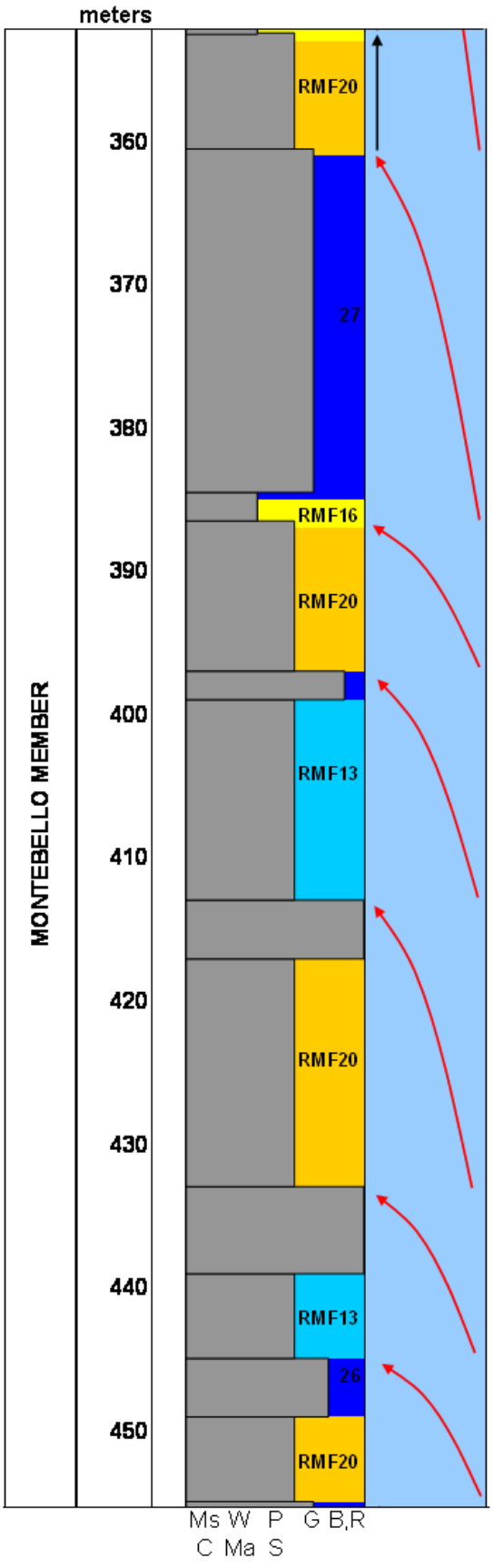
meters
MONTEBELLO MEMBER
360
370
380
390
400
410
420
430
440
450
RMF20
27
RMF16
RMF20
RMF13
RMF20
RMF13
26
RMF20
Ms W P G B,R
C Ma S

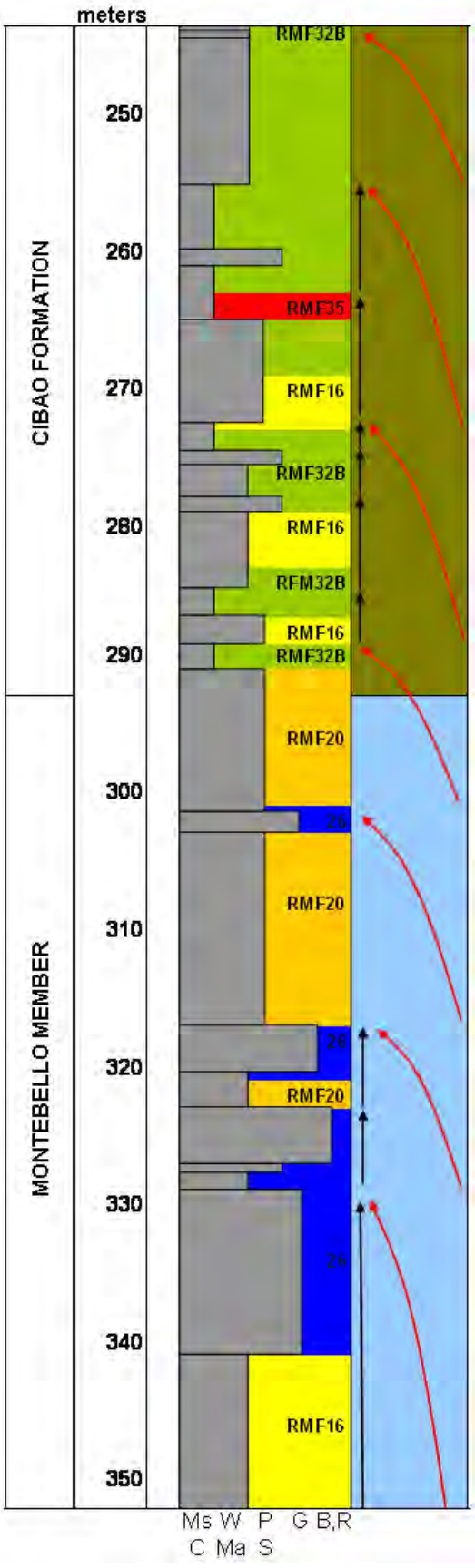
meters
CIBAO FORMATION
MONTEBELLO MEMBER
250
260
270
280
290
300
310
320
330
340
350
RMF32B
RMF35
RMF16
RMF32B
RMF16
RFM32B
RMF16
RMF32B
RMF20
26
RMF20
26
RMF20
26
RMF16
Ms W P G B,R
C Ma S

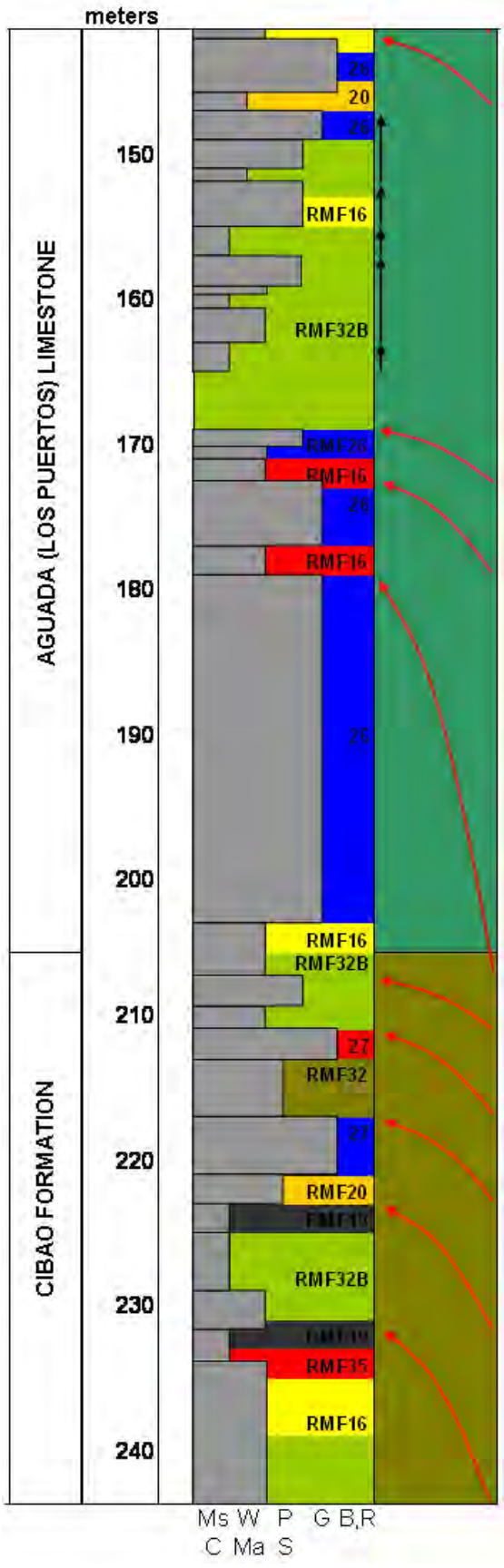
meters
AGUADA (LOS PUERTOS) LIMESTONE
CIBAO FORMATION
150
160
170
180
190
200
210
220
230
240
26
20
26
RMF16
RMF32B
RMF26
RMF16
26
RMF16
26
RMF16
RMF32B
27
RMF32
27
RMF20
RMF32B
RMF35
RMF16
Ms W P G B,R
C Ma S

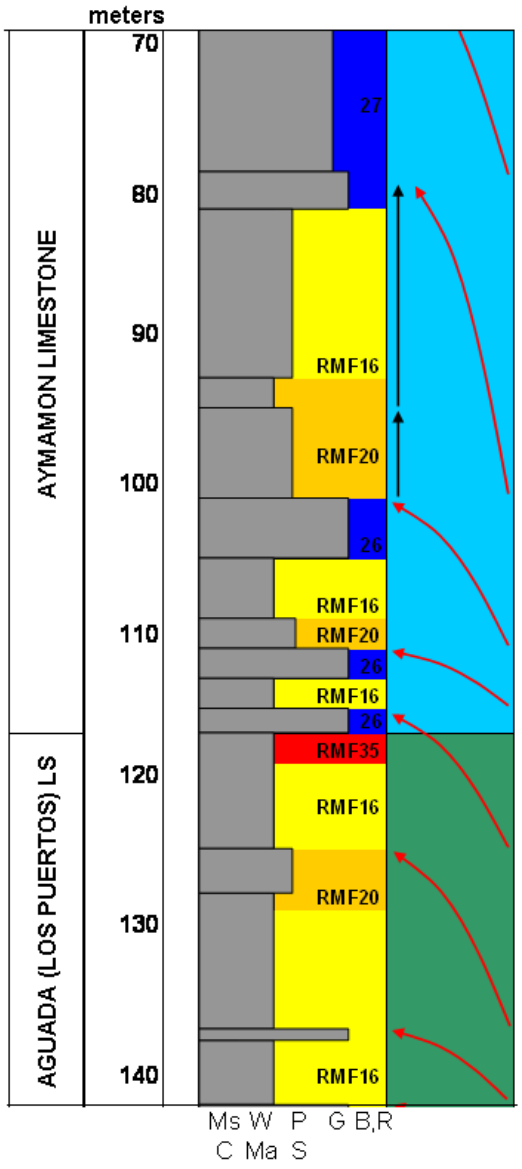
meters
70
80
90
100
110
120
130
140
AYMAMON LIMESTONE
AGUADA (LOS PUERTOS) LS
27
RMF16
RMF20
26
RMF16
RMF20
26
RMF16
26
RMF35
RMF16
RMF20
RMF16
Ms W P G B,R
C Ma S

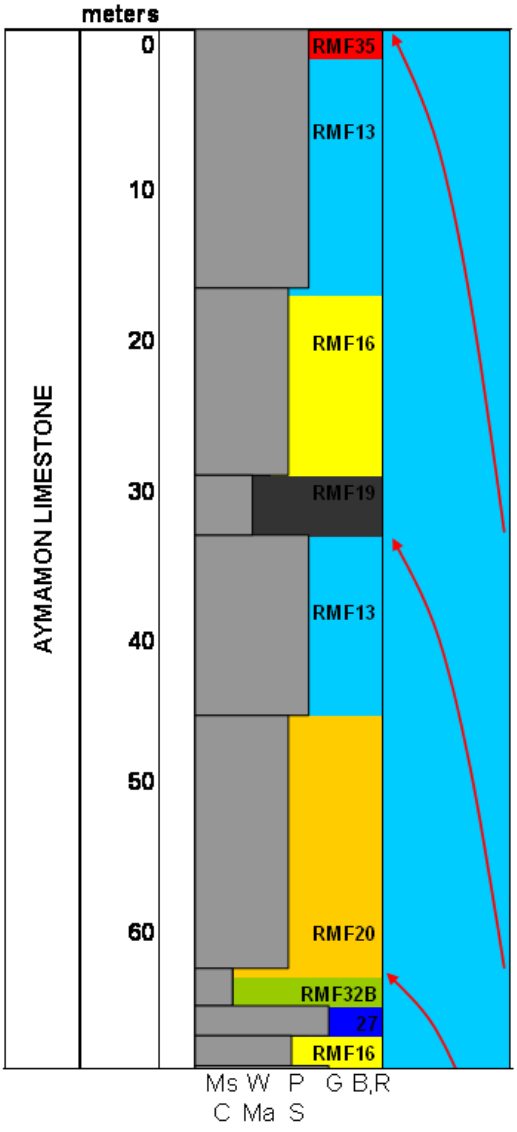
meters
0
10
20
30
40
50
60
AYMAMON LIMESTONE
RMF35
RMF13
RMF16
RMF19
RMF13
RMF20
RMF32B
27
RMF16
Ms W P G B,R
C Ma S

PR-10 AND PR-22 OUTCROPS

PR-10 OUTCROPS : COLUMNS, FACIES, DEPOSITIONAL ENVIRONMENTS AND PARASEQUENCES INTERPRETATIONS

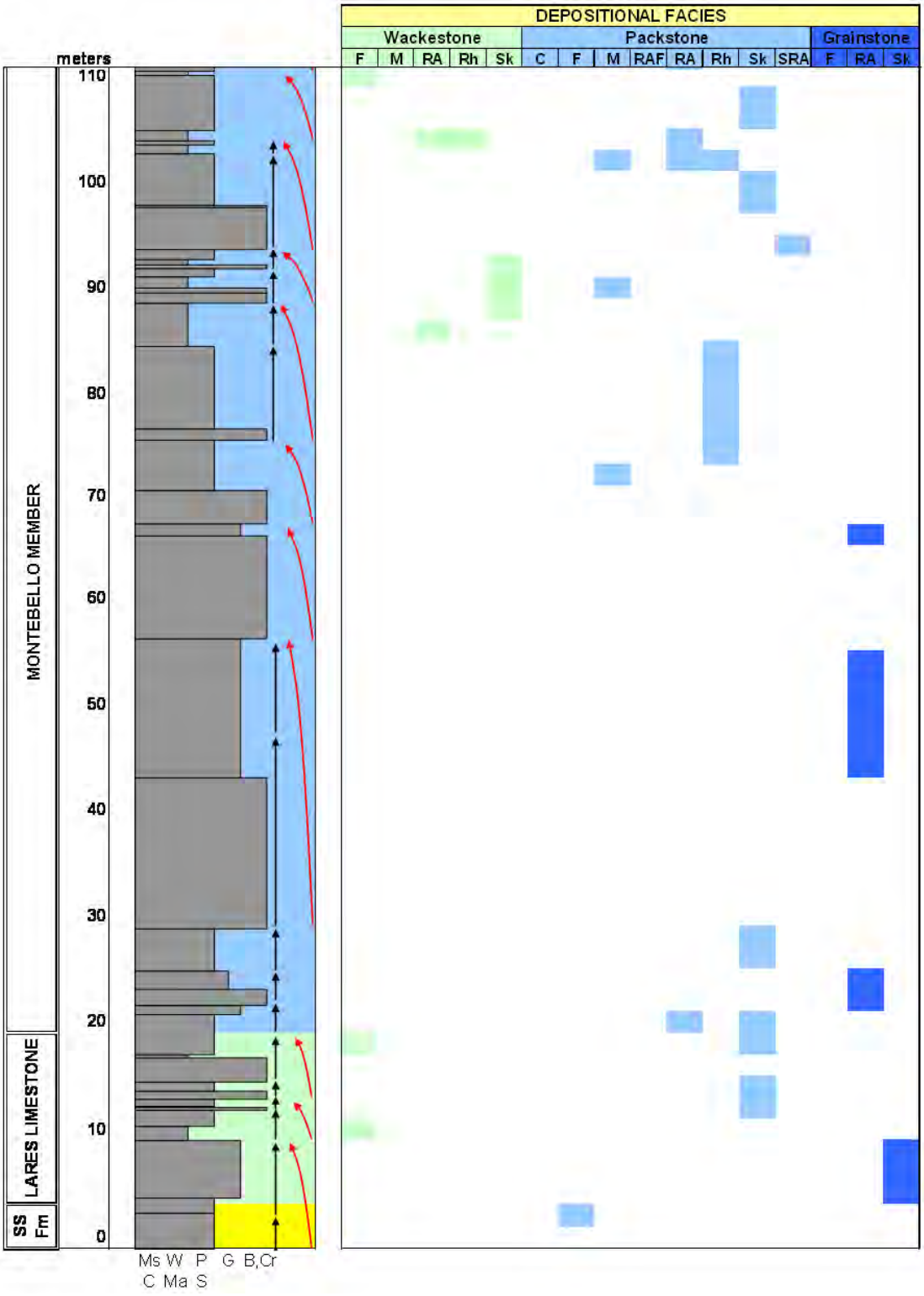

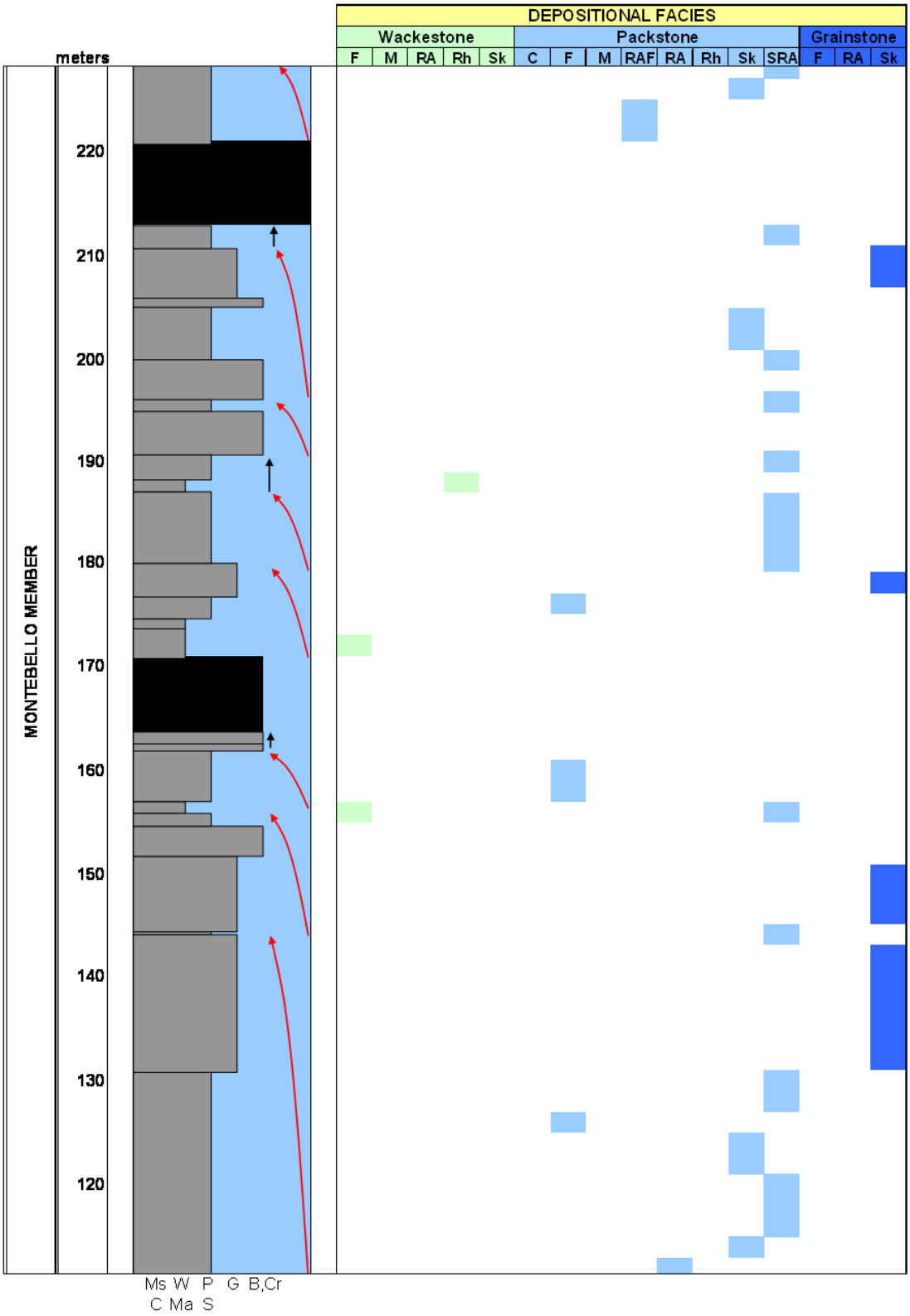
DEPOSITIONAL FACIES
Wackestone
Packstone
Grainstone
F M RA Rh Sk C F M RAF RA Rh Sk SRA F RA Sk
meters
MONTEBELLO MEMBER
220
210
200
190
180
170
160
150
140
130
120
Ms W P G B,Cr
C Ma S

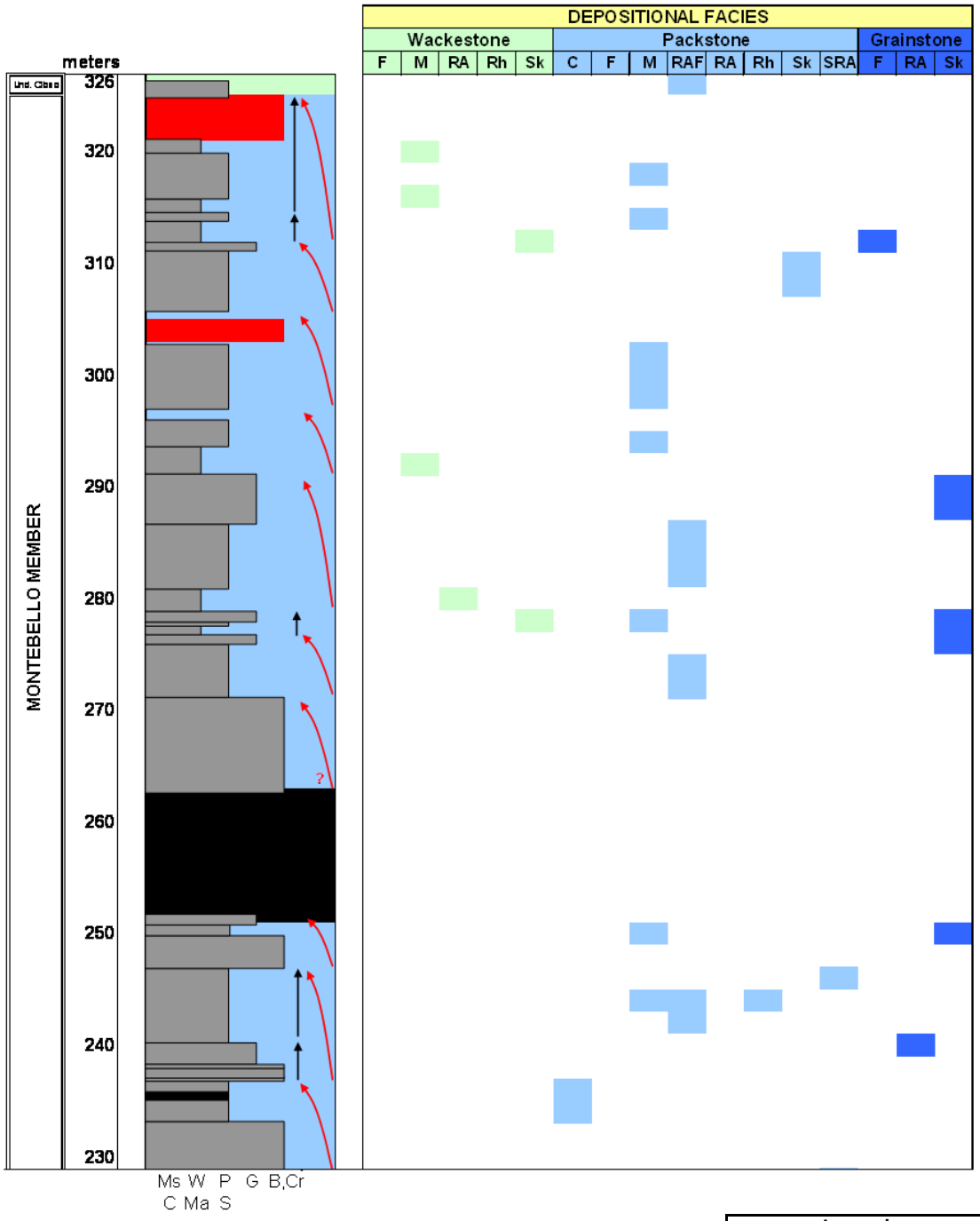
DEPOSITIONAL FACIES
Wackestone
Packstone
Grainstone
F M RA Rh Sk C F M RAF RA Rh Sk SRA F RA Sk
meters
326
320
310
300
290
280
270
260
250
240
230
MONTEBELLO MEMBER
Ms W P G B,Cr
C Ma S
covered section
Legend
F - foraminiferal
M - mollusc
RA - red algal
Rh - rhodolitic
Sk - skeletal
C - coral
RAF - red algal foraminiferal
SRA - skeletal red algal

PR-22 OUTCROP : COLUMN, CONSTITUENTS, DEPOSITIONAL ENVIROMENT AND PARASEQUENCES INTERPREATIONS

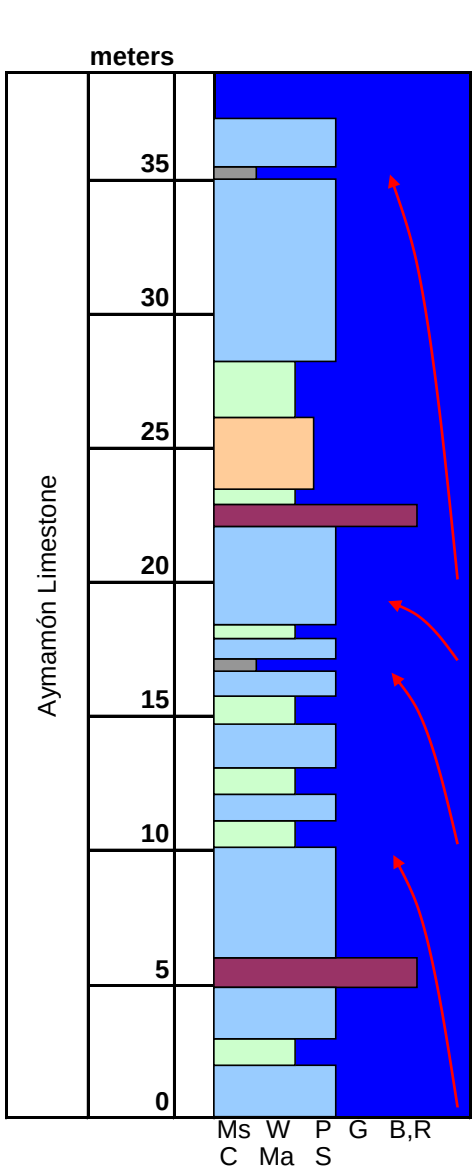

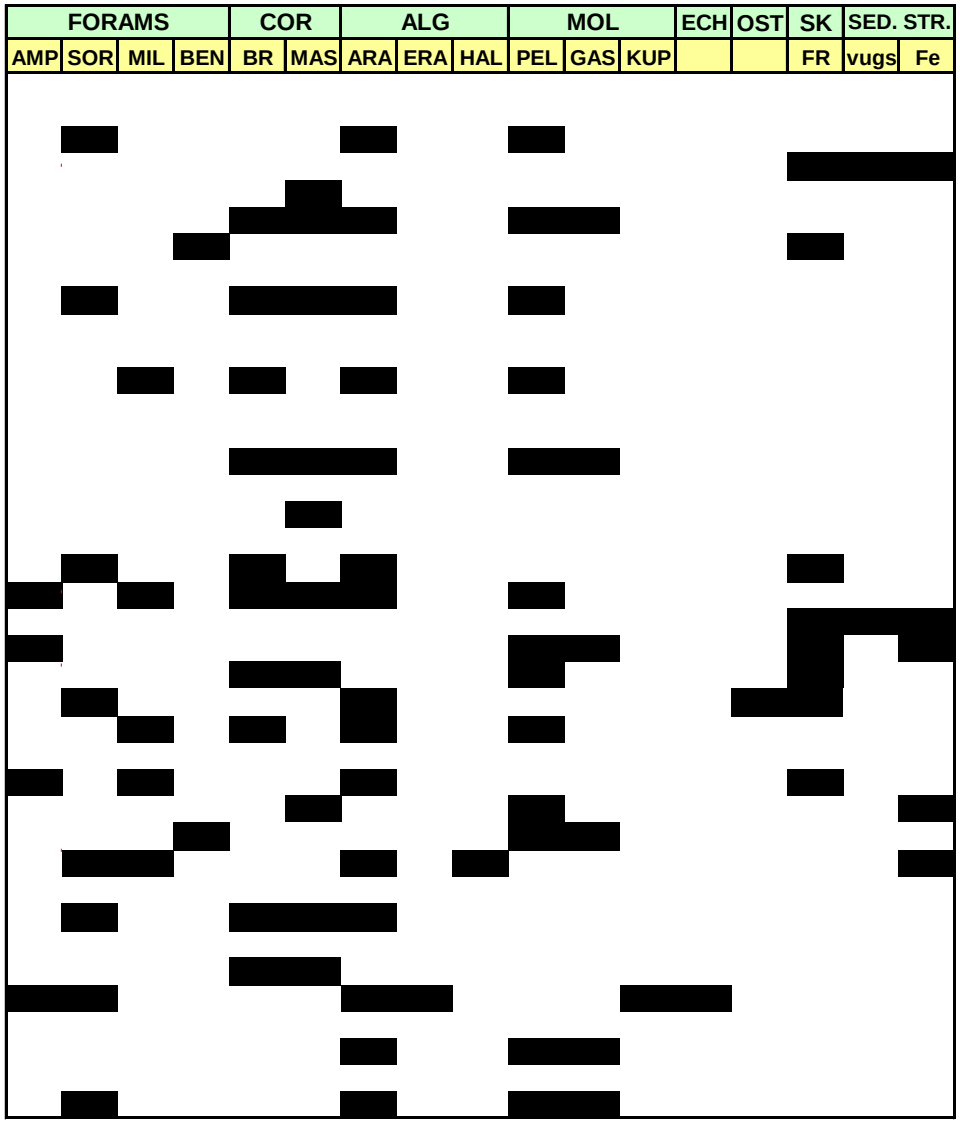

Legend

Foraminifers
Amp - Amphistegina
Sor - Soritid
Mil - Miliolids
Ben - Benthics

Corals
Br - Branching
Mas - Massive

Algae
ARA - Articulated Red Algae
ERA - Encrusting Red Algae
Hal - Halimeda

Mollusks
Pel - Pelecypods
Gas - Gastropods
Kup - Kuphus

Echinoids
Ostracodes
Skeletal fragments und.

clay filled vugs
Fe-oxide stains

APPENDIX 3A AND 3B
STABLE ISOTOPE ANALYSES OF *Kuphus incrassatus* TUBES AND OYSTERS FROM MARCH 10 AND 18, 2009

APPENDIX 3A. Stable isotope analyses of *Kuphus incrassatus* tubes and oysters from March 10, 2009.

		Run 1					
#	Analysis ID	Mass 45/44 $^{13}C^{16}O^{16}O/^{12}C^{16}O^{16}O$	Mass 46/44 $^{12}C^{16}O^{18}O/^{12}C^{16}O^{16}O$	$\delta^{13}C$ (meas.)	$\delta^{18}O$ (meas.)	$\delta^{13}C$ (corr.)	$\delta^{18}O$ (corr.)
1	CFN 1	1.2079E-02	4.0279E-03	-5.41	-8.56	-5.30	-7.88
2	NBS-19-1	1.2166E-02	4.0517E-03	1.93	-2.60	——	——
3	KCC 1	1.2218E-02	4.0359E-03	6.71	-6.56	6.82	-5.88
4	PR-111 M2	1.2128E-02	4.0506E-03	-1.25	-2.97	-1.14	-2.29
5	PR-111 M8	1.2131E-02	4.0521E-03	-1.03	-2.53	-0.92	-1.85
6	PR-111 T1	1.2163E-02	4.0560E-03	1.81	-1.56	1.92	-0.88
7	PR-10 2 K1-4	1.2094E-02	4.0530E-03	-4.17	-2.30	-4.06	-1.62
8	PR-10 3 M2	1.2099E-02	4.0528E-03	-3.68	-2.41	-3.57	-1.73
9	PR-10 Km 67.6-2	1.2138E-02	4.0554E-03	-0.28	-1.70	-0.17	-1.02
10	PR-10 Km 67.6-3	1.2124E-02	4.0528E-03	-1.51	-2.37	-1.40	-1.69
11	PR-111 OL-2	1.2148E-02	4.0519E-03	0.64	-2.65	0.75	-1.97
12	PR-10 GAS3	1.2057E-02	4.0415E-03	-7.21	-5.14	-7.10	-4.46
13	PR-111 GPS	1.2157E-02	4.0525E-03	1.46	-2.44	1.57	-1.76
14	NBS-19-2	1.2160E-02	4.0501E-03	1.79	-3.08	——	——
15	NC-6 LP 1380-77-1	1.2142E-02	4.0499E-03	0.19	-3.02	0.30	-2.34
16	NC-11-1181-2	1.2161E-02	4.0562E-03	1.95	-1.48	2.06	-0.80
17	NC-11-1149-46	1.2150E-02	4.0596E-03	0.97	-0.66	1.08	0.02
18	NC-11-1145-1	1.2151E-02	4.0566E-03	1.06	-1.36	1.17	-0.68
19	NC-11-1165-4	1.2153E-02	4.0565E-03	1.31	-1.47	1.42	-0.79
20	PR-111 OL-3	1.2126E-02	4.0527E-03	-1.07	-2.32	-0.96	-1.64
21	NC-13-526	1.2164E-02	4.0567E-03	2.28	-1.34	2.39	-0.66
22	C1-CIBAO	1.2046E-02	4.0427E-03	-7.95	-4.87	-7.84	-4.19
23	C2-CIBAO	1.2055E-02	4.0425E-03	-7.15	-4.90	-7.04	-4.22
24	NC-11-1145-2	1.2163E-02	4.0541E-03	2.28	-1.97	2.39	-1.29
25	CFN 2	1.2069E-02	4.0261E-03	-5.60	-8.91	-5.49	-8.23
26	NBS-19-3	1.2156E-02	4.0498E-03	1.81	-2.97	——	——
27	KCC 2	1.2209E-02	4.0342E-03	6.60	-6.90	6.71	-6.22
	NBS-19 (average)			1.84	-2.88	1.95	-2.20
	Correction factor applied to samples			+0.11	+0.68		

CFN and KCC are in-house standards at the UPRM Stable Isotope Laboratory.
Samples and standards are listed in chronological order of analysis.
All δ values are in ‰ on the PDB scale. meas. = measured; corr. = corrected

APPENDIX 3B. Stable isotope analyses of *Kuphus incrassatus* tubes and oysters from March 18, 2009.

		Run 2					
#	Analysis ID	Mass 45/44 $^{13}C^{16}O^{16}O/^{12}C^{16}O^{16}O$	Mass 46/44 $^{12}C^{16}O^{18}O/^{12}C^{16}O^{16}O$	$\delta^{13}C$ (meas.)	$\delta^{18}O$ (meas.)	$\delta^{13}C$ (corr.)	$\delta^{18}O$ (corr.)
1	CFN 1	1.2108E-02	4.0379E-03	-5.71	-8.09	-5.63	-7.77
2	NBS-19-1	1.2196E-02	4.0617E-03	1.94	-2.31	——	——
3	KCC 1	1.2250E-02	4.0448E-03	6.81	-6.44	6.89	-6.12
4	PR-111 M2	1.2161E-02	4.0611E-03	-1.16	-2.33	-1.08	-2.01
5	PR-111 M8	1.2160E-02	4.0599E-03	-1.27	-2.57	-1.19	-2.25
6	PR-111 T1	1.2196E-02	4.0670E-03	1.89	-0.85	1.97	-0.53
7	PR-10 2 K1-4	1.2130E-02	4.0630E-03	-4.03	-1.65	-3.95	-1.33
8	PR-10 3 M2	1.2134E-02	4.0621E-03	-3.55	-1.96	-3.47	-1.64
9	PR-10 Km 67.6-2	1.2168E-02	4.0617E-03	-0.61	-1.97	-0.53	-1.65
10	PR-10 Km 67.6-3	1.2157E-02	4.0617E-03	-1.51	-1.98	-1.43	-1.66
11	PR-111 OL-2	1.2182E-02	4.0611E-03	0.68	-2.16	0.76	-1.84
12	PR-10 GAS3	1.2091E-02	4.0507E-03	-7.22	-4.66	-7.14	-4.34
13	PR-111 GPS	1.2195E-02	4.0622E-03	1.75	-1.75	1.83	-1.43
14	NBS-19-2	1.2195E-02	4.0590E-03	1.82	-2.57	——	——
15	NC-6 LP 1380-77-1	1.2177E-02	4.0581E-03	0.26	-2.81	0.34	-2.49
16	NC-11-1181-2	1.2199E-02	4.0671E-03	2.14	-0.57	2.22	-0.25
17	NC-11-1149-46	1.2187E-02	4.0677E-03	0.97	-0.38	1.05	-0.06
18	NC-11-1145-1	1.2187E-02	4.0662E-03	1.13	-0.84	1.21	-0.52
19	NC-11-1165-4	1.2190E-02	4.0655E-03	1.35	-0.99	1.43	-0.67
20	PR-111 OL-3	1.2163E-02	4.0608E-03	-1.11	-1.99	-1.03	-1.67
21	NC-13-526	1.2201E-02	4.0676E-03	2.32	-0.47	2.40	-0.15
22	C1-CIBAO	1.2084E-02	4.0510E-03	-7.96	-4.46	-7.88	-4.14
23	C2-CIBAO	1.2090E-02	4.0503E-03	-7.30	-4.70	-7.22	-4.38
24	NC-11-1145-2	1.2201E-02	4.0638E-03	2.32	-1.36	2.40	-1.04
25	CFN 2	1.2108E-02	4.0351E-03	-5.69	-8.33	-5.61	-8.01
26	NBS-19-3	1.2194E-02	4.0583E-03	1.84	-2.69	——	——
27	KCC 2	1.2250E-02	4.0424E-03	6.71	-6.58	6.79	-6.26
	NBS-19 (average)			1.87	-2.52	1.95	-2.20
	Correction factor applied to samples			+0.08	+0.32		

CFN and KCC are in-house standards at the UPRM Stable Isotope Laboratory
Samples and standards are listed in chronological order of analysis
All δ values are in ‰ on the PDB scale. meas. = measured; corr. = corrected

APPENDIX 4A AND 4B
STRONTIUM ISOTOPE ANALYSES FROM TECTONICS AND GEOCHRONOLOGY ISOTOPE GEOCHEMISTRY SAMPLE PREPARATION FACILITIES AT THE UNIVERSITY OF KANSAS

APPENDIX 4A. Summary of strontium isotope analyses.

Anal. No.	Sample ID	Sample wt. (g)	Spike Tracer wt. (g)	$^{87}Sr/^{86}Sr$ (blank corr.)	$(^{87}Sr/^{86}Sr)n$* (norm. NBS-987)	Sr conc. (ppm)	sample /blank
1	PR-10 2K1-4	0.0786	0.0088	0.708133	**0.708128**	396.42	30130
2	NC-6 LP 1380-77 -1	0.0573	0.0102	0.708800	**0.708795**	742.77	41153
3	NC 13-526	0.0544	0.0100	0.708863	**0.708858**	836.69	44011
4	PR-10KM67.6 #3	0.0253	0.0094	0.708114	**0.708109**	715.72	17510
5	PR111OL-3	0.0554	0.0100	0.708151	**0.708146**	701.28	37569
6	NC 11-1149-46	0.0564	0.0101	0.708850	**0.708845**	611.32	33338
7	NC 11-1145-1	0.0395	0.0094	0.708856	**0.708851**	587.46	22437
8	PR-10KM67.6 #2	0.0209	0.0099	0.708090	**0.708085**	951.64	19233
9	NC-11 1145-2	0.0456	0.0101	0.708859	**0.708854**	670.72	29573
10	PR-10 10 3M2	0.0403	0.0095	0.708203	**0.708198**	406.97	15860
11	PR111-GPS	0.0181	0.0097	0.708172	**0.708167**	1153.73	20193
12	NC-11 1181-2	0.0267	0.0082	0.708840	**0.708835**	915.71	23641
13	NC 11-1165-4	0.0214	0.0099	0.708848	**0.708843**	870.33	18009
14	PR 111-OL-2	0.0318	0.0084	0.708176	**0.708171**	486.12	14948
15	PR-111 T1	0.0237	0.0098	0.708167	**0.708162**	871.89	19982
16	PR-111 M8	0.0160	0.0090	0.708126	**0.708121**	1306.21	20209
17	PR-111 M2	0.0291	0.0100	0.708135	**0.708130**	1226.33	34508

* Analytical uncertainty of each analysis is +/- 20 ppm (+/- 0.000015)

Anal. = Analysis; wt = weight; corr. = corrected; norm. = normalized; conc. = concentration

APPENDIX 4B. STRONTIUM ISOTOPE DATA REDUCTION

Sample ID	**PR-10 2K1-4**		Date	4/7/2009		
Sample Wt (g)	0.07860					
Aliquot (frac)	1.0000	(Sr88/Sr84)t	(Sr87/Sr84)t	(Sr86/Sr84)t	[Sr84]t	
Tracer ID	#11 Sr84	0.00039	0.00010	0.00059	1.0300	
Tracer Wt. (g)	0.0088					
		Sr88/Sr86	Sr87/Sr86	Sr84/Sr86		
Blank Sr86 (ng)	0.100	8.375209	0.709200	0.056490		
Normal Sr		8.375209	0.709000	0.056490		
Measured Sr IC/ID		8.375209	0.708133	0.059570		
			(lin norm)	(norm)		

Sr Reduction	**Iteration 1**		**84**	**86**	**87**	**88**
		Measured	0.0595695	1.000000	0.708133	8.375209
		Sample	0.0564899	0.999998	0.708133	8.375208
		Tracer	0.0030796	0.000002	0.000000	0.000001
			86/88 =	0.119400		8.375223
			Sr87/Sr86 =		0.708134	
	Iteration 2		**84**	**86**	**87**	**88**
		Measured	0.0595696	1.000000	0.708132	8.375195
		Sample	0.0564899	0.999998	0.708132	8.375194
		Tracer	0.0030797	0.000002	0.000000	0.000001
			86/88 =	0.119400		
			Sr87/Sr86 =		0.708133	
	Iteration 3		**84**	**86**	**87**	**88**
		Measured	0.0595696	1.000000	0.708132	8.375195
		Sample	0.0564899	0.999998	0.708132	8.375194
		Tracer	0.0030797	0.000002	0.000000	0.000001
			86/88 =	0.119400		
			Sr87/Sr86 =		0.708133	
	Iteration 4		**84**	**86**	**87**	**88**
		Measured	0.0595696	1.000000	0.708132	8.375195
		Sample	0.0564899	0.999998	0.708132	8.375194
		Tracer	0.0030797	0.000002	0.000000	0.000001
			86/88 =	0.119400		
			Sr87/Sr86 =		0.708133	
	Iteration 5		**84**	**86**	**87**	**88**
		Measured	0.0595696	1.000000	0.708132	8.375195
		Sample	0.0564899	0.999998	0.708132	8.375194
		Tracer	0.0030797	0.000002	0.000000	0.000001
			86/88 =	0.119400		
			Sr87/Sr86 =		0.708133	

		nanomoles	1.9813	35.0735	24.8367	293.7478
		nanogram	166.2578	3013.1376	2158.5303	25822.0802
	blank corr	nanogram		3013.0376		
	blank corr	nanomoles	1.9812	35.0723	24.8359	293.7380
	blank corr	nanogram	166.2523	3013.0376	2158.4585	25821.2232
	blank corr	ppm	2.1152	38.3338	27.4613	328.5143
	Tot Sr (ppm)	(approximate)	396.42			
	Blank Corr Sr87/Sr86		0.708133	Sample/Blank		30130.4

APPENDIX 4B. STRONTIUM ISOTOPE DATA REDUCTION

Sample ID	**NC-6 LP 1380-77 -1**		Date	4/7/2009		
Sample Wt (g)	0.05730					
Aliquot (frac)	1.0000	(Sr88/Sr84)t	(Sr87/Sr84)t	(Sr86/Sr84)t	[Sr84]t	
Tracer ID	#11 Sr84	0.00039	0.00010	0.00059	1.0300	
Tracer Wt. (g)	0.0102					
		Sr88/Sr86	Sr87/Sr86	Sr84/Sr86		
Blank Sr86 (ng)	0.100	8.375209	0.709200	0.056490		
Normal Sr		8.375209	0.709000	0.056490		
Measured Sr IC/ID		8.375209	0.708800	0.059103		
			(lin norm)	(norm)		

Sr Reduction	**Iteration 1**		**84**	**86**	**87**	**88**
		Measured	0.0591034	1.000000	0.708800	8.375209
		Sample	0.0564899	0.999998	0.708799	8.375208
		Tracer	0.0026135	0.000002	0.000000	0.000001
			86/88 =	0.119400		8.375221
			Sr87/Sr86 =		0.708800	
	Iteration 2		**84**	**86**	**87**	**88**
		Measured	0.0591035	1.000000	0.708799	8.375197
		Sample	0.0564899	0.999998	0.708799	8.375196
		Tracer	0.0026136	0.000002	0.000000	0.000001
			86/88 =	0.119400		
			Sr87/Sr86 =		0.708800	
	Iteration 3		**84**	**86**	**87**	**88**
		Measured	0.0591035	1.000000	0.708799	8.375197
		Sample	0.0564899	0.999998	0.708799	8.375196
		Tracer	0.0026136	0.000002	0.000000	0.000001
			86/88 =	0.119400		
			Sr87/Sr86 =		0.708800	
	Iteration 4		**84**	**86**	**87**	**88**
		Measured	0.0591035	1.000000	0.708799	8.375197
		Sample	0.0564899	0.999998	0.708799	8.375196
		Tracer	0.0026136	0.000002	0.000000	0.000001
			86/88 =	0.119400		
			Sr87/Sr86 =		0.708800	
	Iteration 5		**84**	**86**	**87**	**88**
		Measured	0.0591035	1.000000	0.708799	8.375197
		Sample	0.0564899	0.999998	0.708799	8.375196
		Tracer	0.0026136	0.000002	0.000000	0.000001
			86/88 =	0.119400		
			Sr87/Sr86 =		0.708800	
		nanomoles	2.7061	47.9039	33.9543	401.2053
		nanogram	227.0775	4115.3901	2950.9292	35268.1985
	blank corr	nanogram		4115.2901		
	blank corr	nanomoles	2.7060	47.9027	33.9535	401.1955
	blank corr	nanogram	227.0719	4115.2901	2950.8575	35267.3415
	blank corr	ppm	3.9629	71.8201	51.4984	615.4859
	Tot Sr (ppm)	(approximate)	742.77			
	Blank Corr Sr87/Sr86		0.708800	Sample/Blank		41152.9

APPENDIX 4B. STRONTIUM ISOTOPE DATA REDUCTION

Sample ID	**NC 13-526**		Date	4/7/2009		
Sample Wt (g)	0.05440					
Aliquot (frac)	1.0000	(Sr88/Sr84)t	(Sr87/Sr84)t	(Sr86/Sr84)t	[Sr84]t	
Tracer ID	#11 Sr84	0.00039	0.00010	0.00059	1.0300	
Tracer Wt. (g)	0.0100					
		Sr88/Sr86	Sr87/Sr86	Sr84/Sr86		
Blank Sr86 (ng)	0.100	8.375209	0.709200	0.056490		
Normal Sr		8.375209	0.709000	0.056490		
Measured Sr IC/ID		8.375209	0.708863	0.058886		
			(lin norm)	(norm)		

Sr Reduction	**Iteration 1**		**84**	**86**	**87**	**88**
		Measured	0.0588858	1.000000	0.708863	8.375209
		Sample	0.0564899	0.999999	0.708862	8.375208
		Tracer	0.0023959	0.000001	0.000000	0.000001
			86/88 =	0.119400		8.375220
			Sr87/Sr86 =		0.708863	
	Iteration 2		**84**	**86**	**87**	**88**
		Measured	0.0588859	1.000000	0.708862	8.375198
		Sample	0.0564899	0.999999	0.708862	8.375198
		Tracer	0.0023960	0.000001	0.000000	0.000001
			86/88 =	0.119400		
			Sr87/Sr86 =		0.708863	
	Iteration 3		**84**	**86**	**87**	**88**
		Measured	0.0588859	1.000000	0.708862	8.375198
		Sample	0.0564899	0.999999	0.708862	8.375198
		Tracer	0.0023960	0.000001	0.000000	0.000001
			86/88 =	0.119400		
			Sr87/Sr86 =		0.708863	
	Iteration 4		**84**	**86**	**87**	**88**
		Measured	0.0588859	1.000000	0.708862	8.375198
		Sample	0.0564899	0.999999	0.708862	8.375198
		Tracer	0.0023960	0.000001	0.000000	0.000001
			86/88 =	0.119400		
			Sr87/Sr86 =		0.708863	
	Iteration 5		**84**	**86**	**87**	**88**
		Measured	0.0588859	1.000000	0.708862	8.375198
		Sample	0.0564899	0.999999	0.708862	8.375198
		Tracer	0.0023960	0.000001	0.000000	0.000001
			86/88 =	0.119400		
			Sr87/Sr86 =		0.708863	

		nanomoles	2.8940	51.2302	36.3152	429.0638
		nanogram	242.8451	4401.1510	3156.1141	37717.1212
	blank corr	nanogram		4401.0510		
	blank corr	nanomoles	2.8939	51.2291	36.3144	429.0541
	blank corr	nanogram	242.8396	4401.0510	3156.0424	37716.2642
	blank corr	ppm	4.4640	80.9017	58.0155	693.3137
	Tot Sr (ppm)	(approximate)	836.69			
	Blank Corr Sr87/Sr86		0.708863	Sample/Blank		44010.5

APPENDIX 4B. STRONTIUM ISOTOPE DATA REDUCTION

Sample ID	**PR-10KM67.6 #3**		Date	4/7/2009		
Sample Wt (g)	0.02530					
Aliquot (frac)	1.0000	(Sr88/Sr84)t	(Sr87/Sr84)t	(Sr86/Sr84)t	[Sr84]t	
Tracer ID	#11 Sr84	0.00039	0.00010	0.00059	1.0300	
Tracer Wt. (g)	0.0094					
		Sr88/Sr86	Sr87/Sr86	Sr84/Sr86		
Blank Sr86 (ng)	0.100	8.375209	0.709200	0.056490		
Normal Sr		8.375209	0.709000	0.056490		
Measured Sr IC/ID		8.375209	0.708113	0.062150		
			(lin norm)	(norm)		

Sr Reduction	**Iteration 1**		**84**	**86**	**87**	**88**
		Measured	0.0621502	1.000000	0.708113	8.375209
		Sample	0.0564898	0.999997	0.708113	8.375207
		Tracer	0.0056604	0.000003	0.000001	0.000002
			86/88 =	0.119400		8.375235
			Sr87/Sr86 =		0.708115	
	Iteration 2		**84**	**86**	**87**	**88**
		Measured	0.0621504	1.000000	0.708112	8.375184
		Sample	0.0564898	0.999997	0.708112	8.375181
		Tracer	0.0056606	0.000003	0.000001	0.000002
			86/88 =	0.119400		
			Sr87/Sr86 =		0.708114	
	Iteration 3		**84**	**86**	**87**	**88**
		Measured	0.0621504	1.000000	0.708112	8.375184
		Sample	0.0564898	0.999997	0.708112	8.375181
		Tracer	0.0056606	0.000003	0.000001	0.000002
			86/88 =	0.119400		
			Sr87/Sr86 =		0.708114	
	Iteration 4		**84**	**86**	**87**	**88**
		Measured	0.0621504	1.000000	0.708112	8.375184
		Sample	0.0564898	0.999997	0.708112	8.375181
		Tracer	0.0056606	0.000003	0.000001	0.000002
			86/88 =	0.119400		
			Sr87/Sr86 =		0.708114	
	Iteration 5		**84**	**86**	**87**	**88**
		Measured	0.0621504	1.000000	0.708112	8.375184
		Sample	0.0564898	0.999997	0.708112	8.375181
		Tracer	0.0056606	0.000003	0.000001	0.000002
			86/88 =	0.119400		
			Sr87/Sr86 =		0.708114	

		nanomoles	1.1514	20.3831	14.4336	170.7131
		nanogram	96.6216	1751.1014	1254.4078	15006.6436
	blank corr	nanogram		1751.0014		
	blank corr	nanomoles	1.1514	20.3820	14.4328	170.7034
	blank corr	nanogram	96.6161	1751.0014	1254.3360	15005.7867
	blank corr	ppm	3.8188	69.2095	49.5785	593.1141
	Tot Sr (ppm)	(approximate)	715.72			
	Blank Corr Sr87/Sr86		0.708114	Sample/Blank		17510.0

APPENDIX 4B. STRONTIUM ISOTOPE DATA REDUCTION

Sample ID	**PR111OL-3**		Date	4/7/2009		
Sample Wt (g)	0.05540					
Aliquot (frac)	1.0000	(Sr88/Sr84)t	(Sr87/Sr84)t	(Sr86/Sr84)t	[Sr84]t	
Tracer ID	#11 Sr84	0.00039	0.00010	0.00059	1.0300	
Tracer Wt. (g)	0.0100					
		Sr88/Sr86	Sr87/Sr86	Sr84/Sr86		
Blank Sr86 (ng)	0.100	8.375209	0.709200	0.056490		
Normal Sr		8.375209	0.709000	0.056490		
Measured Sr IC/ID		8.375209	0.708151	0.059297		
			(lin norm)	(norm)		

Sr Reduction	**Iteration 1**		**84**	**86**	**87**	**88**
		Measured	0.0592966	1.000000	0.708151	8.375209
		Sample	0.0564899	0.999998	0.708150	8.375208
		Tracer	0.0028067	0.000002	0.000000	0.000001
			86/88 =	0.119400		8.375222
			Sr87/Sr86 =		0.708151	
	Iteration 2		**84**	**86**	**87**	**88**
		Measured	0.0592967	1.000000	0.708150	8.375197
		Sample	0.0564899	0.999998	0.708150	8.375196
		Tracer	0.0028068	0.000002	0.000000	0.000001
			86/88 =	0.119400		
			Sr87/Sr86 =		0.708151	
	Iteration 3		**84**	**86**	**87**	**88**
		Measured	0.0592967	1.000000	0.708150	8.375197
		Sample	0.0564899	0.999998	0.708150	8.375196
		Tracer	0.0028068	0.000002	0.000000	0.000001
			86/88 =	0.119400		
			Sr87/Sr86 =		0.708151	
	Iteration 4		**84**	**86**	**87**	**88**
		Measured	0.0592967	1.000000	0.708150	8.375197
		Sample	0.0564899	0.999998	0.708150	8.375196
		Tracer	0.0028068	0.000002	0.000000	0.000001
			86/88 =	0.119400		
			Sr87/Sr86 =		0.708151	
	Iteration 5		**84**	**86**	**87**	**88**
		Measured	0.0592967	1.000000	0.708150	8.375197
		Sample	0.0564899	0.999998	0.708150	8.375196
		Tracer	0.0028068	0.000002	0.000000	0.000001
			86/88 =	0.119400		
			Sr87/Sr86 =		0.708151	

		nanomoles	2.4704	43.7317	30.9686	366.2619
		nanogram	207.2999	3756.9560	2691.4485	32196.4786
	blank corr	nanogram		3756.8560		
	blank corr	nanomoles	2.4703	43.7305	30.9678	366.2521
	blank corr	nanogram	207.2944	3756.8560	2691.3767	32195.6217
	blank corr	ppm	3.7418	67.8133	48.5808	581.1484
	Tot Sr (ppm)	(approximate)	701.28			
	Blank Corr Sr87/Sr86		0.708151	Sample/Blank		37568.6

APPENDIX 4B. STRONTIUM ISOTOPE DATA REDUCTION

Sample ID	**NC 11-1149-46**		Date	4/9/2009		
Sample Wt (g)	0.05640					
Aliquot (frac)	1.0000	(Sr88/Sr84)t	(Sr87/Sr84)t	(Sr86/Sr84)t	[Sr84]t	
Tracer ID	#11 Sr89	0.00039	0.00010	0.00059	1.0300	
Tracer Wt. (g)	0.0101					
		Sr88/Sr86	Sr87/Sr86	Sr84/Sr86		
Blank Sr86 (ng)	0.100	8.375209	0.709200	0.056490		
Normal Sr		8.375209	0.709000	0.056490		
Measured Sr IC/ID		8.375209	0.708850	0.059684		
			(lin norm)	(norm)		

Sr Reduction	**Iteration 1**		**84**	**86**	**87**	**88**
		Measured	0.0596844	1.000000	0.708850	8.375209
		Sample	0.0564899	0.999998	0.708849	8.375208
		Tracer	0.0031945	0.000002	0.000000	0.000001
			86/88 =	0.119400		8.375224
			Sr87/Sr86 =		0.708851	
	Iteration 2		**84**	**86**	**87**	**88**
		Measured	0.0596845	1.000000	0.708849	8.375195
		Sample	0.0564899	0.999998	0.708849	8.375194
		Tracer	0.0031946	0.000002	0.000000	0.000001
			86/88 =	0.119400		
			Sr87/Sr86 =		0.708850	
	Iteration 3		**84**	**86**	**87**	**88**
		Measured	0.0596845	1.000000	0.708849	8.375195
		Sample	0.0564899	0.999998	0.708849	8.375194
		Tracer	0.0031946	0.000002	0.000000	0.000001
			86/88 =	0.119400		
			Sr87/Sr86 =		0.708850	
	Iteration 4		**84**	**86**	**87**	**88**
		Measured	0.0596845	1.000000	0.708849	8.375195
		Sample	0.0564899	0.999998	0.708849	8.375194
		Tracer	0.0031946	0.000002	0.000000	0.000001
			86/88 =	0.119400		
			Sr87/Sr86 =		0.708850	
	Iteration 5		**84**	**86**	**87**	**88**
		Measured	0.0596845	1.000000	0.708849	8.375195
		Sample	0.0564899	0.999998	0.708849	8.375194
		Tracer	0.0031946	0.000002	0.000000	0.000001
			86/88 =	0.119400		
			Sr87/Sr86 =		0.708850	

		nanomoles	2.1922	38.8069	27.5082	325.0156
		nanogram	183.9550	3333.8689	2390.7111	28570.6935
	blank corr	nanogram		3333.7689		
	blank corr	nanomoles	2.1921	38.8057	27.5074	325.0058
	blank corr	nanogram	183.9495	3333.7689	2390.6394	28569.8365
	blank corr	ppm	3.2615	59.1094	42.3872	506.5574
	Tot Sr (ppm)	(approximate)	611.32			
	Blank Corr Sr87/Sr86		0.708850	Sample/Blank		33337.7

APPENDIX 4B. STRONTIUM ISOTOPE DATA REDUCTION

Sample ID	**NC 11-1145-1**		Date	4/10/2009		
Sample Wt (g)	0.03950					
Aliquot (frac)	1.0000	(Sr88/Sr84)t	(Sr87/Sr84)t	(Sr86/Sr84)t	[Sr84]t	
Tracer ID	#11 Sr810	0.00039	0.00010	0.00059	1.0300	
Tracer Wt. (g)	0.0094					
		Sr88/Sr86	Sr87/Sr86	Sr84/Sr86		
Blank Sr86 (ng)	0.100	8.375209	0.709200	0.056490		
Normal Sr		8.375209	0.709000	0.056490		
Measured Sr IC/ID		8.375209	0.708856	0.060907		
			(lin norm)	(norm)		

Sr Reduction	**Iteration 1**		**84**	**86**	**87**	**88**
		Measured	0.0609073	1.000000	0.708856	8.375209
		Sample	0.0564899	0.999997	0.708855	8.375208
		Tracer	0.0044174	0.000003	0.000000	0.000002
			86/88 =	0.119400		8.375229
			Sr87/Sr86 =		0.708857	
	Iteration 2		**84**	**86**	**87**	**88**
		Measured	0.0609074	1.000000	0.708855	8.375189
		Sample	0.0564899	0.999997	0.708854	8.375188
		Tracer	0.0044176	0.000003	0.000000	0.000002
			86/88 =	0.119400		
			Sr87/Sr86 =		0.708856	
	Iteration 3		**84**	**86**	**87**	**88**
		Measured	0.0609074	1.000000	0.708855	8.375189
		Sample	0.0564899	0.999997	0.708854	8.375188
		Tracer	0.0044176	0.000003	0.000000	0.000002
			86/88 =	0.119400		
			Sr87/Sr86 =		0.708856	
	Iteration 4		**84**	**86**	**87**	**88**
		Measured	0.0609074	1.000000	0.708855	8.375189
		Sample	0.0564899	0.999997	0.708854	8.375188
		Tracer	0.0044176	0.000003	0.000000	0.000002
			86/88 =	0.119400		
			Sr87/Sr86 =		0.708856	
	Iteration 5		**84**	**86**	**87**	**88**
		Measured	0.0609074	1.000000	0.708855	8.375189
		Sample	0.0564899	0.999997	0.708854	8.375188
		Tracer	0.0044176	0.000003	0.000000	0.000002
			86/88 =	0.119400		
			Sr87/Sr86 =		0.708856	

		nanomoles	1.4754	26.1184	18.5142	218.7472
		nanogram	123.8083	2243.8137	1609.0481	19229.1046
	blank corr	nanogram		2243.7137		
	blank corr	nanomoles	1.4754	26.1172	18.5134	218.7374
	blank corr	nanogram	123.8028	2243.7137	1608.9764	19228.2476
	blank corr	ppm	3.1342	56.8029	40.7336	486.7911
	Tot Sr (ppm)	(approximate)	587.46			
	Blank Corr Sr87/Sr86		0.708856	Sample/Blank		22437.1

APPENDIX 4B. STRONTIUM ISOTOPE DATA REDUCTION

Sample ID	**PR-10KM67.6 #2**		Date	4/11/2009		
Sample Wt (g)	0.02090					
Aliquot (frac)	1.0000	(Sr88/Sr84)t	(Sr87/Sr84)t	(Sr86/Sr84)t	[Sr84]t	
Tracer ID	#11 Sr811	0.00039	0.00010	0.00059	1.0300	
Tracer Wt. (g)	0.0099					
		Sr88/Sr86	Sr87/Sr86	Sr84/Sr86		
Blank Sr86 (ng)	0.100	8.375209	0.709200	0.056490		
Normal Sr		8.375209	0.709000	0.056490		
Measured Sr IC/ID		8.375209	0.708090	0.061917		
			(lin norm)	(norm)		

Sr Reduction	**Iteration 1**		**84**	**86**	**87**	**88**
		Measured	0.0619173	1.000000	0.708090	8.375209
		Sample	0.0564898	0.999997	0.708089	8.375207
		Tracer	0.0054275	0.000003	0.000001	0.000002
			86/88 =	0.119400		8.375234
			Sr87/Sr86 =		0.708091	
	Iteration 2		**84**	**86**	**87**	**88**
		Measured	0.0619175	1.000000	0.708089	8.375185
		Sample	0.0564898	0.999997	0.708088	8.375183
		Tracer	0.0054277	0.000003	0.000001	0.000002
			86/88 =	0.119400		
			Sr87/Sr86 =		0.708090	
	Iteration 3		**84**	**86**	**87**	**88**
		Measured	0.0619175	1.000000	0.708089	8.375185
		Sample	0.0564898	0.999997	0.708088	8.375183
		Tracer	0.0054277	0.000003	0.000001	0.000002
			86/88 =	0.119400		
			Sr87/Sr86 =		0.708090	
	Iteration 4		**84**	**86**	**87**	**88**
		Measured	0.0619175	1.000000	0.708089	8.375185
		Sample	0.0564898	0.999997	0.708088	8.375183
		Tracer	0.0054277	0.000003	0.000001	0.000002
			86/88 =	0.119400		
			Sr87/Sr86 =		0.708090	
	Iteration 5		**84**	**86**	**87**	**88**
		Measured	0.0619175	1.000000	0.708089	8.375185
		Sample	0.0564898	0.999997	0.708088	8.375183
		Tracer	0.0054277	0.000003	0.000001	0.000002
			86/88 =	0.119400		
			Sr87/Sr86 =		0.708090	

		nanomoles	1.2647	22.3886	15.8531	187.5091
		nanogram	106.1279	1923.3871	1377.7789	16483.1030
	blank corr	nanogram		1923.2871		
	blank corr	nanomoles	1.2647	22.3874	15.8523	187.4993
	blank corr	nanogram	106.1224	1923.2871	1377.7071	16482.2461
	blank corr	ppm	5.0776	92.0233	65.9190	788.6242
	Tot Sr (ppm)	(approximate)	951.64			
	Blank Corr Sr87/Sr86		0.708090	Sample/Blank		19232.9

APPENDIX 4B. STRONTIUM ISOTOPE DATA REDUCTION

Sample ID	**NC-11 1145-2**		Date	4/12/2009		
Sample Wt (g)	0.04560					
Aliquot (frac)	1.0000	(Sr88/Sr84)t	(Sr87/Sr84)t	(Sr86/Sr84)t	[Sr84]t	
Tracer ID	#11 Sr812	0.00039	0.00010	0.00059	1.0300	
Tracer Wt. (g)	0.0101					
		Sr88/Sr86	Sr87/Sr86	Sr84/Sr86		
Blank Sr86 (ng)	0.100	8.375209	0.709200	0.056490		
Normal Sr		8.375209	0.709000	0.056490		
Measured Sr IC/ID		8.375209	0.708859	0.060091		
			(lin norm)	(norm)		

Sr Reduction	**Iteration 1**		**84**	**86**	**87**	**88**
		Measured	0.0600910	1.000000	0.708859	8.375209
		Sample	0.0564899	0.999998	0.708858	8.375208
		Tracer	0.0036011	0.000002	0.000000	0.000001
			86/88 =	0.119400		8.375226
			Sr87/Sr86 =		0.708860	
	Iteration 2		**84**	**86**	**87**	**88**
		Measured	0.0600911	1.000000	0.708858	8.375193
		Sample	0.0564899	0.999998	0.708858	8.375192
		Tracer	0.0036012	0.000002	0.000000	0.000001
			86/88 =	0.119400		
			Sr87/Sr86 =		0.708859	
	Iteration 3		**84**	**86**	**87**	**88**
		Measured	0.0600911	1.000000	0.708858	8.375193
		Sample	0.0564899	0.999998	0.708858	8.375192
		Tracer	0.0036012	0.000002	0.000000	0.000001
			86/88 =	0.119400		
			Sr87/Sr86 =		0.708859	
	Iteration 4		**84**	**86**	**87**	**88**
		Measured	0.0600911	1.000000	0.708858	8.375193
		Sample	0.0564899	0.999998	0.708858	8.375192
		Tracer	0.0036012	0.000002	0.000000	0.000001
			86/88 =	0.119400		
			Sr87/Sr86 =		0.708859	
	Iteration 5		**84**	**86**	**87**	**88**
		Measured	0.0600911	1.000000	0.708858	8.375193
		Sample	0.0564899	0.999998	0.708858	8.375192
		Tracer	0.0036012	0.000002	0.000000	0.000001
			86/88 =	0.119400		
			Sr87/Sr86 =		0.708859	

		nanomoles	1.9447	34.4250	24.4025	288.3169
		nanogram	163.1840	2957.4301	2120.7947	25344.6768
	blank corr	nanogram		2957.3301		
	blank corr	nanomoles	1.9446	34.4239	24.4017	288.3072
	blank corr	nanogram	163.1785	2957.3301	2120.7229	25343.8198
	blank corr	ppm	3.5785	64.8537	46.5071	555.7855
	Tot Sr (ppm)	(approximate)	670.72			
	Blank Corr Sr87/Sr86		0.708859	Sample/Blank		29573.3

APPENDIX 4B. STRONTIUM ISOTOPE DATA REDUCTION

Sample ID	**PR-10 10 3M2**		Date	4/13/2009		
Sample Wt (g)	0.04030					
Aliquot (frac)	1.0000	(Sr88/Sr84)t	(Sr87/Sr84)t	(Sr86/Sr84)t	[Sr84]t	
Tracer ID	#11 Sr813	0.00039	0.00010	0.00059	1.0300	
Tracer Wt. (g)	0.0095					
		Sr88/Sr86	Sr87/Sr86	Sr84/Sr86		
Blank Sr86 (ng)	0.100	8.375209	0.709200	0.056490		
Normal Sr		8.375209	0.709000	0.056490		
Measured Sr IC/ID		8.375209	0.708203	0.062806		
			(lin norm)	(norm)		

Sr Reduction	**Iteration 1**		**84**	**86**	**87**	**88**
		Measured	0.0628057	1.000000	0.708203	8.375209
		Sample	0.0564898	0.999996	0.708202	8.375207
		Tracer	0.0063159	0.000004	0.000001	0.000002
			86/88 =	0.119400		8.375238
			Sr87/Sr86 =		0.708205	
	Iteration 2		**84**	**86**	**87**	**88**
		Measured	0.0628059	1.000000	0.708201	8.375181
		Sample	0.0564898	0.999996	0.708201	8.375178
		Tracer	0.0063161	0.000004	0.000001	0.000002
			86/88 =	0.119400		
			Sr87/Sr86 =		0.708204	
	Iteration 3		**84**	**86**	**87**	**88**
		Measured	0.0628059	1.000000	0.708201	8.375181
		Sample	0.0564898	0.999996	0.708201	8.375178
		Tracer	0.0063161	0.000004	0.000001	0.000002
			86/88 =	0.119400		
			Sr87/Sr86 =		0.708204	
	Iteration 4		**84**	**86**	**87**	**88**
		Measured	0.0628059	1.000000	0.708201	8.375181
		Sample	0.0564898	0.999996	0.708201	8.375178
		Tracer	0.0063161	0.000004	0.000001	0.000002
			86/88 =	0.119400		
			Sr87/Sr86 =		0.708204	
	Iteration 5		**84**	**86**	**87**	**88**
		Measured	0.0628059	1.000000	0.708201	8.375181
		Sample	0.0564898	0.999996	0.708201	8.375178
		Tracer	0.0063161	0.000004	0.000001	0.000002
			86/88 =	0.119400		
			Sr87/Sr86 =		0.708204	

		nanomoles	1.0429	18.4619	13.0748	154.6225
		nanogram	87.5145	1586.0505	1136.3164	13592.1852
	blank corr	nanogram		1585.9505		
	blank corr	nanomoles	1.0428	18.4608	13.0740	154.6127
	blank corr	nanogram	87.5090	1585.9505	1136.2446	13591.3282
	blank corr	ppm	2.1714	39.3536	28.1947	337.2538
	Tot Sr (ppm)	(approximate)	406.97			
	Blank Corr Sr87/Sr86		0.708203	Sample/Blank		15859.5

APPENDIX 4B. STRONTIUM ISOTOPE DATA REDUCTION

Sample ID	**PR111-GPS**		Date	4/14/2009		
Sample Wt (g)	0.01810					
Aliquot (frac)	1.0000	(Sr88/Sr84)t	(Sr87/Sr84)t	(Sr86/Sr84)t	[Sr84]t	
Tracer ID	#11 Sr814	0.00039	0.00010	0.00059	1.0300	
Tracer Wt. (g)	0.0097					
		Sr88/Sr86	Sr87/Sr86	Sr84/Sr86		
Blank Sr86 (ng)	0.100	8.375209	0.709200	0.056490		
Normal Sr		8.375209	0.709000	0.056490		
Measured Sr IC/ID		8.375209	0.708171	0.061555		
			(lin norm)	(norm)		

Sr Reduction	**Iteration 1**		**84**	**86**	**87**	**88**
		Measured	0.0615548	1.000000	0.708171	8.375209
		Sample	0.0564898	0.999997	0.708171	8.375207
		Tracer	0.0050650	0.000003	0.000000	0.000002
			86/88 =	0.119400		8.375232
			Sr87/Sr86 =		0.708173	
	Iteration 2		**84**	**86**	**87**	**88**
		Measured	0.0615550	1.000000	0.708170	8.375186
		Sample	0.0564898	0.999997	0.708170	8.375184
		Tracer	0.0050651	0.000003	0.000000	0.000002
			86/88 =	0.119400		
			Sr87/Sr86 =		0.708172	
	Iteration 3		**84**	**86**	**87**	**88**
		Measured	0.0615550	1.000000	0.708170	8.375186
		Sample	0.0564898	0.999997	0.708170	8.375184
		Tracer	0.0050651	0.000003	0.000000	0.000002
			86/88 =	0.119400		
			Sr87/Sr86 =		0.708172	
	Iteration 4		**84**	**86**	**87**	**88**
		Measured	0.0615550	1.000000	0.708170	8.375186
		Sample	0.0564898	0.999997	0.708170	8.375184
		Tracer	0.0050651	0.000003	0.000000	0.000002
			86/88 =	0.119400		
			Sr87/Sr86 =		0.708172	
	Iteration 5		**84**	**86**	**87**	**88**
		Measured	0.0615550	1.000000	0.708170	8.375186
		Sample	0.0564898	0.999997	0.708170	8.375184
		Tracer	0.0050651	0.000003	0.000000	0.000002
			86/88 =	0.119400		
			Sr87/Sr86 =		0.708172	

		nanomoles	1.3279	23.5063	16.6465	196.8705
		nanogram	111.4264	2019.4121	1446.7306	17306.0207
	blank corr	nanogram		2019.3121		
	blank corr	nanomoles	1.3278	23.5052	16.6457	196.8607
	blank corr	nanogram	111.4208	2019.3121	1446.6588	17305.1637
	blank corr	ppm	6.1558	111.5642	79.9259	956.0864
	Tot Sr (ppm)	(approximate)	1153.73			
	Blank Corr Sr87/Sr86		0.708172	Sample/Blank		20193.1

APPENDIX 4B. STRONTIUM ISOTOPE DATA REDUCTION

Sample ID	**NC-11 1181-2**		Date	4/15/2009		
Sample Wt (g)	0.02670					
Aliquot (frac)	1.0000	(Sr88/Sr84)t	(Sr87/Sr84)t	(Sr86/Sr84)t	[Sr84]t	
Tracer ID	#11 Sr815	0.00039	0.00010	0.00059	1.0300	
Tracer Wt. (g)	0.0082					
		Sr88/Sr86	Sr87/Sr86	Sr84/Sr86		
Blank Sr86 (ng)	0.100	8.375209	0.709200	0.056490		
Normal Sr		8.375209	0.709000	0.056490		
Measured Sr IC/ID		8.375209	0.708839	0.060147		
			(lin norm)	(norm)		

Sr Reduction	**Iteration 1**		**84**	**86**	**87**	**88**
		Measured	0.0601472	1.000000	0.708839	8.375209
		Sample	0.0564899	0.999998	0.708839	8.375208
		Tracer	0.0036573	0.000002	0.000000	0.000001
			86/88 =	0.119400		8.375226
			Sr87/Sr86 =		0.708840	
	Iteration 2		**84**	**86**	**87**	**88**
		Measured	0.0601473	1.000000	0.708839	8.375193
		Sample	0.0564899	0.999998	0.708838	8.375191
		Tracer	0.0036574	0.000002	0.000000	0.000001
			86/88 =	0.119400		
			Sr87/Sr86 =		0.708840	
	Iteration 3		**84**	**86**	**87**	**88**
		Measured	0.0601473	1.000000	0.708839	8.375193
		Sample	0.0564899	0.999998	0.708838	8.375191
		Tracer	0.0036574	0.000002	0.000000	0.000001
			86/88 =	0.119400		
			Sr87/Sr86 =		0.708840	
	Iteration 4		**84**	**86**	**87**	**88**
		Measured	0.0601473	1.000000	0.708839	8.375193
		Sample	0.0564899	0.999998	0.708838	8.375191
		Tracer	0.0036574	0.000002	0.000000	0.000001
			86/88 =	0.119400		
			Sr87/Sr86 =		0.708840	
	Iteration 5		**84**	**86**	**87**	**88**
		Measured	0.0601473	1.000000	0.708839	8.375193
		Sample	0.0564899	0.999998	0.708838	8.375191
		Tracer	0.0036574	0.000002	0.000000	0.000001
			86/88 =	0.119400		
			Sr87/Sr86 =		0.708840	

		nanomoles	1.5546	27.5195	19.5070	230.4820
		nanogram	130.4501	2364.1844	1695.3275	20260.6614
	blank corr	nanogram		2364.0844		
	blank corr	nanomoles	1.5545	27.5184	19.5061	230.4722
	blank corr	nanogram	130.4446	2364.0844	1695.2557	20259.8044
	blank corr	ppm	4.8856	88.5425	63.4927	758.7942
	Tot Sr (ppm)	(approximate)	915.71			
	Blank Corr Sr87/Sr86		0.708840	Sample/Blank		23640.8

APPENDIX 4B. STRONTIUM ISOTOPE DATA REDUCTION

Sample ID	**NC 11-1165-4**		Date	4/16/2009		
Sample Wt (g)	0.02140					
Aliquot (frac)	1.0000	(Sr88/Sr84)t	(Sr87/Sr84)t	(Sr86/Sr84)t	[Sr84]t	
Tracer ID	#11 Sr816	0.00039	0.00010	0.00059	1.0300	
Tracer Wt. (g)	0.0099					
		Sr88/Sr86	Sr87/Sr86	Sr84/Sr86		
Blank Sr86 (ng)	0.100	8.375209	0.709200	0.056490		
Normal Sr		8.375209	0.709000	0.056490		
Measured Sr IC/ID		8.375209	0.708847	0.062286		
			(lin norm)	(norm)		

Sr Reduction	**Iteration 1**		**84**	**86**	**87**	**88**
		Measured	0.0622861	1.000000	0.708847	8.375209
		Sample	0.0564898	0.999997	0.708846	8.375207
		Tracer	0.0057963	0.000003	0.000001	0.000002
			86/88 =	0.119400		8.375236
			Sr87/Sr86 =		0.708849	
	Iteration 2		**84**	**86**	**87**	**88**
		Measured	0.0622863	1.000000	0.708846	8.375183
		Sample	0.0564898	0.999997	0.708845	8.375181
		Tracer	0.0057965	0.000003	0.000001	0.000002
			86/88 =	0.119400		
			Sr87/Sr86 =		0.708848	
	Iteration 3		**84**	**86**	**87**	**88**
		Measured	0.0622863	1.000000	0.708846	8.375183
		Sample	0.0564898	0.999997	0.708845	8.375181
		Tracer	0.0057965	0.000003	0.000001	0.000002
			86/88 =	0.119400		
			Sr87/Sr86 =		0.708848	
	Iteration 4		**84**	**86**	**87**	**88**
		Measured	0.0622863	1.000000	0.708846	8.375183
		Sample	0.0564898	0.999997	0.708845	8.375181
		Tracer	0.0057965	0.000003	0.000001	0.000002
			86/88 =	0.119400		
			Sr87/Sr86 =		0.708848	
	Iteration 5		**84**	**86**	**87**	**88**
		Measured	0.0622863	1.000000	0.708846	8.375183
		Sample	0.0564898	0.999997	0.708845	8.375181
		Tracer	0.0057965	0.000003	0.000001	0.000002
			86/88 =	0.119400		
			Sr87/Sr86 =		0.708848	

		nanomoles	1.1843	20.9640	14.8603	175.5780
		nanogram	99.3751	1801.0032	1291.4915	15434.2934
	blank corr	nanogram		1800.9032		
	blank corr	nanomoles	1.1842	20.9629	14.8595	175.5683
	blank corr	nanogram	99.3696	1800.9032	1291.4198	15433.4364
	blank corr	ppm	4.6434	84.1544	60.3467	721.1886
	Tot Sr (ppm)	(approximate)	870.33			
	Blank Corr Sr87/Sr86		0.708848	Sample/Blank		18009.0

APPENDIX 4B. STRONTIUM ISOTOPE DATA REDUCTION

Sample ID	**PR 111-OL-2**		Date	4/16/2009		
Sample Wt (g)	0.03180					
Aliquot (frac)	1.0000	(Sr88/Sr84)t	(Sr87/Sr84)t	(Sr86/Sr84)t	[Sr84]t	
Tracer ID	#11 Sr817	0.00039	0.00010	0.00059	1.0300	
Tracer Wt. (g)	0.0084					
		Sr88/Sr86	Sr87/Sr86	Sr84/Sr86		
Blank Sr86 (ng)	0.100	8.375209	0.709200	0.056490		
Normal Sr		8.375209	0.709000	0.056490		
Measured Sr IC/ID		8.375209	0.708175	0.062415		
			(lin norm)	(norm)		

Sr Reduction	**Iteration 1**		**84**	**86**	**87**	**88**
		Measured	0.0624148	1.000000	0.708175	8.375209
		Sample	0.0564898	0.999997	0.708174	8.375207
		Tracer	0.0059250	0.000003	0.000001	0.000002
			86/88 =	0.119400		8.375236
			Sr87/Sr86 =		0.708177	
	Iteration 2		**84**	**86**	**87**	**88**
		Measured	0.0624150	1.000000	0.708174	8.375182
		Sample	0.0564898	0.999997	0.708173	8.375180
		Tracer	0.0059252	0.000003	0.000001	0.000002
			86/88 =	0.119400		
			Sr87/Sr86 =		0.708176	
	Iteration 3		**84**	**86**	**87**	**88**
		Measured	0.0624150	1.000000	0.708174	8.375182
		Sample	0.0564898	0.999997	0.708173	8.375180
		Tracer	0.0059252	0.000003	0.000001	0.000002
			86/88 =	0.119400		
			Sr87/Sr86 =		0.708176	
	Iteration 4		**84**	**86**	**87**	**88**
		Measured	0.0624150	1.000000	0.708174	8.375182
		Sample	0.0564898	0.999997	0.708173	8.375180
		Tracer	0.0059252	0.000003	0.000001	0.000002
			86/88 =	0.119400		
			Sr87/Sr86 =		0.708176	
	Iteration 5		**84**	**86**	**87**	**88**
		Measured	0.0624150	1.000000	0.708174	8.375182
		Sample	0.0564898	0.999997	0.708173	8.375180
		Tracer	0.0059252	0.000003	0.000001	0.000002
			86/88 =	0.119400		
			Sr87/Sr86 =		0.708176	

		nanomoles	0.9830	17.4013	12.3231	145.7392
		nanogram	82.4867	1494.9294	1070.9911	12811.2927
	blank corr	nanogram		1494.8294		
	blank corr	nanomoles	0.9829	17.4001	12.3223	145.7294
	blank corr	nanogram	82.4811	1494.8294	1070.9193	12810.4357
	blank corr	ppm	2.5937	47.0072	33.6767	402.8439
	Tot Sr (ppm)	(approximate)	486.12			
	Blank Corr Sr87/Sr86		0.708176	Sample/Blank		14948.3

APPENDIX 4B. STRONTIUM ISOTOPE DATA REDUCTION

Sample ID	**PR-111 T1**		Date	4/18/2009		
Sample Wt (g)	0.02370					
Aliquot (frac)	1.0000	(Sr88/Sr84)t	(Sr87/Sr84)t	(Sr86/Sr84)t	[Sr84]t	
Tracer ID	#11 Sr818	0.00039	0.00010	0.00059	1.0300	
Tracer Wt. (g)	0.0098					
		Sr88/Sr86	Sr87/Sr86	Sr84/Sr86		
Blank Sr86 (ng)	0.100	8.375209	0.709200	0.056490		
Normal Sr		8.375209	0.709000	0.056490		
Measured Sr IC/ID		8.375209	0.708167	0.061661		
			(lin norm)	(norm)		

Sr Reduction	**Iteration 1**		**84**	**86**	**87**	**88**
		Measured	0.0616612	1.000000	0.708167	8.375209
		Sample	0.0564898	0.999997	0.708166	8.375207
		Tracer	0.0051714	0.000003	0.000001	0.000002
			86/88 =	0.119400		8.375233
			Sr87/Sr86 =		0.708168	
	Iteration 2		**84**	**86**	**87**	**88**
		Measured	0.0616614	1.000000	0.708166	8.375186
		Sample	0.0564898	0.999997	0.708165	8.375184
		Tracer	0.0051715	0.000003	0.000001	0.000002
			86/88 =	0.119400		
			Sr87/Sr86 =		0.708167	
	Iteration 3		**84**	**86**	**87**	**88**
		Measured	0.0616614	1.000000	0.708166	8.375186
		Sample	0.0564898	0.999997	0.708165	8.375184
		Tracer	0.0051715	0.000003	0.000001	0.000002
			86/88 =	0.119400		
			Sr87/Sr86 =		0.708167	
	Iteration 4		**84**	**86**	**87**	**88**
		Measured	0.0616614	1.000000	0.708166	8.375186
		Sample	0.0564898	0.999997	0.708165	8.375184
		Tracer	0.0051715	0.000003	0.000001	0.000002
			86/88 =	0.119400		
			Sr87/Sr86 =		0.708167	
	Iteration 5		**84**	**86**	**87**	**88**
		Measured	0.0616614	1.000000	0.708166	8.375186
		Sample	0.0564898	0.999997	0.708165	8.375184
		Tracer	0.0051715	0.000003	0.000001	0.000002
			86/88 =	0.119400		
			Sr87/Sr86 =		0.708167	

		nanomoles	1.3140	23.2600	16.4720	194.8076
		nanogram	110.2588	1998.2518	1431.5620	17124.6804
	blank corr	nanogram		1998.1518		
	blank corr	nanomoles	1.3139	23.2589	16.4712	194.7978
	blank corr	nanogram	110.2533	1998.1518	1431.4903	17123.8234
	blank corr	ppm	4.6520	84.3102	60.4004	722.5242
	Tot Sr (ppm)	(approximate)	871.89			
	Blank Corr Sr87/Sr86		0.708167	Sample/Blank		19981.5

APPENDIX 4B. STRONTIUM ISOTOPE DATA REDUCTION

Sample ID	**PR-111 M8**		Date	4/19/2009		
Sample Wt (g)	0.01600					
Aliquot (frac)	1.0000	(Sr88/Sr84)t	(Sr87/Sr84)t	(Sr86/Sr84)t	[Sr84]t	
Tracer ID	#11 Sr819	0.00039	0.00010	0.00059	1.0300	
Tracer Wt. (g)	0.0090					
		Sr88/Sr86	Sr87/Sr86	Sr84/Sr86		
Blank Sr86 (ng)	0.100	8.375209	0.709200	0.056490		
Normal Sr		8.375209	0.709000	0.056490		
Measured Sr IC/ID		8.375209	0.708126	0.061186		
			(lin norm)	(norm)		

Sr Reduction	**Iteration 1**		**84**	**86**	**87**	**88**
		Measured	0.0611855	1.000000	0.708126	8.375209
		Sample	0.0564898	0.999997	0.708125	8.375208
		Tracer	0.0046957	0.000003	0.000000	0.000002
			86/88 =	0.119400		8.375231
			Sr87/Sr86 =		0.708127	
	Iteration 2		**84**	**86**	**87**	**88**
		Measured	0.0611857	1.000000	0.708125	8.375188
		Sample	0.0564898	0.999997	0.708124	8.375186
		Tracer	0.0046958	0.000003	0.000000	0.000002
			86/88 =	0.119400		
			Sr87/Sr86 =		0.708126	
	Iteration 3		**84**	**86**	**87**	**88**
		Measured	0.0611857	1.000000	0.708125	8.375188
		Sample	0.0564898	0.999997	0.708124	8.375186
		Tracer	0.0046958	0.000003	0.000000	0.000002
			86/88 =	0.119400		
			Sr87/Sr86 =		0.708126	
	Iteration 4		**84**	**86**	**87**	**88**
		Measured	0.0611857	1.000000	0.708125	8.375188
		Sample	0.0564898	0.999997	0.708124	8.375186
		Tracer	0.0046958	0.000003	0.000000	0.000002
			86/88 =	0.119400		
			Sr87/Sr86 =		0.708126	
	Iteration 5		**84**	**86**	**87**	**88**
		Measured	0.0611857	1.000000	0.708125	8.375188
		Sample	0.0564898	0.999997	0.708124	8.375186
		Tracer	0.0046958	0.000003	0.000000	0.000002
			86/88 =	0.119400		
			Sr87/Sr86 =		0.708126	

		nanomoles	1.3289	23.5254	16.6589	197.0298
		nanogram	111.5166	2021.0468	1447.8088	17320.0297
	blank corr	nanogram		2020.9468		
	blank corr	nanomoles	1.3289	23.5242	16.6581	197.0201
	blank corr	nanogram	111.5110	2020.9468	1447.7370	17319.1727
	blank corr	ppm	6.9694	126.3092	90.4836	1082.4483
	Tot Sr (ppm)	(approximate)	1306.21			
	Blank Corr Sr87/Sr86		0.708126	Sample/Blank		20209.5

APPENDIX 4B. STRONTIUM ISOTOPE DATA REDUCTION

Sample ID	**PR-111 M2**		Date	4/20/2009		
Sample Wt (g)	0.02910					
Aliquot (frac)	1.0000	(Sr88/Sr84)t	(Sr87/Sr84)t	(Sr86/Sr84)t	[Sr84]t	
Tracer ID	#11 Sr820	0.00039	0.00010	0.00059	1.0300	
Tracer Wt. (g)	0.0100					
		Sr88/Sr86	Sr87/Sr86	Sr84/Sr86		
Blank Sr86 (ng)	0.100	8.375209	0.709200	0.056490		
Normal Sr		8.375209	0.709000	0.056490		
Measured Sr IC/ID		8.375209	0.708135	0.059546		
			(lin norm)	(norm)		

Sr Reduction	**Iteration 1**		**84**	**86**	**87**	**88**
		Measured	0.0595455	1.000000	0.708135	8.375209
		Sample	0.0564899	0.999998	0.708134	8.375208
		Tracer	0.0030556	0.000002	0.000000	0.000001
			86/88 =	0.119400		8.375223
			Sr87/Sr86 =		0.708136	
	Iteration 2		**84**	**86**	**87**	**88**
		Measured	0.0595456	1.000000	0.708134	8.375195
		Sample	0.0564899	0.999998	0.708134	8.375194
		Tracer	0.0030557	0.000002	0.000000	0.000001
			86/88 =	0.119400		
			Sr87/Sr86 =		0.708135	
	Iteration 3		**84**	**86**	**87**	**88**
		Measured	0.0595456	1.000000	0.708134	8.375195
		Sample	0.0564899	0.999998	0.708134	8.375194
		Tracer	0.0030557	0.000002	0.000000	0.000001
			86/88 =	0.119400		
			Sr87/Sr86 =		0.708135	
	Iteration 4		**84**	**86**	**87**	**88**
		Measured	0.0595456	1.000000	0.708134	8.375195
		Sample	0.0564899	0.999998	0.708134	8.375194
		Tracer	0.0030557	0.000002	0.000000	0.000001
			86/88 =	0.119400		
			Sr87/Sr86 =		0.708135	
	Iteration 5		**84**	**86**	**87**	**88**
		Measured	0.0595456	1.000000	0.708134	8.375195
		Sample	0.0564899	0.999998	0.708134	8.375194
		Tracer	0.0030557	0.000002	0.000000	0.000001
			86/88 =	0.119400		
			Sr87/Sr86 =		0.708135	

		nanomoles	2.2692	40.1693	28.4453	336.4262
		nanogram	190.4133	3450.9147	2472.1479	29573.7560
	blank corr	nanogram		3450.8147		
	blank corr	nanomoles	2.2691	40.1681	28.4445	336.4165
	blank corr	nanogram	190.4078	3450.8147	2472.0761	29572.8990
	blank corr	ppm	6.5432	118.5847	84.9511	1016.2508
	Tot Sr (ppm)	(approximate)	1226.33			
	Blank Corr Sr87/Sr86		0.708135	Sample/Blank		34508.1